Rainfall Variability over Southern Africa

Author:
Penny Driver

Supervisors:
Prof. Chris Reason
Dr. Babatunde Abiodun

Thesis presented for the degree of

Doctor of Philosophy

Department of Oceanography

Faculty of Science

University of Cape Town

August, 2014

Acknowledgments

To my parents, without whose love and support I could never have achieved this goal.

To my father, who gave me so much strength and support, kept me laughing at the worst of times, and never had any doubt in my ability to succeed. Although he didn't live to see me finish, I know he would have been so proud of me and excited to see what comes next.

To my mother, who has always been an inspiration and the most amazing role model any girl in science could have wished for. Thank you for all the hours spent chatting about everything under the sun and most of all for my lifetime of encouragement and support.

To my supervisor Chris Reason, for being a rock star scientist and the most amazing and efficient supervisor I've ever had the pleasure of witnessing in action.

To my co-supervisor Babatunde Abiodun, for turning a very reluctant mathematician into a proficient programmer and always having time to debug my code in 5 minutes after I'd worked on it for days and days.

To Joe Prusa, for the endless hours spent teaching me about model development over email and never making me feel that I was an unwelcome burden even when I'm sure I was.

To Frank Shillington and George Philander, for all your guidance and support in the early years of my studies.

To Dave Ogier, for being my company in misery while we learned how to install a climate model on a cluster and program in Fortran and Ferret. Also for that friend thing.

To my friends and colleagues in Oceanography, for all the tea room chats, shared stories of pain, and encouraging stories of success.

To the support team at the Centre for High Performance Computing, for all the hours spent trying to get my model running on the cluster, and

a special thanks to Eric Mbele who always took my calls and solved my problems even though I'm fairly certain that he is employed far out of the realm of dealing with users directly.

To the National Research Foundation and the University of Cape Town, for funding my studies.

To Joe Byrne, my love, for putting up with me and all the crazy that goes with dating a PhD student.

To my friends and family both here and back home, for all the love, encouragement, teasing, and torture. You'll have to find something else to give me a hard time about now! Thanks for making my trips home full of fun and laughter, you lot helped keep me sane.

To all those left unnamed who helped me along the way, you have my deepest gratitude.

Contents

Abstract

Southern Africa is subject to high interannual rainfall variability and the factors influencing southern African rainfall are not fully understood. The variability has been linked with various sea surface temperature anomalies (SSTAs) in each of the three major ocean basins as well as variability in the strength and position of regional atmospheric features. One of the atmospheric factors that may play a substantial role in southern African rainfall variability is the Botswana high, a high pressure cell which exists at the 500 hPa level and is centred over central Namibia and western Botswana during austral summer. 20th Century reanalysis data is used to further investigate this feature and analysis reveals an association between the strength of the Botswana high and ENSO. Further analysis indicates that a connection between the Botswana high and rainfall over southern Africa not only exists during ENSO years, but is also apparent during neutral years that display ENSO-like characteristics in the Botswana high. This result may assist in producing better rainfall forecasts for non-ENSO years.

The frequency of dry days over southern Africa during austral summer is investigated using GPCP observational data. Correlation analysis is generally in agreement with previous studies and showed that dry day frequency (DDF) over the Limpopo and North East Zambia regions is correlated with ENSO, while DDF over coastal northern Angola and central South Africa is correlated with SSTs in the Indian and Atlantic Oceans. The possible role played by DDF during JFM 1998 and JFM 2010 is investigated and results indicate that the distribution of DDF over southern Africa was notably different during these two seasons and may have contributed to the unexpected rainfall experienced over southern Africa.

Further investigations into the unexpectedly high rainfall anomalies over southern Africa during JFM 1998 and 2010 are carried out in a series of modeled sensitivity experiments. A non-hydrostatic, stretch grid global atmospheric model CAM-EULAG (CEU) is used to assess the relative impact of each of the three major ocean basin SSTs on rainfall over southern Africa. In three of the experiments, SSTs in one major ocean basin are replaced by the climatology of that ocean, which acts to neutralise the impact of that

ocean basin on southern African rainfall. In another three experiments, SSTs in two ocean basins are replaced with their climatology, which acts to isolate the impact of the remaining ocean basin on southern African rainfall. Results suggest that although these experiments indicate that no single ocean basin SSTAs were responsible for the anomalous rainfall, the unexpectedly strong Angola low that occurred during JFM 1998 and 2010 did appear to have had a strong impact on rainfall over southern Africa during these two seasons.

Chapter 1

Introduction

Southern Africa is subject to high interannual and interdecadal rainfall variability (Tyson, 1986; Mason and Jury, 1997; Fauchereau et al., 2003b; Richard et al., 2001) and is prone to drought and flood events (Richard et al., 2001; Rouault and Richard, 2005; Washington and Preston, 2006). A number of factors have been implicated in rainfall variability over the region, chief among them being ENSO (El Niño Southern Oscillation) (Rocha and Simmonds, 1997; Nicholson and Kim, 1997; Nicholson and Selato, 2000; Nicholson and Entekhabi, 1987; Lindesay, 1988; Hastenrath et al., 1993; Goddard and Graham, 1999; Mason and Jury, 1997; Mulenga et al., 2003; Reason et al., 2000; Reason and Rouault, 2002; Reason and Jagadheesha, 2005; Richard et al., 2000, 2001; Lyon and Mason, 2007, 2009). Regional sea surface temperature (SST) variability in the Indian and Atlantic Oceans has also been shown to have a substantial impact on southern African rainfall (Rocha and

Simmonds, 1997; Hirst and Hastenrath, 1983; Goddard and Graham, 1999; Mason and Jury, 1997; Reason et al., 2006b; Reason and Mulenga, 1999; Hermes and Reason, 2005; Reason, 2001, 2002; Hansingo and Reason, 2009; Cook et al., 2004; Saji et al., 1999; Behera and Yagamata, 2001; Rouault et al., 2003a; Cook, 2000; Walker, 1990; Landman and Mason, 1999; Richard et al., 2001; Washington and Preston, 2006; Cook et al., 2004; Lyon and Mason, 2007, 2009). There is an ongoing discussion among climate scientists as to which particular ocean-forcing mechanism has the greatest impact on southern African rainfall. Apart from oceanic factors, southern African rainfall is also influenced by the strength and position of regional atmospheric features such as the ITCZ, Angola low and Walker circulation (Tyson, 1986; Jury and Pathack, 1991; Todd and Washington, 1999; Rouault et al., 2003a; Wu et al., 2003; Cook et al., 2004; Reason et al., 2006b).

It is challenging to predict rainfall with a high degree of accuracy on long range or seasonal time scales over many global regions including southern Africa (Kane, 1999; Lyon and Mason, 2007; Landman and Beraki, 2010). However, it is vitally important to a large number of user groups to predict seasons during which rainfall may differ significantly from the annual or seasonal average. The provision of an adequate water supply for domestic consumption, as well as for industrial and commercial use, is one of the key requirements for economic progress and stability. Reliable predictions of extreme weather events, especially periods of drought or the occurrence of

floods, facilitate forward and contingency planning and enable communities and governments to marshal their resources and minimise the negative impact of such events. Developing countries are at particular risk from extreme weather events because they often lack the communication infrastructure that would facilitate rapid emergency intervention when and where required. In rural areas, rain-fed subsistence farming as well as commercial agricultural products and livestock are vulnerable to periods of drought or floods and those seasons during which rainfall is significantly different from average can have a devastating impact on local and regional food security as well as export revenue.

The variability of total rainfall year-on-year must be distinguished from both a fluctuation in the intensity and also the seasonal distribution of rainfall. Richard et al. (2001) substantiated the contention that there were no significant changes in the average rainfall over southern Africa during the 20th century when aggregated on an annual basis. However, the intensity of precipitation showed substantial variability from year to year during that period. Fauchereau et al. (2003a) analysed observational rainfall data for the 20th century and concluded that some regions in southern Africa experienced a noticeable shift towards more extreme rainfall events in the later decades of that century. Nevertheless, with regard to annual totals, they agreed with the observations of Richard et al. (2001) that no overall trend towards drier or wetter conditions could be established. Observational data, as well as out-

put from their model, supported the conclusion that there were fewer days on which rain fell but, when it did, there was more of it. Further evidence of an increase in the intensity of high rainfall events between 1931 and 1990 was provided by Mason et al. (1999a). New et al. (2006) concurred with earlier findings and showed that regionally averaged total rainfall decreased over the time period between 1961 and 2000, but not to an extent that is statistically significant. However, the authors deduced that there was statistically significant increase in the intensity of daily regional rainfall as well as a marked change in the duration of dry spells during those fifty years. These studies indicate that attention should be paid to individual rainfall seasons and the incidence of extreme rainfall events, rather than only focussing on seasonal or annual rainfall totals.

More than half of the population of sub-Saharan Africa makes a living from rain-fed agricultural activities (Food and Agriculture Organisation of the United Nations). Crop growth can be affected by the number of dry or wet spells, with the majority of rain-fed crops more likely to flourish with uniformly spread light rainfall than with a few heavy events interrupted by dry spells (Usman and Reason, 2004; Reason et al., 2005). Staple crops such as maize, sorghum or millet need to be planted at the correct time before the rains are too heavy and the seed is washed away. On the other hand, the rains need to be sufficiently substantial to ensure proper germination of the seeds. In this context, reliable prediction of rainfall variables such as the number

of dry days in the summer rainy season and the duration of dry spells would be of huge benefit to subsistence farmers in southern Africa. Thus, dry day frequency over southern Africa is generally of more interest to user groups (e.g. water resources, agriculture) than more common parameters provided by meteorological services such as seasonal rainfall totals, and these groups would benefit from more accurate forecasts of these variables.

One of the atmospheric factors that may play a substantial role in southern African rainfall variability is the Botswana high, a high pressure cell which exists at the 500 hPa level and is centred over central Namibia and western Botswana during austral summer. This high pressure feature over the southern part of the subcontinent has not been extensively studied except in connection with rainfall over Zimbabwe (Matarira, 1990; Magadza, 1994; De Groen and Savenije, 1995; Unganai and Mason, 2002; Jury, 2002; Ratna et al., 2013). The relative strength and position of the Botswana high is known to impact rainfall over the region and a stronger than usual Botswana high is usually associated with below average rainfall over Zimbabwe (Ratna et al., 2013).

A better understanding of the relative influence of the ocean / atmosphere and regional / remote forcings on rainfall variability over southern Africa could improve forecasting ability over the region. Landman and Beraki (2010) assessed the probabilistic rainfall forecast skill over southern Africa

during DJF for the period 1980-2002 using a number of multi-model ensembles. One of the main results of their study was that the forecasts perform better during El Niño and La Niña seasons than during neutral years. El Niño events are usually associated with drought conditions over southern Africa (Hastenrath et al., 1993; Goddard and Graham, 1999; Reason et al., 2000; Reason and Rouault, 2002; Reason and Jagadheesha, 2005; Richard et al., 2000, 2001; Lyon and Mason, 2007, 2009). Most seasonal climate forecasts indicated an enhanced probability of below-average rainfall over southern Africa during the austral summer rainfall season 1997-1998 (Mason et al., 1999b; Buizer et al., 2000; Lyon and Mason, 2007). However, the widespread drought conditions that were expected generally failed to materialise and in fact, seasonal rainfall in some regions was observed to be near or above average (Richard et al., 2001). Similarly, the rainfall forecast for the summer rainfall season 2009-2010 showed mostly enhanced probabilities for dry conditions over southern Africa. However, DJF 2009-2010 rainfall over South Africa was anomalously high, something that was largely missed by most forecasting systems. The association of enhanced forecast skill with El Niño years may partially explain the level of confidence in the forecast of dry conditions for the austral summer seasons during 1997-1998 and 2009-2010. Chipanshi and Ringrose (2001) argue that the poor crop yield during the 1997-1998 rainfall season in Botswana may have been more influenced by the drought forecasts than rainfall levels themselves. The area planted in 1997-1998 was the smallest nationally since 1980, which could have been due

to the early warning messages to expect drought conditions.

This thesis focuses on the following questions:

1. What impact does the Botswana high have on rainfall over southern Africa and how does it relate to ENSO?

2. Which SSTAs have the greatest impact on dry day frequency over southern Africa during JFM and did changes in dry day frequency play a role in the unexpected rainfall during JFM 1998 and JFM 2010?

3. What was the relative impact of each ocean basin on rainfall over southern Africa during JFM 1998 and JFM 2010 and can they shed light on why anticipated levels of rainfall did not occur during these seasons?

Chapter 2 reviews studies pertaining to rainfall and general atmospheric circulation over southern Africa. Features that influence the annual cycle of southern African rainfall are presented separately from interannual factors that occur on an irregular basis but also impact rainfall over the region. A discussion of the impact of various SST anomalies (SSTAs) on southern African rainfall is split by basin, followed by a summary of those studies that have considered the influence of more than one SSTA on rainfall over the region. A review of studies investigating the 1997-1998 and 2009-2010

summer rainfall seasons follows. **Chapter 3** gives a detailed description of the data and methods used in this study. The non-hydrostatic, stretch grid global atmospheric model CAM-EULAG (CEU) is introduced. The stretch grid capability enables the grid on which the model runs to be stretched to achieve a higher resolution over a particular region and then slowly move to lower resolution over the rest of the globe. Spacial resolution of global climate models can be increased in parallel with an increase in computing capacity and, as resolution increases, non-hydrostatic behaviour emerges. In CEU, the stretch grid capabilities are coupled with a non-hydrostatic model to maximise results at high resolution.

Chapter 4 presents an analysis of the Botswana high and its association with rainfall over southern Africa. This high pressure feature over the southern part of the subcontinent has not been extensively studied except in connection with rainfall over Zimbabwe (Matarira, 1990; Magadza, 1994; De Groen and Savenije, 1995; Unganai and Mason, 2002; Jury, 2002; Ratna et al., 2013). In this study, the evolution of the Botswana high is described, followed by an analysis of the correlation of this feature with global SSTs. Given the results of the correlation analysis, an association between the Botswana high and southern African rainfall is investigated.

Chapter 5 considers dry day frequency (DDF) over southern Africa and correlations between DDF over southern Africa and global SSTs are consid-

ered. This chapter also investigates whether DDF may have contributed to the unexpected seasonal rainfall during JFM 1998 and JFM 2010.

Model validation is performed in **Chapter 6**. The primary region of interest in this study is southern Africa. However, global-scale validation is necessary to confirm that the model adequately captures global climate features and processes that are important for southern African climate. A comparison between validation of CEU and CAM3, which have the same physics cores, is made to identify which problems might be a result of the physics parametrisations rather than the dynamics cores. A validation of the two years of interest, 1998 and 2010, is also performed.

The model CEU is used in **Chapter 7** to perform a series of sensitivity experiments for the 1997-1998 and 2009-2010 periods. In these idealised experiments, the grid is stretched to a resolution of 0.5 x 0.5 degrees over southern Africa, 1x1 degrees over much of the rest of the globe and 2x2.5 degrees over the Pacific Ocean and the poles. A spacial resolution of 0.5^o is the typical resolution used in regional climate models, for example see the CORDEX experiments (Nikulin et al., 2012). Six idealised experiments are performed for each of the years 1997-1998 and 2009-2010 in which the model is forced with idealised monthly SSTs. In three of the experiments, SSTs in one major ocean basin are replaced by the climatology of that ocean which neutralises the impact of that ocean on rainfall over southern Africa. In the

remaining three experiments, SSTs in two ocean basins are replaced with climatology which emphasises the impact on southern African rainfall of SST anomalies (SSTAs) in the remaining ocean. The objective of these experiments is to isolate the impact of SSTAs in each ocean basin on southern African rainfall during JFM 1998 and JFM 2010.

Chapter 2

Literature review

There have been many studies focusing on the possible links between regional or remote SSTAs and rainfall variability over southern Africa (Tyson, 1986; Mason and Jury, 1997; Fauchereau et al., 2003b; Richard et al., 2001; Rouault and Richard, 2005; Washington and Preston, 2006). The link between southern African rainfall variability and remote forcing by ENSO has been extensively discussed (Rocha and Simmonds, 1997; Nicholson and Kim, 1997; Nicholson and Selato, 2000; Nicholson and Entekhabi, 1987; Lindesay, 1988; Hastenrath et al., 1993; Goddard and Graham, 1999; Mason and Jury, 1997; Mulenga et al., 2003; Reason et al., 2000; Reason and Rouault, 2002; Reason and Jagadheesha, 2005; Richard et al., 2000, 2001; Lyon and Mason, 2007, 2009). Regional SST variability of the Indian and Atlantic Oceans also has a substantial impact on southern African rainfall (Rocha and Simmonds, 1997; Hirst and Hastenrath, 1983; Goddard and Graham,

1999; Mason and Jury, 1997; Reason et al., 2006b; Reason and Mulenga, 1999; Hermes and Reason, 2005; Reason, 2001, 2002; Hansingo and Reason, 2009; Cook et al., 2004; Saji et al., 1999; Behera and Yagamata, 2001; Rouault et al., 2003a; Cook, 2000; Walker, 1990; Landman and Mason, 1999; Richard et al., 2001; Washington and Preston, 2006; Cook et al., 2004; Lyon and Mason, 2007, 2009). There is an ongoing discussion among climate scientists as to which particular ocean-forcing mechanism has the greatest impact on southern African rainfall. While the influence of the Indian Ocean has been extensively investigated, the influence of the Atlantic Ocean has received less attention. This is partly due to the fact that most of the moisture input into rain-bearing weather systems over southern Africa during summer tend to come from the warmer Indian Ocean on the east coast. However, the influence of the Atlantic Ocean should not be discounted as there is evidence that its impact may be substantial (Reason et al., 2006b).

El Niño events are usually associated with drought conditions over southern Africa (Hastenrath et al., 1993; Goddard and Graham, 1999; Reason et al., 2000; Reason and Rouault, 2002; Reason and Jagadheesha, 2005; Richard et al., 2000, 2001; Lyon and Mason, 2007, 2009). Landman and Beraki (2010) assessed the probabilistic rainfall forecast skill over southern Africa during DJF for the period 1980-2002 using a number of multi-model ensembles. One of the main results of their study was that the forecasts perform better during El Niño and La Niña seasons than during neutral years.

Many seasonal climate forecasts indicated an enhanced probability of below-average rainfall over southern Africa during the austral summer rainfall season 1997-1998 (Mason et al., 1999b; Buizer et al., 2000; Lyon and Mason, 2007; Kane, 1999; Curtis et al., 2001). This prediction of dry conditions was linked to the strong El Niño that occurred during 1997-1998 and the typical association of El Niño with drought conditions over southern Africa. However, the widespread drought conditions that were expected generally failed to materialise and in fact, seasonal rainfall in some regions was observed to be near or above average (Richard et al., 2001; Lyon and Mason, 2007; Kane, 1999). Yuan et al. (2014) found that the model SINTEX-F was overconfident in simulating the link between ENSO and southern African rainfall and suggested this might explain why the forecasts for the 1997-1998 summer rainfall season were not in line with observations. The rainfall forecast for the 2009-2010 DJF El Niño season made by the three coupled models discussed in Landman and Beraki (2010) showed mostly enhanced probabilities for dry conditions over southern Africa. A similar forecast was also made by centres such as the IRI and the South African Weather Service. However, DJF 2009-2010 rainfall over South Africa was anomalously high, something that was largely missed by most forecasting systems. The association of enhanced forecast skill with El Niño years may partially explain the level of confidence in the forecast of dry conditions for the austral summer seasons during 1997-1998 and 2009-2010.

This chapter reviews literature describing the main factors that influence southern African rainfall as well as those studies that are relevant to this thesis. The features of the annual cycle are discussed in section 2.1, followed by interannual modes and phenomena in section 2.2. A discussion of factors that influence rainfall over southern Africa is given in section 2.3. Section 2.4 covers the literature which focused on the 1997-1998 time period, followed by section 2.5 which discusses the literature that focused on the 2009-2010 time period.

2.1 Annual cycle

Southern Africa has a strong seasonal cycle with most of the region experiencing summer rainfall due to convective thunderstorms (Tyson, 1986). The exceptions are the south-western Cape which is a winter rainfall region and the southern Cape coastal region which experiences rainfall year round. Factors that influence rainfall variability over southern Africa may change over time, and the nature of the relationship between these factors and rainfall variability over the region is also subject to variation (Reason et al., 2006b). A complex and complicated inter-related system makes it difficult to isolate and identify the impact or influence of an individual variable or group of variables. A basic description of features of the annual cycle that influence southern African rainfall is given below.

The Intertropical Convergence Zone. The northeasterly trade winds and southeasterly trade winds converge along the tropics in a low pressure zone known as the Intertropical Convergence Zone (ITCZ). The movement of the ITCZ over Africa displays a clear seasonal cycle (Tyson, 1986). The location of the ITCZ varies throughout the year and moves faster and further over land than it does over the ocean due to the higher temperatures experienced on land. The ITCZ is a region of low-level convergence with strong upward motion and is usually associated with a band of heavy rainfall around the tropics. It has a distinct seasonal migration across the equator, that manifests via a precipitation maximum that shifts from 8^oN in April-November to 8^oS in December-March (Wu et al., 2003). Jury and Pathack (1991) found that the ITCZ was most intense over Africa on the 10^oS latitude, shifted southward in the Mozambique Channel, and is relatively weak over the southwest Indian Ocean. There is a meridional arm of the ITCZ through the Congo basin and it exists over the Atlantic Ocean somewhere over coastal West Africa. The ITCZ in the western Indian Ocean is located at approximately 10^oS during austral summer as the northern hemisphere trades intrude into the southern hemisphere. The continental ITCZ is found between Tanzania and central Mozambique during December-February (Behera and Yagamata, 2001).

The ITCZ typically reaches its northern-most position over Africa in July

when it lies just below the Tropic of Cancer in a tilde-like $\sim$ shape. The ITCZ maintains this shape as it migrates southward. Much of southern and eastern African rainfall between September and February is determined by the seasonal migration of the ITCZ. The "short rains" in eastern Africa occur during OND when the ITCZ migrates from north of the equator southward over Kenya, the lake countries, and northern Tanzania. The ITCZ then moves rapidly between December and February across southern Tanzania into Zambia, Zimbabwe, Malawi, and central Mozambique (Goddard and Graham, 1999). Jury and Pathack (1991) found that convergence associated with the ITCZ is highest over northern Zambia and considerably reduced over the southwest Indian Ocean. Cook et al. (2004) noted that wet summers in South Africa are often associated with an anomalous southward shift and strengthening of the ITCZ over tropical southeastern Africa.

The South Atlantic and South Indian anticyclones. The South Atlantic anticyclone is a semi-permanent high-pressure system in the southern part of the Atlantic Ocean that shifts 6^o latitudinally between seasons and has a zonal shift of approximately 13^o. These seasonal fluctuations drive changes in surface winds which impact on SSTs particularly in the upwelling zones along the western coast of southern Africa and the Atlantic cold tongue (Reason et al., 2006b). An anomalously strong South Atlantic Anticyclone is associated with wet conditions over some parts of southern Africa (Walker, 1990; Tyson, 1986).

The South Indian Ocean Anticyclone is a region of high atmospheric pressure over the Indian Ocean between 20^oS and 35^oS. It is one of the centres of anticyclonic activity in the southern hemisphere subtropical belt and is thought to play an important role in the evolution of subtropical Indian Ocean dipole events, which are discussed in more detail in the next section.

The Angola low. A shallow heat low located over southern Angola and northern Namibia, referred to as the Angola low, starts developing around October each year. It strengthens during January and February and acts as the tropical source region for the tropical-extratropical cloudbands that bring most of the summer rainfall over southern Africa south of approximately 15^oS (Mason and Jury, 1997; Todd and Washington, 1999; Reason et al., 2006b; Hart et al., 2010, 2013). A confluence zone stretches eastward from the Angola low toward the ITCZ (Reason et al., 2006b). SSTAs over the tropical southeast Atlantic Ocean affect the strength of the Angola low which may significantly influence southern African rainfall (Rouault et al., 2003a; Cook et al., 2004). Easterly wind anomalies over the northern Angola low region are consistent with a weaker low and less moisture import from the tropical Atlantic (Reason and Jagadheesha, 2005).

Much of the summer rainfall over southern Africa south of approximately 15^oS can be attributed to tropical temperate troughs (TTTs). The Angola

low is a tropical source region for these TTTs and their associated cloud bands and the presence of a strong Angola low generally results in higher levels of rainfall (Reason et al., 2006b; Mason and Jury, 1997; Cook et al., 2004; Hart et al., 2010). Cook et al. (2004) found that wet spells and seasons over South Africa may be associated with an anomalous easterly or north-easterly moisture flux alongside a TTT or a ridging anticyclone along the east coast of South Africa.

2.2 Interannual factors influencing rainfall

The El Niño Southern Oscillation (ENSO). ENSO is a coupled ocean-atmosphere phenomenon that occurs approximately every two to seven years in the equatorial Pacific Ocean. The Southern Oscillation is characterised by an interannual fluctuation in tropical sea level pressure between the western and eastern parts of the Pacific Ocean, accompanied by a strengthening or weakening of the easterly trade winds over the tropical Pacific Ocean. El Niño (La Niña) is characterised by anomalously warm (cold) water in the eastern and/or central Pacific Ocean (**Figure 2.1**). Bjerknes (1969) was the first to recognised that El Niño and the Southern Oscillation were in fact two aspects of the same phenomenon which is now referred to as ENSO (El Niño Southern Oscillation). NOAA's operational definitions of El Niño and La Niña conditions are based upon the Oceanic Niño Index (ONI). The ONI is defined as the 3-month running means of SSTAs in the Niño 3.4 region

[5N-5S, 120-170W] in relation to the 1971-2000 SST climatology. If the ONI exceeds +0.5 (-0.5) for at least five consecutive months, the event is classified as El Niño (La Niña).

The tropical Indian Ocean dipole (TIOD). The tropical Indian Ocean dipole is a naturally occurring coupled ocean-atmosphere phenomenon that influences global climate (Saji et al., 1999; Webster et al., 1999). This phenomenon is known by many names, but in this study, it is referred to as the tropical Indian Ocean Dipole (TIOD). A positive phase TIOD is characterised by positive SSTAs in the tropical west Indian Ocean and negative SSTAs in the tropical east Indian Ocean (**Figure 2.2**). The equatorial winds reverse direction from westerlies to easterlies during the peak phase of positive TIODs. This causes changes in atmospheric circulation and water vapour transport which can result in anomalous summer rainfall over parts of Africa (Yamagata et al., 2004).

The Subtropical Indian Ocean Dipole (SIOD). An interannual dipole event in the subtropical Indian Ocean is known by various names, such as the subtropical dipole pattern or the Indian Ocean subtropical dipole. In this study we refer to it as the subtropical Indian Ocean Dipole (SIOD). The SIOD has a positive phase characterised by unusually warm SSTs in the southwest Indian Ocean south of Madagascar and anomalously cool SSTs in the southeast Indian Ocean off Australia and it is related to the occurrence

of high pressure anomalies in the midlatitude South Indian Ocean (**Figure 2.3**). Positive events tend to result in above average rainfall over parts of southern Africa during the austral summer (Behera and Yagamata, 2001; Reason, 2001, 2002).

The Southern Annular Mode (SAM) The Southern Annular Mode (SAM), also called the Antarctic Oscillation (AAO), is the principal mode of atmospheric variability between the extratropics and high latitudes in the southern hemisphere. It consists of an oscillation in atmospheric pressure between the Antarctic region and the southern midlatitudes. A positive (negative) event is characterised by anomalously low (high) pressure over Antarctica and anomalously high (low) pressure over the midlatitudes of the southern hemisphere. There is usually an associated movement of the winds whereby the midlatitude westerlies and the upper-level subtropical jet shift poleward (equatorward) during the positive (negative) events. Gillett et al. (2006) found a positive association between the SAM and rainfall over south-eastern southern Africa, as well as subtropical Australia and South America, while a negative association is apparent over southern South America, New Zealand and Tasmania due to a southward shift of the stormtrack (Thompson and Wallace, 2000). Reason and Rouault (2005) also found a negative association between SAM and winter rainfall over the western Cape region of South Africa.

Benguela Niño. The Benguela upwelling system is caused by surface water located near the western coast of southern Africa being forced offshore by strong southerly winds and deeper cold water rising to the surface and replacing the warmer water. The Benguela upwelling system has not been stable over time. It was disrupted by an intrusion of warm water from the Angolan Current during ten austral summers between 1959 and 2006, causing an anomalous SST regime (Rouault et al., 2009). This phenomenon is referred to as a Benguela Niño event because it is reminiscent of El Niño although a clear causal link between the two has not been established (Reason et al., 2006a). A warm event in the southwestern Atlantic Ocean is classified as a Benguela Niño provided the FMA SSTA is greater than 1 standard deviation (Shannon et al., 1986). Benguela Niño events usually occur when anomalies in the trade winds in the western-to-central equatorial Atlantic basin excite eastward propagating Kelvin waves a few months earlier. It is interesting that the interval between successive occurrences of Benguela Niño events has been as short as one year (1998 to 1999) and as long as nineteen years (1965 to 1984), although smaller warm events occur more frequently (Florenchie et al., 2004). When the Kelvin waves reach the southern African coast, coastal trapped waves are generated which propagate southward and induce SSTA in the Angola Benguela frontal area (Lubbecke et al., 2010; Florenchie et al., 2003, 2004) where the thermocline shouls towards the surface suggesting that these events are remotely rather than regionally forced. Significant increases in rainfall over the adjacent continent are correlated with

strong Benguela Niño events notably during 1984 and 1995 (Rouault et al., 2003a).

2.3 Sea Surface Temperature Anomalies That Influence Rainfall Over Southern Africa

The influence of remote and regional SSTAs on southern African rainfall has been a topic of study and debate among climate scientists for some time. This section presents a summary of a selection of studies on the topic, divided into Pacific, Indian and Atlantic Ocean forcing, as well as a section on those studies that examined the relative impact of more than one set of SSTAs on southern African rainfall.

2.3.1 El Niño Southern Oscillation

The existence of a correlation between ENSO events and rainfall variability over some global regions fuelled a strong response from climate scientists. One of the priorities was to develop tools or techniques that would enable accurate forecasting of the occurrence of ENSO events and then to use these forecasts as a predictive tool to anticipate seasonal rainfall on an annual basis. Bjerknes (1969) posited that ENSO was caused by a positive ocean-atmosphere feedback involving the Walker circulation. However, ENSO was not intensively studied until the very strong El Niño of 1982-1983 (Wang

et al., 2012). This event helped motivate the ten year international TOGA (Tropical Ocean Global Atmosphere) program to study and predict ENSO which successfully built an ENSO observing system and greatly advanced understanding of ENSO. Another coordinated multi-national initiative, known as the Global Tropical Moored Buoy Array, commenced in 1984 to facilitate the provision of real-time data for forecasting as well as climate research (McPhaden et al., 2009). This array collects data on oceanographic phenomena with particular emphasis given to ENSO in the Pacific; the Atlantic dipole mode, equatorial warm events, and hurricane activity in the Atlantic; as well as the monsoons, the Indian Ocean Dipole, and intraseasonal variability in the Indian Ocean.

An El Niño event typically begins with a westerly wind burst and an associated depression of the thermocline in the eastern Pacific Ocean. As a result of the smaller east-west SST gradient, the pressure gradient is reduced and hence the winds weaken. The weaker winds promote weaker upwelling which in turn deepens the thermocline further and slows the transport of colder water to the surface. This is the positive feedback that Bjerknes proposed in 1969 (Bjerknes, 1969; Cane, 2005; Wang et al., 2012). Equatorial Kelvin waves propagate the thermocline signal to the east, leading to warming (cooling) during El Niño (La Niña). After an El Niño reaches its peak, a negative feedback is required for terminating a continued growth of El Niño. There are two major theories for the mechanisms explaining ENSO. The first

is that El Niño is one phase of a self-sustained, unstable and naturally oscillatory mode of the coupled ocean-atmosphere system. The second is that El Niño is a stable mode triggered by stochastic forcing or noise such as westerly wind bursts and Madden-Julian Oscillation events and the tropical instability waves in the eastern Pacific Ocean (see Wang et al. (2012) for more details).

The relationship between rainfall over southern Africa and ENSO has evolved, and also changed in nature, over time (Reason et al., 2000; Richard et al., 2001, 2000; Landman and Mason, 1999). Between 1940 and 1970, the incidence of dry conditions over the region did not appear to be correlated with either El Niño or La Niña occurrences. During these three decades, periods of lower-than-average rainfall were mainly associated with, and attributed to, cold SST conditions over the southwest Indian Ocean (Fauchereau et al., 2003b; Richard et al., 2001, 2000). However, after the late 1970s, a significant correlation emerged between rainfall over southern Africa and ENSO events, namely that periods of drought are linked with El Niño while abundant rainfall is associated with La Niña (Lindesay, 1988; Reason and Jagadheesha, 2005; Reason et al., 2006b; Mason and Jury, 1997). Richard et al. (2001) investigated drought conditions over southern Africa and their results indicated that between the years 1950 and 1969, droughts were associated mainly with SSTAs over the southwest Indian Ocean while after 1970, extreme dry conditions became associated with El Niño events.

Rouault and Richard (2005) concluded that the most severe droughts occurred after 1970 and hypothesised that this was due to a stronger ENSO-rainfall relationship over the region. There is evidence to suggest that the levels of rainfall over southern Africa are remotely forced by El Niño Southern Oscillation as well as regionally forced by the SSTs of the Atlantic and Indian Oceans (Reason et al., 2006b).

ENSO has the greatest influence on rainfall over southern Africa during its mature phase between the austral summer months of December and March when the upper westerlies have retreated poleward south of Africa (Mason and Jury, 1997). El Niño events are usually associated with dry conditions over most of southern Africa, while La Niña events are typically associated with wet conditions over southern Africa (Hastenrath et al., 1993; Goddard and Graham, 1999; Reason et al., 2000; Reason and Rouault, 2002; Reason and Jagadheesha, 2005; Richard et al., 2000, 2001; Lyon and Mason, 2007, 2009; Meque and Abiodun, 2014). During most El Niño years, southern Africa is dominated by a continental high pressure centre which acts to suppress convection (Mulenga et al., 2003). However, during La Niña events, the region is dominated by low level convergence and thus rainfall is enhanced (Reason and Jagadheesha, 2005). Meque and Abiodun (2014) found that the correlation between ENSO and surface temperature over southern Africa is stronger than the correlation between ENSO and rainfall over southern Africa which indicates that rainfall alone may not adequately capture the in-

fluence of ENSO over the region. Cook (2000) described two possible mechanisms for how the ENSO signal reaches southern Africa. The first is an atmosphere-ocean interaction in which the atmospheric response to Pacific Ocean SSTAs causes Indian Ocean warming which, in turn, changes southern African rainfall through sensitivity to more local SSTs. The second occurs when atmospheric Rossby waves are generated by shifts in the site of the strongest atmospheric convection in the tropical Pacific which then leads to the Pacific South American pattern. Cook (2001) used idealised GCM experiments to study the impact of ENSO on southern hemisphere waves. Two statistically significant wave anomalies were found. The eastern hemisphere wave anomaly was associated with a northeastward shift of the South Indian convergence zone (SICZ), and the western hemisphere wave anomaly resulted from the northeastward shift of the South Pacific convergence zone (SPCZ).

During El Niño years, the rising branch of the Walker circulation from tropical Africa into the central Indian Ocean is displaced and this is associated with a northeastward shift in the SICZ (Harrison, 1984; Lindesay, 1988). This displacement is associated with an equatorward shift in the subtropical jet and reduced rainfall over southern Africa. During La Niña events, convection over tropical Africa is typically enhanced as the strength of the rising branch of the Walker cell is increased, while the continental location of cloud band formation is strongly favoured which leads to above average rainfall over southern Africa (Harrison, 1986). However, the teleconnections

between ENSO and southern African rainfall may be modified by other climate signals, for example the Angola low, extratropical westerly waves and the Madden Julian Oscillation (Todd and Washington, 1999; Reason and Jagadheesha, 2005; Pohl et al., 2007; Ratnam et al., 2014).

Hart et al. (2013) found that El Niño NDJF seasons are characterised by a strong reduction in the total number of TTTs developing both continentally and over Madagascar, which challenges the general contention that TTTs move offshore during El Niño dry events. La Niña years typically experience a climatological number of TTTs but those that do occur are more likely to be more intense and persistent systems. However, Hart et al. (2013) noted that TTT variability is not a good indicator of rainfall variability since the year with the greatest number of TTTs had near average rainfall.

A new type of El Niño, characterised by anomalously warm SSTAs in the central equatorial Pacific Ocean, has been occurring with more frequency in the last few decades. These events can be described using the Niño 4 index (Kao and Yu, 2009; Yeh et al., 2009). It is known by many names including the central Pacific (CP) El Niño, dateline El Niño, warm pool (WP) El Niño or El Niño Modoki (Ashok et al., 2007a; Kao and Yu, 2009; Yu and Kim, 2010; Kug et al., 2009; Larkin and Harrison, 2005). However, the "Modoki" definition requires cold SSTAs in the western and eastern Pacific (Ashok et al., 2007a) and can thus be considered as a special type of CP El Niño.

Thus far, there have been at least three different mechanisms proposed to explain the dynamics of the CP El Niño (Ashok and Yamagata, 2009; Kug et al., 2009; Yu and Kim, 2010). Studies have shown that the canonical, or eastern Pacific (EP) El Niño, and CP El Niño may impact the global climate differently due to differences in the Walker circulation as well as differences in the atmospheric teleconnections (Ashok et al., 2007a; Weng et al., 2009; Kim et al., 2011; Ashok and Yamagata, 2009). Ratnam et al. (2012) provide global precipitation anomalies for a composite of EP El Niño years and also those of CP El Niño years and showed that there is a negative anomaly over southern Africa in the EP composite, while the CP composite displays almost no impact on rainfall over southern Africa.

The intensity of CP El Niño events has almost doubled in the past three decades. Lee and McPhaden (2010) used satellite data to distinguish between the increases in the intensity of CP El Niño and background SST anomalies. Their analysis suggests that the warming trend in the central Pacific is primarily a consequence of more frequent and intense CP El Niño events since SSTs during La Niña and neutral years have not become significantly warmer. Mo (2010) suggested that the possible different climate impacts of the canonical and CP El Niños could be a source of uncertainty in El Niño impact prediction in the US. Landman and Beraki (2012) suggested that El Niño plays a substantial role in seasonal model forecasting over southern Africa, and this "new" El Niño could impact future predictions in

an unexpected way.

Ratnam et al. (2014) investigated the difference between the impact of CP and EP El Niños on rainfall over southern Africa during DJF. They created composite CP and EP El Niño years using years between 1982 and 2011. They found that, although CP El Niño events result in below average rainfall over southern Africa, the region experiences substantially less rainfall during EP El Niño events when compared with CP El Niño. They identified two teleconnections responsible for the lower than average rainfall during EP El Niño events. The first arises due to the Matsuno-Gill response to the anomalously high precipitation over the Pacific Ocean which results in an anomalous anticyclone extending from the equatorial Indian Ocean to the subtropical South Indian Ocean. These anomalous anticyclonic winds weaken the tropical moisture flow into southern Africa. The second teleconnection is an upper level anomalous tropospheric stationary wave from the Pacific which propagates towards southern Africa and maintains an anomalous anticyclone over southern Africa. These two teleconnections are intense during EP El Niño events and cause dry conditions over southern Africa. However, they are weaker during CP El Niño events.

A cyclostationary EOF analysis on Pacific SSTs found three main modes of variability (Yeo and Kim, 2013). The first mode exhibits a clear trend and represents global SST warming with an El Niño-like SST pattern, the

second mode indicates a close connection between the tropical and north Pacific regions, and the third mode shows a see-saw pattern between El Niño and La Niña within a two year period. The most extreme El Niño events, such as the 1997-1998 event, are attributed to the positive contribution of all three modes. Yeo and Kim (2013) also found that the CP El Niño events of the early 1990s and 2000s originated from different modes, namely the second and first mode, respectively. In particular, the 2009-2010 El Niño was strongly affected by the global warming mode.

Yeh et al. (2014) noticed that differences in the SSTAs and SLPAs in the tropical Pacific Ocean between CP El Niño and EP El Niños suggested a different response of the Walker circulation and global precipitation anomalies. As a result, they suggested two new indices that might be able to better indicate the interannual variability and intensity of the Walker circulation coupled with CP and EP El Niño, respectively. They found that in the case of an EP El Niño, the anomalous Walker circulation exhibits a large-scale dipole structure over the Pacific Ocean, while the CP El Niño-associated Walker circulation exhibits a tripole structure. The ascending branch is located over the central Pacific and the two descending branches are located over the eastern tropical Indian Ocean and the western Atlantic Ocean.

CP El Niños seem to be occurring more frequently in recent decades. Yeh et al. (2009) compared the ratio of EP and CP El Niño events in CMIP3

model simulations and noted that the ratio is projected to increase under global warming scenarios. They argue that the recent increase in CP El Niños is related to a weakening in the mean Walker circulation and a flattening of the mean thermocline in the equatorial Pacific Ocean, which might be a result of global warming. It has also been argued that the increase of CP El Niños could be a natural multidecadal variability and not necessarily a consequence of anthropogenic forcing (Newman et al., 2011; McPhaden et al., 2011).

In their study, Landman and Beraki (2010) assessed the probabilistic rainfall forecast skill over southern Africa during DJF for the period 1980-2002 using a number of multi-model ensembles. They found that multi-model forecasts outperform single model forecasts of rainfall over southern Africa and that they can be used with confidence during ENSO events. In particular, predictions during El Niño seasons were more accurate than those during neutral years. Nevertheless, the rainfall forecasts made using an improved version of the multi-model used in this study for the DJM 2009-2010 rainfall season over southern Africa showed enhanced probabilities for dry conditions to occur. Similar forecasts were issued by the IRI and the SAWS with high confidence due to the fact that it was an El Niño season. However, DJF rainfall over South Africa was anomalously high, particularly over the central and western parts of the country. One of the main results of their study was that the forecasts perform better during El Niño and La Niña seasons than

they do during neutral years.

2.3.2 Indian Ocean SSTAs

Just as the association of southern African rainfall with ENSO has changed over time, so too has the association of southern African rainfall and SSTAs over the tropical Indian Ocean. Landman and Mason (1999) used the United Kingdom Meteorological Office Historical Sea-Surface Temperature data set to create a three month mean December to February SST data set for the 40 year period 1957-1997. They performed a principal component analysis to identify the relationship between SSTs and South African and Namibian rainfall variability. They found that, during the years after the late 1970s, warm events in the tropical western Indian Ocean became associated with wet conditions over southern Africa whereas in previous decades they had been associated with dry conditions over the region. They also found that, around the same time, SST variability in the tropical western Indian Ocean became substantially independent of ENSO.

There are two primary interannual modes of Indian Ocean SSTAs, namely the TIOD and the SIOD. The TIOD was first characterised in 1999 by Saji et al. (1999) and Webster et al. (1999). Saji et al. (1999) performed an analysis of 40 years of observational SST data over the Indian Ocean which revealed a dipole mode that is unique and independent of ENSO. They described a pattern of internal variability with anomalously cold SSTs in the

tropical eastern Indian Ocean and anomalously warm SSTs in the tropical western Indian Ocean, with associated wind and precipitation anomalies. They introduced the dipole mode index (DMI) which is generally used to represent the TIOD. The occurrence of a TIOD typically weakens or reverses the Walker circulation across the Indian Ocean which then shifts the convergence zone and leads to drought in Indonesia and floods over East Africa.

Webster et al. (1999) concluded that the 1997-1998 Indian Ocean SSTAs were primarily an expression of internal dynamics rather than a response to the strong El Niño that occurred that year. They gave a number of reasons as to why they suggest that these two events were separate. The climate pattern around the Indian Ocean rim was very different during the 1997-1998 event from that usually associated with an El Niño event. They also note that the rainfall anomalies during 1997-1998 were out of line with expectations for an El Niño event, with drought over Indonesia far more intense than was expected, droughts that did not materialise over India or Australia, and East African rainfall that was far higher than expected. Correlation analysis suggests that the association between East African rainfall and ENSO (r=0.24) is not as strong as the equatorial Indian Ocean - East African rainfall association (r=0.62). They also pointed out that not all the examples of other instances in which the Indian Ocean SSTAs were similarly anomalous co-occurred with ENSO. In fact, they claimed that, of the 16 years in which the equatorial Indian Ocean SSTs reversed gradient for at least a month,

only three were El Niño years and none were La Niña years.

An analysis of the six most recent extreme TIOD events was performed in Saji et al. (1999) which enabled them to present the life cycle of a typical TIOD. Cool SSTAs develop during May-June in the tropical eastern Indian Ocean, accompanied by moderate south-easterly wind anomalies. In the following months, the cold anomalies intensify and migrate northwest towards the Equator, while the tropical western Indian Ocean begins to warm. The zonal wind anomalies over the Equator and alongshore wind anomalies over Indonesia intensify with the SST dipole. These features peak rapidly in October and then decline very quickly in the following two months to the extent that SSTAs are not evident by January.

In a later paper, Saji and Yamagata (2003) investigated the possible impacts of the TIOD on global climate and found that temperatures and rainfall are anomalously high over countries west of the Indian Ocean, such as in East Africa, and anomalously low to its east. The also found that the TIOD affects remote regions and, in particular, positive TIOD events are associated with increased temperatures and reduced rainfall over South Africa.

Since the late 1970s, SST variability in the equatorial Indian Ocean has been characterised by increasing temperatures. SST variability in the equatorial Indian Ocean was closely related to ENSO prior to the late 1970s and

these warming events were typically associated with dry conditions over much of southern Africa. The ENSO signal in Indian Ocean SSTs has weakened since the late 1970s. SSTs in the region seem to modulate the influence of ENSO events on rainfall over parts of southern Africa (Landman and Mason, 1999).

The TIOD cannot be viewed in isolation from ENSO. In some years, a strong ENSO can predispose the Indian Ocean to a TIOD event (Black et al., 2003; Murtugudde et al., 2000) whereas there have been years during which a TIOD occurred but no ENSO was observed (Saji et al., 1999). Yamagata et al. (2004) identified that only one third of TIOD events are associated with ENSO. They found that the TIOD, independent of ENSO, can lead to above average rainfall over East Africa through changes in atmospheric circulation and water vapour transport. Black et al. (2003) described a sequence of events that may explain how an El Niño event can trigger a TIOD, namely, that El Niño must be sufficiently strong to perturb the convection and circulation in the vicinity of the Maritime Continent and that this perturbation must be strong enough to generate a persistent change in the local Hadley circulation with enhanced southerly winds in the eastern Indian Ocean. These southerly winds must, in turn, be strong and persistent enough to cool the eastern Indian Ocean via enhanced upwelling so that the zonal SST gradient across the Indian Ocean is reversed. In addition, the easterly anomalies over the Indian Ocean must extend across the entire ocean basin in order for a

TIOD to occur.

Abram et al. (2008) used coral oxygen-isotope records to reconstruct an index of tropical IOD (TIOD) behaviour since 1846. Analysis of this index indicated that there has been an increase in both frequency and strength of TIOD events during the 20th century which may be attributed to anthropogenic greenhouse warming. In the same paper, a strong positive correlation was established between TIOD events and ENSO during the years prior to 1905, as well as after 1960, supporting the contention that a TIOD event may be triggered by ENSO but ENSO is not a necessary precondition (Saji et al., 2006).

Kug and Kang (2006) investigated a feedback process between ENSO and the Indian Ocean SSTs. An outcome of their study was a conjecture that Indian Ocean warming triggered by a relatively strong El Niño, leads to the development of anomalous easterly winds in the western Pacific which contribute to the reversal of an El Niño into a La Niña.

Shinoda et al. (2004) used NCEP reanalysis data and both atmospheric and coupled atmosphere-ocean models to conduct idealised experiments in order to clarify the impact of ENSO on surface flux, and therefore SST, variations in the Indian Ocean. Their results corroborated the view that SSTAs in the eastern Indian Ocean are remotely forced by ENSO. However,

the western Indian Ocean anomalies were not reproduced in their model experiments suggesting that internal Indian Ocean dynamics contribute to the Indian Ocean dipole events.

There is another SST dipole in the Indian Ocean that occurs in the subtropics (known as the subtropical Indian Ocean Dipole (SIOD)). The positive phase of an SIOD is characterised by a negative SSTA in the southeastern Indian Ocean and a positive SSTA in the southwestern Indian Ocean. This dipole has been associated with increased rainfall over southern Africa during the austral summer (Behera and Yagamata, 2001; Reason, 2001, 2002).

The SIOD index is obtained from the SSTA difference between the western (55^oE-65^oE, 37^oS-27^oS) and eastern (90^oE-100^oE, 28^oS-18^oS) subtropical Indian Ocean (Behera and Yagamata, 2001). The evolution of a positive SIOD is detailed in Behera and Yagamata (2001) and summarised here. A SIOD usually develops in December-January, peaks in February, and then declines in May-June. As a result of the South Indian Ocean Anticyclone, the mean surface winds in the south Indian Ocean are predominantly westerly south of 35^oS and easterly north of 35^oS. The centre of the subtropical high shifts eastward during the austral summer, and the resulting pressure gradient along the edge of the subtropical high and Australia leads to southeasterly winds off the coast of Australia. The anomalous southeasterlies cause cooling due to increased evaporation and upper ocean mixing. The deforma-

tion of the subtropical high causes anomalous easterlies around 40^{o}S which leads to a weakening of the seasonal midlatitude westerlies. The related reduction of seasonal latent heat loss results in a warming of the southwestern Indian Ocean. Another mechanism by which the anomalous easterlies may contribute to warming in the southwestern Indian Ocean is by decreasing the equatorial Ekman transport of colder high latitude waters. Near the end of the austral summer, the subtropical high migrates northwest as the Australian continent cools and an anticyclonic feature is established over the country. The associated shift in winds leads to the decay of the SIOD (Behera and Yagamata, 2001).

Reason and Mulenga (1999) investigated the relationship between South African rainfall and SSTAs in the southwest Indian Ocean. They performed idealised experiments using the Melbourne University atmospheric global climate model and found that warm (cold) SSTAs in the southwest Indian Ocean are associated with increased (decreased) rainfall over eastern South Africa and neighbouring regions. The mechanism by which rainfall responds to this SSTA seems to involve changes in the convergence over southeastern Africa of moist air streams originating from either the tropical South Indian Ocean or the tropical South Atlantic Ocean. Low level westerly anomalies over tropical southern Africa along with higher level easterly anomalies, which are associated with increased rainfall over South Africa (Tyson, 1986), were also observed in the model simulations.

Walker (1990) suggested that warmer SSTs in the southwest Indian Ocean were associated with increased easterlies which promoted moisture flux convergence over eastern southern Africa. They posited that the associated changes in the tropical and midlatitude atmosphere encouraged the formation of TTTs which led to increased rainfall.

An analysis of observational and reanalysis data suggested that the SIOD influence on rainfall over southern Africa is related to a weakening of the maritime ITCZ over the Indian Ocean and enhanced moisture transport towards southeastern Africa via stronger southeasterlies (Behera and Yagamata, 2001). Reason (2001) used an atmospheric general circulation model to investigate the relationship between the SIOD and southern African rainfall and results suggested that summer rains are increased by enhanced evaporation of water from the warm SST pole. This moisture-rich air is advected towards southern Africa as a result of the low pressure anomaly that is generated over this warm pole. Reason (2002) performed idealised experiments to investigate the sensitivity of precipitation over southern Africa to the location of the warm pole and also the presence of the cold pole off the coast of Western Australia. The results indicated that the rainfall response over southern Africa is stronger if the warm pole is located closer to the subcontinent while sensitivity to the cold pole off Western Australia is only apparent over the subtropical, rather than the tropical, African continent.

Suzuki et al. (2004) used a coupled general circulation model to describe the complete life cycle of the SIOD and found that the anomalous latent heat flux is the dominant factor in the formation of both positive and negative dipole events. This flux anomaly is caused by variations in the climatological wind field which is associated with a pressure anomaly in the central region of the southern Indian Ocean. They postulated that, since the flux anomaly begins during austral autumn and develops over the next nine months, atmosphere-ocean interaction must play a role in the formation of the SIOD. It remains uncertain exactly how the subtropical SSTA reinforces the sea level pressure anomaly that drives a corresponding subtropical SSTA. Behera and Yagamata (2001) noted that the SIOD is locked to austral summer and Suzuki et al. (2004) suggested that this is due to the more efficient influence of the latent heat flux on SST in summer when the depth of the surface mixed layer is shallowest.

Washington and Preston (2006) questioned whether extremely wet rainfall years over southern Africa during the twentieth century were due to unusually strong La Niña events or whether other factors played a consequential role. A series of multi-model experiments using the ensemble mean of five AGCMs illustrated the importance of global SSTs. Idealised experiments then isolated the role of Indian Ocean SSTAs by removing the ENSO signal. The results indicated that the cold SSTA in the northern south west

Indian Ocean has a critical influence on rainfall over southern Africa. Further, the circulation changes resulting from this cool anomaly were greater in magnitude and spatial extent than those arising from the warm SSTA reminiscent of the warm pole of the SIOD. However, the strongest response was observed when both the northern and subtropical south west Indian Ocean SSTAs were included. Wet years are characterised by anomalous anticyclonic circulation in the Mascarene region which drives anomalous low-level easterly moisture flux along 10^oS-20^oS, resulting in enhanced moist convective uplift over eastern southern Africa.

2.3.3 Atlantic Ocean SSTAs

Hirst and Hastenrath (1983) used observational data in a study that investigated the links between local SSTAs off the Angolan coast and rainfall variability in Angola. They identified occurrences of above and below average rainfall events and created a composite of an above and below average year using data from each of the specified years. For the composite of wetter-than-usual years, they found that the South Atlantic trade winds were greatly enhanced. In addition, positive SSTAs in the tropical Atlantic were prevalent, most significantly so in the waters off the coast of Angola.

A link between the occurrence of a Benguela Niño event and an increase in coastal rainfall over the African continent lying approximately between the equator and 25^oS was established in Nicholson and Entekhabi (1987).

Further studies, including those by Rouault et al. (2003a) and Hansingo and Reason (2009) have confirmed that there is a significant increase in rainfall over adjacent western Southern Africa, as well as further inland, during Benguela Niño events.

Vigaud et al. (2007) discussed two strong modes of variability affecting the onshore flow of moisture along the west coast of southern Africa. The first of these modes is linked to the South Atlantic anticyclone and the other is linked with the zonal mode of the westerly flux of moisture from the Atlantic. In a subsequent study, Vigaud et al. (2009) further explored the connection between southern African climate and the South Atlantic Ocean during the austral summer. They found that increased rainfall over the Congo basin is associated with increased moisture flux input from the tropical Atlantic Ocean and increased convection. This excess water vapour is then channelled from the Congo basin to the east and southeast at the surface, while the African Easterly Jet may transport moist air southward at mid-tropospheric levels. McHugh and Rogers (2001) suggested that wet conditions over southern Africa are linked to a strong westerly current from the South Atlantic as it brings moist air and includes an element of uplift due to topography as it moves eastward.

The Atlantic Multidecadal Oscillation (AMO) is a coherent pattern of interdecadal SST variability in the Atlantic Ocean with a period of approx-

imately 65 years. The positive (negative) phase is characterised by warm (cool) SSTAs in the North Atlantic Ocean and cool (warm) SSTAs in the South Atlantic Ocean. The impact of the AMO has been discussed in relation to the Sahel drought (Folland et al., 1986), the frequency of Atlantic hurricanes (Goldenberg et al., 2001), Northeast Brazilian rainfall (Folland et al., 2001), North American and European summer climate (Sutton and Hodson, 2005; Nigam et al., 2011), and the Asian summer monsoon (Lu et al., 2006). However the AMO has not previously been associated with rainfall variability over southern Africa.

The warming of the subtropical North Atlantic SSTs can probably be attributed to the combined forcings from the El Niño and negative NAO that often warms the subtropical and high latitude SSTs and cools the midlatitude SSTs in the North Atlantic by modifying evaporative heat loss (Deser and Blackmon, 1993). McHugh and Rogers (2001) found that heavier, convective, DJF rainfall occurs over Tanzania, northern Mozambique, Zambia and part of the western DRC during the negative NAO phase, when the North Atlantic westerlies are unusually weak. Todd and Washington (2004) also found a negative correlation between the NAO and central African rainfall, although their study focused on the FMA season.

Todd and Washington (2004) found that positive rainfall anomalies over this region are associated with anomalous westerly mid-tropospheric zonal

winds over the central equatorial African and Atlantic Ocean on multi-annual time-scales. They used NCEP reanalysis data to investigate the influence from the Atlantic sector on rainfall over the Central Equatorial African (CEA) region. The CEA is defined in their study as the area which lies inside the box 10^oS - 10^oN; 15^oE - 35^oE, and we note that the DRC makes up the majority of this region. They found a strong teleconnection between rainfall over the CEA and the large-scale circulation over the North Atlantic. Anomalous westerly mid-tropospheric zonal winds over the CEA/Atlantic region were associated with positive rainfall anomalies over the CEA and both interannual and multi-annual time-scales. They went on to perform idealised model experiments using HadAM3 which suggest that these anomalous westerlies may be associated with SST forcing from the tropical North Atlantic on multi-annual time-scales, but at interannual time-scales they appear to be relatively independent of the tropical North Atlantic SSTs.

2.3.4 Comparative ocean influence

A principal component analysis was performed on SSTs in the oceans bordering southern Africa between 1953 and 1989 to determine which regional SST variations have the greatest impact on rainfall over the region (Mason et al., 1994). Principal component analysis is a mathematical procedure that converts a set of observations of possibly correlated variables into a set of values of uncorrelated variables called principal components. The

first principal component has as high a variance as possible which means that it accounts disproportionately for the variability in the data in this model analysis. Mason et al. (1994) deduced from the principal component analysis performed in their paper that SST changes in the central South Atlantic Ocean, the South Atlantic subtropical convergence region and the western equatorial Indian Ocean each had a significant effect on southern African rainfall during the period between 1953 and 1989. Moreover, notwithstanding the demonstrated efficacy of El Niño or La Niña events as predictors of southern African rainfall in the years after 1970, other variables also play a significant role.

Rocha and Simmonds (1997) used observational data to investigate the variability of south-eastern African summer rainfall. Their results indicated that ENSO is only moderately related to rainfall over some parts of south-eastern Africa, while SSTAs in the western Indian Ocean play a substantial role in rainfall variability over the region. Part II of their study further corroborated their findings. The Melbourne University General Circulation Model was forced with idealised global SSTs to isolate the impact of each Ocean's SSTAs on southeastern African rainfall. Warm SSTAs in the tropical Pacific and Indian Oceans typical of an El Niño event were used to force the experiment *global*. The experiments *Ind+WPac* and *PInd* used the same input SSTs as *global* but *Ind+WPac* excluded the SSTAs over the central and eastern Pacific and *PInd* excluded the SSTAs over the entire Pacific

Ocean. The result of these experiments indicated that the central Indian Ocean SSTAs had the largest impact on rainfall over southeastern Africa but a slightly stronger atmospheric response was evident when the Pacific Ocean SSTs were included whereas the Atlantic Ocean has little or no effect on southeastern African rainfall. Warm central Indian Ocean SSTs led to low-level cyclonic circulation anomalies east of Madagascar which diverted moisture from the trades and monsoonal air masses toward the Indian Ocean. This resulted in above average precipitation over the central Indian Ocean and a decrease in moisture over southeast Africa and Indonesia which, coupled with subsidence over Africa, led to below average rainfall.

Idealised atmospheric model experiments were performed in Goddard and Graham (1999) to differentiate between the relative impact of the Indian and Pacific Oceans on rainfall variability over eastern central and southern Africa. Global observed SSTs were used in their control run and the relevant rainfall patterns over eastern and southern Africa were well simulated. Two idealised experiments used observed SSTs over the Indian (respectively Pacific) Ocean and replaced SSTs over the remaining two ocean basins with climatology. Their results indicated that although the tropical Pacific exerts some influence over southern African rainfall, the Indian Ocean SSTAs are an essential feature in generating the rainfall response seen in the control run.

Summer rainfall variability over southern Africa is affected by tropical

SSTAs in the central Indian and eastern South Atlantic Oceans. The relationship between western Indian Ocean SSTs and southern African rainfall exhibits significant decadal variability (Reason and Mulenga, 1999). They used the Melbourne University AGCM to investigate the relationship between South African rainfall and warm SSTAs in the southwest Indian Ocean. The results found that this pattern of SSTs is associated with increased rainfall over eastern South Africa and neighbouring regions and *vice versa*. The mechanism by which rainfall responds to this SSTA seems to involve changes in the convergence over southeastern Africa of moist air streams originating from either the tropical South Indian Ocean or the tropical South Atlantic Ocean. Low level westerly anomalies over tropical southern Africa along with higher level easterly anomalies, which are associated with increased rainfall over South Africa (Tyson, 1986), were also observed in the model simulations.

Camberlin et al. (2001) investigated the influence of tropical SST changes in the Atlantic and Pacific to determine which ocean has a greater influence on southern African rainfall. The authors used NCEP reanalysis data from 1951 to 1997 and concluded that El Niño Southern Oscillation plays a dominant role in southern African rainfall.

Hermes and Reason (2005) used a global ocean model called ORCA2 to investigate the evolution of a dipole-like SST variability in the South Indian and South Atlantic Oceans. The South Atlantic dipole is characterised

by warm (or cold) SSTAs in the northeast South Atlantic and the opposite SSTA in the midlatitude southwest Atlantic Ocean. Their study focused on those events that occurred during the same season as a SIOD, noting that the SIOD lagged the dipole in the Atlantic by one or two months. The events considered in their study were those in which there is a significantly warm (cool) SSTA in the southwest of both the South Indian and South Atlantic Oceans and a cool (warm) anomaly in the eastern subtropics. Their results indicated that a significant modulation of the wavenumber -3 or -4 pattern in the atmospheric circulation of the Southern Hemisphere forces these concurrent dipole events. This forcing shifts the semi-permanent subtropical anticyclone in each basin from its summer mean position and its strength is modulated.

Idealized experiments using the HadAM3 AGCM were performed to investigate the sensitivity of southern African rainfall to anomalous SST patterns in the southern Indian and Atlantic Oceans with a particular focus on Benguela Niño events (Hansingo and Reason, 2009). Analysis of the model output suggested that southwest Indian Ocean SSTAs may further amplify or oppose the influence of the Benguela Niño, depending on the sign of the anomaly.

2.4 The 1997-1998 Southern African Rainfall Season

The time period 1997-1998 was particularly interesting due to a number of strong SSTAs that occurred globally. In particular, there was a very strong El Niño event (McPhaden, 1999; Latif et al., 1999; Murtugudde et al., 2000; Reason and Jagadheesha, 2005; Lyon and Mason, 2007), a strong tropical Indian Ocean Dipole (Webster et al., 1999; Latif et al., 1999; Murtugudde et al., 2000) and a subtropical Indian Ocean dipole (Behera and Yagamata, 2001). In the South Atlantic Ocean, a strong Benguela Niña was observed in April 1997 and, from January 1998, a Benguela Niño developed which increased rainfall over the southwestern coast of Africa (Rouault et al., 2009), while the tropical Atlantic SSTs were warmer than usual (Trenberth, 1998).

The strong El Niño event that began in the second half of 1997 was distinguished in several respects from those that had occurred in previous years (McPhaden, 1999; Trenberth, 1998; Kane, 1999). The first few months of 1997 had seen the weakening and reversal of the trade winds in the western and equatorial Pacific which led to anomalously warm SSTs in the western Pacific. This warm pool extended eastward replacing the equatorial cold tongue. The development of El Niño in 1997 was so rapid that a new monthly record high for SST in the eastern equatorial Pacific was achieved in successive months between June and December 1997. The greatest SSTAs occurred

in December 1997 and were the largest on record in the eastern equatorial Pacific Ocean averaging nearly 4^oC. In early 1998, the warmer trend continued with actual eastern Pacific SSTs exceeding 29^oC. In mid-May 1998, the trade winds abruptly returned to near normal strength and cold La Niña conditions began. These events were recorded and measured by the "El Niño Southern Oscillation Observing System" which incorporates satellite and in situ data recording.

Webster et al. (1999) discussed the evolution of the 1997-1998 TIOD. A strong, cool SSTA developed in the tropical eastern Indian Ocean in July 1997 and reached a maximum greater than -2^oC in November 1997. A warm SSTA had started developing in the tropical western Indian Ocean around the same time in June 1997, which reached a maximum greater than 2^oC in February 1998. Together, these anomalies produced a reversed SST gradient between November 1997 and June 1998 with SSTs now increasing from east to west. As the warm SSTA developed in the tropical western Indian Ocean in June 1997, the usually weak climatological equatorial westerly winds were replaced by surface easterly winds. This warming period may end in a number of ways. The monsoon season following the Indian Ocean warming should have stronger winds in the western basin, which would lead to greater mixing, greater upwelling, and greater evaporation, and contribute to cooling. Another mechanism of cooling could be related to the weakening of El Niño and the associated movement of convection towards Indonesia which may

lead the equatorial winds over the Indian Ocean to revert back to westerlies.

Murtugudde et al. (2000) raised the question of the nature of the connection between the 1997-1998 ENSO event and the evolution of the TIOD in the same year. An ocean general circulation model was used to investigate the dynamic and thermodynamic processes that underpin the evolution of a TIOD. Starting in July 1997, warm SSTAs occurred in the western Indian Ocean, peaking in February 1998. Stronger local alongshore winds, as well as remote equatorial and coastal Kelvin waves, contributed to an unusually strong Sumatran upwelling and this caused significant cooling in the eastern Indian Ocean. The strength of the winds over the eastern Indian Ocean weakened by the end of 1997 and the consequent reduction in latent heat loss led to the decline of the cold SSTAs in the east. Warming over the western Indian Ocean followed weaker Southwest Monsoon winds and higher SSTs continued as a result of increased precipitation, which resulted in a barrier layer structure. Murtugudde et al. (2000) analysed the mixed layer temperature equation and deduced that a downwelling Rossby wave contribution was instrumental for sustaining the warming trend into February 1998. They also speculated that TIOD events represent a natural mode of oscillation in the Indian Ocean which is partially externally forced by ENSO but also triggered by ocean-atmosphere interactions internal to the Indian Ocean.

A single case study of rainfall over eastern equatorial Africa during the

months December 1997 and January 1998 was performed by Latif et al. (1999). They used an atmospheric global climate model to highlight the significance of the role played by anomalous SSTs over the tropical Indian Ocean. Their results suggested that the strong TIOD that occurred in 1997-1998 may have been remotely forced by ENSO. However, a different conclusion as to the origin of the 1997-1998 TIOD was reached by Webster et al. (1999), namely that this TIOD was primarily an expression of internal Indian Ocean dynamics rather than a direct response to ENSO.

The 1997-1998 El Niño was not well predicted, although some models did forecast warming in the Pacific one season in advance. The Climate Prediction Center (CPC, NOAA) published a number of model predictions of SST warming in the Pacific Ocean during 1997 (Experimental Long-Lead forecast Bulletin 5, No.4) in December 1996 (Kane, 1999). The Cane-Zebiak model forecast for equatorial SSTs over the Pacific Ocean during 1996-1997 was 'below normal for winter 1996-1997, normal by fall 1997, warming thereafter.' This was particularly misleading due in part to its success in forecasting the 1986-1987 event. The most successful models were those that coupled both full atmospheric and dynamical ocean models together, and this was the first time coupled models outperformed their individual counterparts (Trenberth, 1998). However, none of the models were without errors and none correctly predicted the evolution of the 1997-1998 El Niño (Barnston et al., 1999).

Many seasonal climate forecasts indicated an enhanced probability of below-average rainfall over southern Africa during the austral summer rainfall season 1997-1998 (Mason et al., 1999b; Buizer et al., 2000; Lyon and Mason, 2007; Kane, 1999; Curtis et al., 2001). The association between El Niño and dry conditions over southern Africa has been well studied and established (Ropelewski and Halpert, 1987; Hastenrath et al., 1993; Goddard and Graham, 1999; Reason et al., 2000; Reason and Rouault, 2002; Reason and Jagadheesha, 2005; Richard et al., 2000, 2001; Lyon and Mason, 2007, 2009; Meque and Abiodun, 2014). However, while southern Zimbabwe and Namibia experienced drought during the summer of 1997-1998, the rest of southern Africa received average rainfall totals for the season despite a dry start to the summer rainy season (Cook, 2000). In particular, there was drought in South Africa before December 1997, but heavy rains occurred thereafter. Rainfall was low in Namibia, almost normal in south southern Africa, and excessive in southeastern southern Africa (Kane, 1999). There have been a number of studies that have attempted to explain the apparent inconsistency between the forecast and observed rainfall over southern Africa during this season.

Su et al. (2001) used the quasi-equilibrium tropical circulation model to study the tropical teleconnections to SSTAs during the 1997-1998 El Niño. They found that SSTAs in the Indian Ocean impacted strongly on equatorial Africa during the austral summer season and cancelled the remote effect

of ENSO. They suggested that the Indian Ocean SSTAs contributed to the negative precipitation anomalies in southwestern Africa, working to enhance the impact of ENSO over this region.

Reason and Jagadheesha (2005) used the UKMO HadAM3 atmospheric model to investigate the impacts on southern African rainfall of five ENSO events between 1991 and 2003. The model was forced with observed SSTs and, of the five events studied, it was most successful in reflecting observed rainfall during the 1997-1998 El Niño event. HadAM3 does not adequately represent the Angola low which is typically weakened during ENSO events, but this weakening did not occur in 1997-1998 in spite of the occurrence of one of the strongest El Niño events on record. During the austral summer of 1997-1998, a positive Indian Ocean Dipole occurred as well as warm SST anomalies off the Angola coast which led to increased evaporation over this region. The resulting enhanced moisture levels, together with the strong Angola low, mitigated the drought conditions that often coincide with an El Niño event.

Lyon and Mason (2007) performed a diagnostic study of NCEP reanalysis data in which they compared the summer rainfall response over southern Africa during the 1997-98 El Niño to the 1982-83 event with a composite of 8 El Niño events. They found that JFM 1998 had significantly different atmospheric circulation when compared to the 1983 and composite events. The

features they identified as most influential in JFM 1998 included an unusually strong Angola low; high SSTs in the western Indian Ocean and east tropical south Atlantic; and enhanced northerly moisture flux from the continental interior and the western tropical Indian Ocean. An investigation of tropical storm track data revealed that the monthly and seasonal rainfall anomalies were not simply the results of a few extreme weather events. OND 1997 was similar to the "typical" El Niño response, while JFM 1998 was not as dry. The Angola low was unusually strong in JFM 1998 compared with JFM 1983 which contributed to enhanced northerly moisture flux from the tropical interior and, to a smaller extent, from the equatorial east tropical Atlantic. In a follow up study, Lyon and Mason (2009) used three atmospheric models forced with observed SSTs and found them generally unable to reproduce the observed rainfall over southern Africa and also over the eastern and southern Indian Ocean. As a consequence, they attempted to obtain a better correlation between observed rainfall and model output, by using three coupled ocean-atmosphere models. Two of their three models produced output that more accurately reflected the rainfall during JFM 1998. However, none of these models generated the anomalous stationary wave patterns consistent with observations over the South Atlantic and Pacific Oceans. The models also failed to reproduce the associated enhanced Angola Low which is positively associated with rainfall over southern Africa. This suggested to the authors that the two coupled models that were consistent with wetter conditions over southern Africa may have succeeded for partially the wrong

reasons.

During strong ENSO events, the Angola low is typically weakened and therefore supplies less moisture to the cloudbands over southern Africa with resulting dryer-than-average conditions (Mulenga et al., 2003; Reason and Jagadheesha, 2005). However, this connection between a strong ENSO and a weak Angola low was not observed during 1997-1998 and may have been partially responsible for the wetter-than-expected conditions over southern Africa (Reason and Jagadheesha, 2005).

2.5 The 2009-2010 Southern African Rainfall Season

Compared with the 1997-1998 El Niño, the 2009-2010 event has received relatively less attention, although both events are often cited as examples of anomalous rainfall responses to El Niño. The El Niño event of 2009-2010 is considered to have been a CP El Niño event, however it was unusual since SSTAs over the eastern equatorial Pacific Ocean were also high. The SSTAs over the south eastern Pacific Ocean were below average which is typical of an CP El Niño and, despite the anomalous warm equatorial eastern Pacific waters, the 2009-2010 event falls into the categorization of CP El Niño when the indices are consulted (Lee and McPhaden, 2010; Kim et al., 2011; Ratnam et al., 2012).

The rainfall forecast for the 2009-2010 DJF season that was made by the three coupled models discussed in Landman and Beraki (2010) showed mostly enhanced probabilities for dry conditions over southern Africa. A similar forecast was also made by international centres such as the IRI (International Research Institute for Climate and Society) and the South African Weather Service (SAWS). However, DJF 2009-2010 rainfall over South Africa was anomalously high. The Vaal Dam in South Africa was more than 100% full for the first time in 13 years during the summer of 2010. The association of enhanced forecasting skill with El Niño years may partially explain the level of confidence in the forecast of dry conditions for the austral summer season during 2009-2010.

Ratnam et al. (2012) studied the impact of the 2009-2010 CP El Niño on global rainfall during the austral summer between December 2009 and February 2010 (DJF09). They used an atmospheric global climate model based on the NCEP seasonal forecast model which was modified by the Environmental Climate Prediction Center (ECPC) at Scripps. They performed sensitivity experiments in which they altered the SST input over the Pacific Ocean in order to identify the relative impact of the central and eastern equatorial Pacific Ocean SSTAs on global rainfall during DJF09. The model did not reflect the above average rainfall over southern Africa seen in the observations. However, the experiments did indicate that the rainfall over the region was

largely due to the eastern Pacific SSTs and the opposite signal was apparent in the central Pacific experiment. This suggests that the anomalously warm eastern Pacific SSTAs played a secondary role to the central Pacific SSTAs over southern Africa during the DJF09 season.

There was a strong negative phase NAO during JFM 2010 and a tripole SSTA pattern is evident in the North Atlantic Ocean. The warming of the subtropical North Atlantic SSTs can probably be attributed to the combined forcings from the El Niño and negative NAO that often warms the subtropical and high latitude SSTs and cools the midlatitude SSTs in the North Atlantic by modifying evaporative heat loss (Deser and Blackmon, 1993). McHugh and Rogers (2001) found that heavier, convective, DJF rainfall occurs over Tanzania, northern Mozambique, Zambia and part of the western DRC during the negative NAO phase, when the North Atlantic westerlies are unusually weak. Todd and Washington (2004) also found a negative correlation between the NAO and central African rainfall, although their study focused on the FMA season. There was also a weak positive TIOD during JFMA 2010, although the strength, and therefore its classification as a dipole event, varies depending on which SST data set is used (Blunden et al., 2011). The AMO was in a warm phase during JFM 2010 and the SAM was in a negative phase (Blunden et al., 2011). Gillett et al. (2006) found a positive association between the SAM and rainfall over southeastern southern Africa.

2.6 Summary

Most of southern African receives the majority of its annual rainfall during the austral summer months. The seasonal shift in rainfall over the region tracks the movement of the band of strong convergence associated with the ITCZ which reaches its southernmost position over southern Africa during the austral summer (Tyson, 1986; Jury and Pathack, 1991; Goddard and Graham, 1999). TTTs and their associated cloudbands account for much of the rainfall over southern Africa south of approximately 15^oS (Todd and Washington, 1999; Hart et al., 2013). Since the Angola low acts as a tropical source of moisture for these TTTs, an enhanced Angola low generally results in higher levels of rainfall over parts of southern Africa (Reason et al., 2006b; Mason and Jury, 1997; Cook et al., 2004; Hart et al., 2010).

Southern African rainfall is impacted by several interannual climate modes, of which ENSO has received the most attention to date. ENSO has the greatest influence on rainfall over southern Africa during its mature phase between the austral summer months of December and March when the upper westerlies have retreated poleward south of Africa (Mason and Jury, 1997). El Niño events are usually associated with dry conditions over most of southern Africa, while La Niña events are typically associated with wet conditions over southern Africa (Hastenrath et al., 1993; Goddard and Graham, 1999; Reason et al., 2000; Reason and Rouault, 2002; Reason and Jagadheesha, 2005;

Richard et al., 2000, 2001; Lyon and Mason, 2007, 2009; Meque and Abiodun, 2014). Cook (2000) describes two possible mechanisms for how the ENSO signal reaches southern Africa. The first is an atmosphere-ocean interaction where the atmospheric response to Pacific Ocean SSTAs causes Indian Ocean warming that in turn changes southern African rainfall through sensitivity of the atmospheric circulation and air mass characteristics over southern Africa to regional SST forcing. The second occurs when atmospheric Rossby waves are generated by shifts in the site of the strongest atmospheric convection in the tropical Pacific which then leads to the Pacific South American pattern and hence atmospheric circulation anomalies over southern Africa that modulate the rainfall.

A new type of El Niño, characterised by anomalously warm SSTAs in the central equatorial Pacific Ocean, has been occurring with more frequency in the last few decades. These events can be described using the Niño 4 index (Kao and Yu, 2009; Yeh et al., 2009). It is known by many names including the central Pacific (CP) El Niño, dateline El Niño, warm pool (WP) El Niño or El Niño Modoki (Ashok et al., 2007a; Kao and Yu, 2009; Yu and Kim, 2010; Kug et al., 2009; Larkin and Harrison, 2005). Studies have shown that the canonical, or eastern Pacific (EP) El Niño, and CP El Niño may impact the global climate differently due to differences in the Walker circulation as well as differences in the atmospheric teleconnections (Ashok et al., 2007a; Weng et al., 2009; Kim et al., 2011; Ashok and Yamagata, 2009). Ratnam

et al. (2014) investigated the difference between the impact of CP and EP El Niños on rainfall over southern Africa during DJF. They found that although CP El Niño events result in below average rainfall over southern Africa, the region experiences substantially less rainfall during EP El Niño events when compared with CP El Niño. That is to say that CP El Niño events also appear to be associated with dry conditions over southern Africa, although conditions are not as dry over the region as they are during an EP El Niño.

There are two primary interannual Indian Ocean climate modes, namely the TIOD and the SIOD. A positive phase TIOD is characterised by positive SSTAs in the equatorial west Indian Ocean and negative SSTAs in the tropical east Indian Ocean. Saji and Yamagata (2003) investigated the possible impacts of the TIOD on global climate and found that temperatures and rainfall are anomalously high over countries west of the Indian Ocean, such as in East Africa, and anomalously low to its east. The also found that the TIOD affects remote regions and ,in particular, positive TIOD events are associated with increased temperatures and reduced rainfall over northern South Africa. The positive phase of an SIOD is characterised by a cold SSTA in the southeastern Indian Ocean and a warm SSTA in the southwestern Indian Ocean. This SST dipole pattern has been associated with increased rainfall over southern Africa during the austral summer (Behera and Yagamata, 2001; Reason, 2001, 2002).

A link between the occurrence of a Benguela Niño event in the Atlantic Ocean and an increase in coastal rainfall over the African continent lying approximately between the equator and 25^{o}S was established in Nicholson and Entekhabi (1987). Further studies, including those by Rouault et al. (2003a) and Hansingo and Reason (2009) have confirmed that there is a significant increase in rainfall over adjacent western Southern Africa, as well as sometimes further inland, during Benguela Niño events.

Two years that experienced a number of these SST anomaly patterns were 1997-1998 and 2009-2010. 1997-1998 in particular experienced a very strong El Niño event (McPhaden, 1999; Latif et al., 1999; Murtugudde et al., 2000; Reason and Jagadheesha, 2005; Lyon and Mason, 2007), a strong tropical Indian Ocean Dipole (Webster et al., 1999; Latif et al., 1999; Murtugudde et al., 2000) as well as a subtropical Indian Ocean dipole (Behera and Yagamata, 2001). In the South Atlantic Ocean, a strong Benguela Niña was observed in April 1997 and from January 1998 a Benguela Niño developed which increased rainfall over western Angola and Namibia (Rouault et al., 2009), and the tropical Atlantic SSTs were warmer than usual (Trenberth, 1998). The summer rainfall during JFM 1998 was also much higher than forecast over much of southern Africa which has generated a lot of interest in the teleconnections between ENSO and southern African rainfall and why the normal association did not hold during this season.

Compared with the 1997-1998 El Niño, the 2009-2010 event has received relatively less attention, although both events are often cited as examples of anomalous rainfall responses to El Niño. The El Niño event of 2009-2010 is considered to have been a CP El Niño event, however it was unusual since SSTAs over the eastern equatorial Pacific Ocean were also high. The SSTAs over the south eastern Pacific Ocean were below average which is typical of an CP El Niño and despite the anomalous warm equatorial eastern Pacific waters, the 2009-2010 event falls into the categorization of CP El Niño when the indices are consulted (Lee and McPhaden, 2010; Kim et al., 2011; Ratnam et al., 2012).

This thesis attempts to add to the body of knowledge about southern African rainfall variability and which factors impact it most. It is felt that a better understanding of the relative impacts of regional and remote forcing as well as large scale atmospheric and oceanic influences may help to improve understanding and hence long range forecasting in the region.

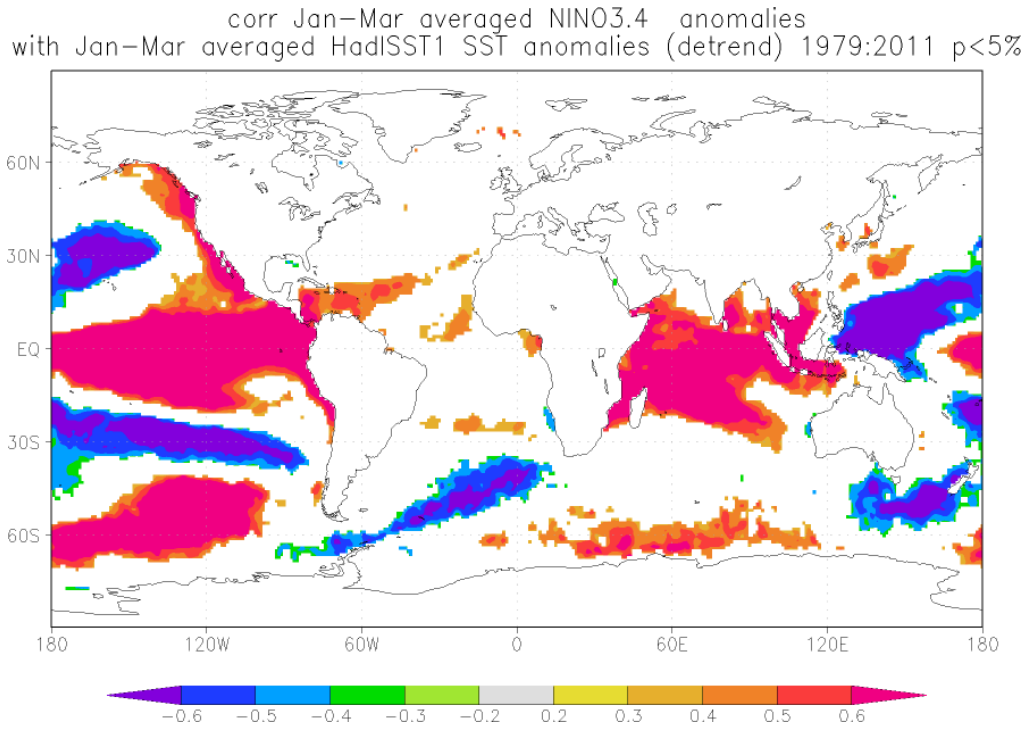

Figure 2.1: Correlation between ENSO (Niño 3.4) and global SST (HadISST) for the JFM season created on Climate Explorer, which shows ENSO over the equatorial Pacific Ocean.

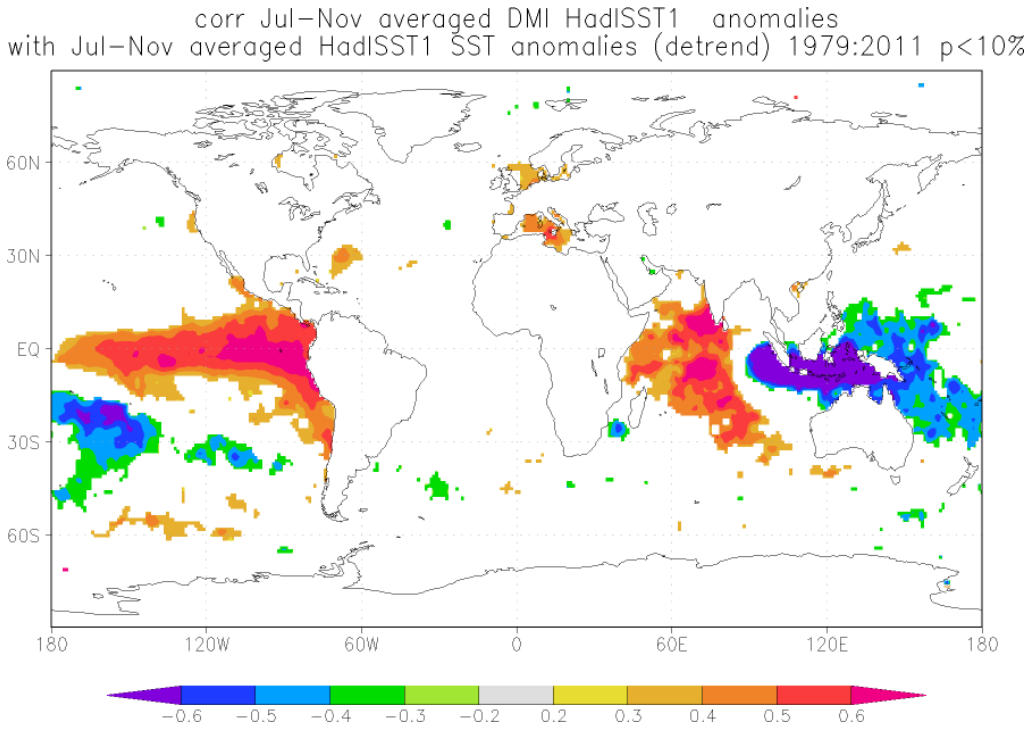

Figure 2.2: Correlation between the TIOD and global SST (HadISST) for the months July-November created on Climate Explorer, which shows the TIOD over the western equatorial Indian Ocean.

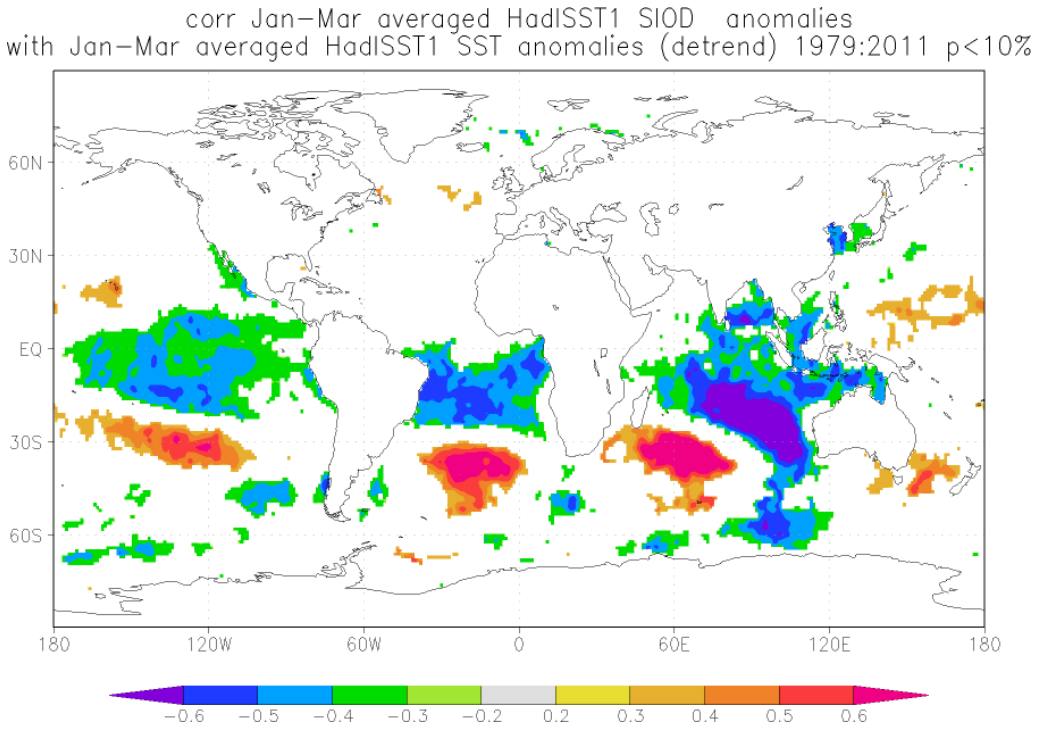

Figure 2.3: Correlation between the SIOD and global SST (HadISST) for the JFM season created on Climate Explorer, which shows the SIOD over the southern Indian Ocean.

Chapter 3

Data and Methods

This chapter provides a description of the data and methods used throughout the course of this study. Section 3.1 details all the observational and reanalysis data sets, including where they are used, in this study. A list of software and online tools used is provided in section 3.2. The model CAM-EULAG, which is used to perform idealised experiments in Chapter 8, is discussed in section 3.3.

3.1 Data

3.1.1 Climatic Research Unit (CRU)

The Climatic Research Unit (CRU) at the University of East Anglia has developed a number of data sets that are widely used in climate research. The data set CRU TS3.20 is a monthly global data set consisting of a few

variables having a spatial resolution of 0.5^o x 0.5^o and spanning the years from 1901 to 2011 (Harris et al., 2013). In this study, the variables used are precipitation and temperature, during the period from January 1979 to December 2010. A climatology is calculated using this subset of the data provided by CRU. This data is used in model validation in Chapters 7 and 8 and was sourced from BADC (http://badc.nerc.ac.uk/data/cru/).

3.1.2 ERA-Interim (ERA)

The ECMWF (European Centre for Medium-Range Weather Forecasts) improved on their previous reanalysis data set ERA-40 by using an improved atmospheric model and assimilation technique to create ERA-Interim. The newer reanalysis data set has been successful in correcting some of the errors in the previous version such as the high levels of rainfall over the oceans from the 1990s as well as an anomalously strong Brewer-Dobson circulation in the stratosphere (Dee et al., 2011). It has a spacial resolution of 1.5^ox1.5^o for the period 1979 to the present and is available in both monthly and daily time scales. This study uses the monthly data in model validation in Chapters 7 and 8. It is available for download at http://apps.ecmwf.int/data sets/.

3.1.3 20th Century Reanalysis (20thCR)

The Twentieth Century Reanalysis (20thCR) project is a collaborative effort to create a global 2 degree spacial grid resolution data set at 6-hourly time

intervals for the period 1871 to present (Compo et al., 2011). This project is being run through the US National Energy Research Scientific Computing Center (NERSC) in the US and the data is freely available online. (20th Century Reanalysis V2 data provided by the NOAA/OAR/ESRL PSD, Boulder, Colorado, USA, from their Web site at http://www.esrl.noaa.gov/psd/). Monthly 20th Century data is used to describe atmosphere circulation and in model validation in Chapters 4,5,7, and 8. Divergence and velocity potential are calculated from winds using the software CDO.

3.1.4 Global Precipitation Climatology Project (GPCP)

The Global Precipitation Climatology Project (GPCP) daily precipitation Version 1DD data set is a global 1^o x 1^o resolution daily data set that runs from October 1996 to the present (Huffman et al., 2001; Bolvin et al., 2009). The Version 2 data set contains monthly data and there is also a companion pentad data set. The data covers the period from 1979 to near current time at a resolution of 2.5^ox2.5^o. The monthly data is used in model validation in Chapters 7 and 8, while the pentad and daily data sets are the primary data sets used in Chapter 5. The raw data for all three temporal resolutions is available at http://www1.ncdc.noaa.gov/pub/data/gpcp/.

3.1.5 CPC Merged Analysis of Precipitation (CMAP)

The CPC Merged Analysis of Precipitation (CMAP) data set merges observations and rainfall estimates from several satellite-based algorithms to produce a pentad and monthly global 2.5^o x 2.5^o grid precipitation data set. This data set begins in 1979 and continues to the near present (Xie and Arkin, 1997). The monthly data is used in model validation in Chapter 7 and 8, while the pentad data set is used for comparison in Chapter 5.

3.1.6 Sea Surface Temperature Data

The National Oceanic and Atmospheric Administration (NOAA) in the US produced a 0.25^o x 0.25^o daily gridded optimally interpolated data set for SST (Reynolds et al., 2007). This data set is used to show the SSTAs during JFM 1998 and 2010 throughout this thesis.

All analysis performed using SST data on Climate Explorer uses HadISST1 which is the Met Office Hadley Centre's sea ice and SST data set. This is a monthly global 1x1 SST and sea ice concentration data set that runs from 1870 to present. This data set is used extensively in correlation analysis performed using Climate Explorer in Chapters 4 and 5.(Hadley Centre for Climate Prediction and Research/Met Office/Ministry of Defence/United Kingdom. 2000, updated monthly. Hadley Centre Global Sea Ice and Sea Surface Temperature (HadISST). Research Data Archive at the National Center for

Atmospheric Research, Computational and Information Systems Laboratory. http://rda.ucar.edu/data sets/ds277.3/. Accessed§ 03 Mar 2014).

3.2 Methods

Software used during the course of this thesis includes CDO, NCO, Ferret, Fortran, and Climate Explorer.

The mathematical development of empirical orthogonal functions (EOFs) followed from the desire to find a basis set that explains as much as possible of the variance of a data set with the fewest possible unit vectors (Kutzbach, 1967). The eigenvectors of the covariance matrix of the data set of interest are orthogonal if the eigenvalues are distinct and form a new basis that can be used to describe the data set. It is convenient to order the eigenvalues and eigenvectors in order of decreasing magnitude of the eigenvalue. The first eigenvector thus has the largest λ and explains the largest amount of variance in the data set used to construct the covariance matrix. In climate studies, only the first few eigenvalues and their corresponding eigenvectors, the leading modes of variability, are used. EOF analysis is the same as performing a principal components analysis (PCA), except that the EOF method calculates both time series and spatial patterns.

The EOF analysis in this study in Chapter 4 was performed using the

EOFSVD functions in Ferret. The program code was contributed by Billy Kessler and generates traditionally-scaled EOFs using a Singular Value Decomposition routine. Traditionally-scaled means that the units of the EOFs are the units of the variable, while the principal components are dimensionless. The routine is based on Numerical Recipes routine svdcmp.f. More details can be found on the Ferret user-guide (http://ferret.pmel.noaa.gov/Ferret /documentation/users-guide).

The correlation analysis performed in this chapter was carried out using the KNMI Climate Explorer web application (http://climexp.knmi.nl). The KNMI Climate Explorer is a web application that can be used to analyse climate data statistically. The code of the Climate Explorer itself is freely available. Due to its humble origins, it consists of a set of shell scripts and Fortran programs and runs under Linux and Mac OS X.

3.3 The CAM-EULAG Model

The Community Atmospheric Model – Euler-Lagrange, abbreviated as CAM-EULAG (or CEU), is a non-hydrostatic global atmospheric climate model with grid stretching capability that uses Community Atmospheric Model (CAM) physics and Euler-Lagrangian (EULAG) dynamics.

The Community Atmosphere Model was developed at the National Center for Atmospheric Research (NCAR) for the weather and climate research communities and acts as the atmospheric component of the coupled climate model Community Climate System Model (CCSM). A complete description of CAM can be found in Collins et al. (2004). Community Atmosphere Model Version 3 (CAM3) is an atmospheric model that includes the Community Land Model (CLM3), an optional slab ocean model, and a thermodynamic sea ice model. The model physics is designed to allow for multiple dynamics as well as a wide range of spatial resolutions. This is achieved by making the model time step and other adjustable parameters dependent on the resolution and dynamics. The adjustable parameters affect the parametrisations of cloud and precipitation processes. The CAM physics package consists of parametrised components that are sequentially computationally processed including precipitation processes, clouds and radiation, the surface model, and turbulent mixing.

Version 3 of CAM incorporated improvements to the physics parametrisations used in previous versions of CAM which increase the capacity of the model to investigate interactions between global scale and mesoscale flows and also better represents the impact of mesoscale systems on regional climates. A particular feature of version 3 of CAM is the use of a microphysical parametrisation scheme which resembles those used in cloud resolving models (Grabowski and Smolarkiewicz, 2002; Collins et al., 2004, 2006). Higher grid

resolutions are required in order to realise the benefits derived from these refinements in the model. CAM version 3 has been shown to adequately capture the precipitation response to ENSO (Hack et al., 2006b).

The variables within the parametrisation suite of CAM are separate from those that are processed in the dynamics core. This separation enables the replacement of the dynamics analysis by EULAG, a non-hydrostatic, parallel computational model. EULAG is a research model designed for geophysical flows and a complete description can be found in Prusa et al. (2008). The non-hydrostatic behaviour of the variables in EULAG is achieved through anelastic approximation of the equations of motion. The underlying anelastic equations are either solved in an EULerian (flux form), or a LAGrangian (advective form) framework.

Coordinate Mapping A signature feature of EULAG is its formulation in generalised time-dependent curvilinear coordinates. The code uses mappings from a physical space $\mathbb{S}_p$ in which the problem is formulated to a transform space $\mathbb{S}_t$ where the problem is solved numerically. The physical space $\mathbb{S}_p$ is a Lorentz space $\mathbb{S}_p(\mu)$ which is defined (Hélein, 2002) as the set of all measurable functions $f : \mathbb{R}^n \to \mathbb{R}^n$ for which the L^p norm of f^* on $\mathbb{R}^+$ with respect to the measure μ is finite, i.e..

$$\left\{ \int_0^\infty [f^*(x)]^p v(x) dx \right\}^{\frac{1}{p}} < \infty$$

where $d\mu(x) = v(x)dx$ and $v(x)$is a non-negative (weight) function on $[0, \infty)$, while f^* is the non-increasing rearrangement of f with respect to the measure μ defined as

$$f^*(t) = \inf\{\alpha \in \mathbb{R}^+ : d_f(\alpha) \leq t\}$$

where $d_f(\alpha)$ is the distribution function of f defined by

$$d_f(\alpha) := \mu(\{x \in \mathbb{R}^n : |f(x)| < \alpha\}).$$

The problem is formulated in a Lorentz space which has zero space-time (Riemannian) curvature. This characteristic is preserved by the transformation mapping from $\mathbb{S}_p$ to $\mathbb{S}_t$ and the invariance of Riemannian curvature is important in order to preserve tensor identities that are required in the transformed space. The mapping from $\mathbb{S}_p \to \mathbb{S}_t$ is defined by

$$(\bar{t}, \bar{x}, \bar{y}, \bar{z}) := (t, E(t, x, y), D(t, x, y), C(t, x, y, z)) \tag{3.1}$$

where the functions E, D and C are twice continuously differentiable and $\bar{x}$ and $\bar{y}$ are independent of the vertical coordinate z. The assumption that $\bar{x}$ and $\bar{y}$ do not vary with z simulates the primary hydrostatic structure of the atmosphere and, in conjunction with the identity map for the time variable, achieves a simplification of the metric terms. The equations of motion can be formulated in terms of any orthogonal coordinate system and the default orthogonal coordinate system for $\mathbb{S}_p$ is spherical for global applications

of CEU. The mapping from $\mathbb{S}_p$ to $\mathbb{S}_t$ is an "almost global" diffeomorphism (Prusa et al., 2008) and accommodates the implementation of grid stretching where the grid may appear non-uniform in physical space but is uniform in the transform space where computations are performed.

The vertical component $\bar{z} := C(t, x, y, z)$ is only constrained *a priori* by smoothness conditions in (3.1), but the CEU model used in this study incorporates an exponential vertical stretch in a similarity transformation, namely

$$\bar{z} = C(\zeta) = \frac{H_o(1 - e^{-\zeta/H_z})}{1 - e^{-H_o/H_z}}$$

where $\zeta = \frac{H_o(z - z_s)}{H - z_s}$ and $z_s(t, x, y)$ and $H(t, x, y)$ are the lower and upper boundary altitudes, respectively; while H_o is a representative domain depth and $H_z = 8.0$ km is the scale height. This choice of scale height maximises vertical resolution at lower and mid levels of the atmosphere where the dynamics play an important role.

Governing Equations Let ν^j denote the physical velocity vector; θ, ρ, and π denote potential temperature, density, and a density-normalised pressure, respectively; g is gravitational acceleration; q_v, q_c, q_i are the specific humidity for water vapour, cloud water, and cloud ice, respectively, while P_v, P_c and P_i are their corresponding time derivatives; $\rho^* := \rho_b \bar{G}$ where ρ_b

denotes the basic potential density and $\bar{G}$ is the Jacobian of the transformation from Cartesian space to $\mathbb{S}_t$. Renormalised elements of the Jacobi matrix appearing in the momentum equations (3.3) below are denoted by $\tilde{G}_j^k$; while δ_j^3 is the Kronecker delta. Primes denote perturbations with respect to the environmental state (denoted by subscript e), while subscript b refers to the basic state. The index $i = 0, 1, 2, 3$ corresponds to the variables t, x, y and z respectively.

In CEU, the dynamics model EULAG solves the generalised anelastic equations in the transformed space $\mathbb{S}_t$ which incorporates a horizontally homogeneous hydrostatic basic state. EULAG uses the Lipps-Hemler anelastic approximation (JAS 1982) which consists of two approximations. The first arises from the assumption that the Mach number $<< 1$ which is valid for all atmospheric processes except for very high wind speeds that might occur in tornadoes or strong hurricanes as well as deep barotropic modes like tides which move at near sonic velocities. The second assumption is that potential temperature scale height $>>$ vertical scales of flow which makes allowances for nearly all gravity waves. The anelastic approximation enhances computational accuracy since the model does not expend effort by computing effects arising from hydrostatic balance. In particular, it filters sound waves out of the equations and thus the Courant number limit allows a much larger value of dt. The equations of motion are

$$\frac{\partial(\rho^* \bar{\nu}^{s^k})}{\partial \bar{x}^k} = 0, \quad k = 1, 2, 3 \tag{3.2}$$

$$\frac{d\nu^j}{d\bar{t}} = -\tilde{G}^k_j \frac{\partial \pi'}{\partial \bar{x}^k} + g\frac{\theta'_d}{\theta_b}\delta^3_j + S_j, \quad j, k = 1, 2, 3 \tag{3.3}$$

$$\frac{d\theta'}{d\bar{t}} = -\bar{\nu}^{s^k} \frac{\partial \theta_e}{\partial \bar{x}^k} + H_\theta, \quad k = 1, 2, 3 \tag{3.4}$$

$$\frac{dq_\nu}{d\bar{t}} = P_\nu \ ; \quad \frac{dq_c}{d\bar{t}} = P_c \ ; \quad \frac{dq_i}{d\bar{t}} = P_i \tag{3.5}$$

where $\frac{d}{d\bar{t}} = \bar{\nu}^{*i}\frac{\partial}{\partial \bar{x}^i}$ denotes the total derivative; $\bar{\nu}^{s^j} = \tilde{G}^j_k \nu^k$ denotes solenoidal velocity and $\bar{\nu}^{*j} := \frac{d\bar{x}^j}{d\bar{t}} \equiv \frac{\partial \bar{x}^j}{\partial x^i}\nu^i$ denotes contravariant velocity. In the transformed space $\mathbb{S}_t$, solenoidal velocity differs from contravariant velocity by the grid speeds and preserves the incompressible feature of the equations of motion. The moist potential temperature is denoted by $\theta_d = \theta + \theta_b(\varepsilon q_v - q_c - q_i)$, where θ is the dry potential temperature, and ε is defined as the difference between 1 and the ratio of water vapour and dry gas constants, i.e.. $\varepsilon + 1 = R_v/R_d$. The buoyancy perturbation term appearing in equation (3.3) is $\theta'_d = \theta_d - \theta_{de}$ where $\theta_{de} = \theta_e + \varepsilon\theta_b q_{\nu e}$. H_θ includes adiabatic forcing that is a consequence of CAM physics and numerical absorbers. S_j are additional momentum forcings from CAM physics, deviation of inertial forces (Coriolis and geospherical metric accelerations) from the geostrophically-balanced ambient (e.g.. environmental) state, and absorbers. The Lipps-Hemler equa-

tions (Lipps and Hemler, 1982, 1986) describe a deep and moist anelastic model which Grabowski and Smolarkiewicz (2002) first implemented in EULAG, utilized subsequently by Abiodun et al. (2008) in CEU.

Equations (3.3) and (3.4) are in Lagrangian form and can be equivalently reformulated in Eulerian flux conservation form. Each of the reformulated equations can be approximated to second-order accuracy in space and time using a non-oscillatory forward-in-time (NFT) approach (see Smolarkiewicz and Prusa (2004)). The combination of NFT numerics and tensor formulation within the EULAG package admits a class of mappings described by (3.1). EULAG is noteworthy for its robust elliptic Krylov solver, grid adaptivity, and scalability on massive parallel processor machines. CEU solves the fluid equations in Eulerian mode with uniformly second order accuracy (Prusa et al., 2008).

Global climate models commonly use hydrostatic governing equations to simulate circulation dynamics. Spacial resolution of global climate models can be increased in parallel with an increase in computing capacity and, as resolution increases, non-hydrostatic behaviour emerges. In the idealised experiments performed in this study, the grid is stretched to a resolution of 0.5 x 0.5 degrees over southern Africa, 1x1 degrees over much of the rest of the globe and 2x2.5 degrees over the Pacific Ocean and the poles (**Figure 3.1**). The main advantages of using a stretch grid include the ability to use a very

high resolution over the area of interest in a global model without requiring a substantial increase in computational power. Regional modes also accommodate increased grid resolution but often encounter the boundary condition problem which is avoided by using a stretch grid model. If the stretched output data is regridded to a uniformly high resolution grid, then little data is lost in interpolation beyond higher levels of conservation and identities that the full solution offers.

CEU is an anelastic model which uses pressure anomalies rather than full pressure. As a result, the pressure levels are not all integers. **Table 3.1** details the approximate pressure at each of the 26 levels in CEU. For convenience and ease of reading, the pressures in CEU are rounded to the more commonly used positive integers. In particular, 202.97 hPa is rounded down to 200 hPa, 504.83 hPa is rounded down to 500 hPa, 700.63 hPa is rounded down to 700 hPa, and 851.30 hPa is rounded down to 850 hPa.

Since anelastic models do not require full pressure for calculations, it is challenging to deduce the full pressure and geopotential height. The algorithm for calculating geopotential height in CEU needs more work, but for the moment is unsuitable for use in this thesis.

After the implementation of the dynamics core EULAG into the global atmospheric climate model CAM3 was completed, the new model had to be

validated to test that this new dynamics core did not cause anomalous behaviour in the model. Abiodun et al. (2008) carried out three aqua-planet simulations using CAM3 with each of the dynamics cores EULAG (CEU), finite volume (CFV) and Eulerian spectral (CES), and on comparison found that CEU adequately reproduces the results of CAM at uniform grid resolutions, and is therefore appropriate for use in climate simulations. Abiodun et al. (2011) went on to compare rainfall in CEU to CFV over West Africa during the boreal summer from 1996 to 2000. They found that CEU with a uniform grid of the same resolution of 2^ox2.5^o outperformed CFV, and when a stretch grid was introduced over their region of interest, the results improved further.

3.3.1 Model Spin-Up and Optimisation

Atmospheric models typically take a period of time after initialisation to converge towards a state of quasi-stationary behaviour. Such a state is usually characterised by a substantial change in fluctuation of parameters such as temperature, wind and moisture. The period of time before this state is reached is called the spin-up time of the model. After the spin-up is completed, the output is considered to have negligible climate drift and hence the most accurate statistics for the model climate will be simulated (Johns et al., 1997).

One of the difficulties in calculating the spin-up time of a realistically

initiated climate model is that since the global forcing changes with time, no true quasi-stationary state exists. This makes it harder to ascertain the end of the spin-up period.

Abiodun et al. (2008) found that CEU output reached statistical stationarity in approximately 40 days. They looked at the time evolution of the zonal average of zonal wind, potential temperature and specific humidity (Figure 3 in Abiodun et al. (2008)). All three variables show a trend of reaching a quasi-stationary (QS) state in the tropics before the midlatitudes. Zonal wind reached QS after approximately 25 days, potential temperature after 18 days, and specific humidity no sooner than 20 days. The minimum spin-up time is therefore 25 days, but 40 days is more robust.

A similar figure for daily climatological CEU data initialised with more realistic atmospheric conditions is found in **Figure 3.2**. The time evolution of zonal wind displays a sudden shift south in the zero wind line in the northern hemisphere at approximately 5^oN to 10^oN at roughly 15 days. This structural change is not repeated elsewhere in the plot and this variable appears reasonably stable after this anomaly. Potential temperature shows some variability before 10 days that seems to calm into a QS between 15 and 20 days. Moisture is almost always the variable to set the limit as it is the slowest to reach QS balance and that is the case in this application. The structures in the tropics do not reach a QS until around 25 to 35 days. In

light of these individual spin-up times, it is reasonable to select a spin-up time of more than 35 days for CEU experiments.

Sensitivity experiments were run to determine the optimum number of processors on which to run the model. Since the grid size was predetermined by the desired resolution, the only variables to test were processor geometry (i.e. the way in which the x and y component of the grid is split between processors) and the total number of nodes to be used. Parallel processing reaches its optimum level of efficiency when the time spent passing messages between processors is less than the time saved by having extra processors. CEU runs optimally when the x component of the processor geometry is set to equal the number of processors per node, which in this case was eight. With nprocx = 8, maximum efficiency in computational time was achieved with nprocy also equal to eight. Hence all experiments were run on 64 processors made up of 8 nodes with 8 processors each.

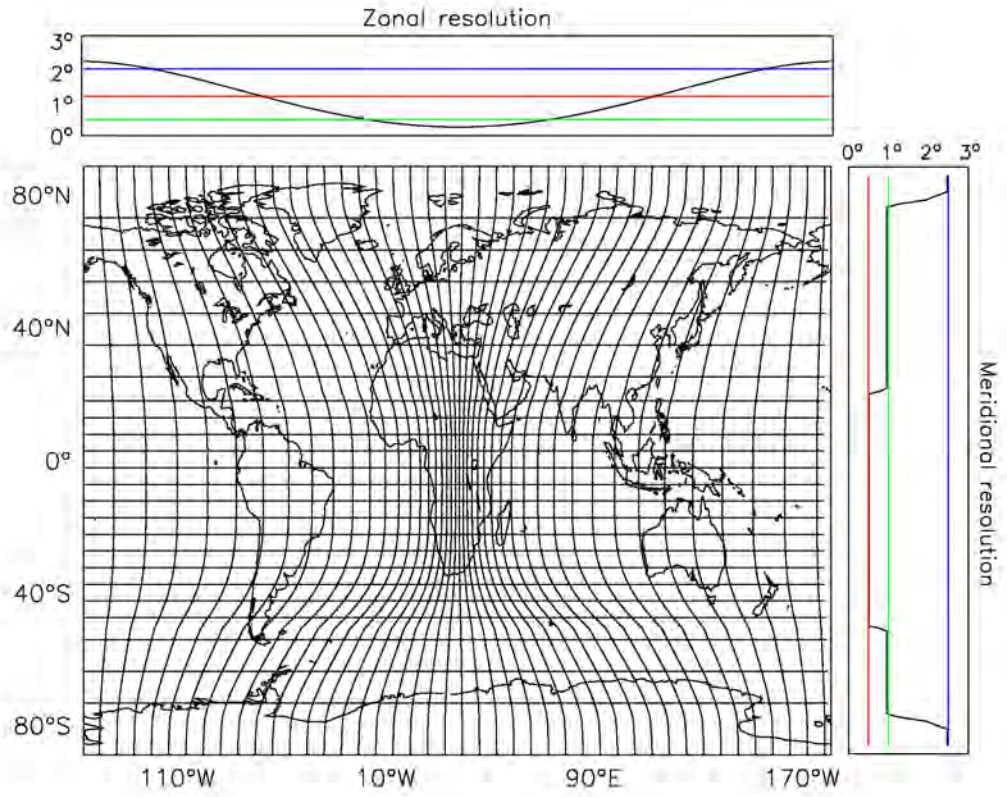

Figure 3.1: Grid indicating zonal and meridional resolution used in all validation and experiments of CEU

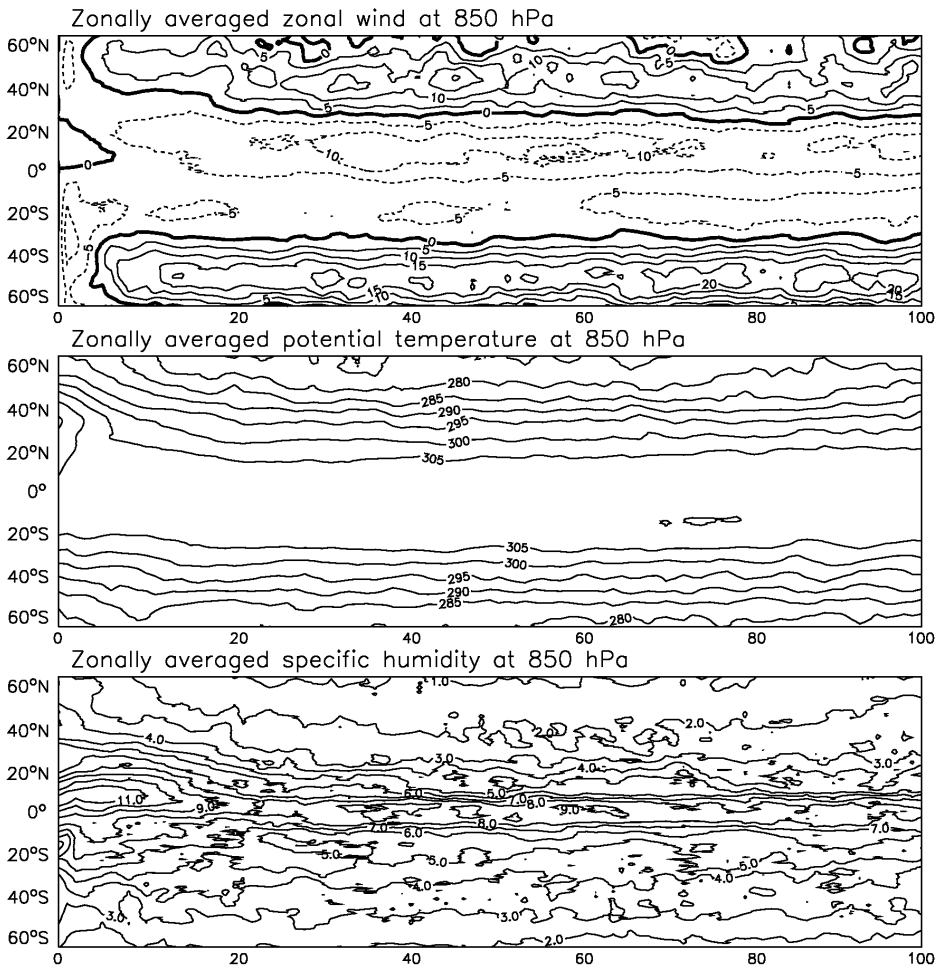

Figure 3.2: Daily time evolution of CEU zonally averaged zonal wind, potential temperature, and specific humidity at 850 hPa

Level	Pressure
1	11.79
2	37.20
3	69.58
4	111.02
5	156.72
6	202.97
7	248.82
8	293.84
9	337.98
10	380.82
11	423.00
12	465.00
13	504.83
14	545.99
15	584.95
16	624.35
17	663.41
18	700.63
19	739.89
20	777.09
21	814.64
22	851.30
23	887.51
24	923.10
25	958.40
26	993.17

Table 3.1: Approximate pressure level (in hPa) at each of the 26 levels in CEU

Chapter 4

The Botswana High

The Botswana high, sometimes referred to as the Botswana upper high, is a high pressure cell which exists at the 500 hPa level and is centred over central Namibia and western Botswana during the late austral summer (**Figure 4.1**). This high pressure feature over the southern part of the subcontinent has not been extensively studied except in connection with rainfall over Zimbabwe (Matarira, 1990; Magadza, 1994; De Groen and Savenije, 1995; Unganai and Mason, 2002; Jury, 2002; Ratna et al., 2013). The relative strength and position of the Botswana high is known to impact rainfall over the region and a stronger than usual Botswana high is usually associated with below average rainfall over Zimbabwe (Ratna et al., 2013).

Matarira (1990) found that a composite of 500 hPa geopotential height for anomalously wet (dry) summers was associated with a negative (positive)

anomaly over the southern part of the subcontinent indicating a relationship between the Botswana high and precipitation over Zimbabwe (see Figure 6 in Matarira (1990)). In terms of agriculture, it was noted in Magadza (1994) that those countries that experience the highest levels of variation in yield per unit harvested are generally those which lie on the extremity of the ITCZ and levels of rainfall depend on the southward movement of this feature. The study indicated that periods of high rainfall are characterised by a persistence of the ITCZ while drought is associated with the dominance of the Botswana High. In another study investigating the long term predictability of rainfall over Zimbabwe, Unganai and Mason (2002) similarly concluded that, while rainfall variability over the region depends mainly on the location and strength of the ITCZ, it is also influenced by the passage of upper westerly waves of midlatitude origin. The influence of these waves is sometimes affected by the presence of a strong Botswana high or a persistent blocking high extending from the Indian Ocean. The Botswana high merits further study since it appears to influence rainfall variability over large parts of southern Africa.

4.1 Evolution of the Botswana High

The late summer (JFM) mean Botswana high is shown in **Figure 4.1** while the monthly evolution of the Botswana high over the course of the austral summer from September until April is shown in **Figure 4.2**. Broadly

speaking, the high develops during the early summer when it is at its strongest, shifts southward and weakens, and then migrates northward, a seasonal shift that roughly tracks the movement of the ITCZ. A more detailed description of the evolution of the Botswana high is given below.

A region of high pressure is present over southern Angola in September and covers most of Angola south of 10^oS. Two arms of lower pressure extend from this high, one to the west to cover a band of the tropical South Atlantic Ocean between 5^oS and 15^oS, the other extending to the northeast over eastern Africa. The centre of the Botswana high shifts southwest and increases in strength during October, while the bands extending from the high are no longer evident. The high continues to shift southwest during November moving to northern Namibia / northern Botswana and reducing in strength. By December, the Botswana high only exists in the latitudinal band between approximately 15^oS and 25^oS and its strength reduces further, although the arm over the tropical South Atlantic Ocean is again apparent. In January, the Botswana high becomes weaker still and occupies a smaller latitudinal band, with a new high presenting in the central tropical South Atlantic Ocean. February is much the same as January except for a slight reduction of pressure in the band between 20^oS and 30^oS. The Botswana high increases both in size and strength during March extending north to cover most of the northern half of Namibia with extensions over both adjacent oceans. The high decreases and shifts further northward in April.

4.2 EOF Analysis

An empirical orthogonal function (EOF) analysis is performed over southern Africa on monthly 20th Century data between the years 1979 and 2011 for the early and late summer seasons OND and JFM, respectively. The eigenvectors are derived from anomalies of the seasonal totals and have been computed on the covariance matrix. Since the Botswana high lies over the southern portion of the subcontinent, the region lying between 10^oW to 40^oE and the equator to 35^oS was chosen in an effort to exclude the surrounding oceans and their anticyclones. The semi-permanent high pressure cells over the South Atlantic and South Indian Oceans are known to extend into the 500 hPa level of the atmosphere and their presence may have interfered in the search for signals over the landmass of interest here.

4.2.1 The Early Summer OND Season

The three month period from October to December (OND) is considered to be the early austral summer season. Although the focus of this thesis is the late summer rainfall season (JFM), the early summer rainfall season is included in this chapter for completeness. The first two EOFs during this season account for approximately 81% of the total variance of the 500 hPa geopotential height over the region 10^oW to 40^oE and 0^oS to 35^oS. The first EOF (EOF1) carries most of this variance (55%) and shows the variability of the pressure gradient over southern Africa. The second EOF (EOF2) is

reminiscent of the Botswana high and accounts for approximately 25% of the variance of 500 hPa geopotential height over this region (**Figure 4.3**).

The time series associated with EOF2 indicates that the Botswana high was strongest in the early summer months during the years 1987, 1997, 1998, 2002, and 2003 (3 out of 5 are peak phase El Niño summers) and weakest during the years 1984, 1985, 2000, 2007, and 2010 (4 out of 5 are peak phase La Niña summers) (**Figure 4.4**). Thus, some of the variability of the Botswana high during the early summer may be associated with ENSO. **Figure 4.5** shows the 500 hPa geopotential height during the OND season for the 5 strong and 5 weak EOF2 years identified above and the association between the EOF2 time series and the relative strength of the Botswana high is demonstrated. Since the EOF2 pattern in **Figure 4.3** is generally negative, the strong instances of the Botswana high in the left hand column correspond to the negative values in the time series, while the weaker Botswana highs in the right hand column correspond to years that had positive values in the time series. The centre of the Botswana high varies from year to year which is likely to have an impact on regional rainfall. During OND 2007, it was centered over southern Zimbabwe and eastern Botswana which is far east of its usual position. The OND Botswana high was at its strongest during 2002 and was centered over the border of northern Namibia and Botswana which is its expected location. The weakest example of an OND Botswana high occurred during 1985 and was centered over northern Botswana, northern

Namibia and part of southern Angola. The 10 examples in **Figure 4.3** give some indication of the variability of this circulation system.

4.2.2 The Late Summer JFM Season

The first EOF (EOF1) during the JFM season accounts for approximately 75% of the variance of 500 hPa geopotential height and has a pattern that is reminiscent of the Botswana high (**Figure 4.6**). The second EOF (EOF2) lies in the confluence region between the Angola low and the ITCZ and appears to resemble a mode where the Botswana high is shifted northwestward and is weaker than in mode 1. It accounts for approximately 13% of the variance.

The time series associated with EOF1 shown in **Figure 4.7** indicates that the feature was particularly strong during the JFM season in the years 1983, 1988, 1998 and 2010 and weak during the years 1989, 1996, 2000 and 2001. **Figure 4.8** shows the 500 hPa geopotential height for these 4 strong and 4 weak years and each corresponds to strong and weak Botswana highs, respectively. It is interesting to note that all four incidences of the strongest Botswana highs occurred during mature phase El Niño summers (1983, 1988, 1998, and 2010) while all the weakest Botswana highs occurred during mature phase La Niña summers (1988, 1996, 2000, and 2001). The Botswana high was exceptionally strong during JFM 1983, and comparatively weak and shifted slightly southward during JFM 1988. Although the 500 hPa geopo-

tential height was generally high over the band of southern Africa between 10^oS and 30^oS, it is difficult to identify a centre of the Botswana high. In the JFM 2010 case, the Botswana high was centered very far south across the border of southern Botswana and Namibia. In the cases of weak Botswana highs, the JFM 1989 case is unusual since it is centered over the most common region. In the 1996 and 2001 JFM seasons, the high is centered over Namibia, while in 2000 it is difficult to pin down a location.

The pattern emerging from the EOF analysis of both the OND and JFM seasons suggests a strong association between ENSO and the Botswana high. This is investigated in the next section using correlation techniques.

4.3 Correlation Between the Botswana high and global SSTs

All correlation analyses are performed using the built-in correlation functions in Climate Explorer (detailed in Chapter 3) and only those correlations that produced 95% or higher statistically significant values at lags of between -3 and 3 months are included. Each of the SST indices used in this study appear within the monthly climate indices folder in Climate Explorer and the following details are taken from the site. ENSO is measured via the Niño 3.4 SST index (Barnston and Ropelewski, 1992) and the TIOD is measured via the dipole mode index (DMI; Saji et al. (1999)). The SIOD is measured using

the subtropical dipole index (SDI; Behera and Yagamata (2001)). The NAO index is taken from the Climate Prediction Centre (Barnston and Livezey, 1987). The AMO index is calculated as defined in Trenberth and Shea (2006). The SAM index is sourced from the British Antarctic Survey (Limpasuvan and Hartmann, 1999).

4.3.1 The Early Summer OND Season

A correlation between the EOF time series during OND that represents the Botswana high (EOF2) and climatological global SSTs is shown in **Figure 4.9**. The Botswana high displays strong positive correlations over the tropical Pacific Ocean, the tropical Atlantic Ocean north of the equator, and the tropical Indian Ocean. The patterns of correlation over the Pacific and Indian Oceans are also present in the correlation between ENSO and global SSTs during OND (**Figure 4.10**). This indicates that the Botswana high is positively correlated with ENSO and also with the tropical North Atlantic Ocean SSTs during the OND season.

Time series correlations between the Botswana high EOF and individual SST indices produced statistically significant results for ENSO and the TIOD, but the only Atlantic Ocean index to have a relevant value correlation was the NAO. At a lag of 1 month, the NAO and OND Botswana high were correlated with a value of r= 0.36 (96% statistically significant). The correlation between the Botswana high and ENSO as well as the TIOD is shown in

Table 4.1 which supports the previous suggestion that the Botswana high is well correlated with ENSO. This correlation is r= 0.51 (100% statistically significant) getting progressively weaker (stronger) as a negative (positive) lag is introduced, while maintaining a statistical significance higher than 99%. The Botswana high has a correlation coefficient of r= 0.36 (96% statistically significant) with the TIOD, and this correlation becomes stronger if a lag of -1,-2 or -3 months is introduced.

Correlation analysis suggests that the Botswana high during the early summer OND season is positively correlated with the positive phases of both ENSO and the TIOD. Although the tropical North Atlantic Ocean SSTs are also correlated with the Botswana high, this signal does not present strongly in any of the conventional Atlantic Ocean indices.

4.3.2 The Late Summer JFM Season

A correlation analysis of the leading EOF time series during JFM against climatological global SSTs is shown in **Figure 4.11**. The pattern of correlation between the Botswana high and global SSTAs is strikingly similar to the correlation between the ENSO signal and global SSTAs (**Figure 4.12**). The main difference can be seen over the tropical North Atlantic Ocean where the correlation between SSTs there and the Botswana high are stronger than those of SSTs over the region and ENSO. The strong similarities between these two correlations indicates that the Botswana high is strongly corre-

lated with ENSO and also with the global SSTAs that are associated with ENSO.

Individual time series correlations between the Botswana high EOF time series and the Niño 3.4 index are summarised in **Table 4.2**. This correlation is very high with a value of r= 0.87 (at approximately 100% statistical significance). The correlation gets progressively weaker as negative monthly lags are introduced and the ENSO signal typically decays after reaching its mature phase. However, the correlation is similar when positive month lags are introduced which indicates that the ENSO signal leading up to the mature phase of ENSO has a similar influence on the JFM Botswana high as the mature phase ENSO itself.

Figure 4.12 correlates Niño 3.4 with global SSTs. A number of studies have attempted to identify the extent to which each of these other SST modes are independent from ENSO. In particular, the TIOD-ENSO relationship has received a lot of attention (Webster et al., 1999; Murtugudde et al., 2000; Black et al., 2003; Yamagata et al., 2004). It is now generally accepted that a sufficiently strong ENSO event may trigger a TIOD. However, it is not a necessary condition for the dipole to occur as it may result from internal dynamics in the Indian Ocean (Saji et al., 2006; Kug and Kang, 2006). Thus, although many of the SST modes considered in the following correlation analysis are associated with ENSO, they also merit individual analysis.

The correlation between the Botswana high EOF time series and the TIOD is r= 0.45 (99% statistically significant) with a lag of 1 month (**Table 4.2**). This correlation increases to r= 0.53 (100% statistically significant) when a lag of 2 or 3 months is introduced. This implies that a positive TIOD, which typically peaks in the early summer, may have a positive association with a strong JFM Botswana high. **Table 4.3** summarises the correlations between the Botswana high EOF time series and the AMO as well as SAM. The AMO is correlated with a value of r= −0.36 (96% statistically significant), which increases to a correlation of r= −0.42 (98% statistically significant) when a lag of 1 month is introduced, and is r= −0.40 (98% statistically significant) when the lag is 2 months. The Botswana high EOF is correlated with SAM at lags of 2 and 3 months with values of r= −0.50 (100% statistically significant) and r= −0.49 (98% statistically significant), respectively. This implies that a negative phase occurrence of the AMO or SAM during the early austral summer may be associated with a strong Botswana high.

Correlation analysis suggests a very strong association between the Botswana high and ENSO. The correlations with the TIOD, AMO and SAM at positive month lags could simply be part of the ENSO signal, or they may have independent relationships with the Botswana high. The interdependence (or otherwise) of these modes will not be investigated in this thesis.

4.4 Association with Rainfall

A relationship between ENSO and rainfall over southern Africa has been established (Lindesay, 1988; Reason et al., 2000). Correlation analysis indicates a strong association between ENSO and the Botswana high. The question as to whether or not the Botswana high is simply another manifestation of the ENSO signal or if it can give additional insight into rainfall conditions over the region is addressed in this section. A percentage difference is used for rainfall rather than standardised anomalies since this is the method used for model comparison in Chapter 8.

4.4.1 The Early Summer OND Season

During OND, the main differences between the Botswana highs that occurred during El Niño as opposed to La Niña events is that they were generally stronger during El Niño and their centre was slightly to the west of those that occurred during La Niña (**Figure 4.13**, **Figure 4.14**). The Botswana highs during OND 1982 and 1986 were the weakest that occurred during the El Niño events and while there was above average rainfall over most of the subcontinent, that was not the case over Zimbabwe, southern Mozambique, and much of eastern South Africa during 1982 and Namibia and western South Africa in 1986 (**Figure 4.15**). The driest season over southern Africa occurred during OND 1994 although the Botswana high was relatively weak during that season. The strongest Botswana high occurred in 2002 where

the rainfall anomalies showed much the same pattern as 1982, although with a lower magnitude. These examples demonstrate that a linear relationship between rainfall and the Botswana high is not directly evident during OND in El Niño years.

The strongest Botswana highs during La Niña events occurred during 1988, 1995, 1998, 2008, and 2011 (**Figure 4.14**). These years were generally associated with higher than average rainfall over parts of southern Africa, particularly in 2011 (**Figure 4.16**). The years 1984, 2000 and 2007 had relatively weak Botswana highs and did not receive as much rainfall as most La Niña years. The association between the strength of the Botswana high and rainfall does appear to have been reversed and is not what was expected.

The neutral years Botswana highs and rainfall are shown in **Figures 4.17** and **4.18**. No relationship between the two is readily apparent.

4.4.2 The Late Summer JFM Season

Figure 4.19 shows the 500 hPa geopotential height during the JFM seasons of the El Niño years between 1979 and 2011, while **Figure 4.20** shows the percentage difference between rainfall for that season and the climatology. The pattern of geopotential height is different in each year, but an overall pattern emerges in which the highest values are typically located at the centre of the Botswana high. Moreover, if there are high values over the

adjacent oceans, they are usually higher over the subtropical South Atlantic Ocean. **Figure 4.21** shows the 500 hPa geopotential height during the JFM seasons of the La Niña years that occurred between 1979 and 2011 with a general pattern in which the highest values are split across each of the adjacent oceans. Alternatively, if the strongest values occur over land, they are not restricted to the usual location of the Botswana high.

The Botswana high that occurred during JFM 1983 was very strong and, during that season, southern Africa experienced one of the most widespread droughts ever recorded. The weakest Botswana highs occurred during 1989 and 2000 and in both cases southern Africa received widespread heavy rainfall. El Niño years are generally associated with a strong Botswana high and below average rainfall (**Figure 4.20**), while La Niña years are usually associated with a weak Botswana high and above average rainfall (**Figure 4.22**); however, there are exceptions in both cases. The El Niño years 1988, 1998 and 2010 were all anomalous in the sense that above average rainfall was experienced over most of the subcontinent. There does not appear to be any indication as to why this occurred. However, the 1998 and 2010 Botswana highs were both more in line with the La Niña pattern than with the El Niño pattern. The strongest component of the Botswana high covered a larger area along the zone between 10^oS and 30^oS than is typical during El Niño years (**Figure 4.19**). This is also true for the year 2005 which shows slightly above average rainfall over some regions of southern Africa. The La

Niña years were more consistent, although less rainfall than average occurred over most of southern Africa during 2008 which more closely resembled an El Niño pattern of 500 hPa geopotential height (**Figure 4.21**).

If the neutral years are split into two categories, namely those whose 500 hPa geopotential height over South Africa resembles the same pattern identified in the El Niño years versus those in the La Niña years, a pattern emerges. The years 1979, 1980, 1982, 1984, 1986, 1993 and 2002 bear a resemblance to El Niño years while the years 1981, 1990, 1991, 1994, 1997 and 2004 bear a resemblance to the La Niña years (**Figure 4.23**). These years also correspond very well to the below and above average rainfall seasons with the exceptions of 1980 and 1990 (**Figure 4.24**).

This analysis suggests that the Botswana high may be useful in predicting rainfall over southern Africa during neutral ENSO years. It could also be used to indicate the possibility of unexpected rainfall events over southern Africa during El Niño years.

4.5 Summary and Conclusions

The Botswana high, a high pressure cell which exists at the 500 hPa level and is centred over central Namibia and western Botswana during summer, is described and analysed and its relationship with rainfall over southern Africa

is examined. The monthly evolution of the Botswana high is detailed and it is seen to track a similar migration pattern to that of the ITCZ. Its movement and strength between the months of September and April is described in detail.

An EOF analysis of 500 hPa geopotential height over southern Africa reveals that the Botswana high accounts for approximately 25% of the variance of geopotential height during the early summer OND season, which increases to 75% during the late summer JFM season. In the time series associated with the EOF that represents the Botswana high for OND, the majority of years during which a strong or weak Botswana high occurred were ENSO years. The time series associated with the EOF representing the Botswana high during JFM showed an even stronger relationship since every strong or weak Botswana high occurred during an ENSO year. This indicates an association between the strength of the Botswana high and ENSO.

Correlation analysis was then used to further investigate the relationship between the Botswana high and ENSO. A correlation coefficient of r= 0.51 was found for the early summer OND season, while the late summer JFM season showed a correlation coefficient of r= 0.87. This confirmed that there is indeed an association between the Botswana high and ENSO and that it is stronger in the later summer JFM season than in the early summer OND season.

With regard to the question of whether the Botswana high may give additional insight into rainfall over southern Africa outside the context of ENSO, the JFM 2002 season is noteworthy. A very strong Botswana high occurred during JFM 2002 (**Figure 4.25**) and there was no ENSO event during the 2001-2002 austral summer. The OND 2001 season was relatively wet and the Botswana high was not much stronger than average (**Figure 4.18**). The region of southern Africa south of approximately 15^{o}S and east of approximately 20^{o}E experienced below-average rainfall. This is one example of a non-ENSO year during which much of the southern African region received below average rainfall and a strong Botswana high occurred.

The question arises as to whether the Botswana high is simply another manifestation of ENSO. To address this, the association between rainfall over southern Africa and the relative strength and position of the Botswana high is investigated. No obvious pattern was found for the early OND season, however there may be a connection between the Botswana high and rainfall over southern Africa during the late summer JFM season which not only exists during ENSO years but also during those neutral years that have ENSO-like characteristics in the Botswana high over southern Africa. Thus, if the strength and location of the Botswana high could be accurately predicted, this may give an indication of the levels of rainfall that could be expected over parts of southern Africa. This could be particularly useful

because seasonal rainfall predictions over the region only seem to be reasonably accurate during strong ENSO seasons (Landman and Goddard, 2002). The results presented suggest that seasonal forecasters and climate scientists should pay attention not only to ENSO indicators but also to the Botswana high in investigating rainfall variability over southern Africa.

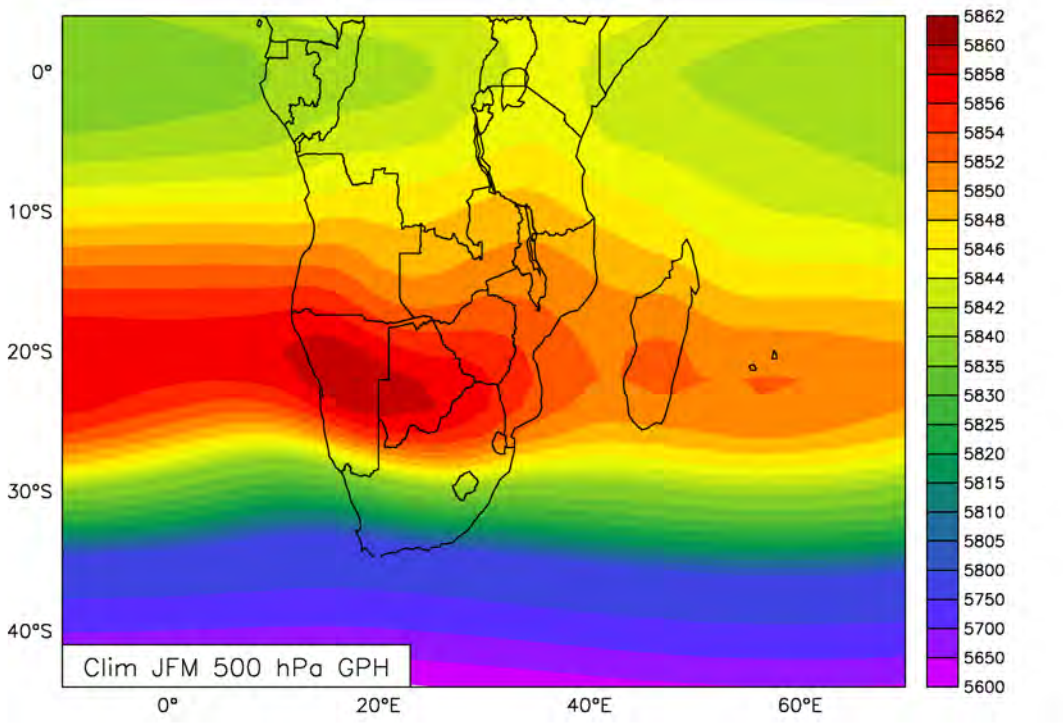

Figure 4.1: 20th Century climatological 500 hPa geopotential height for the JFM Season (in hPa)

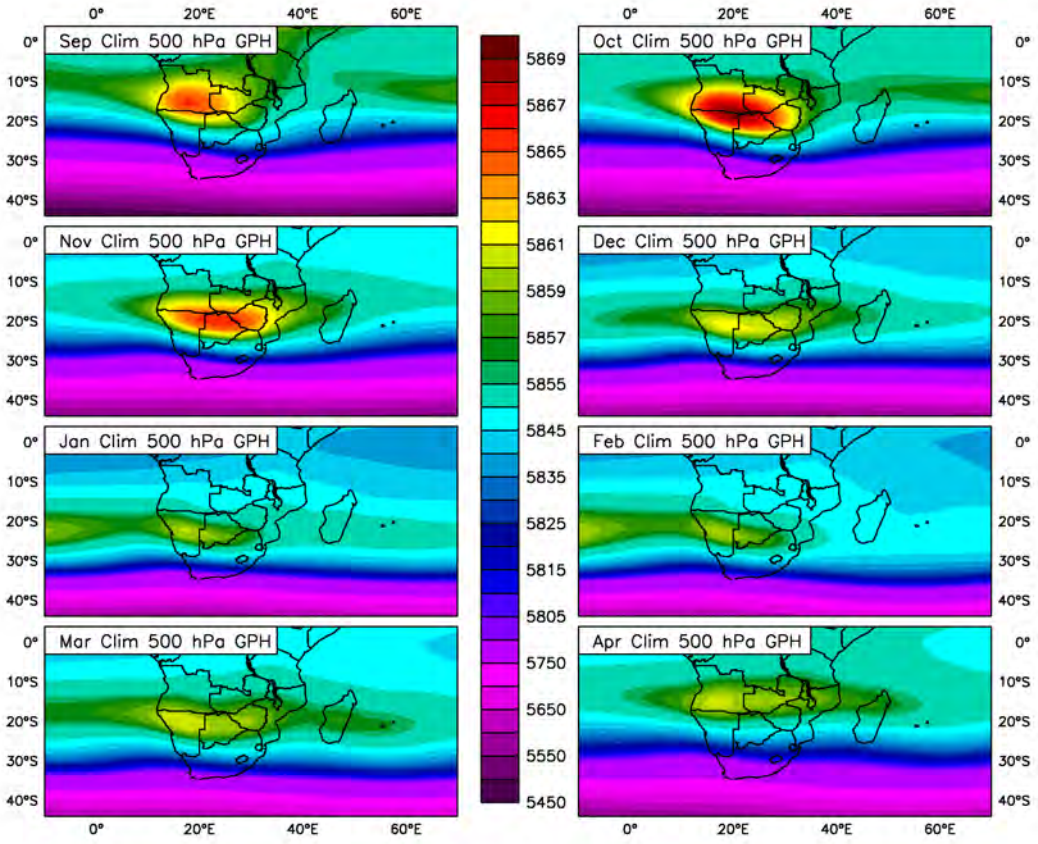

Figure 4.2: 20th Century climatological 500 hPa geopotential height for September - April (in hPa)

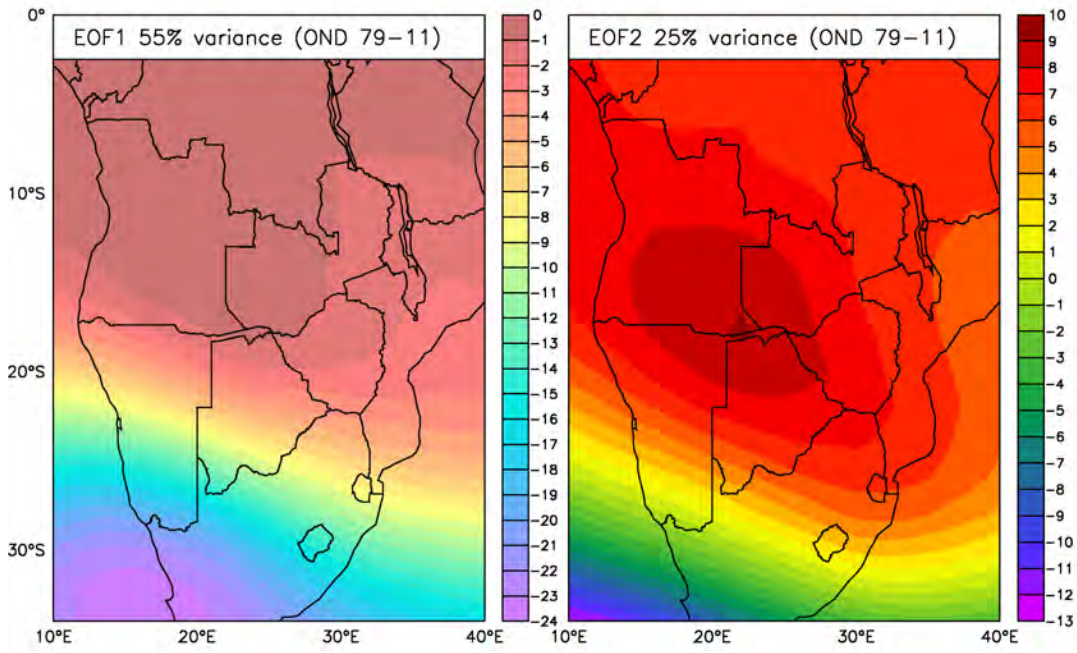

Figure 4.3: First two modes of EOF analysis using monthly 20th Century 500 hPa geopotential height for OND between 1979 and 2011

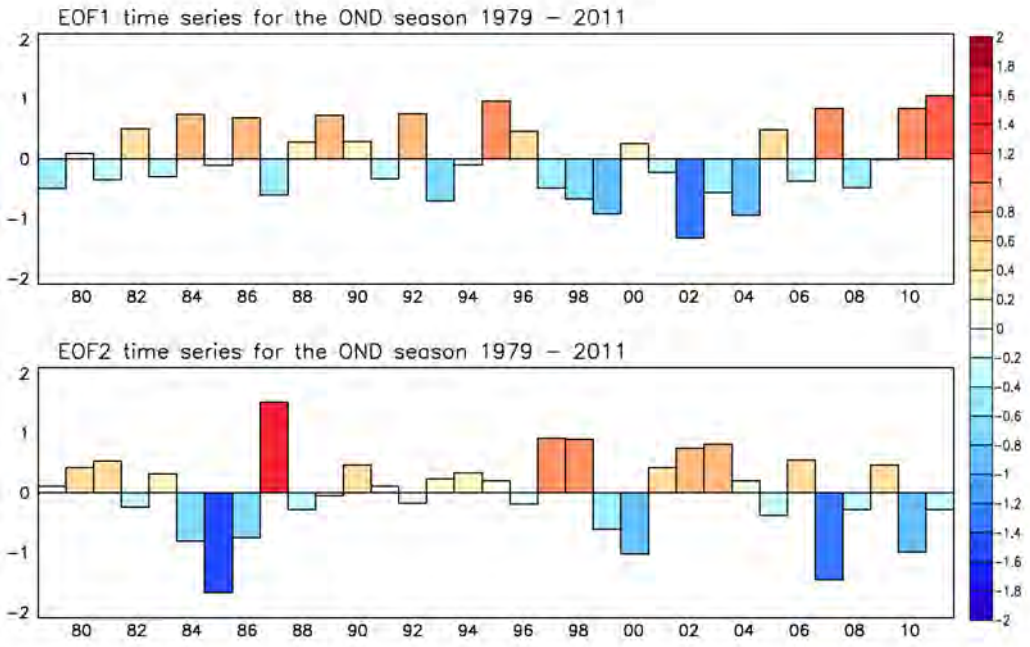

Figure 4.4: Time series corresponding to the OND EOFs in Figure 4.3

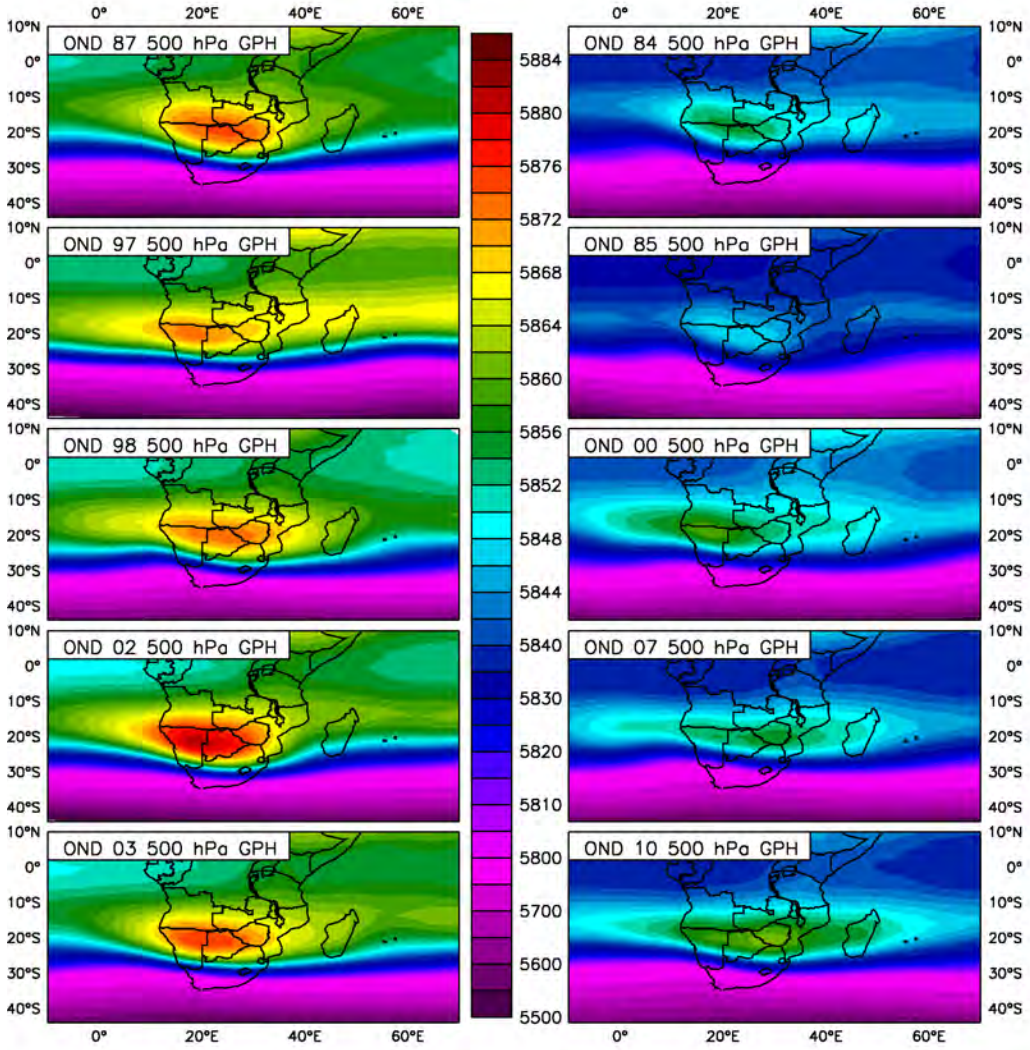

Figure 4.5: 20th Century 500 hPa geopotential height for OND 1987, 1997, 1998, 2002 and 2003 (the left hand side column) as well as 1984, 1985, 2000, 2007 and 2010 (the right hand side column) (in hPa)

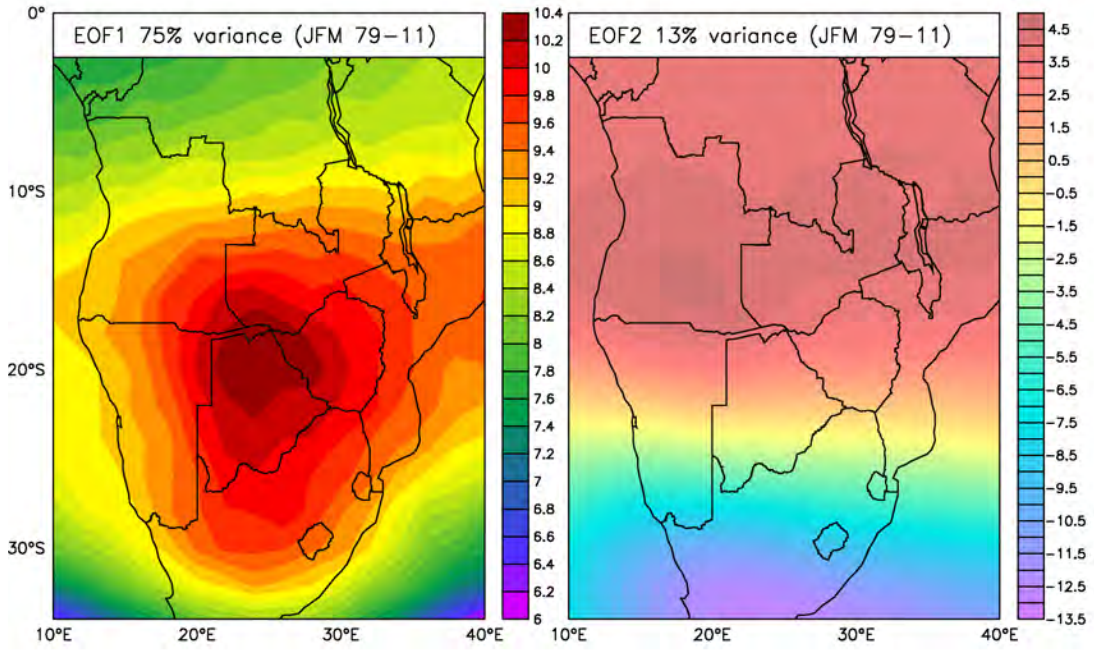

Figure 4.6: First two modes of EOF analysis using monthly 20th Century 500 hPa geopotential height for JFM between 1979 and 2011

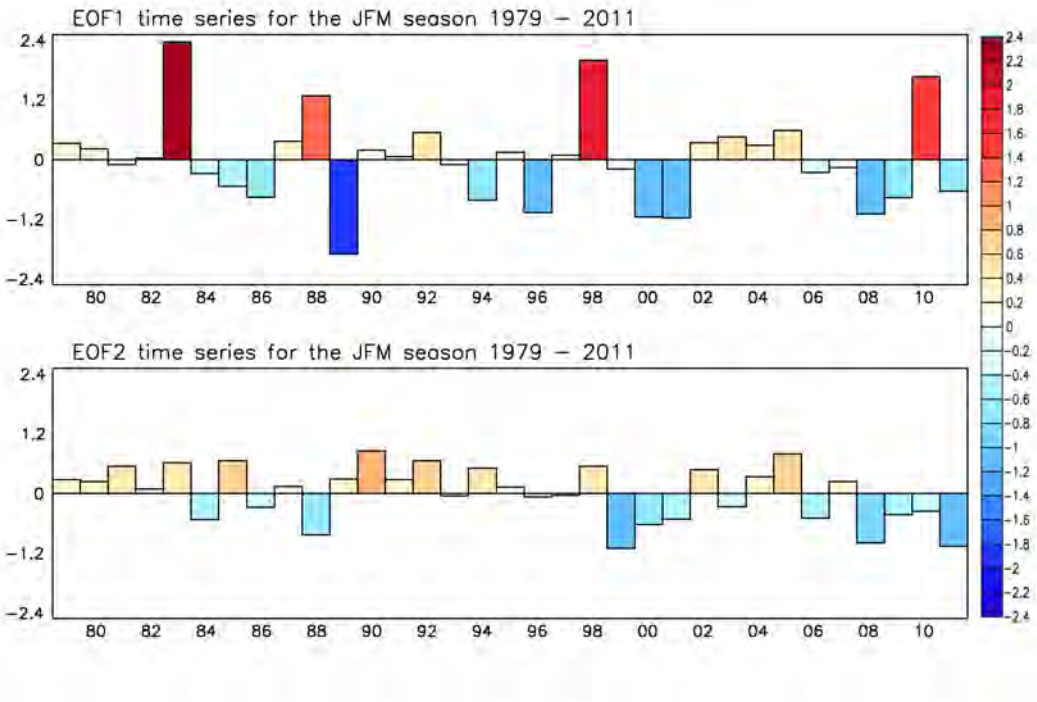

Figure 4.7: Time series corresponding to the EOFs in Figure 4.6

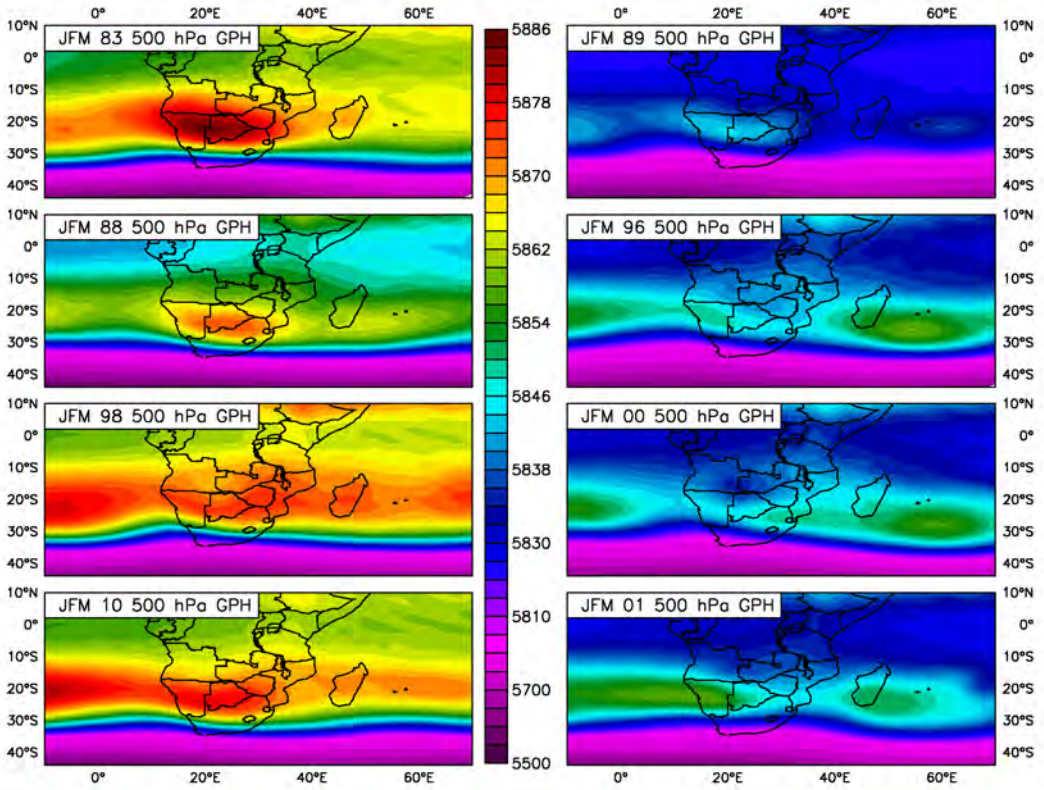

Figure 4.8: 20th Century 500 hPa geopotential height for JFM 1983, 1988, 1998 and 2010 as well as 1989, 1996, 2000 and 2001 (in hPa)

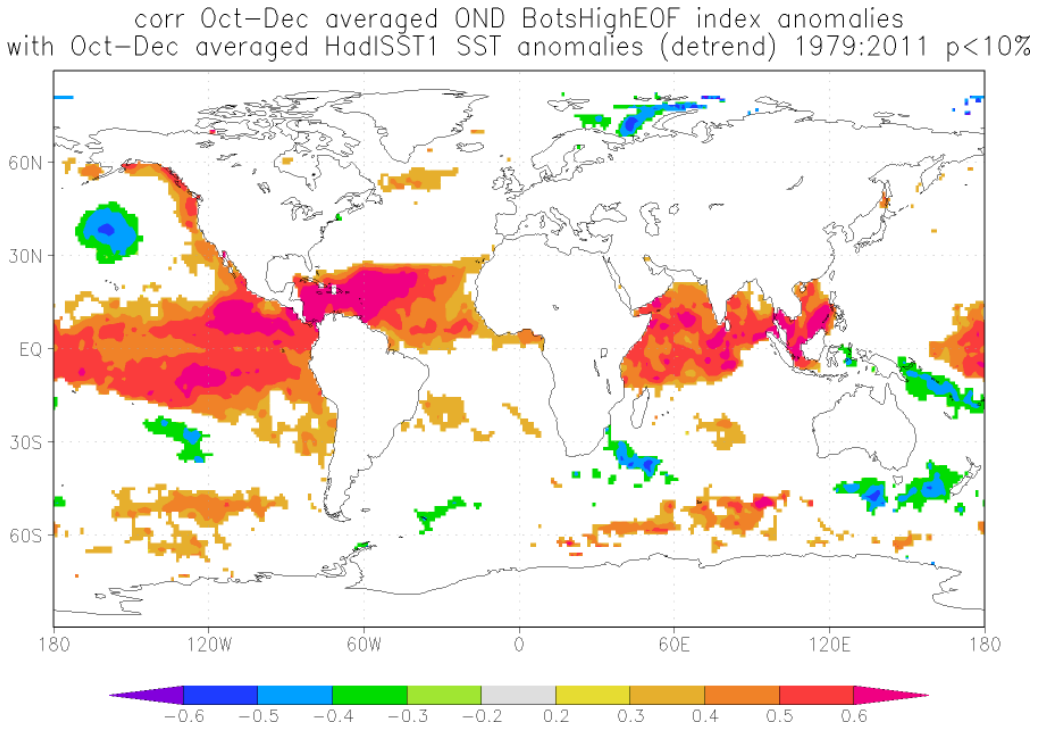

Figure 4.9: Correlation between the Botswana high (EOF2) and global SST (HadISST) for the OND season created on Climate Explorer

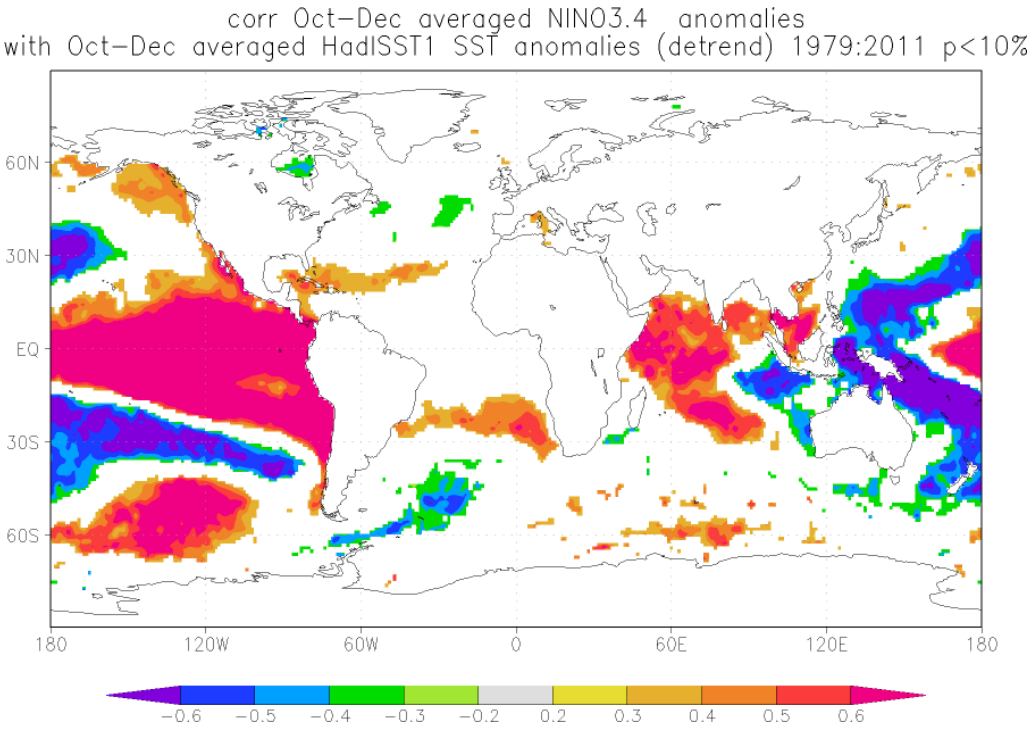

Figure 4.10: Correlation between ENSO and global SST (HadISST) for the OND season created on Climate Explorer

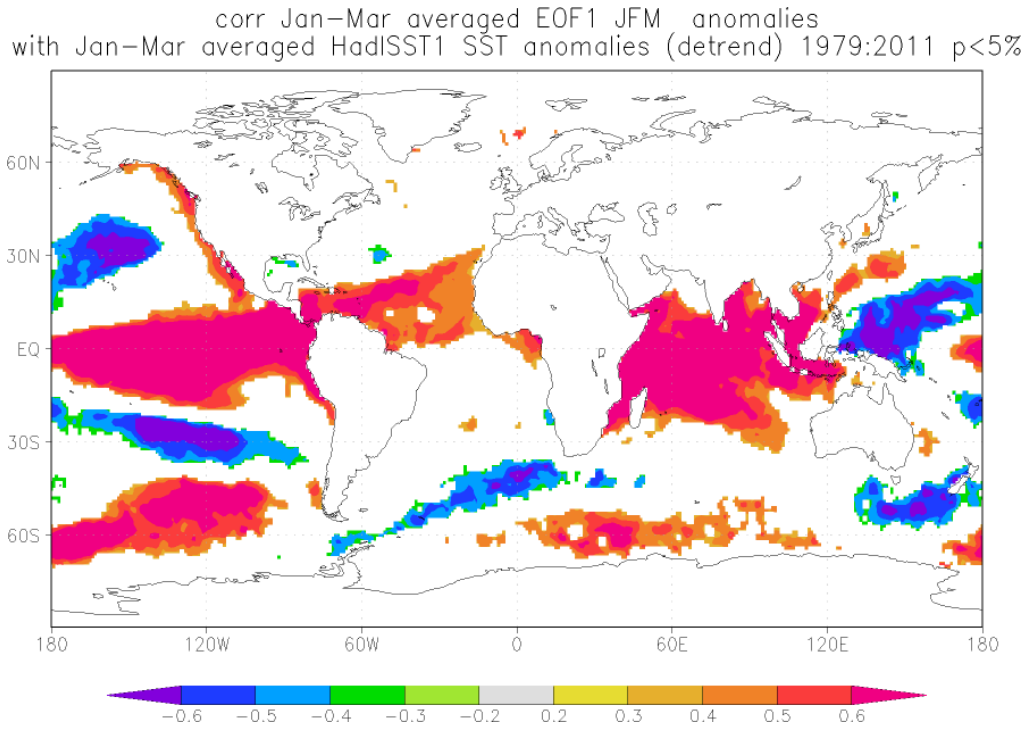

Figure 4.11: Correlation between the Botswana high (EOF1) and global SST (HadISST) for the JFM season created on Climate Explorer

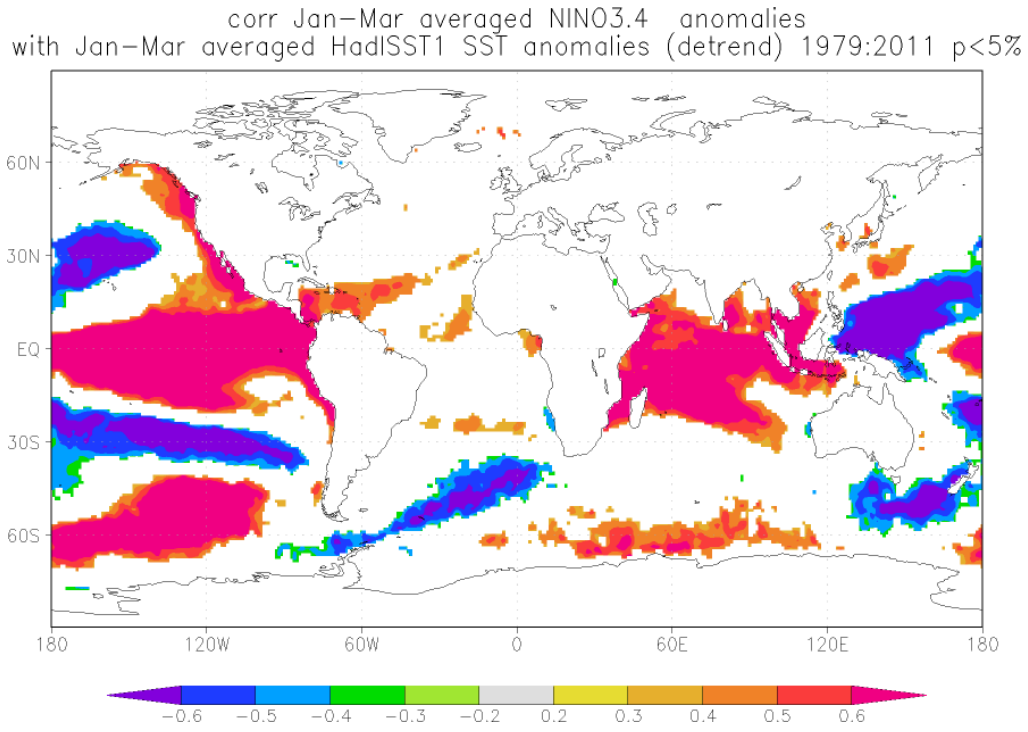

Figure 4.12: Correlation between ENSO (Niño 3.4) and global SST (HadISST) for the JFM season created on Climate Explorer

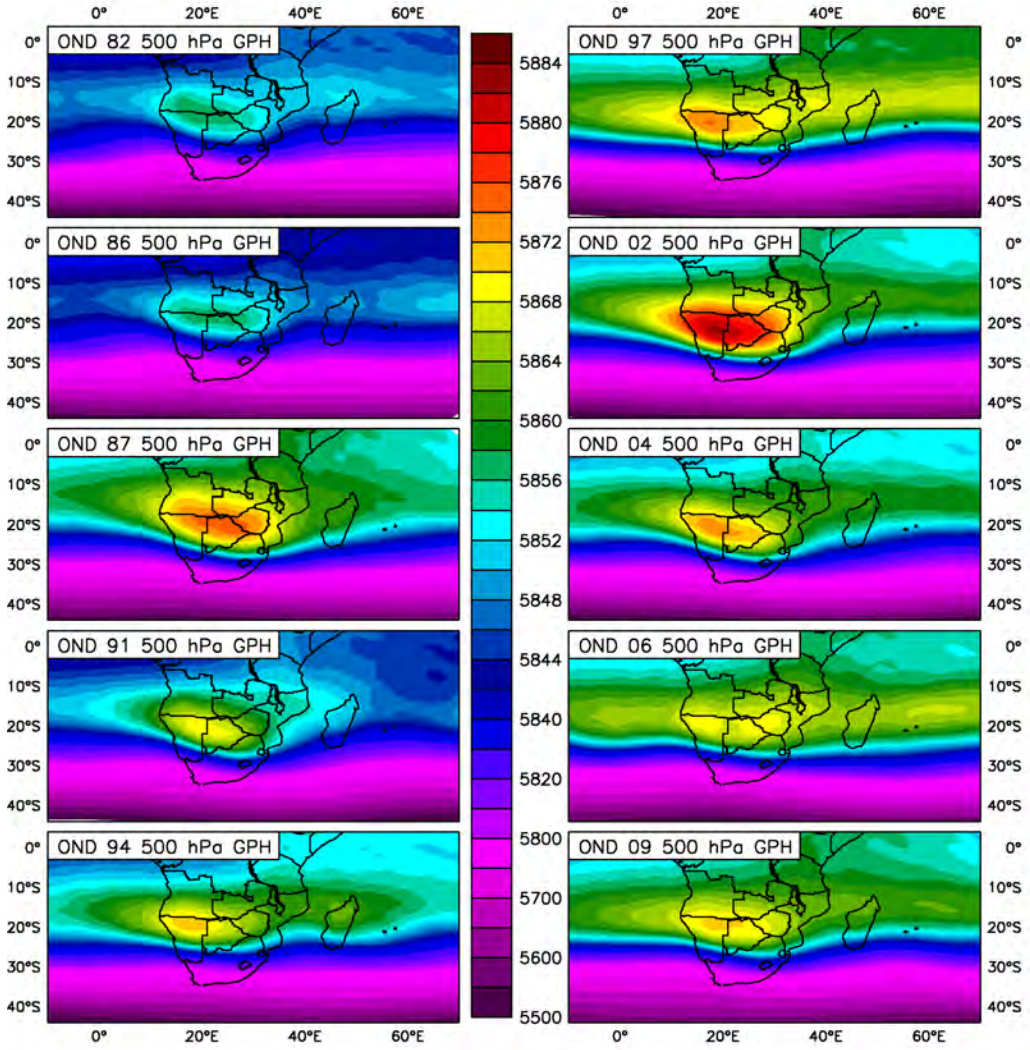

Figure 4.13: 20th Century 500 hPa geopotential height for the OND season during El Niño years (in hPa)

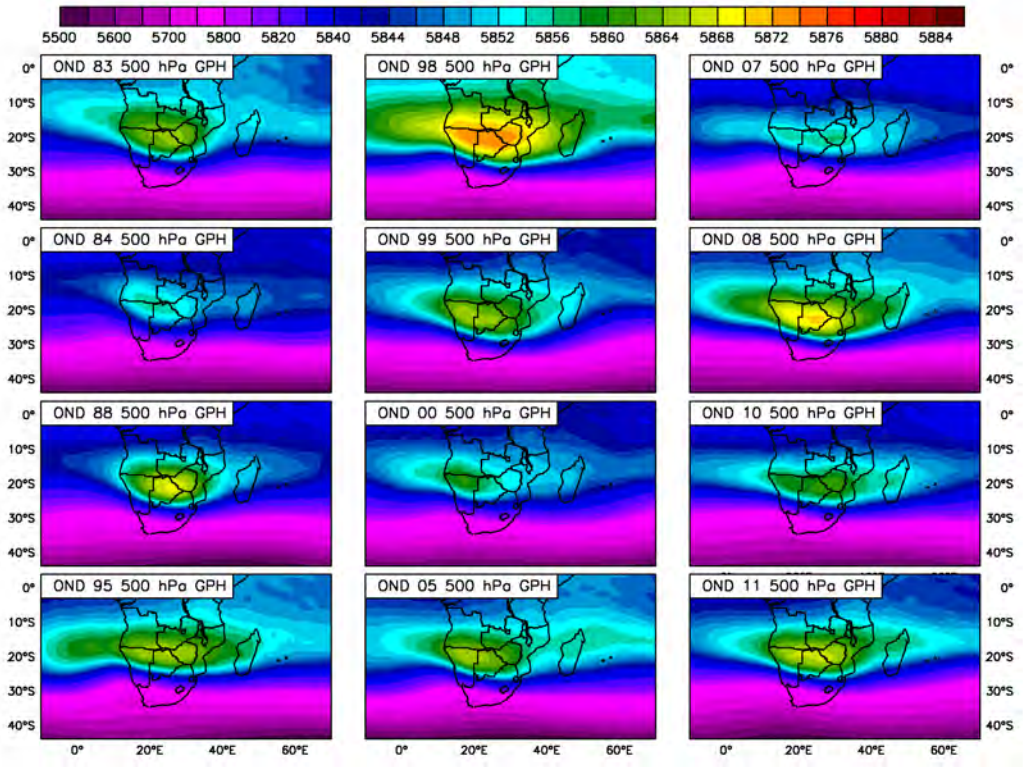

Figure 4.14: 20th Century 500 hPa geopotential height for the OND season during La Niña years (in hPa)

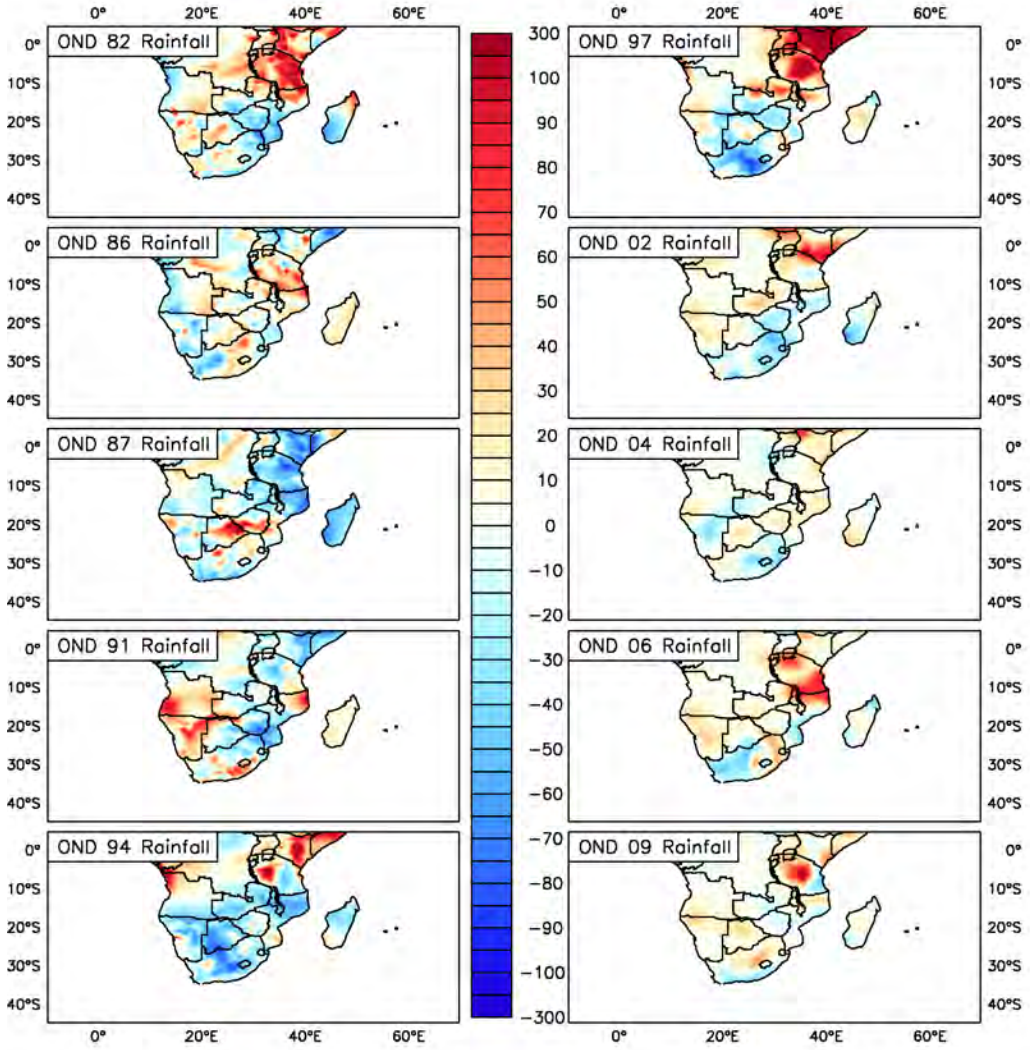

Figure 4.15: CRU Rainfall % Difference with Rainfall for the OND season during El Niño years between 1979 and 2011 (in $m \cdot s^{-1}$)

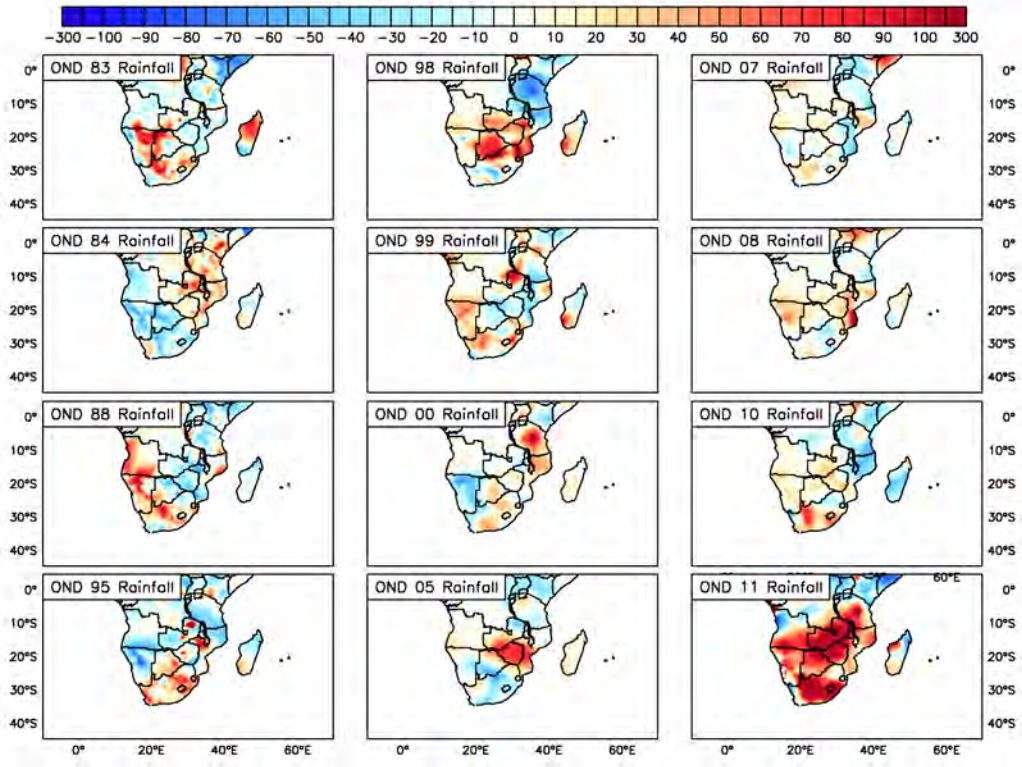

Figure 4.16: CRU Rainfall % Difference with Rainfall for the OND season during La Niña years between 1979 and 2011 (in $m \cdot s^{-1}$)

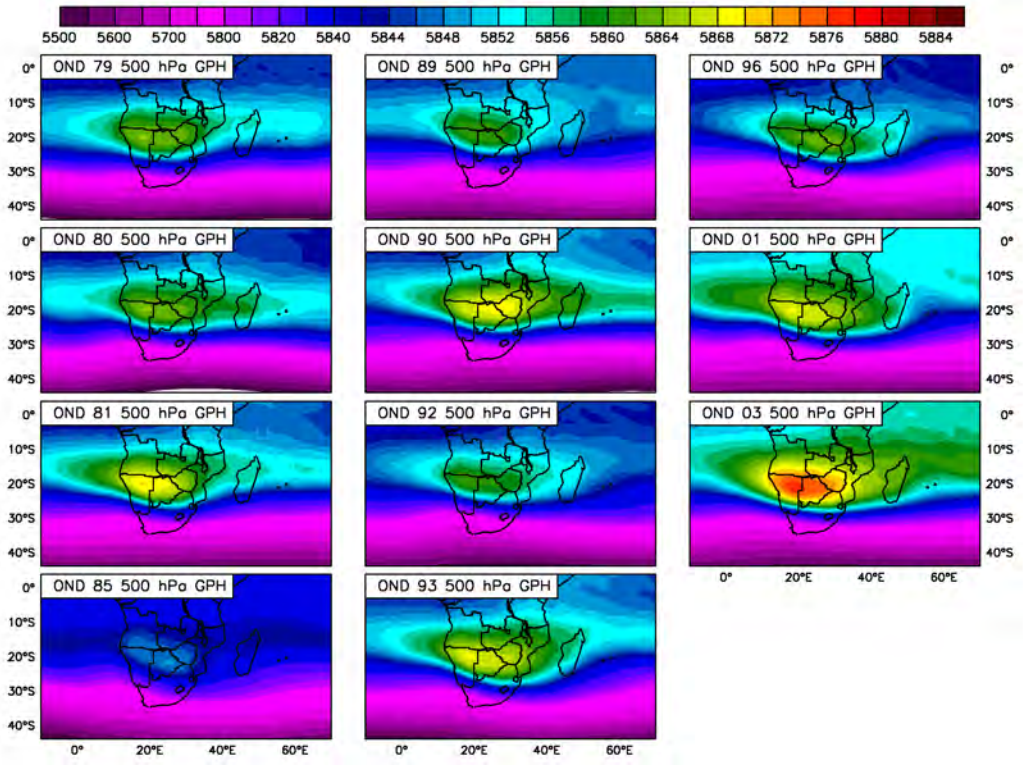

Figure 4.17: 20th Century 500 hPa geopotential height for the OND season during neutral years (in hPa)

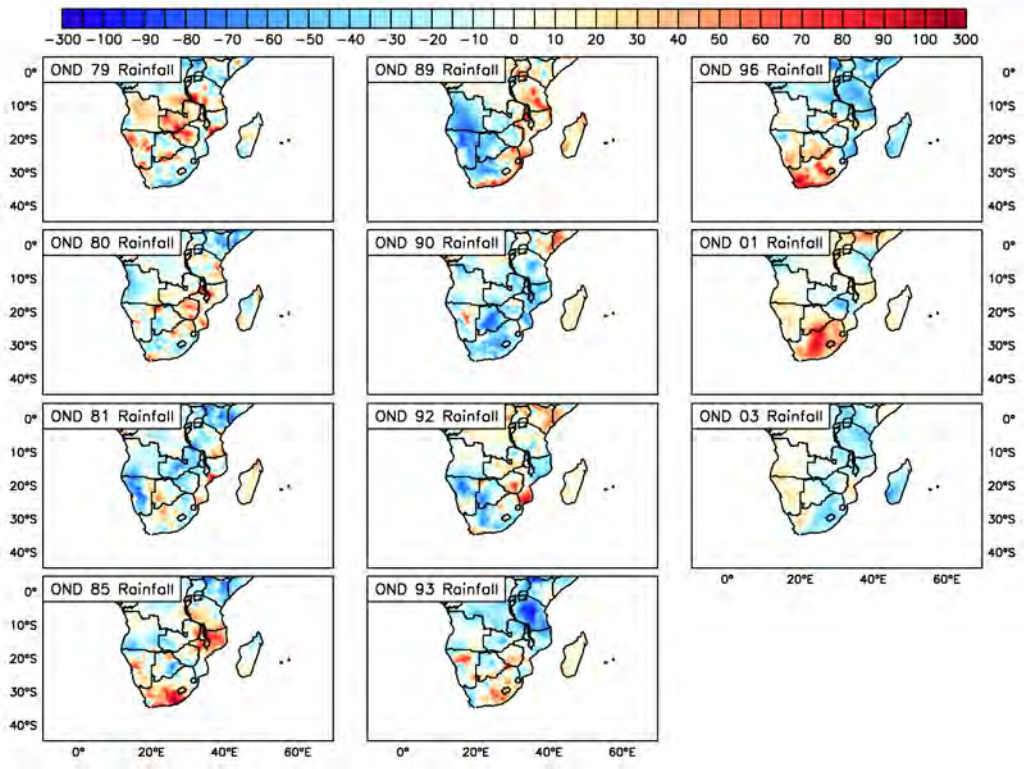

Figure 4.18: CRU Rainfall % Difference with Rainfall for the OND season during neutral years between 1979 and 2011 (in $m \cdot s^{-1}$)

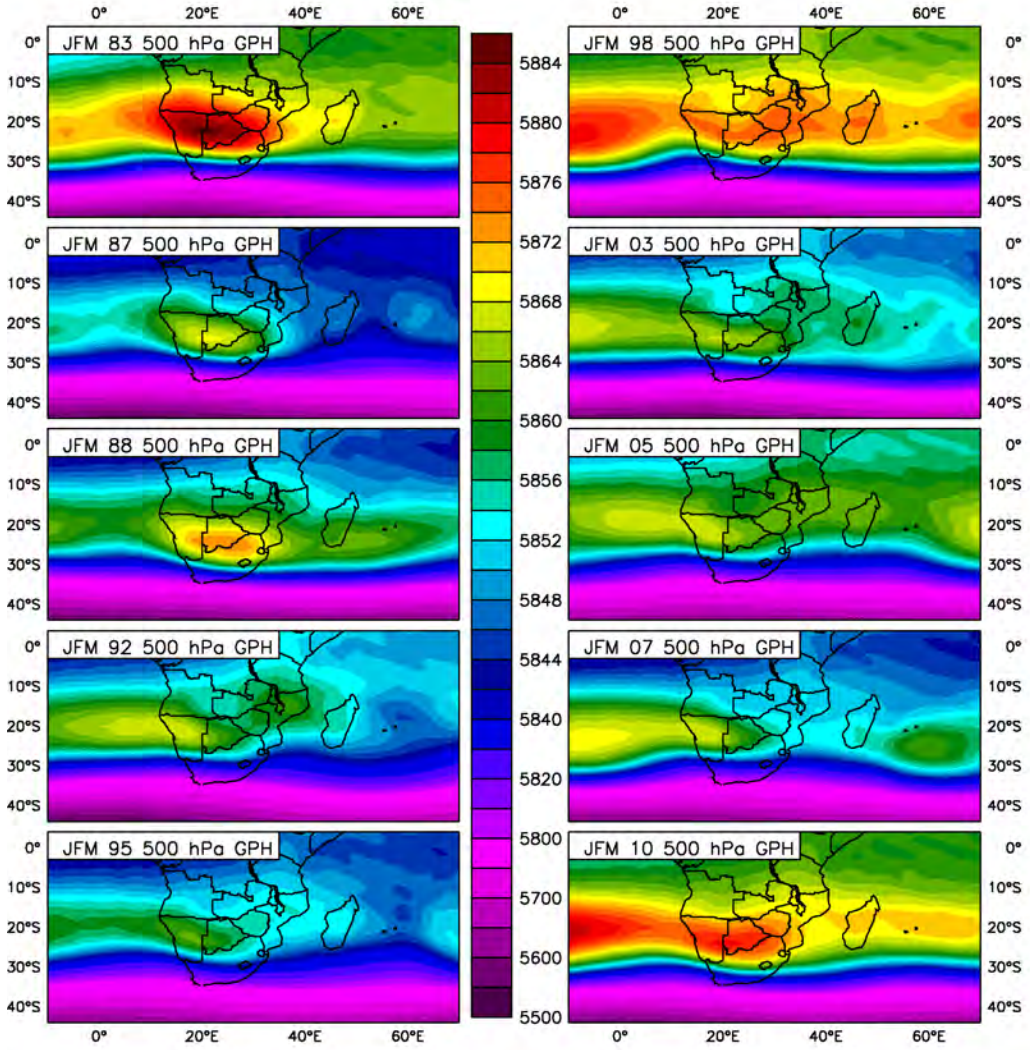

Figure 4.19: 20th Century 500 hPa geopotential height for the JFM season during El Niño years (in hPa)

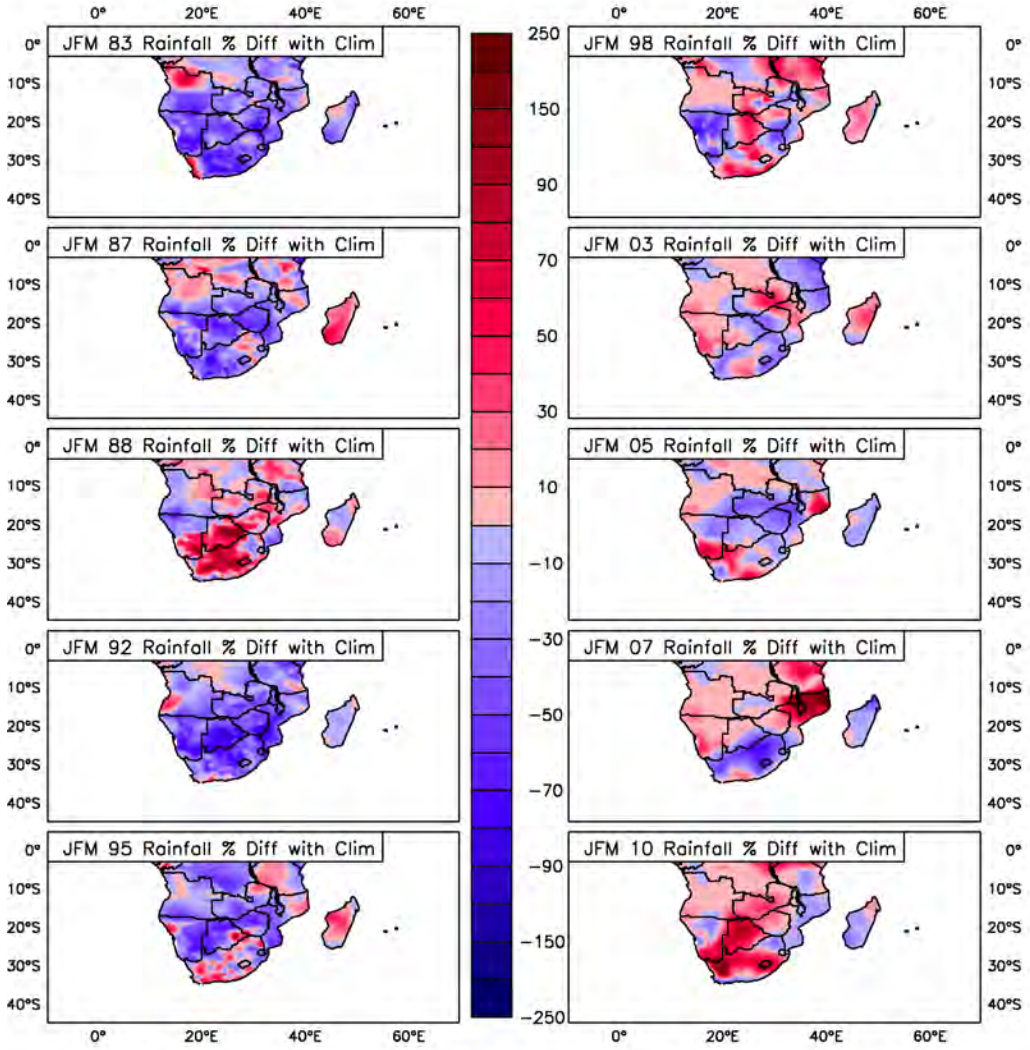

Figure 4.20: CRU Rainfall % Difference with Rainfall for the JFM season during El Niño years between 1979 and 2011 (in $m{\cdot}s^{-1}$)

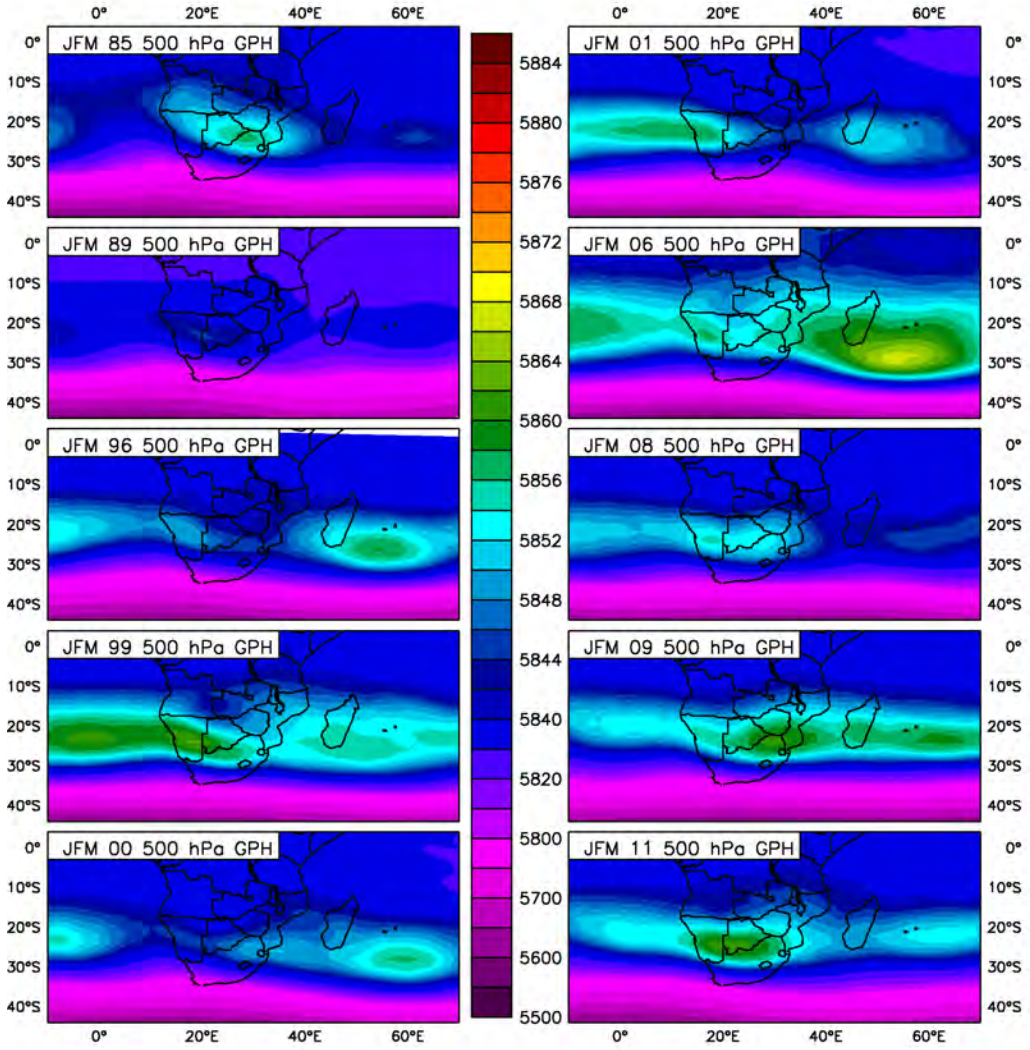

Figure 4.21: 20th Century 500 hPa geopotential height for the JFM season during La Niña years (in hPa)

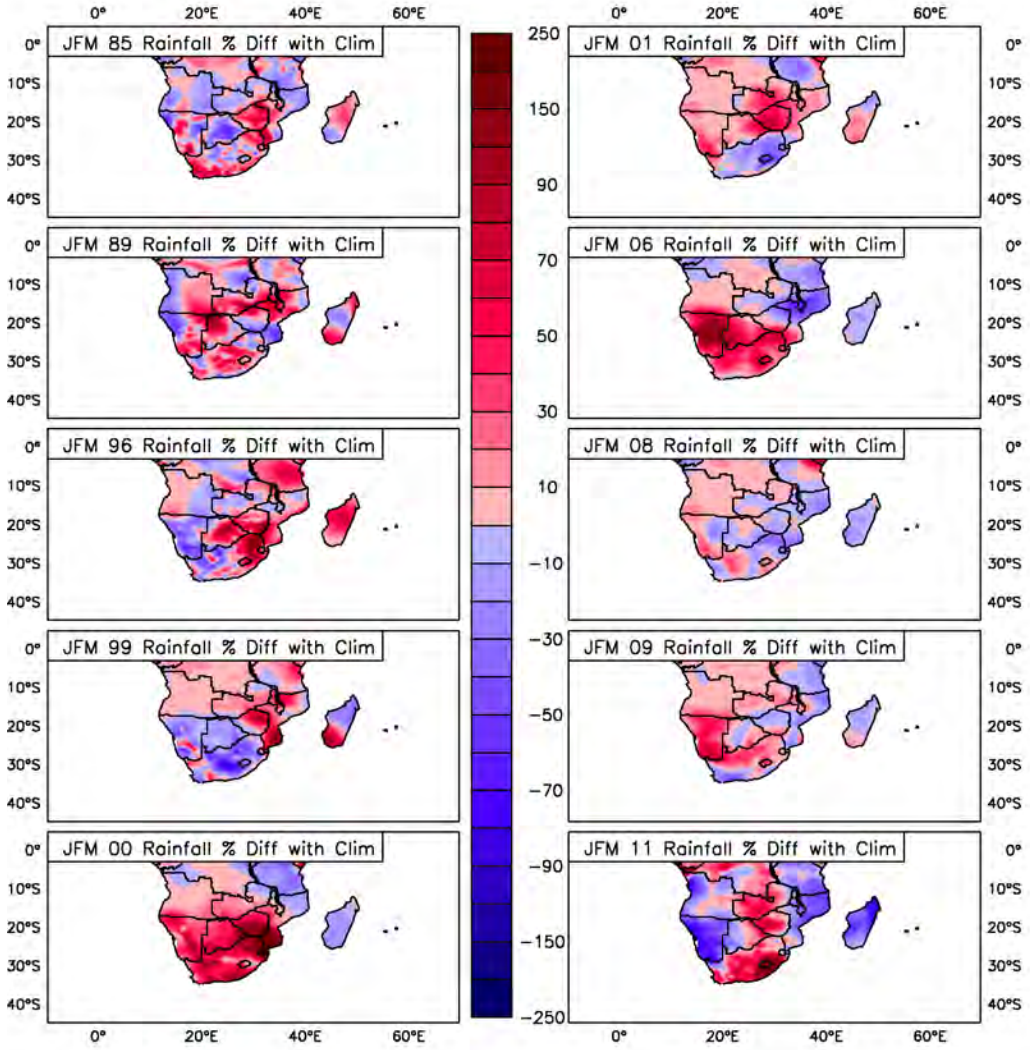

Figure 4.22: CRU Rainfall % Difference with Rainfall for the JFM season during La Niña years between 1979 and 2011 (in $m{\cdot}s^{-1}$)

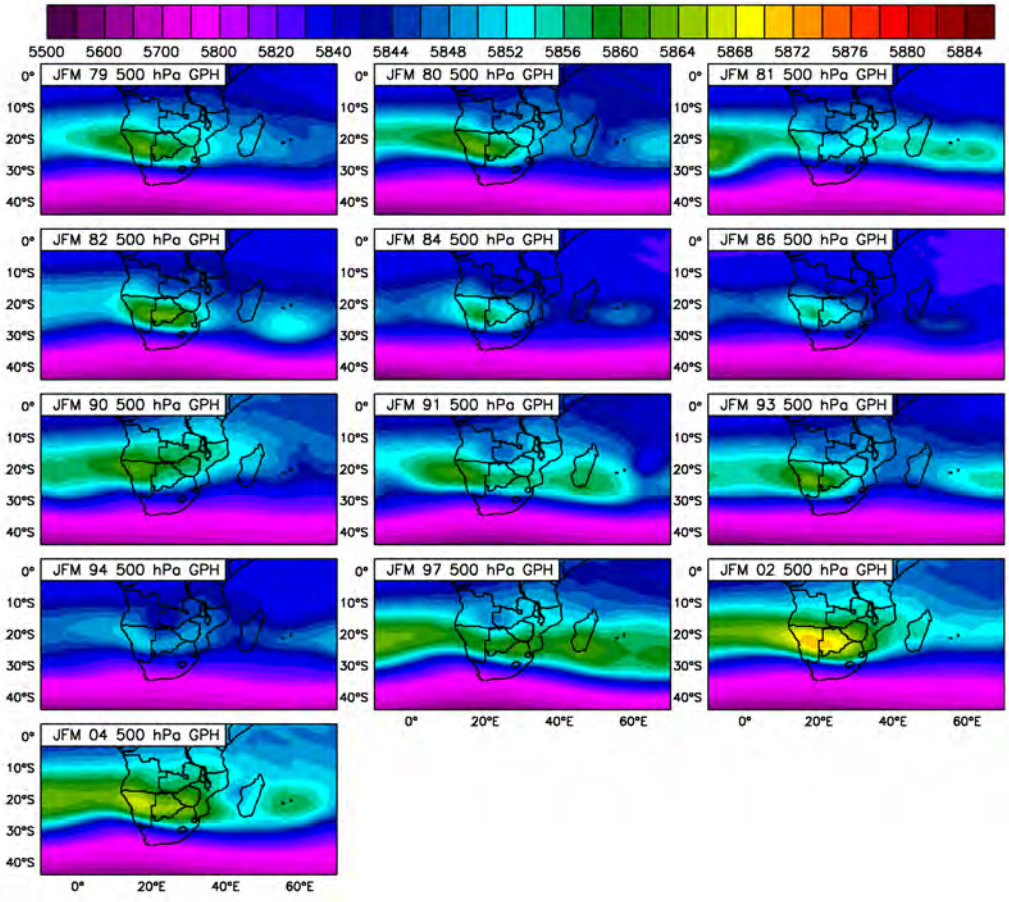

Figure 4.23: 20th Century 500 hPa geopotential height for the JFM season during neutral years (in hPa)

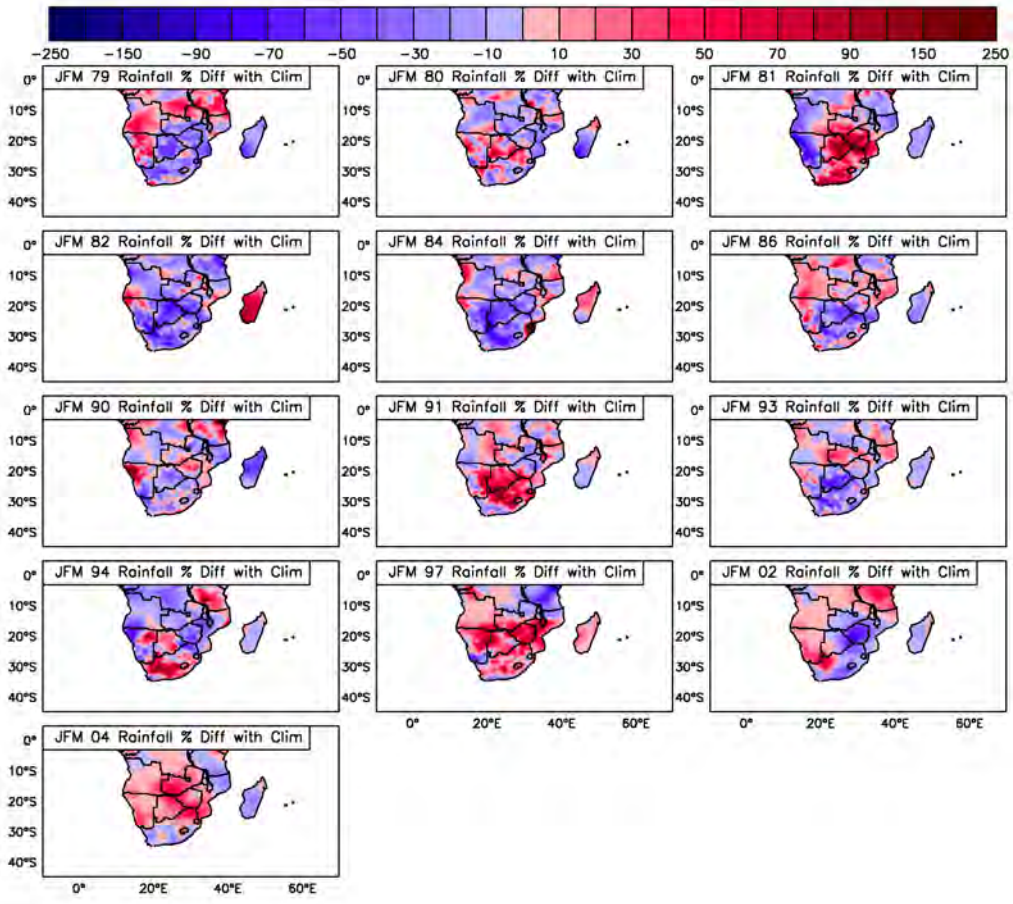

Figure 4.24: CRU Rainfall % Difference with Rainfall for the JFM season during neutral years between 1979 and 2011 (in $m{\cdot}s^{-1}$)

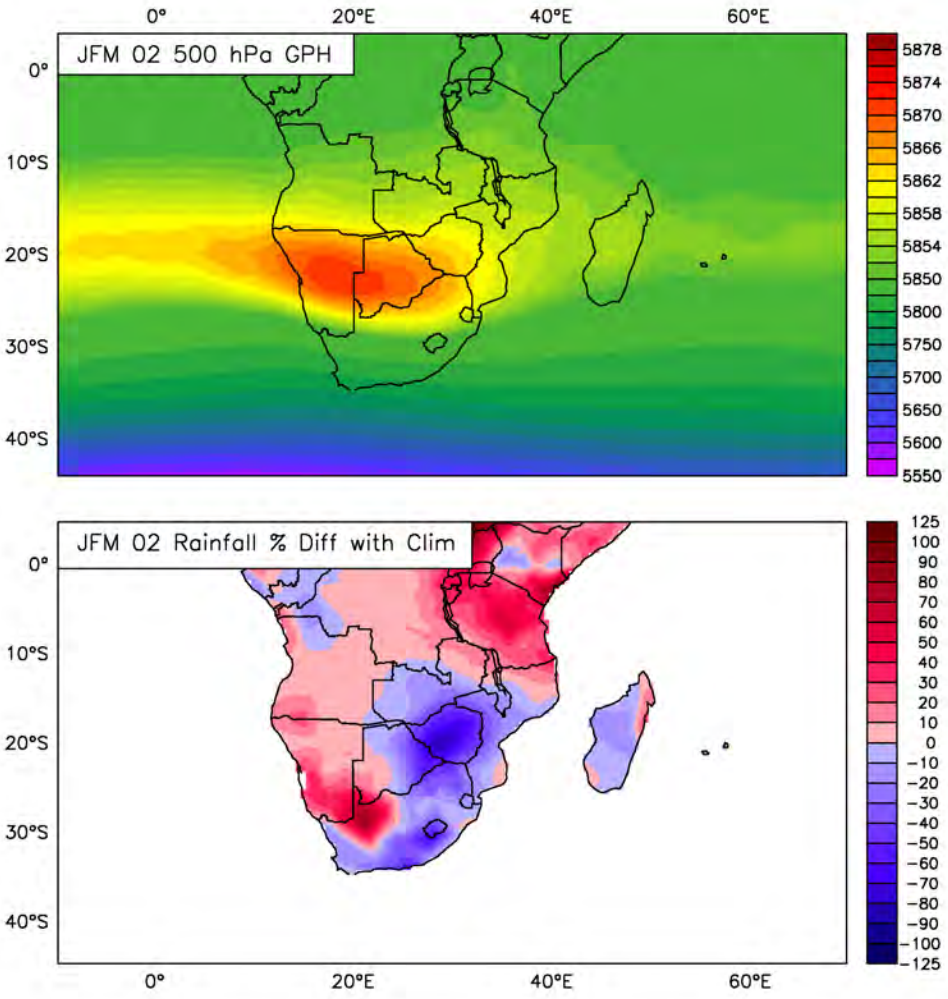

Figure 4.25: 20th Century 500 hPa geopotential height for the JFM 2002 season (top) and the % rainfall anomaly for JFM 2002 (in hPa)

Botswana high and Niño 3.4			**Botswana high and TIOD**		
Lag	Correlation	% Significance	Lag	Correlation	% Significance
-3	**0.43**	**99**	**-3**	**0.43**	**99**
-2	**0.47**	**99**	**-2**	**0.56**	**100**
-1	**0.49**	**100**	**-1**	**0.44**	**99**
0	**0.51**	**100**	**0**	**0.36**	**96**
1	**0.53**	**100**	1	0.25	85
2	**0.55**	**100**	2	0.23	80
3	**0.86**	**100**	3	0.18	68

Table 4.1: Summary of correlations between the Botswana high and Niño 3.4 as well as the TIOD for the OND seasons 1979-2011

Botswana high and Niño 3.4			**Botswana high and TIOD**		
Lag	Correlation	% Significance	Lag	Correlation	% Significance
-3	**0.46**	**99**	-3	0.13	52
-2	**0.73**	**100**	-2	-0.00	2
-1	**0.83**	**100**	-1	0.03	15
0	**0.87**	**100**	0	0.21	76
1	**0.87**	**100**	**1**	**0.45**	**99**
2	**0.87**	**100**	**2**	**0.53**	**100**
3	**0.86**	**100**	**3**	**0.53**	**100**

Table 4.2: Summary of correlations between the Botswana high and Niño 3.4 as well as the TIOD for the JFM seasons 1979-2011

Botswana high and AMO			**Botswana high and SAM**		
Lag	Correlation	% Significance	Lag	Correlation	% Significance
-3	-0.22	77	-3	-0.01	2
-2	-0.13	53	-2	-0.1	41
-1	-0.27	87	-1	-0.03	12
0	**-0.36**	**96**	0	-0.20	74
1	**-0.42**	**98**	1	-0.23	84
2	**-0.40**	**98**	**2**	**-0.50**	**100**
3	-0.33	94	**3**	**-0.42**	**98**

Table 4.3: Summary of correlations between the Botswana high and the AMO as well as the SAM for the JFM seasons 1979-2011

Chapter 5

Dry Day Frequency Over Southern Africa

This chapter investigates the frequency of dry days over southern Africa. This parameter is generally of more interest to user groups (e.g. water resources, agriculture) than more common parameters provided by meteorological services such as seasonal rainfall totals. Most rain-fed crops are more likely to flourish with uniformly spread light rainfall than with a few heavy events interrupted by dry spells (Usman and Reason, 2004; Reason et al., 2005). Crops such as maize, sorghum or millet need to be planted at the correct time before the rains are too heavy and cause the seed to be washed away. On the other hand, the rains need to be sufficiently substantial to ensure proper germination of the seeds. In this context, information regarding rainfall variables such as number of dry days in the summer rainy season

and their duration would be of huge benefit to subsidence farmers living in southern Africa.

In line with previous work (e.g. Mulenga et al. (2003); Reason et al. (2005); Hachigonta and Reason (2006); Hachigonta et al. (2008)), two tropical regions and two subtropical regions are chosen for the purpose of investigating dry day frequency (hereafter referred to as DDF). These four regions are identified in **Figure 5.1** and are referred to in the text as coastal northern Angola [Box 1]; central South Africa [Box 2]; Limpopo [Box 3]; and North East Zambia [Box 4].

A full description of the data used in this chapter is given in Chapter 3. However, a short discussion is necessary here to clarify the choice of datasets in the different sections. The daily GCPC rainfall dataset has a relatively high resolution of 1^ox1^o and is available from the year 1997 to the present. Due to its high resolution, it was chosen for the study of DDF over southern Africa. However, since this dataset only starts in 1997, the time series of JFM seasons is perhaps not long enough for robust correlation analysis. On the other hand, GPCP has also produced a lower spatial resolution (2.5^ox2.5^o) dataset for rainfall which is available from 1979 to the present at pentad (5 day) intervals. The dataset covering the longer period of time is more appropriate for use in correlation analysis. Therefore, the longer time series pentad data is used to investigate correlations between the DDF over the

four regions of interest and global SSTs, while the higher spatial resolution data is used to investigate the DDF over the four regions of interest during the JFM season. For the purpose of this study, a dry day is defined to be a day on which less than 1mm of rainfall is recorded and a heavy rain day is one on which more than 10mm of rainfall is recorded. This is the same definition used by the Famine and Early Warning System (FEWS) and was also the basis of the definition of wet and dry spells in numerous other studies including Usman and Reason (2004); Reason et al. (2005); Hachigonta and Reason (2006); Hachigonta et al. (2008).

5.1 Dry Day Frequency During the JFM Season

Two plots of the number of dry days over southern Africa during the JFM season are given in **Figure 5.2**. The top panel uses GPCP mean daily rainfall data at 1^ox1^o grid resolution averaged from 1997 to 2012. The bottom panel uses CMAP mean pentad rainfall data (previously analysed by Usman and Reason (2004) in their study of dry spell frequency) at 2.5^ox2.5^o grid resolution averaged from 1979 to 2011. The GPCP data was processed as daily data rather than pentads but, for ease of comparison with CMAP, the days are grouped into pentads. Usman and Reason (2004) produced a very similar figure using CMAP pentad data, however their season of interest was DJF and the data used to create their climatology ran from 1979 until 2002.

Figure 1 in Usman and Reason (2004) and both plots in **Figure 5.2** produce the same general pattern of dry days over southern Africa despite the data set differences mentioned. There are significant dry regions over the South Atlantic Ocean corresponding to the South Atlantic Anticyclone. The high incidence of dry days persists along the western coast of southern Africa up to a latitude just north of the Angola Benguela Frontal Zone. There is another dry region over the Central South Indian Ocean which also corresponds to a semi-permanent high pressure system (the South Indian Anticyclone). The region lying within the area between approximately 5-15^{o}S and 15-35^{o}E displays a reduced number of dry days which is to be expected since this region corresponds with the position of the ITCZ during the JFM season. Usman and Reason (2004) identified the band of high DDF between 20^o and 25^{o}S as the drought corridor that runs across subtropical southern Africa. There is also a low DDF region over eastern South Africa below the drought corridor. This region of relatively low DDF over Lesotho and southern KwaZulu Natal/northern Eastern Cape provinces is related to the Drakensberg and Maluti Mountains and the onshore flow of moist marine air as migratory anticyclones ridge into the South West Indian Ocean (**Figure 5.3**). Orographic effects are also apparent over eastern and northern Madagascar as well as in a rain shadow effect west of southern Madagascar.

In general, CMAP pentad data (lower panel) has a lower frequency of

dry days than GPCP (upper panel) which is also reflected in the rainfall climatology where CMAP displays reduced JFM rainfall over southern Africa compared to GPCP (**Figure 5.4**). There is also a more complex pattern of DDF over central southern Africa in the GPCP plot which is likely to be due to the higher resolution data capturing more small scale features of rainfall and lower topographic effects.

5.2 Correlations Between Dry Day Frequency and Sea Surface Temperature Indices

Pentad GPCP rainfall data is used in this section to create DDF time series from 1979 to 2011 for the four regions of interest and correlate them with global SST indices. The correlations obtained may indicate which global SSTs impact the frequency of dry days over each region. All correlation analyses are performed using the built-in correlation functions in Climate Explorer (detailed in Chapter 3) and only those correlations that produced 95% or higher statistically significant values at lags of between -3 and 3 months are included. ENSO is measured via the Niño 3.4 SST index (Barnston and Ropelewski, 1992) and the TIOD is measured via the dipole mode index (DMI; Saji et al. (1999)). The SIOD is measured using the subtropical dipole index (SDI; Behera and Yagamata (2001)). The NAO index is taken from the Climate Prediction Centre (Barnston and Livezey, 1987). The AMO index is calculated as defined in Trenberth and Shea (2006). The SAM

index is sourced from the British Antarctic Survey (BAS) (Limpasuvan and Hartmann, 1999).

5.2.1 Coastal Northern Angola

The time series showing the standardised anomalies of the area average DDF over coastal northern Angola between 1979 and 2011 is shown in **Figure 5.5**. This time series is correlated with a number of SST indices in order to identify those which might impact the DDF. **Figure 5.6** shows the correlation between this time series and global SSTs which indicates that SSTs over the tropical South Atlantic Ocean are correlated with dry spells over coastal northern Angola, as are those over the tropical South Indian Ocean. On the other hand, there is a statistically significant correlation between the DDF and the AMO and the NAO over the Atlantic Ocean. The correlations between the DDF time series over coastal northern Angola and the AMO as well as the NAO are summarised in **Table 5.1**. DDF over coastal northern Angola has a correlation of r= 0.51 with the AMO (at 100% statistical significance). The correlation is slightly stronger, r= 0.56 at 100% statistical significance, when a lag of -1 month is introduced, which is to say that JFM DDF over the region is correlated with the FMA AMO, and remains statistically significant for almost the entire range of lags presented here. The impact of the AMO has been discussed in relation to the Sahel drought (Folland et al., 1986), the frequency of Atlantic hurricanes (Goldenberg et al., 2001), Northeast Brazilian rainfall (Folland et al., 2001), North

American and European summer climate (Sutton and Hodson, 2005; Nigam et al., 2011), and the Asian summer monsoon (Lu et al., 2006). However the AMO has not previously been associated with rainfall variability over southern Africa.

The NAO and DDF over coastal northern Angola are correlated with a value of r= 0.38 (at 97% statistical significance) and this correlation rises to r= 0.50 (at 100% statistical significance) with a lag of 1 month, which is to say that JFM DDF over the region is correlated with the DJF NAO. This positive correlation is consistent with the results of Todd and Washington (2004), who documented a strong teleconnection between central equatorial African (CEA) rainfall and the large-scale circulation over the North Atlantic Ocean, similar to those associated with the NAO. The region over which they define the CEA includes part of coastal northern Angola and, although the CEA region is generally fairly insensitive to global tropical ocean SST forcings, they do appear to be associated with tropical North Atlantic Ocean forcings.

There was no statistically significant correlation between the DDF over coastal northern Angola and the Niño 3.4 index suggesting that ENSO does not play a significant role in dry spells over this region. There were also no statistically significant correlations when considering the Benguela Niño region, which was defined to be the region within 8^oE-15^oE and 10^oS-20^oS

(Rouault et al., 2009). Although Benguela Niños (Niñas) have been associated with increased rainfall over western and northern Angola, the main rainy season in Angola occurs during FMA and the region of interest covered in this study is to the north of the landmass adjacent to where the maximum SSTAs would occur during a Benguela Niño event (Rouault et al., 2003a; Grimm and Reason, 2011).

The correlations between the time series and the SAM are summarised in **Table 5.2**. The correlation between the dry day time series and SAM is r= 0.5 (at 100% statistical significance) and approximately the same when a 1 month lag is considered, which means that JFM DDF over coastal northern Angola is correlated with the DJF SAM. It is most likely that SAM could influence the strength and position of the South Atlantic Anticyclone and hence rainfall over Africa, and in particular coastal northern Angola (Pohl et al., 2010; Malherbe et al., 2014).

The correlation between the DDF series and the Botswana high index is r= -0.37 (at 96% statistical significance, not shown) at a lag of -1 month, so JFM DDF over the region is correlated with the FMA Botswana high. A possible explanation for this correlation is the northward shift of the Botswana high in April when it centres over southern Angola (**Figure 4.2**).

5.2.2 Central South Africa

The second panel in **Figure 5.5** shows the time series for the standardised anomalies of the area average DDF over central South Africa during the JFM season from 1979-2011. The correlation map between this time series and global SSTs can be seen in **Figure 5.7** which displays a strong correlations over the western Indian Ocean. The TIOD does correlate at a statistically significant value despite the absence of the eastern Indian Ocean pole, while the SIOD does not. Correlations between the DDF over central South Africa and the TIOD and AMO are summarised in **Table 5.4**. A correlation of r= -0.36 (at 96% statistical significance) exists with the TIOD implying that there are more dry days when the TIOD is in its negative phase. This correlation is higher at a lag of both 1 and -1 months which means that JFM DDF over central South Africa is correlated at a value of r= -0.37 (at 97% and 96% statistical significance, respectively) with the DJF and FMA TIOD, respectively, and is still significant at a lag of -2 months. The DDF of central South Africa has a correlation of r= 0.47 (at 99% statistical significance) with the AMO. The time series is also correlated with the AMO at lags of -1, 1 and 2 months. A possible association between rainfall over South Africa and the AMO does not seem to have been studied as yet.

5.2.3 Limpopo

The time series of standardised anomalies of the area averaged DDF over the Limpopo region from 1979-2011 is shown in the third panel of **Figure 5.5**. The correlation map of this time series with global SSTs indicates that there is a relationship between ENSO and DDF over the Limpopo region (**Figure 5.8**). The correlation coefficient between the DDF and the Niño 3.4 index is r= 0.37 (at 96% statistical significance, **Table 5.5**). This is less than the correlation coefficient of r= 0.5 that Reason et al. (2005) found when using CMAP pentad data over almost the same region during DJF for the period 1979-2002, which could be due to the fact that 9 more years were included in this study. The correlation between DDF over the Limpopo region and the Niño 3.4 index strengthens when a lag of -1,-2 and -3 months are introduced. The JFM DDF is correlated with the decaying ENSO signal during the season of FMA (r= 0.4 at 98% statistical significance), MAM (r= 0.44 at 99% statistical significance), and AMJ (r= 0.41 at 98% statistical significance). DDF over this region is also correlated with the Botswana high at r= 0.37 (at 96% statistical significance) at zero lag.

5.2.4 North East Zambia

The lower panel in **Figure 5.5** shows the time series of standardised anomalies of the area averaged DDF over North East Zambia. The correlation map of this series with global SSTs is shown in **Figure 5.9** which

indicates a strong relationship with both ENSO and the South East Atlantic Ocean. **Table 5.6** shows the correlations between the DDF over NE Zambia and the Niño 3.4 index as well as the Benguela Niño index. The correlation between the DDF time series and the Niño 3.4 index is r= 0.48 (at 99% statistical significance) and, in fact, the JFM seasonal DDF over North East Zambia is correlated with the Niño 3.4 index at values between r= 0.47 and r= 0.54 (at statistical significance greater than 99%) when lags of up to 3 months in both directions are considered. El Niño is associated with below average rainfall over the region and Hachigonta and Reason (2006) established that there was an increase in the frequency of dry spells and a decrease in the frequency of wet spells over the region during El Niño events during the DJF season.

The DDF over this region is also correlated with Benguela Niño with a value of r= -0.36 (at 95% statistical significance). This indicates that Benguela Niña events may contribute to DDF as far inland as North East Zambia. The DDF over North East Zambia has a correlation coefficient of r= 0.37 (at 95% statistical significance, not shown) with the Botswana high at a lag of 1 month, ie. the DJF Botswana high. This association could be due to the northward position of the Botswana high during December as well as its elongated shape extending eastward over much of the subcontinent (**Figure 4.2**).

5.3 Dry Day Frequency During JFM 1998

The JFM rainfall levels for both the 1998 and 2010 JFM seasons were above average over much of southern Africa which was not expected from the predictions made for the mature phase El Niño seasons. This section examines whether the number of dry days during these two rainfall seasons was also anomalous, and, if so, the role that dry days may have played in the JFM 1998 and 2010 late summer seasons. The prediction of dry conditions over southern Africa during the 1997-1998 austral summer rainfall season (Mason et al., 1999b; Buizer et al., 2000; Lyon and Mason, 2007) was linked with the strong El Niño that occurred during 1997-1998 and the typical association of El Niño with drought conditions over southern Africa. However, the widespread drought conditions that were expected generally failed to materialise and, in fact, seasonal rainfall in some regions was observed to be near or above average (Richard et al., 2001). The rainfall forecast for the 2009-2010 DJF El Niño season that was made by the three coupled models discussed in Landman and Beraki (2010) showed mostly enhanced probabilities for dry conditions over southern Africa. A similar forecast was also made by international centres such as the IRI (International Research Institute for Climate and Society) and the South African Weather Service (SAWS). However, DJF 2009-2010 rainfall over South Africa was anomalously high. The association of enhanced forecasting skill during El Niño years may partially explain the level of confidence in the forecast of dry conditions for the austral summer

seasons during 1997-1998 and 2009-2010.

Figure 5.10 shows the global SSTAs during JFM 1998. An El Niño occurred which was subsequently found to be the strongest El Niño on record. A strong positive TIOD event also took place during the second half of 1997 and, although it is not typical for these events to last into the beginning of the following year, the DMI remained greater than 0.5 until February 1998, only decaying in March 1998 (Webster et al., 1999). In addition to the positive TIOD, the South Indian Ocean showed SSTAs reminiscent of a negative phase SIOD event which is confirmed in Feng et al. (2014). Behera and Yagamata (2001) also note that the positive SIOD of 1997 changed phase to become a negative SIOD in early 1998. It has also been suggested that 1998 was a Benguela Niño year (Rouault et al., 2009). El Niño events typically lead to drought conditions over southern Africa (Lindesay, 1988; Reason et al., 2000), and negative SIOD events have been associated with dry conditions over parts of southern Africa, while a Benguela Niño, and positive TIOD events usually result in above average rainfall over parts of southern Africa (Rouault et al., 2003a; Behera and Yagamata, 2001).

Many parts of southern Africa experienced more dry days during JFM 1998 when compared with the climatology (**Figure 5.11**). In particular, the drought corridor identified in Usman and Reason (2004) expanded and moved further north. There was an increase in the number of dry days dur-

ing JFM 1998 over northern Namibia and southern Angola, Botswana, much of Zambia, and north Mozambique. The position of this band of positive anomalies, as well as the strong negative anomalies just north of it, indicate that it may be related to a shift in the position of the ITCZ. The region of high climatological DDF over western Namibia and South Africa expanded eastward during JFM 1998.

The seasonal rainfall anomalies shown in **Figure 5.12** indicate that central and south western South Africa, northern Angola, parts of northern Zambia, coastal Mozambique and all of Tanzania experienced above average rainfall during JFM 1998. The rest of the subcontinent received less than average seasonal total rainfall.

20th Century reanalysis data is used to compare the atmospheric circulation over southern Africa during JFM 1998 with its climatology in order to asses potential mechanisms associated with rainfall and dry day anomalies. **Figure 5.13** shows a negative velocity potential anomaly at 200 hPa over the western South Indian Ocean which indicates relative ascent over this region. SSTs in this area were still higher than average due to the strong positive TIOD as well as the ongoing El Niño event (**Figure 5.10**). The warm waters present over the western Indian Ocean have been linked with increased rainfall over East Africa (Webster et al., 1999; Saji et al., 1999) and may have also contributed to a reduction in the number of dry days over

Tanzania, Kenya and Somalia. El Niño events have also been associated with an increase in rainfall over the region (Ogallo, 1988; Kijazi and Reason, 2005).

Most of south eastern Africa displays positive geopotential height anomalies at 850 hPa which implies relative subsidence and reduced convection and hence more dry spells (**Figure 5.14**). The Angola low was close to average during JFM 1998 (**Figure 5.14**) and thus, for an El Niño event, this Angola low was anomalously strong considering that it is typically weakened during ENSO (Reason and Jagadheesha, 2005). Reason and Jagadheesha (2005) suggested that the presence of this relatively strong Angola low during JFM 1998, coupled with warmer SSTs over the tropical South East Atlantic, may have encouraged the transport of moist air from the tropical South East Atlantic Ocean which is favourable for cloud band development and was warmer than average (**Figure 5.10**) over Angola and northern Namibia. The northerly moisture flux anomalies (**Figure 5.15**) stretched from Angola to the south of South Africa. This feature, together with relative uplift (**Figure 5.16**), seems to be associated with increased rainfall over southern South Africa despite the number of dry days being close to average there. **Figure 5.17** shows a strong region of relative convergence over southern Angola near the Angola low that extended down through Namibia into western South Africa. This pattern is consistent with the increased rainfall over the western part of the Eastern Cape Province. The Botswana high was much stronger during JFM 1998 when compared with climatology and this fea-

ture may have contributed to the increased DDF over the drought corridor (**Figure 5.18**).

It is now appropriate to consider in more detail the four regions whose dry day frequency time series were analysed earlier in the chapter.

5.3.1 Coastal Northern Angola

Rainfall variability over Angola has been linked to changes in regional SSTs (e.g. Hirst and Hastenrath (1983); Nicholson and Entekhabi (1987)). In particular, Benguela Niño events are usually associated with an increase in rainfall over coastal Angola and occasionally also further inland (Nicholson and Entekhabi, 1987; Rouault et al., 2003a; Hansingo and Reason, 2009). The year 1998 was identified as a Benguela Niño year (Rouault et al., 2009).

The total rainfall over the northern coastal region of Angola, represented as Box 1 in **Figure 5.1**, averaged 397.9mm during the JFM seasons between 1997 and 2012. The total rainfall received during JFM 1998 was higher by almost one (0.9) standard deviation at 450.9 mm (**Table 5.7**). This increase in overall seasonal rainfall was accompanied by a reduction in the number of dry days from an average of 12.9 dry days per season to 8.0 during JFM 1998. The longest stretch of uninterrupted dry days over this region was 4.0 on average and this reduced to 3.0 during JFM 1998. This indicates that, when dry spells occurred over coastal northern Angola during this season,

they were not typically long lived.

The South Atlantic trade winds were enhanced during JFM 1998 (**Figure 5.15**) which Hirst and Hastenrath (1983) associated with increased levels of rainfall over Angola. There was increased moisture flux from the tropical South East Atlantic Ocean towards coastal Angola during JFM 1998 (**Figure 5.15**) which may have contributed to increased rainfall over the region. The increase in available moisture may have been a result of the anomalously warm SSTAs (up to 2^oC higher) just off the Angolan coast (**Figure 5.19**). There was relative convergence over the coastal Angolan region extending over the South East Atlantic Ocean (**Figure 5.17**) which, coupled with the relative uplift over the northern part of the region (**Figure 5.16**), would have further encouraged favourable rainfall conditions.

5.3.2 Central South Africa

For ease of reference, the region encompassed by Box 2 in **Figure 5.1** is called central South Africa. The average total rainfall over central South Africa during the JFM season (1997-2012) is 261.2 mm, while the JFM 1998 rainfall total was 305.1 mm (**Table 5.8**). This higher level of rainfall represents an increase of half a standard deviation above average but it was not accompanied by a decrease in the number of dry days. In fact, dry days increased from an average of 47.1 to 55.0 in JFM 1998, representing a 0.9 standard deviation increase. However, the maximum number of consecutive

dry days over this region was 10.7 on average and slightly lower during JFM 1998 at 10.0. This indicates that at least one dry spell lasting 10 days occurred over central South Africa during JFM 1998.

One explanation for the increased rainfall and increased dry spells can be found by considering the number of heavy rain days. The region generally records 6.6 wet days during the JFM season whereas, during JFM 1998, there were 11 days on which more than 10mm of rainfall fell. This difference of 4.4 wet days translates to at least 44mm of rainfall which (coincidentally almost exactly) accounts for the increase in the total seasonal rainfall over the region. This demonstrates very clearly that a small increase in the number of heavy rainfall days can make a big difference to the seasonal rainfall total. The value of maximum daily rainfall during JFM 1998 (42.8 mm) was also substantially higher at 1.6 standard deviations above the average (25.1 mm).

The moisture influx from the South Indian Ocean was weaker than usual during JFM 1998, while there was a strong increase in moisture input from north of the region originating from the Congo Basin and the South East Atlantic Ocean (**Figure 5.15**). There was strong relative uplift over the region (**Figure 5.16**) favouring convective rainfall and TTT formation. **Figure 5.17** shows mixed signals with some parts of the box experiencing relative convergence and others divergence which indicates that anomalies over this region may have been variable during the course of the season. The increase

in both dry and heavy rain days could account for this on a seasonal time scale.

5.3.3 Limpopo

The Limpopo region in the north east part of South Africa lies within the drought corridor and is prone to severe drought and flood events (Cook et al., 2004; Reason et al., 2005). Limpopo experienced a reduced seasonal rainfall during JFM 1998 of about 0.6 standard deviations below average (**Table 5.9**). However, almost no change in the average number of dry days (51.0 during JFM 1998 while the average is 51.3 days) was experienced while the number of heavy rain days decreased by more than one standard deviation (-1.1) from 8.1 on average to only 1 during JFM 1998.

Cook et al. (2004) found that a number of atmospheric circulation anomalies may be associated with dry spells over eastern South Africa. Most of these circulation anomalies are present when considering this region during the JFM 1998 season. There was weak divergence and relative subsidence over northeastern South Africa (**Figures 5.16** and **5.17**), as well as a cyclonic anomaly just south of the Mozambique Channel (**Figure 5.15**). Moisture influx from the South Indian Ocean was also weaker than usual during JFM 1998 (**Figure 5.15**). The northwesterly anomalies in the central and southern Mozambique Channel indicate that there was less moisture influx from the South Indian Ocean, one of the main sources of moisture over southern

Africa (Reason et al., 2006a). There was also a region of subsidence centred over north east South Africa which makes conditions unfavourable for rainfall (**Figure 5.16**).

5.3.4 North East Zambia

Zambia is a region of high temporal and spacial rainfall variability (Hachigonta et al., 2008; Hachigonta and Reason, 2006) which can have a substantial impact on the rain-fed crops. The region is located near the turning point of the ITCZ and hence the meeting place for the two convergence zones bringing moisture from the Indian and Atlantic Oceans respectively. As such, it is very sensitive to any significant movement of these convergence zones as well as moisture input from the monsoonal flow. Hachigonta and Reason (2006) found that rainfall variability over northern and southern Zambia is sufficiently distinct to justify studying the two regions separately. The north east part of Zambia generally receives more rainfall than the south western part of the country, probably due to the position of the ITCZ which is located over northern Zambia during the rainy season.

El Niño is associated with below average rainfall over the region and Hachigonta and Reason (2006) established that there was an increase in the frequency of dry spells and a decrease in the frequency of wet spells over the country during El Niño events during the DJF season. A relationship between Indian Ocean SSTAs and dry and wet spell frequency was also ex-

plored but this correlation was found to be weaker than that of ENSO. Low level westerly anomalies over southern Angola and western Zambia are associated with fewer dry spells and more wet spells over Zambia.

Total seasonal rainfall amounts over north east Zambia during JFM 1998 (662mm) were almost the same as the seasonal average (662.4mm) (**Table 5.10**). This region straddles areas of both increased and decreased rainfall (**Figure 5.12**). There was an increase in the number of dry days from an average of 4.7 days per season to 6 days during JFM 1998. Although this is not a large increase, it represents half a standard deviation. The moisture flux anomalies over north east Zambia were not substantial and are consistent with average rainfall (**Figure 5.15**). **Figure 5.16** shows that half of the region had weak relative subsidence while the other half had weak relative uplift and **Figure 5.17** shows a similar pattern with weak divergence and convergence. The area average convergence over the region is zero which is consistent with the average rainfall that occurred during the JFM 1998 season.

5.4 Dry Day Frequency During JFM 2010

The JFM 2010 season was also predicted to be a dry season over southern Africa but, much like JFM 1998, near or above average rainfall levels were recorded over most regions. The global SSTAs during JFM 2010 are

shown in **Figure 5.20**. A Central Pacific (CP) El Niño (Larkin and Harrison, 2005; Yu and Kao, 2007; Ashok et al., 2007b) is evident in which SSTs were approximately 2.5^{o}C warmer than average over the central equatorial Pacific Ocean. These CP El Niño events can be described using the Niño 4 index rather than the Niño 3.4 index which is typically used to describe canonical El Niño's (Kao and Yu, 2009; Yeh et al., 2009). It is known by many names including the central Pacific (CP) El Niño, dateline El Niño, warm pool (WP) El Niño or El Niño Modoki (Ashok et al., 2007a; Kao and Yu, 2009; Yu and Kim, 2010; Kug et al., 2009; Larkin and Harrison, 2005). However, the "Modoki" definition requires cold SSTAs in the western and eastern Pacific (Ashok et al., 2007a) and can thus be considered as a special type of CP El Niño. Studies have shown that the canonical, or eastern Pacific (EP) El Niño, and CP El Niño may impact the global climate differently due to differences in the Walker circulation as well as differences in the atmospheric teleconnections (Ashok et al., 2007a; Weng et al., 2009; Kim et al., 2011; Ashok and Yamagata, 2009). Ratnam et al. (2012) investigated global precipitation anomalies for a composite of EP El Niño years and also those of CP El Niño years and showed that there is a negative anomaly over southern Africa in the EP composite, while the CP composite displays almost no impact on rainfall over southern Africa.

There was a strong negative phase NAO during JFM 2010 and a tripole SSTA pattern is evident in the North Atlantic Ocean. The warming of the

subtropical North Atlantic SSTs can probably be attributed to the combined forcings from the El Niño and negative NAO that often warms the subtropical and high latitude SSTs and cools the midlatitude SSTs in the North Atlantic by modifying evaporative heat loss (Deser and Blackmon, 1993). McHugh and Rogers (2001) found that heavier, convective, DJF rainfall occurs over Tanzania, northern Mozambique, Zambia and part of the western DRC during the negative NAO phase, when the North Atlantic westerlies are unusually weak. Todd and Washington (2004) found a negative correlation between the NAO and central African rainfall, although their study focused on the FMA season. There was also a weak positive TIOD during JFMA 2010, although the strength, and therefore its classification as a dipole event, varies depending on which SST data set is used (Blunden et al., 2011). The AMO was in a warm phase during JFM 2010 and the SAM was in a negative phase (Blunden et al., 2011). Gillett et al. (2006) found a positive association between the SAM and rainfall over southeastern southern Africa.

The changes in the distribution of dry days over southern Africa during JFM 2010 display a different pattern than those of JFM 1998 (**Figure 5.21**). The location of the drought corridor was different during JFM 2010, strengthening (weakening) over Namibia (Botswana), while gaining DDF over Zimbabwe and southern Mozambique. The increase in dry days over the eastern half of the drought corridor may be linked to changes in the moisture flux from the South Indian Ocean. Most of South Africa, Botswana and Zambia

appeared to experience fewer dry days during JFM 2010 than average, while northeast South Africa, Mozambique, Zimbabwe, Namibia and Angola each displayed higher DDF during JFM 2010. The seasonal rainfall anomalies (**Figure 5.22**) correspond very well to the increase and decrease in the number of dry days over southern Africa.

There was a region of very strong subsidence centred over Zimbabwe which contributed to unfavourable rainfall conditions over the region (**Figure 5.23**). Moisture flux from the South Indian Ocean was weaker due to northerly anomalies over the South Mozambique Channel (**Figure 5.24**) and conditions were therefore unfavourable for rainfall over southern Mozambique and Zimbabwe. The monsoonal northwesterlies in the northern Mozambique Channel were weaker in JFM 2010 than in the climatology, implying a weaker ITCZ over eastern southern Africa. On the other hand, the moisture influx from the tropical Atlantic Ocean was stronger than average (**Figure 5.24**) although there was a region of strong divergence over northern Angola which may have disrupted the influx of moisture from the Atlantic (**Figure 5.25**).

5.4.1 Coastal Northern Angola

The SSTAs close to the coast of Angola during JFM 2010 were weakly negative but changed sign to become weakly positive further off the coast. There was a relatively weak negative anomaly of 0.6^{o}C near the Angola Benguela Frontal Zone (**Figure 5.26**).

The total seasonal rainfall over coastal northern Angola was lower than average during JFM 2010 when the region received 323.2mm of rainfall compared with the average of 397.9mm (1.2 standard deviations below). The number of dry days increased by 1.7 standard deviations from an average of 12.9 days to 25 days during JFM 2010, while the number of heavy rainfall days decreased from 5.8 to 2 days. The increase in the number of dry days was accompanied by an increase in the maximum duration of consecutive dry days from a mean of 4 days to 6 days during JFM 2010. There were no consecutive wet days during JFM 2010 (**Table 5.7**).

There was relative divergence over coastal northern Angola during JFM 2010 (**Figure 5.25**) as well as weak relative subsidence over the region (**Figure 5.23**) which would have made conditions unfavourable for rainfall. Although there was an increased influx of moisture from the South East Atlantic Ocean, the region was dominated by moisture flux divergence and therefore this increased moisture did not correspond to increased rainfall over the region (**Figure 5.24**). There was a cyclonic anomaly just off the Angolan coast which may have acted to divert moisture away from the coast.

5.4.2 Central South Africa

The average JFM seasonal rainfall total over central South Africa is 261.2mm which increased to 340.8mm during JFM 2010. This increase rep-

resents a 0.9 standard deviation increase in rainfall and was accompanied by a similar increase in the number of heavy rain days that occurred over the region. The number of dry days decreased by more than 10 days from 47.1 to 37.0 days (-1.1 standard deviations). The maximum number of consecutive dry days decreased from an average of 10.7 to 7.0 which still represents a fairly long time period for an average dry spell in the rainy season. The maximum rainfall amount for any day during JFM 2010 was higher at 34.5mm than the mean of 25.1mm (**Table 5.8**).

The Angola low was slightly weaker during JFM 2010 by 5 hPa (**Figure 5.27**) and shifted westward. Since the Angola low is the source region for the cloudbands that are the most important summer rainfall-producing weather system, the pattern suggests that the TTTs during this summer might have occurred further west. **Figure 5.23** and **Figure 5.25** are consistent with this suggestion implying wetter than average conditions over central South Africa. The northerly moisture flux anomalies over northern South Africa (**Figure 5.24**) facilitated the transport of moisture into the region and also contributed to rainfall there.

5.4.3 Limpopo

Northeast South Africa received less rainfall during JFM 2010 (210.7mm) than average (271.6mm) and experienced an increase in the number of dry days over the region, having 54.0 during JFM 2010, approximately 3 above

average. There were fewer wet days with only 5.0 during JFM 2010 as opposed to the average 8.1 experienced over this region. The maximum number of consecutive dry days increased from 10.3 to 14.0.

Moisture influx into Limpopo from the South Indian Ocean was weaker than average during JFM 2010 and there was weak divergence over the region (**Figure 5.24**, **Figure 5.25**). The easterly moisture flux over the central Indian Ocean east of Madagascar around 20°S was substantially weaker than average during JFM 2010 and as a result there was less moisture influx into Limpopo from the South West Indian Ocean. There was weak divergence over northeastern South Africa (**Figure 5.25**) and relative subsidence over the region (**Figure 5.23**). The positive geopotential height anomalies further indicates relative subsidence and hence reduced convection over the region (**Figure 5.27**).

5.4.4 North East Zambia

North East Zambia experienced a small increase in total seasonal rainfall during JFM 2010 of about 16mm. The number of dry days decreased from 4.7 on average to 3.0 during JFM 2010 (-0.6 standard deviations). The number of heavy rain days increased from 23.1 to 24 days while the maximum number of consecutive dry and wet days were almost the same as the average at 2.0 and 4.0 respectively.

The north-easterly moisture flux from the tropical Atlantic was stronger than average during JFM 2010 and the monsoonal westerlies over the tropical Indian Ocean around 10^oS were below average (**Figure 5.24**). As a result, there was more moisture transported from the tropical South Indian Ocean into Tanzania without as much of it being retroflected back over the central Indian Ocean towards north Madagascar as usually occurs. Thus, there was more moisture available over North East Zambia than average during JFM 2010 as well as strong relative uplift over the north eastern part of the country (**Figure 5.23**). This region was also favoured with relative low level convergence during this season (**Figure 5.25**) which contributed to the higher than average rainfall experienced.

5.5 Summary and Conclusions

The frequency of dry days over southern Africa during JFM was investigated using GPCP observational data. The climatology of DDF over southern Africa during JFM was calculated using daily GPCP data from 1997 to 2012 is shown in **Figure 5.2**. There is a large dry region over the South Atlantic Ocean which corresponds to the South Atlantic Anticyclone, and there is also a dry region over the central South Indian Ocean corresponding the the South Indian Anticyclone. There is a band of relatively low DDF that extends from the equatorial Atlantic Ocean south-eastward centred over northeast Angola, southern DRC, northeast Zambia, extending to

a lesser extent into northern Mozambique, then moving south-eastward to northern Madagascar before heading in a slightly northeastern direction over the Indian Ocean. This region of low DDF appears to be associated with the seasonal position of the ITCZ. Just to the south of this region, running from southern Namibia, across South Botswana, over southern Zimbabwe, most of the Limpopo region, southern Mozambique and into the southern Mozambique Channel is another band, but, in contrast, this band is one of high DDF. Usman and Reason (2004) identified this band of high DDF between 20^o and 25^oS as the drought corridor that runs across subtropical southern Africa. There is also a low DDF region over eastern South Africa below the drought corridor which is related to the Drakensberg and Maluti Mountains and the onshore flow of moist marine air as migratory anticyclones ridge into the South West Indian Ocean.

Pentad rainfall data from 1979 to 2011 was used to perform correlation analysis between DDF and global SSTs since the daily dataset may be too short to produce robust correlation data. The correlation analysis was generally in agreement with previous studies and found that DDF over the Limpopo and North East Zambia regions is correlated with ENSO, while DDF over coastal northern Angola and central South Africa is correlated with SSTs in the Indian and Atlantic Oceans. In particular, the Atlantic Ocean SSTs play an important role in DDF over coastal northern Angola. The role of the Indian Ocean was not as pronounced, but it was still significant

as both the tropical South Indian Ocean and the TIOD showed correlations with DDF over the region. The Pacific Ocean SSTAs do not appear to have a significant relationship with DDF over coastal northern Angola. DDF over central South Africa is influenced by some aspects of SST anomaly patterns over the Atlantic and Indian Ocean while the Pacific Ocean SSTs do not correlate at statistically significant values over this region. The correlation between the DDF over Limpopo and ENSO is consistent with that found by Reason et al. (2005) using CMAP pentad data for 1979-2002, although their correlation was stronger. DDF over this region is also correlated with the strength and position of the Botswana high. Correlation analysis suggests that DDF over North East Zambia is associated with ENSO which is consistent with Hachigonta and Reason (2006). They used both CMAP pentad and station data for the DJF season between 1979 and 2002 and found that correlations between the dry spell and Niño 3.4 anomalies ranged from r= 0.6 to r= 0.8 when calculated using a 10 year running window. Their correlation coefficients may have been higher than those in this study due to the season of interest and the 10 year running windows. DDF over North East Zambia is also found to be correlated with the Benguela Niño index which indicates that cold events may have an impact on DDF as far inland as North East Zambia. DDF over this region is also found to be correlated with the Botswana high when a 1 month lag is introduced.

The late summer rainfall seasons JFM 1998 and JFM 2010 are of partic-

ular interest due to the fact that most climate prediction models forecast dry conditions over southern Africa but the expected dry conditions were not as widespread as anticipated. During JFM 1998, the drought corridor expanded and moved northward and the DDF along the rough seasonal position of the ITCZ increased. This might be linked to a northward shift in the position in the ITCZ. During El Niño events, the ITCZ is typically weakened as high pressure anomalies occur over the South Indian Ocean and southern Africa. The anomalously strong and unusually elongated Botswana high may also have contributed to the increase in size of the drought corridor, as well as the increase in DDF. The decreased moisture flux input from the South Indian Ocean may have been another contributing factor in this region. The stronger South Atlantic Anticyclone may have contributed to the eastward expansion of DDF over western Namibia and South Africa. DDF over Tanzania was reduced which was likely due to a combination of ENSO and TIOD influences.

The distribution of DDF over southern Africa during JFM 2010 was rather different from that of JFM 1998 and the climatology. The drought corridor developed a more pronounced break over Botswana and the band to the right of Botswana increased and expanded further northward into Zimbabwe and Mozambique. This may have been linked to a reduction in moisture flux input from the South Indian Ocean. The movement of the drought corridor may also indicate a northward shift in the ITCZ.

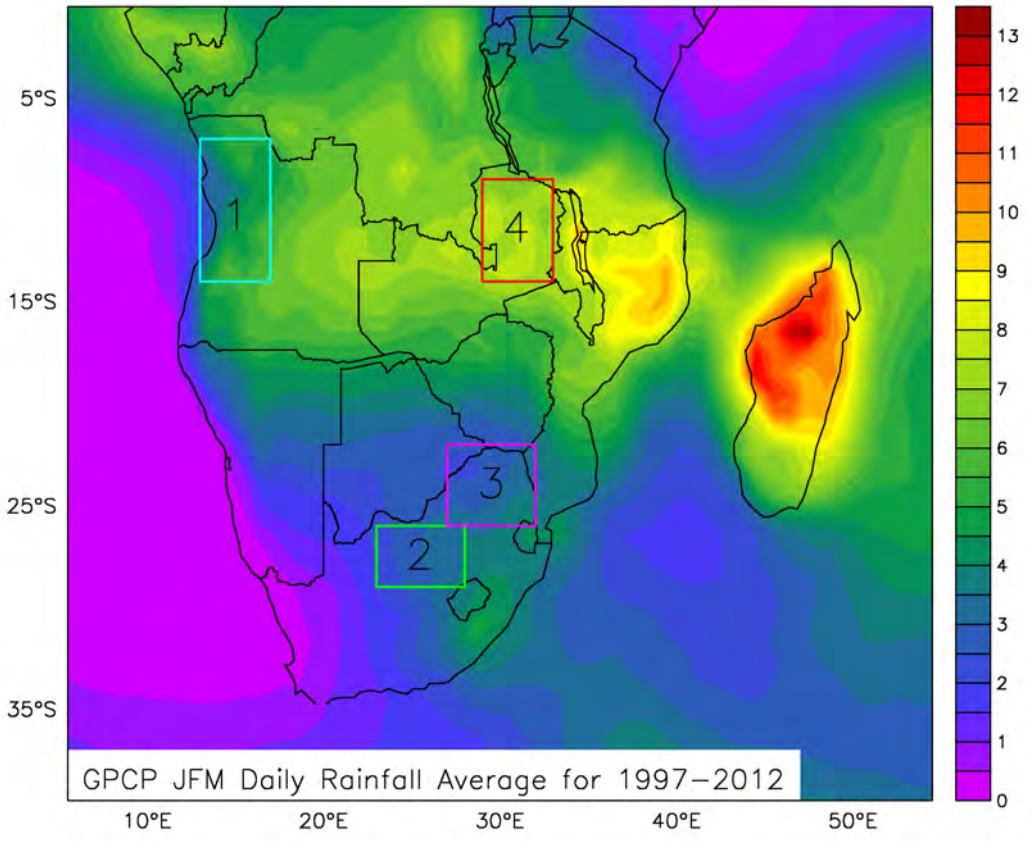

Figure 5.1: GPCP JFM daily rainfall average for 1997-2012. Box 1 - Coastal Northern Angola [13-17^{o}E; 7-14^{o}S]; Box 2 - Central South Africa [23-28^{o}E; 26-29^{o}S]; Box 3 - Limpopo [27-32^{o}E; 22-26^{o}S]; Box 4 - North East Zambia [29-33^{o}E; 9-14^{o}S]

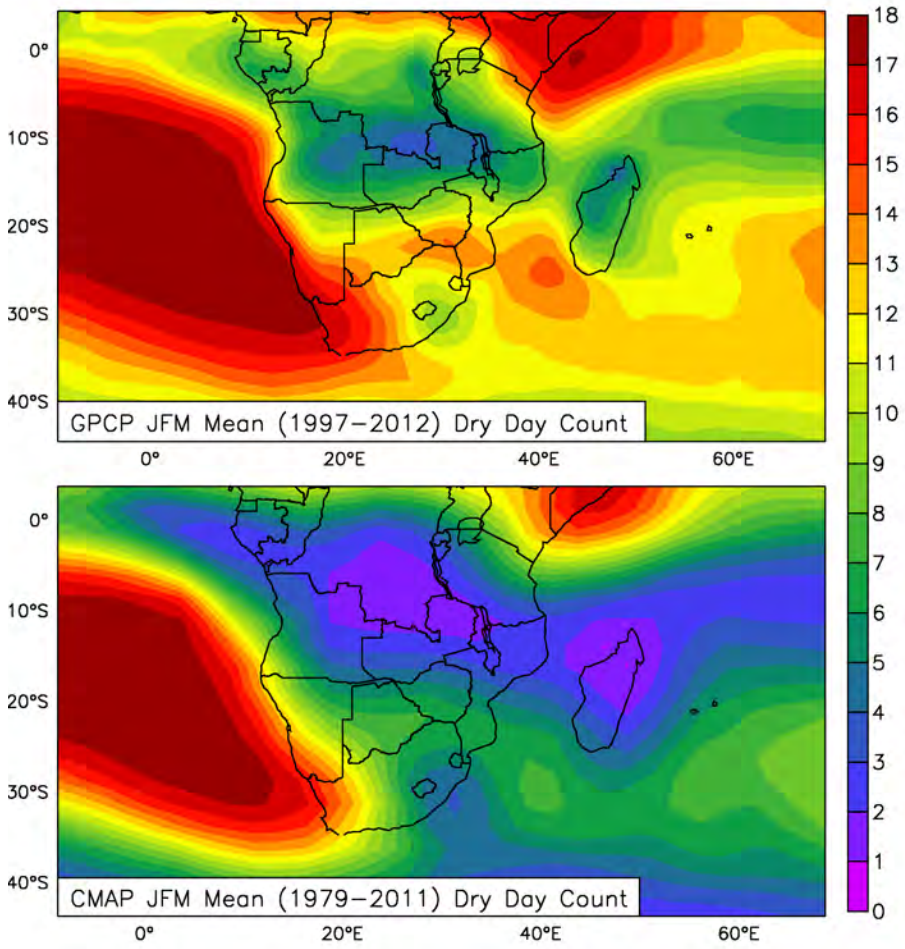

Figure 5.2: Mean number of dry days over southern Africa averaged over JFM using GPCP (top) and CMAP (bottom) data. The GPCP daily data was averaged from 1997 to 2012. Dry days have been considered individually but for ease of comparison the interval in the colour key is pentads. The CMAP pentad data was averaged from 1979 to 2011.

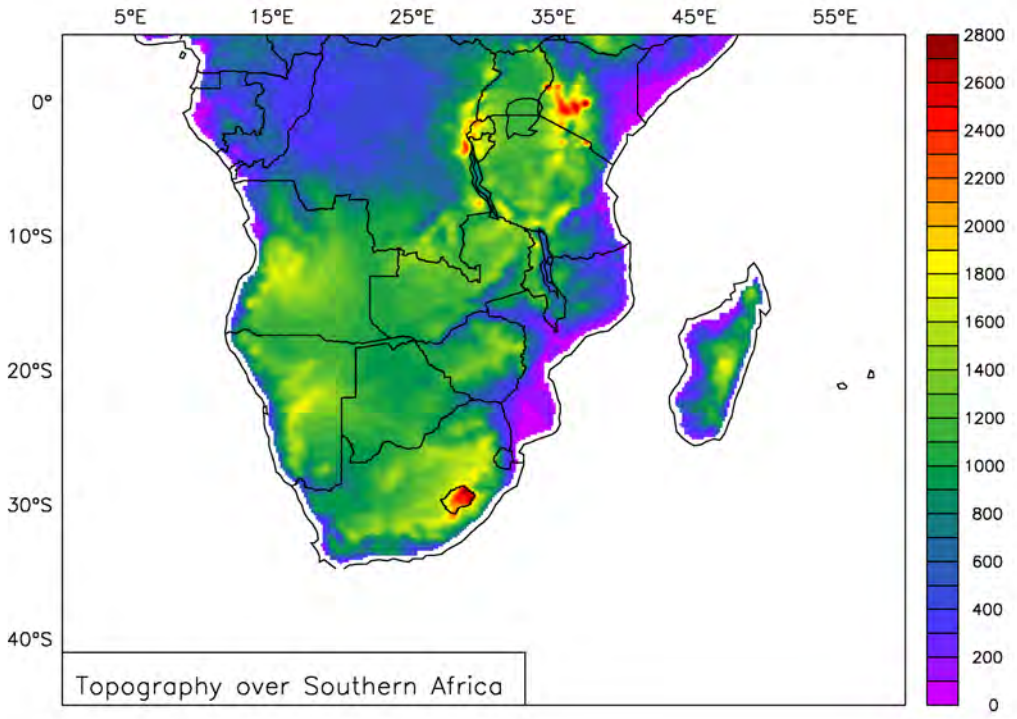

Figure 5.3: Topography over southern Africa in meters above sea level (in m)

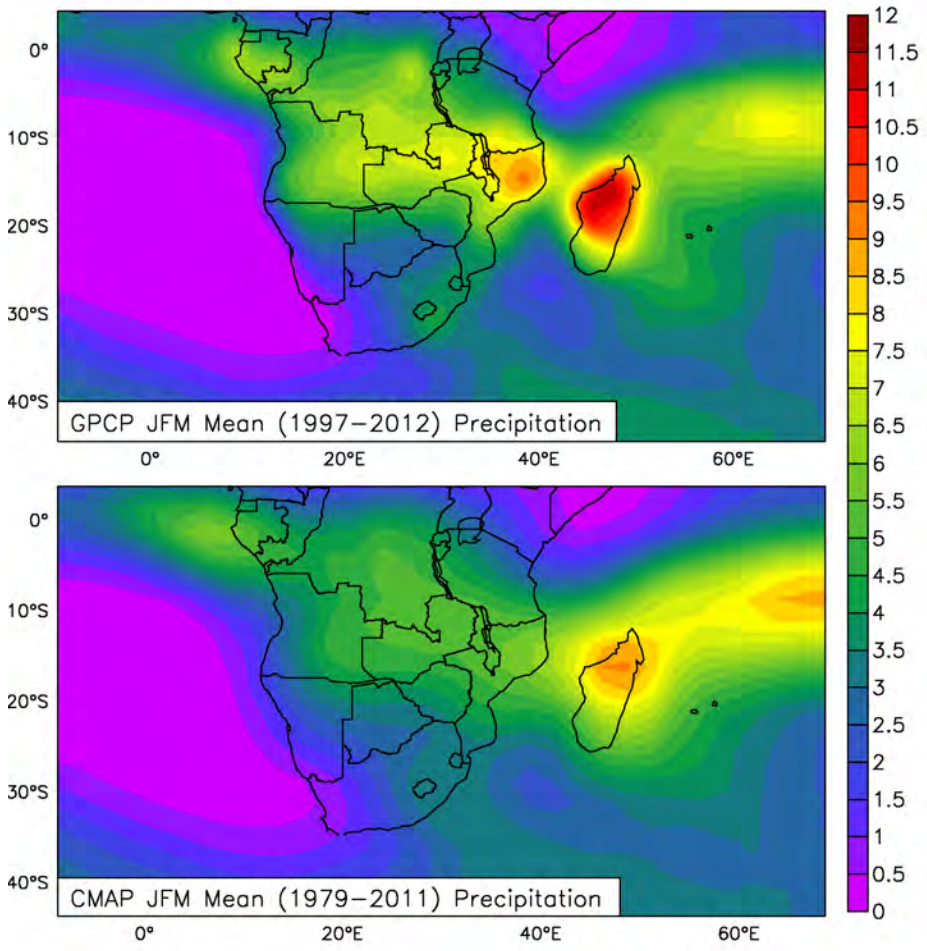

Figure 5.4: Mean rainfall over southern Africa during JFM for GPCP and CMAP (in $\mathrm{m{\cdot}s^{-1}}$)

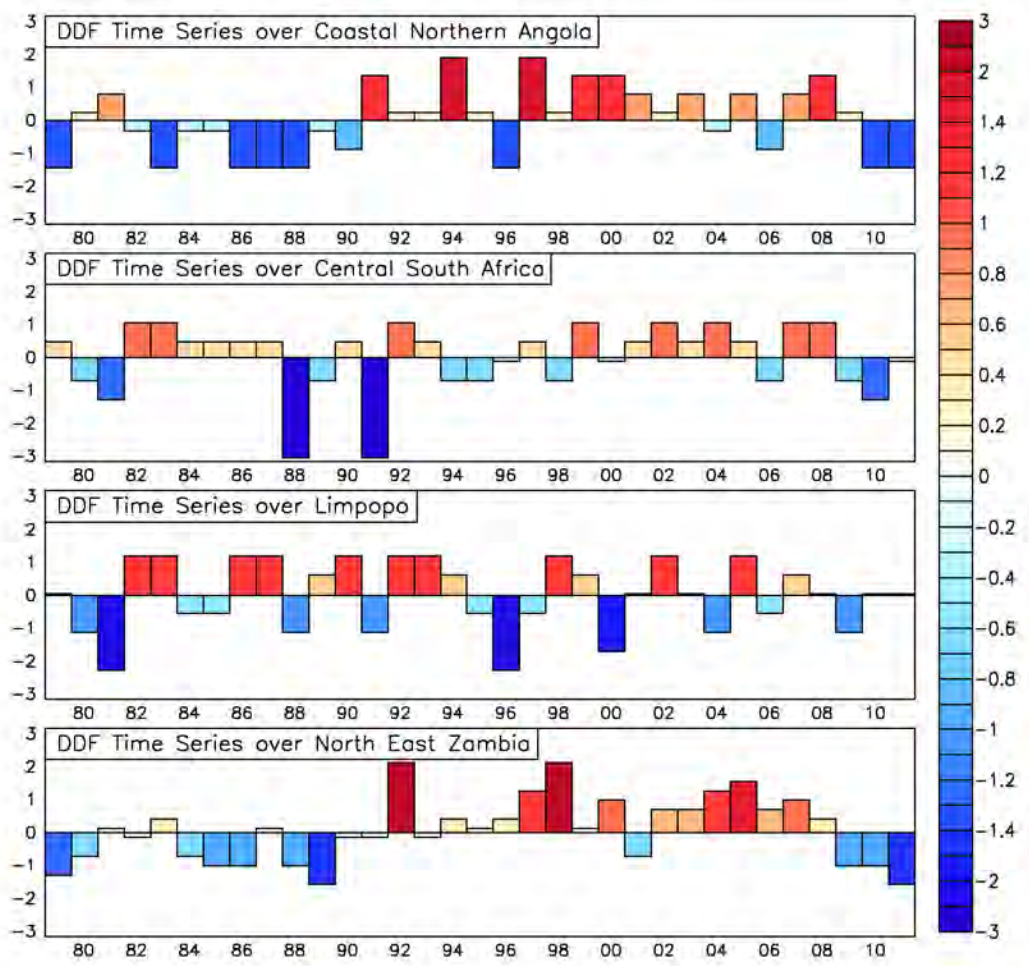

Figure 5.5: Area Averaged Dry Day Frequency Time Series over Coastal Northern Angola and Central South Africa for the period 1979-2011 using GPCP pentad data

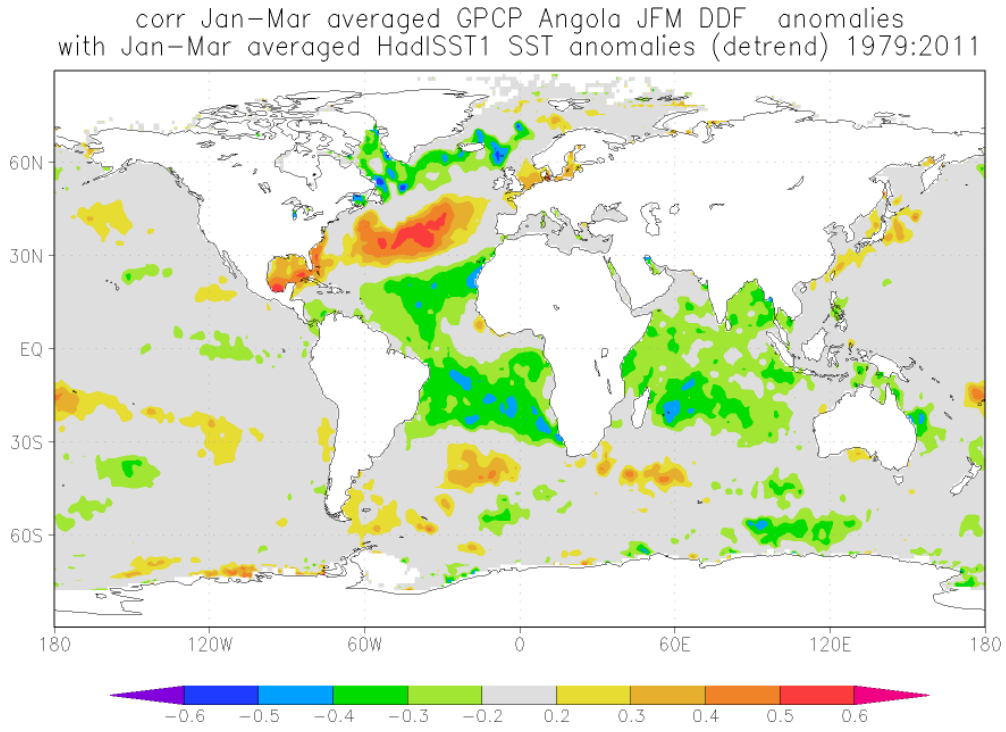

Figure 5.6: Correlation map between the area averaged dry day frequency over coastal northern Angola and global SSTs for the period 1979-2011 using GPCP pentad data

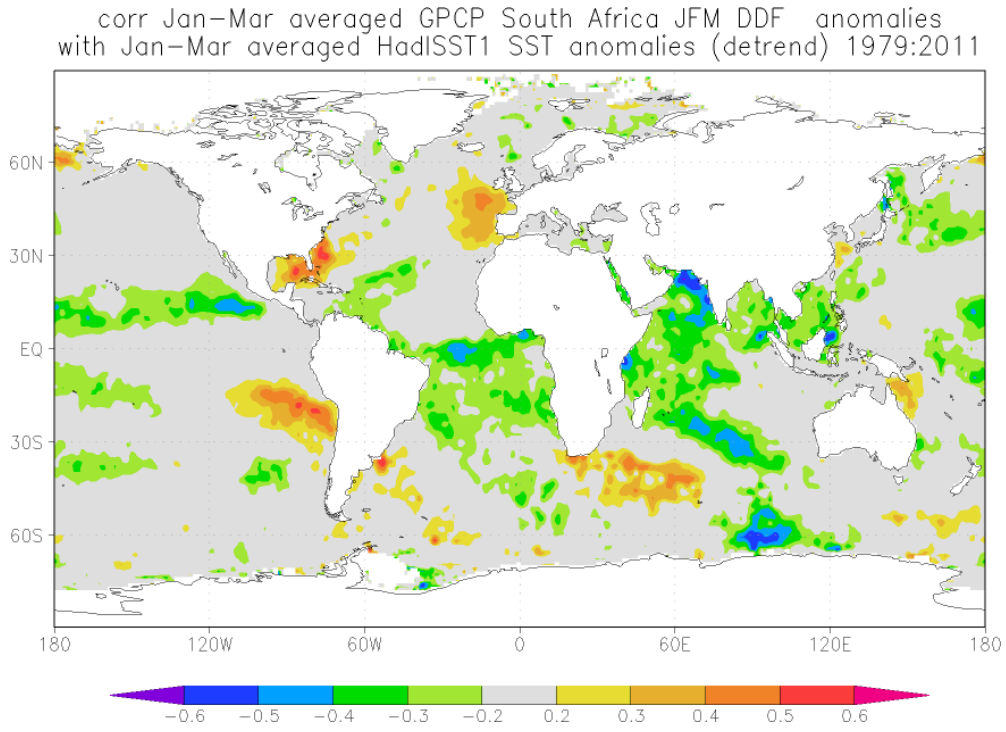

Figure 5.7: Correlation map between the area averaged dry day frequency over central South Africa and global SSTs for the period 1979-2011 using GPCP pentad data

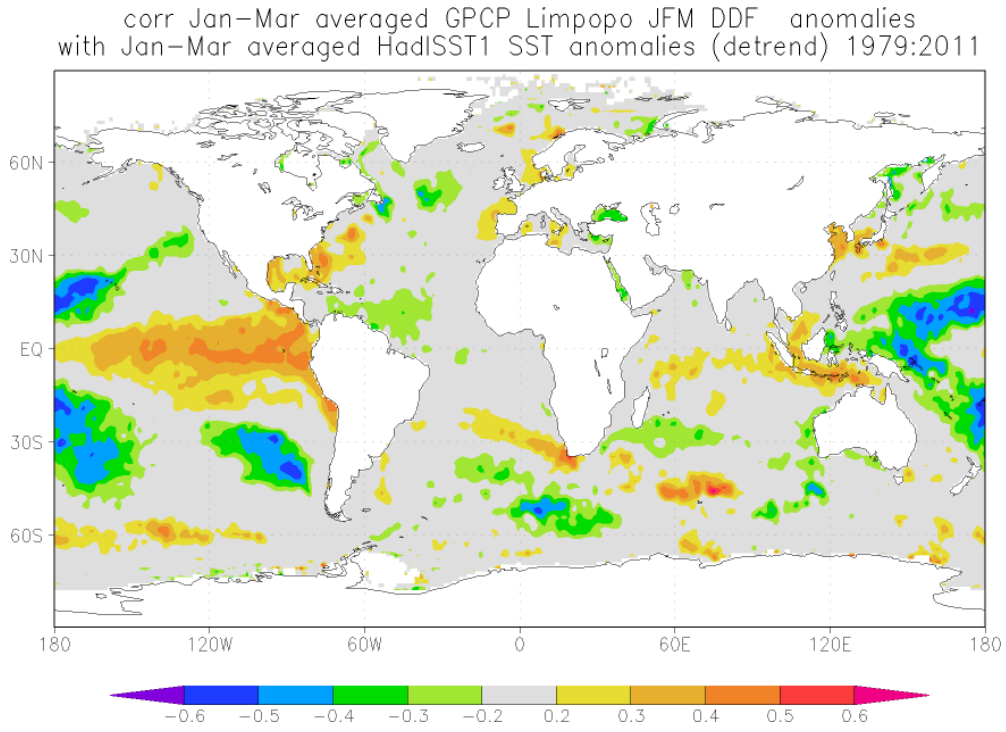

Figure 5.8: Correlation map between the area averaged dry day frequency over Limpopo and global SSTs for the period 1979-2011 using GPCP pentad data

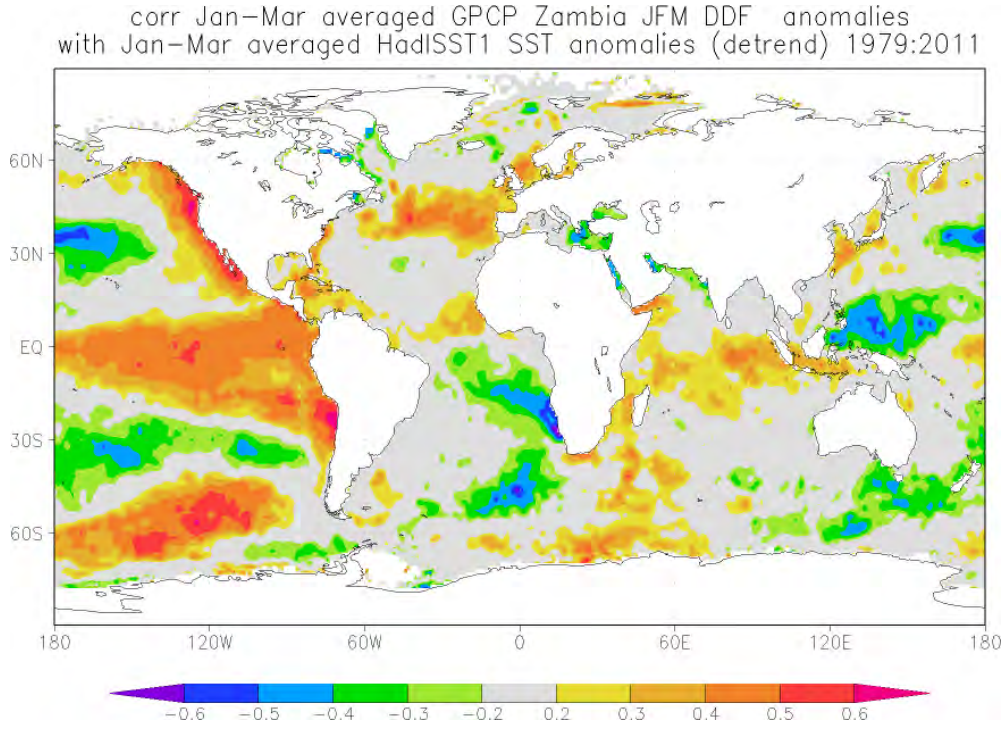

Figure 5.9: Correlation map between the area averaged dry day frequency over North East Zambia and global SSTs for the period 1979-2011 using GPCP pentad data

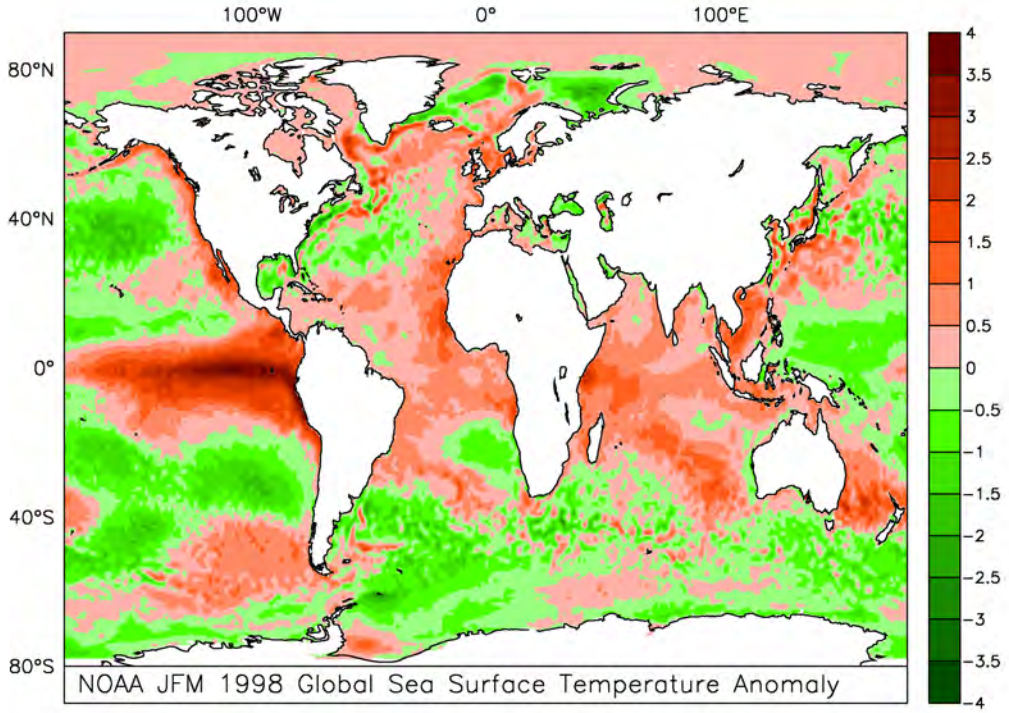

Figure 5.10: NOAA JFM 1998 Global Sea Surface Temperature Anomaly (in ^{o}C)

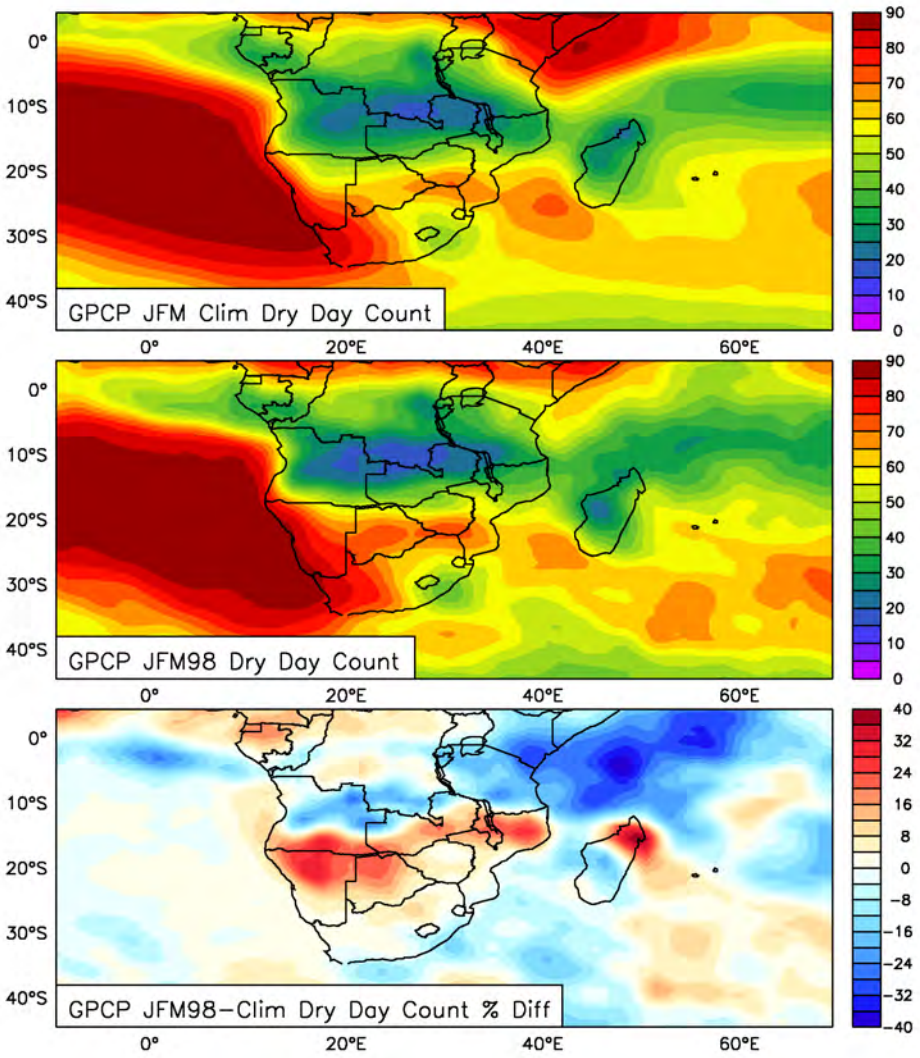

Figure 5.11: GPCP JFM 1998 number of dry days over southern Africa (in days)

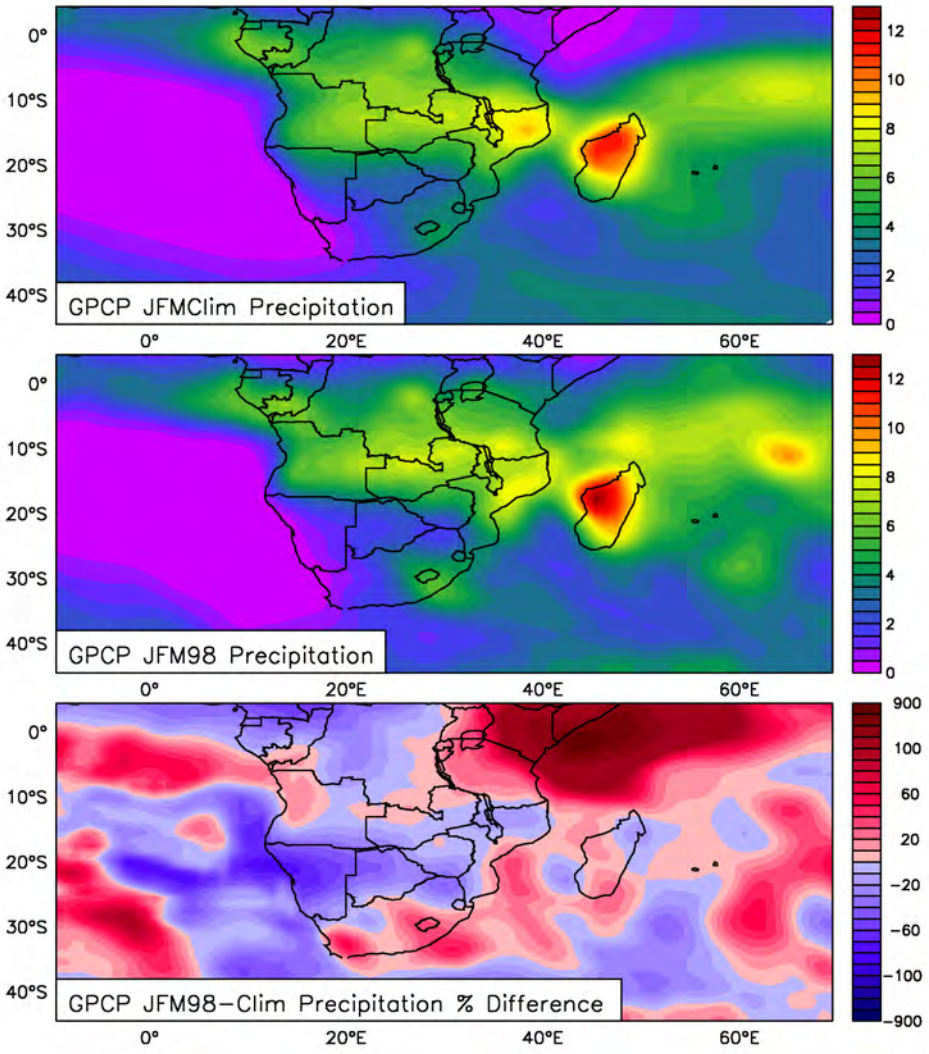

Figure 5.12: GPCP rainfall over southern Africa during JFM 1998 and climatology (in $m \cdot s^{-1}$)

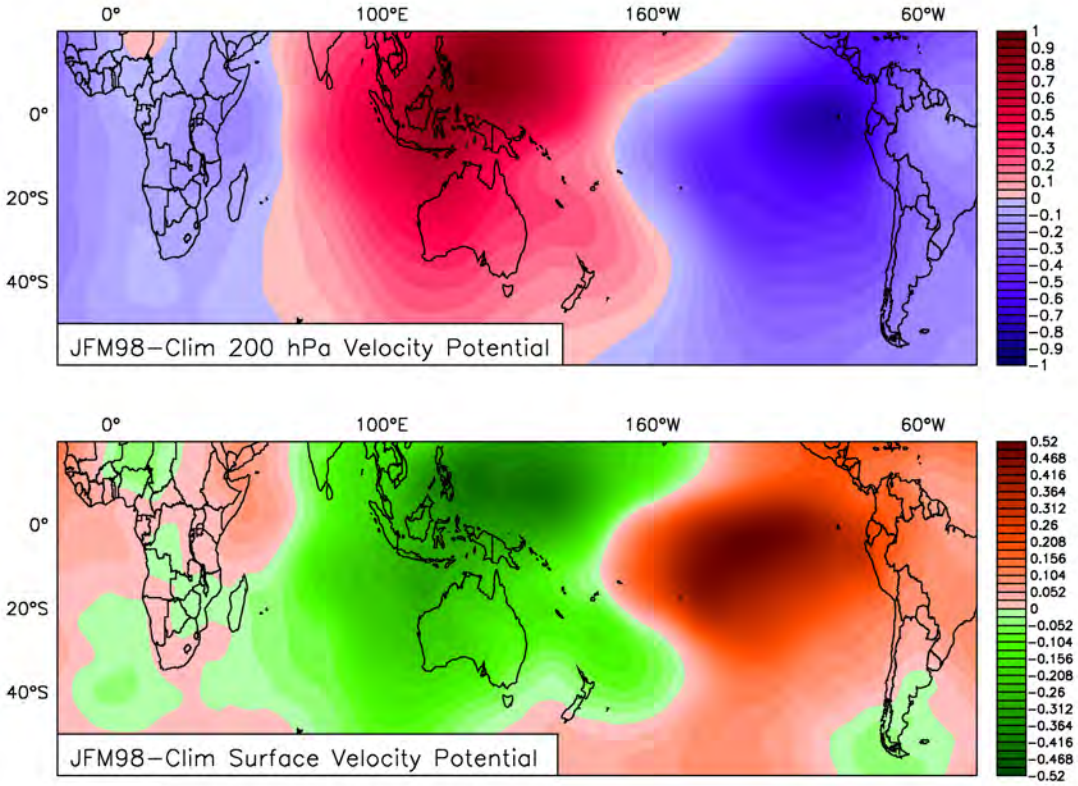

Figure 5.13: NCEP 20th Century JFM 1998 - Clim 200 hPa and Surface Velocity Potential (in hPa)

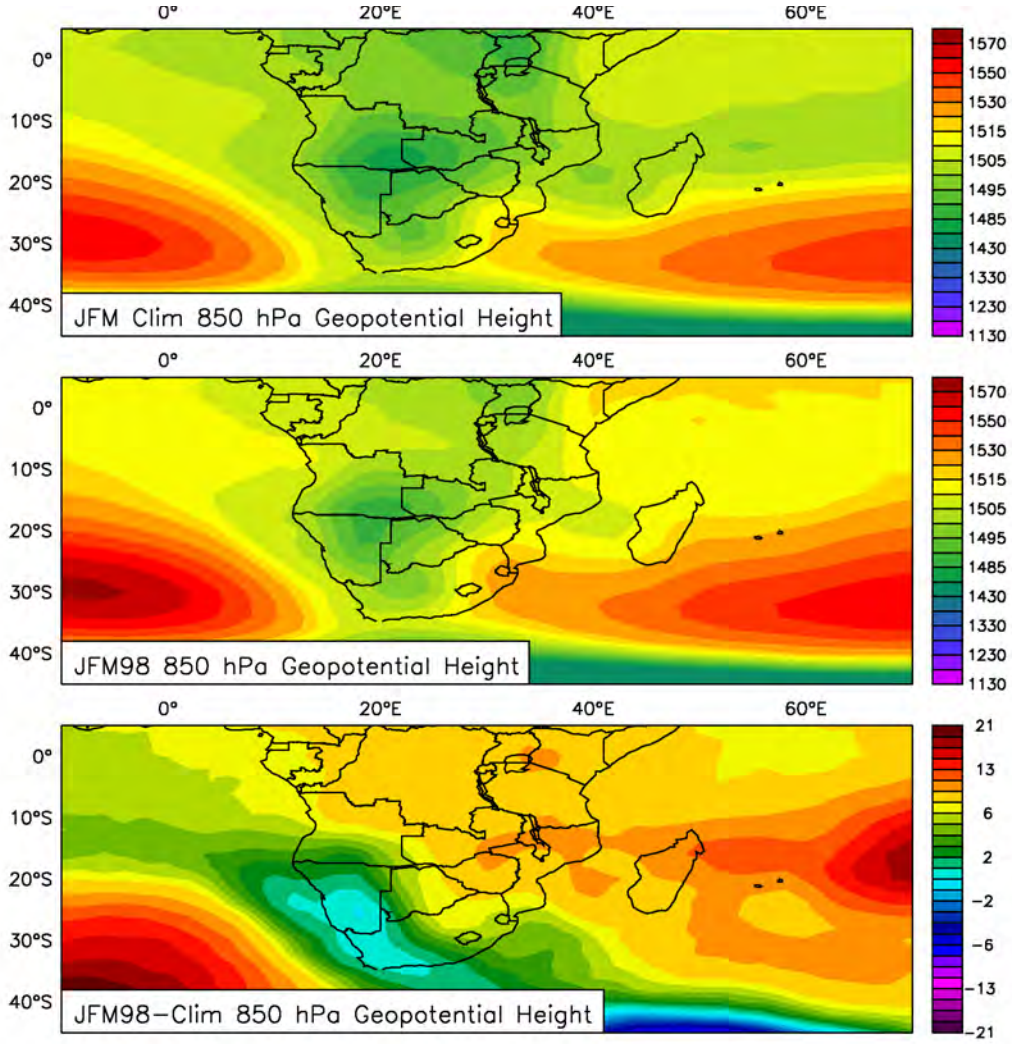

Figure 5.14: NCEP 20th Century JFM 1998 - Clim 850 hPa Geopotential Height (in hPa)

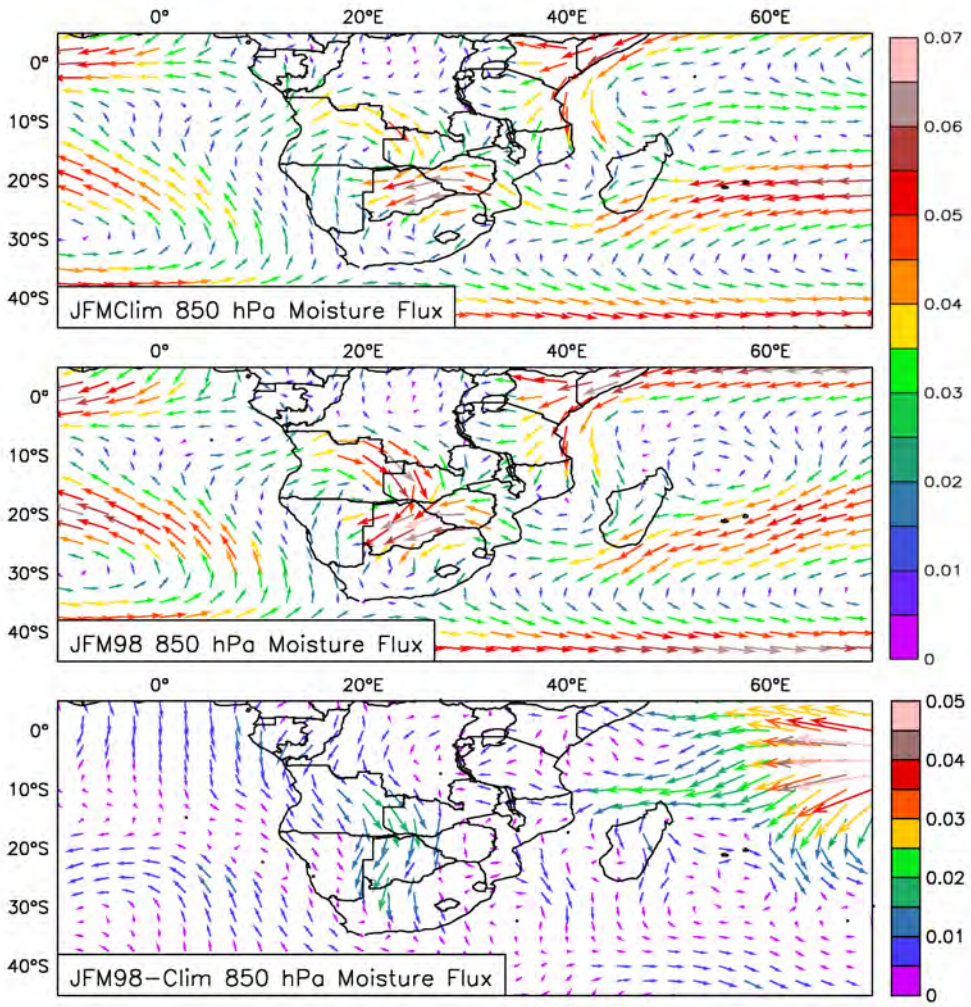

Figure 5.15: NCEP 20th Century JFM 1998 - Clim 850 hPa Moisture Flux (in $\mathrm{m{\cdot}s^{-1}}$)

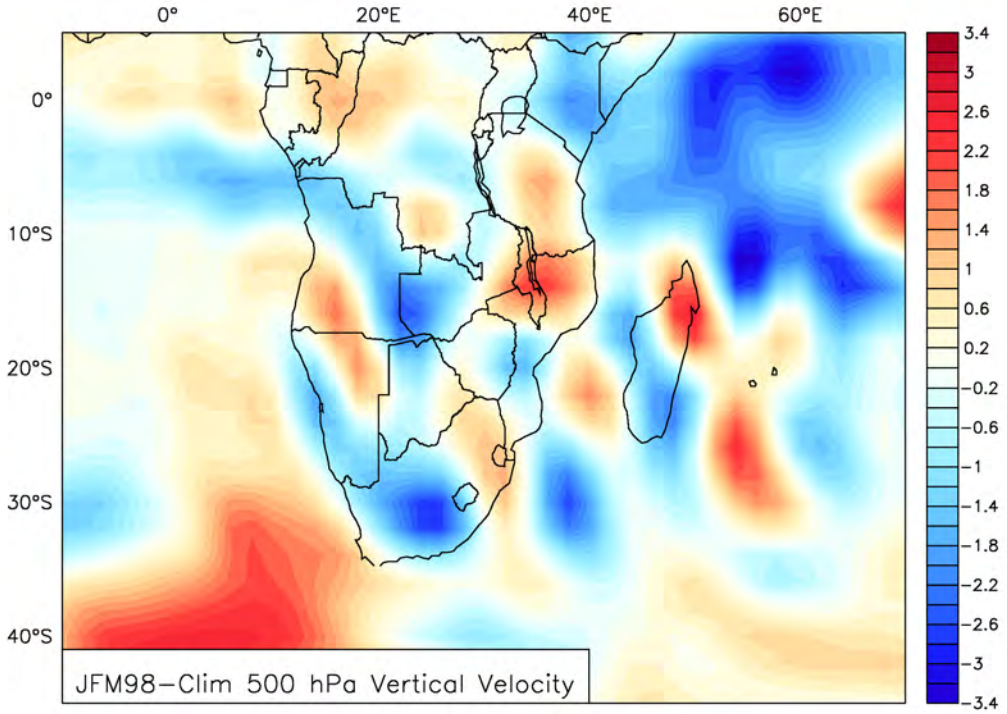

Figure 5.16: NCEP 20th Century JFM 1998 - Clim 500 hPa Vertical Velocity (in 10^2 kg·m^{-1}·s^{-3})

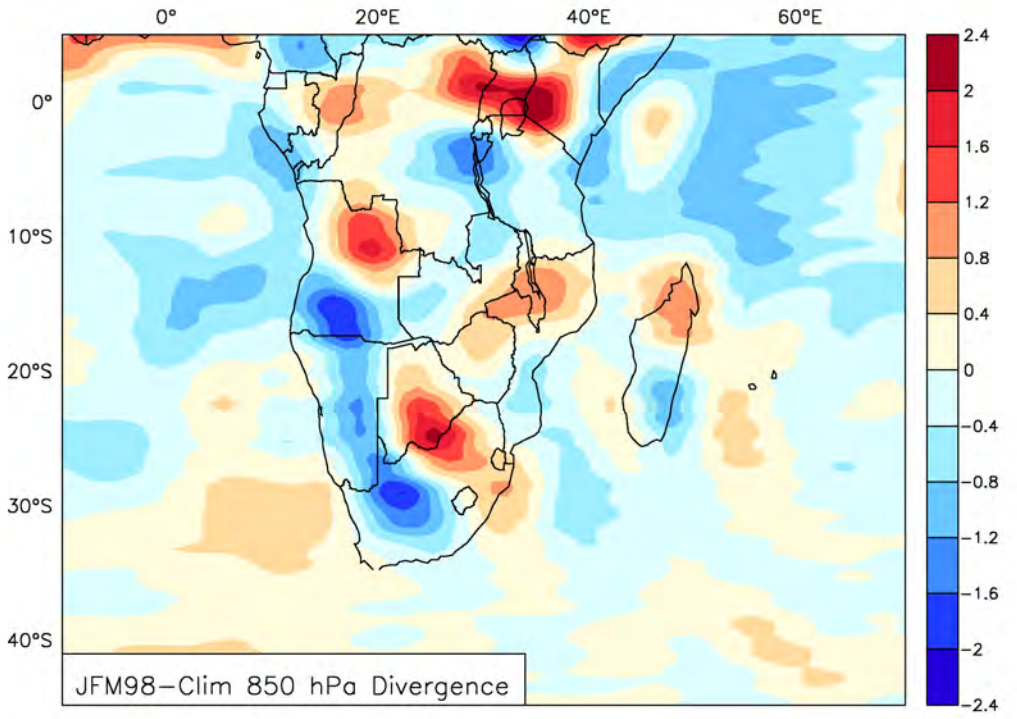

Figure 5.17: NCEP 20th Century JFM 1998 - Clim 850 hPa Divergence (in s^{-1})

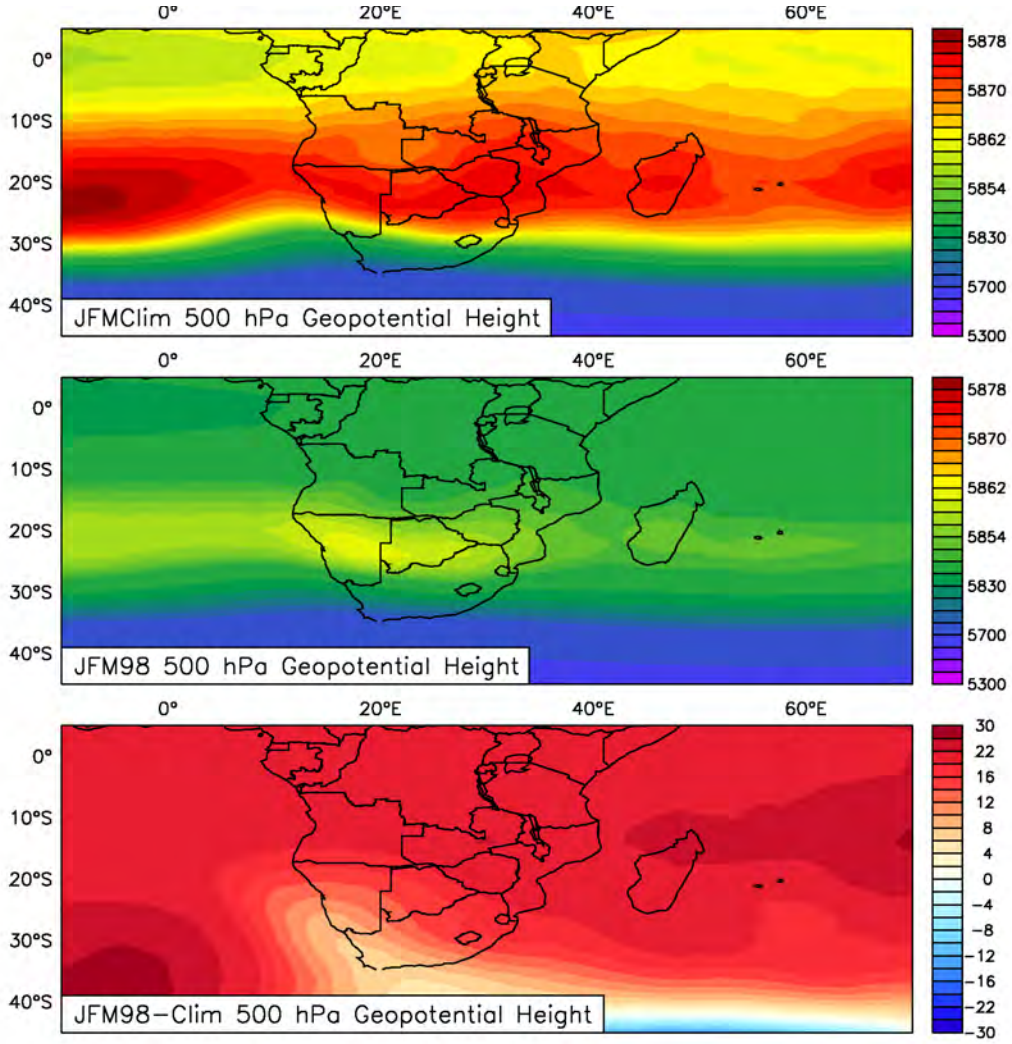

Figure 5.18: 20th Century JFM 1998 - Clim 500 hPa Geopotential Height (in hPa)

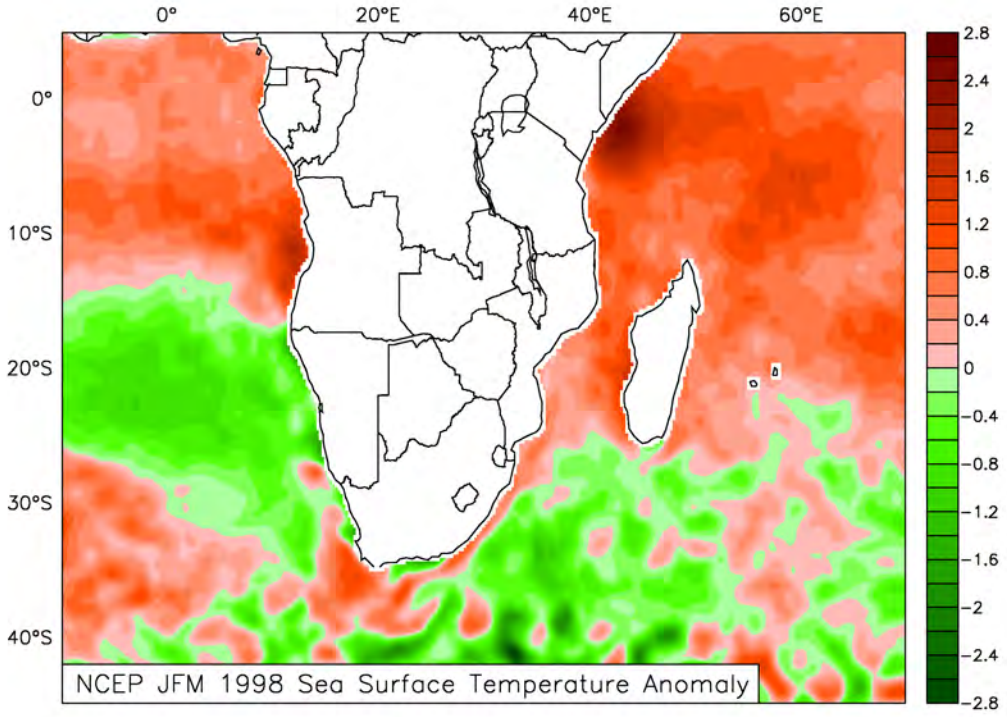

Figure 5.19: NOAA JFM 1998 Regional Sea Surface Temperature Anomaly (in ^{o}C)

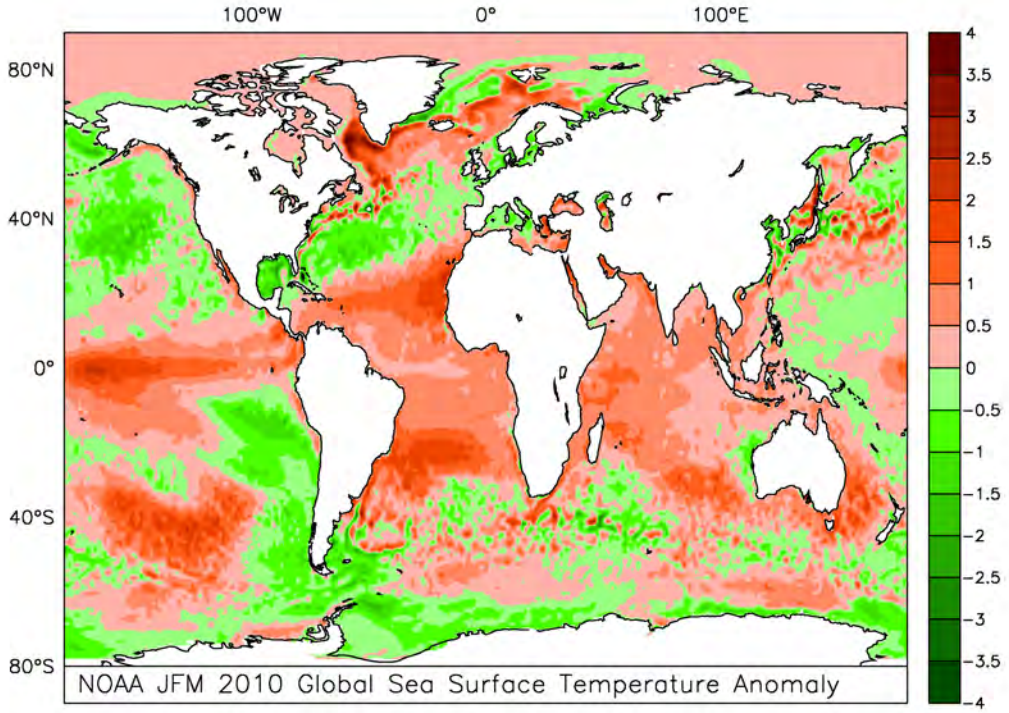

Figure 5.20: NOAA JFM 2010 Global Sea Surface Temperature Anomaly (in ^{o}C)

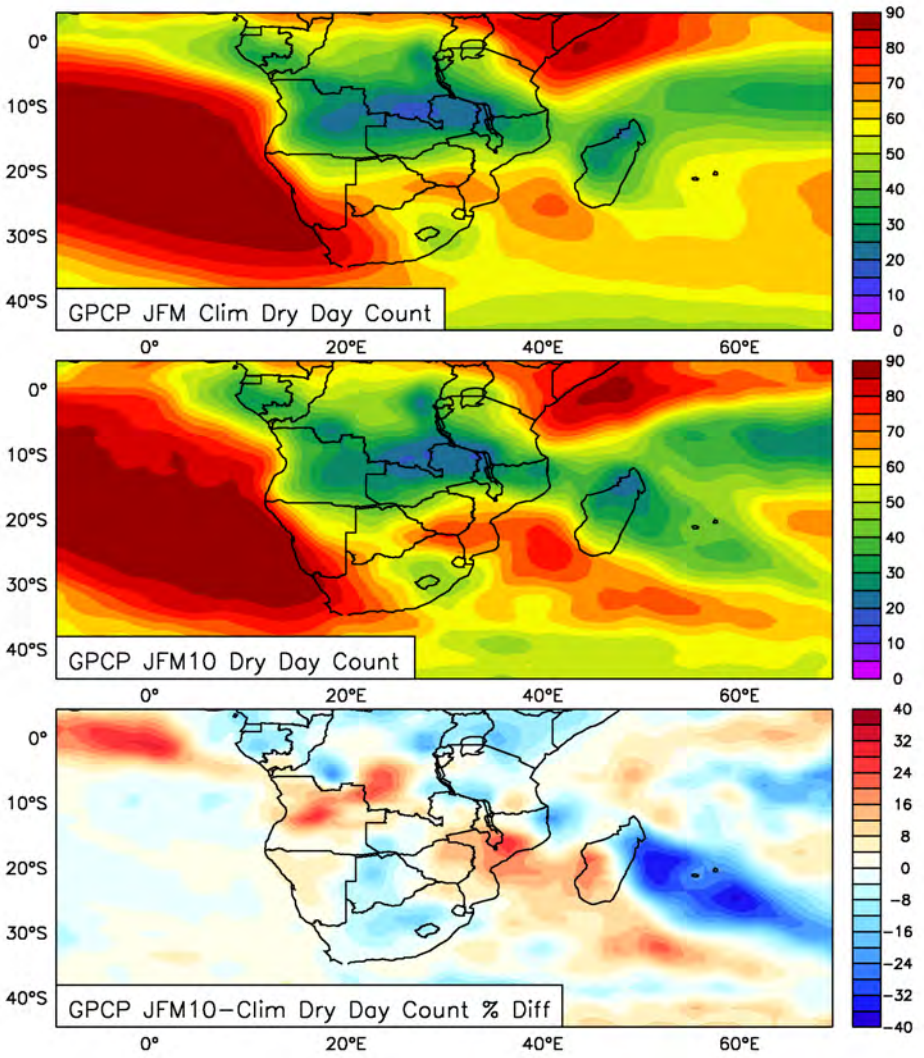

Figure 5.21: GPCP JFM 2010 number of dry days over southern Africa (in days)

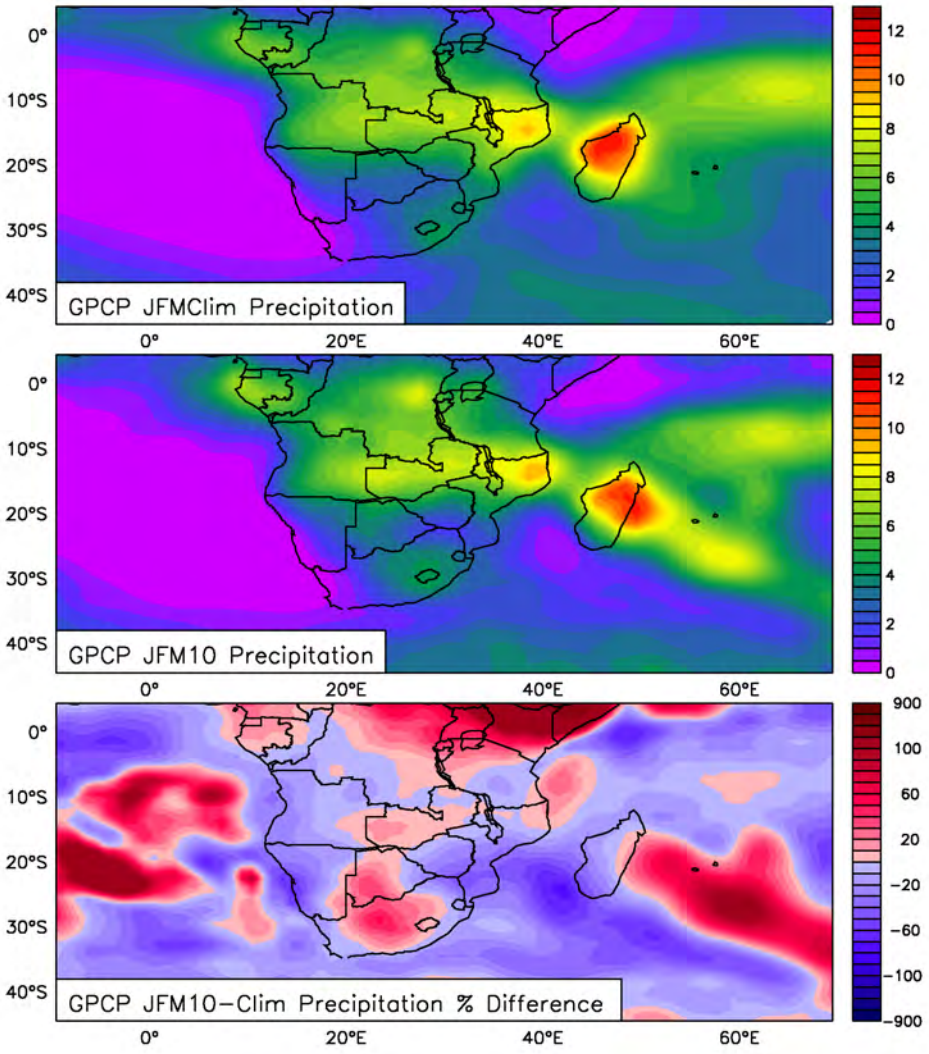

Figure 5.22: GPCP rainfall over southern Africa during JFM 2010 and climatology (in $m \cdot s^{-1}$)

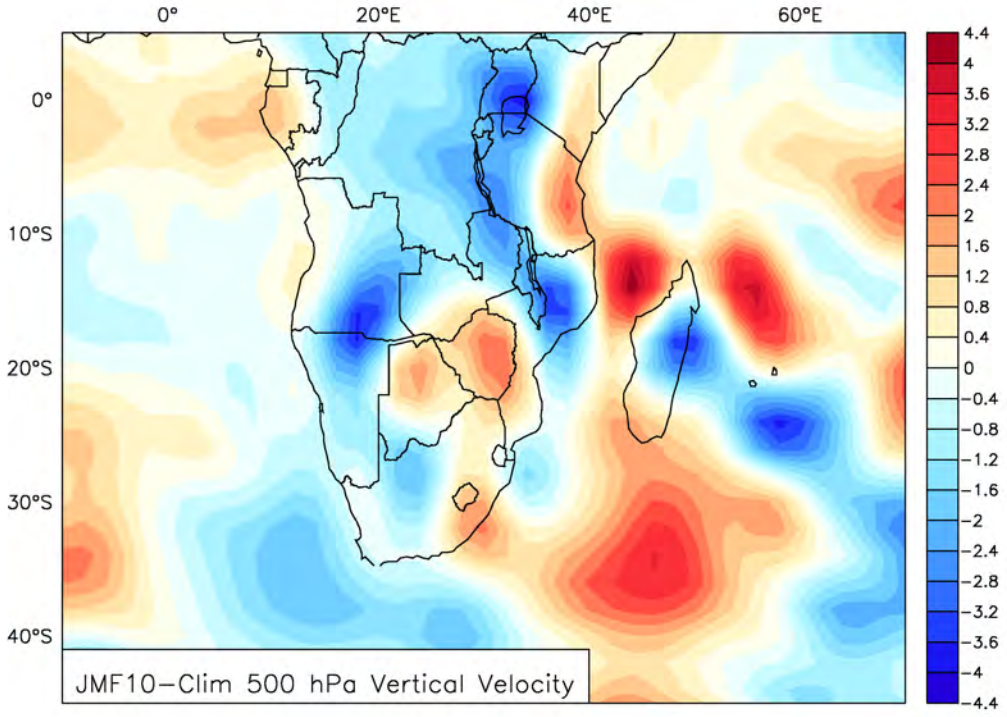

Figure 5.23: 20th Century JFM 2010 - Clim 500 hPa Vertical Velocity (in 10^2 kg·m^{-1}·s^{-3})

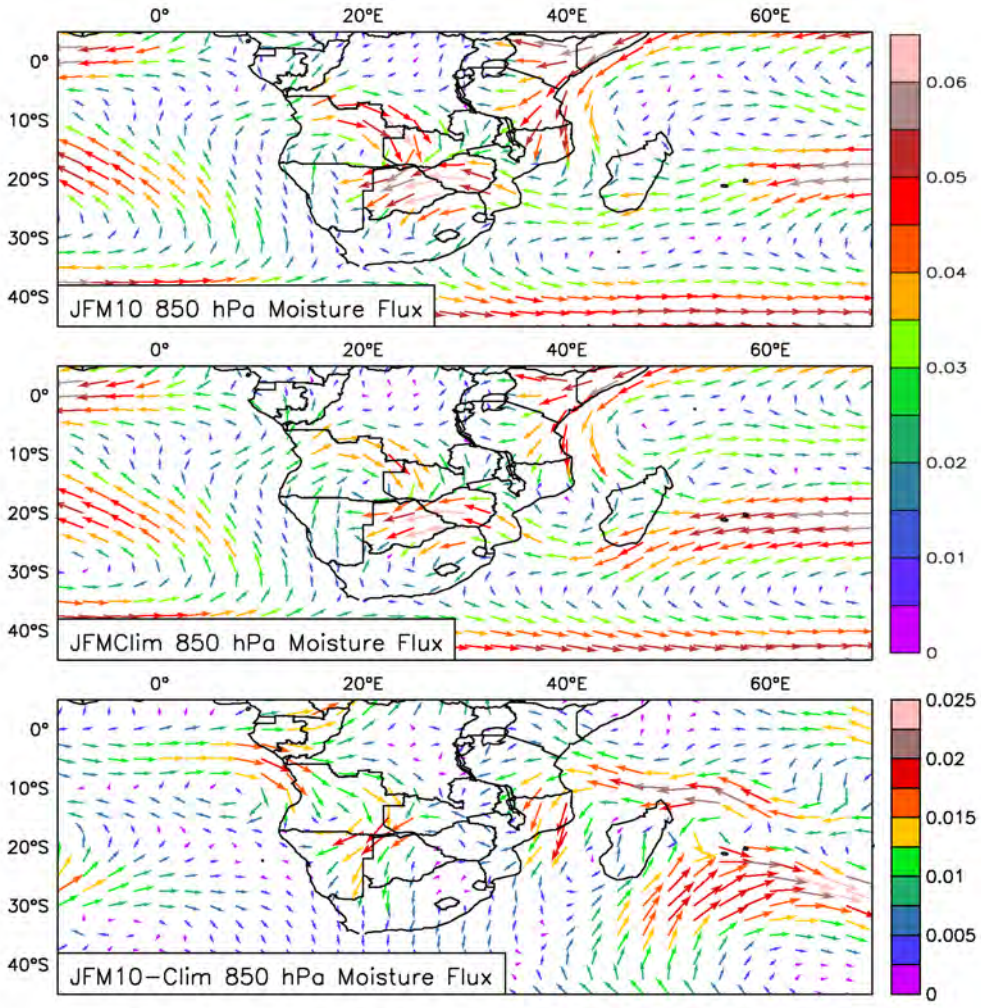

Figure 5.24: 20th Century JFM 2010 - Clim 850 hPa Moisture Flux (in $m \cdot s^{-1}$)

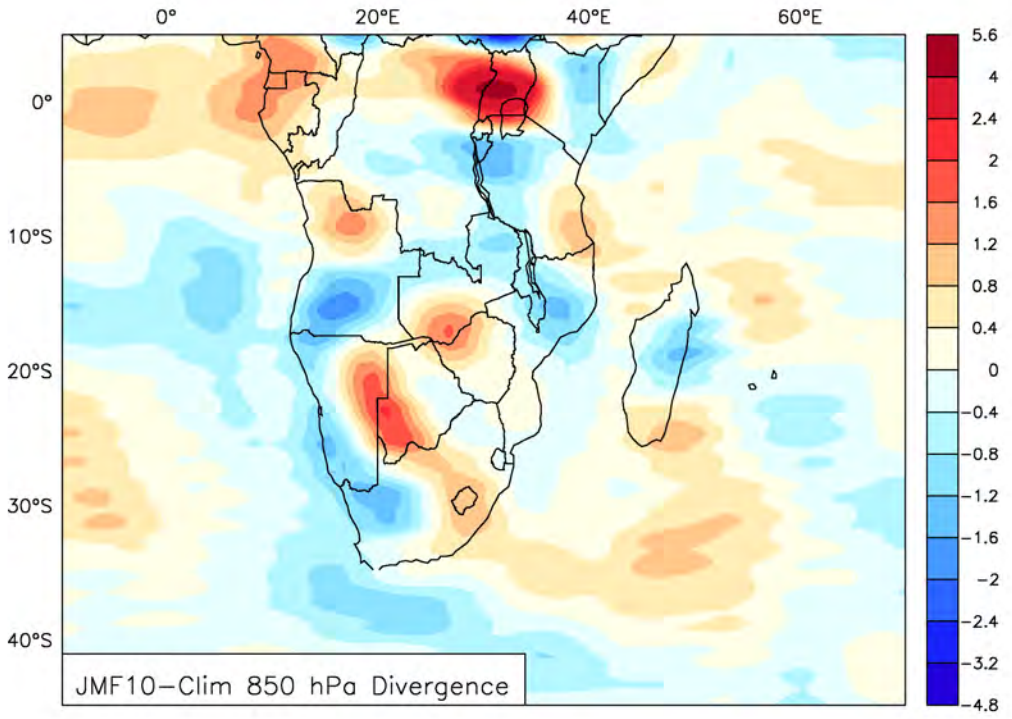

Figure 5.25: 20th Century JFM 2010 - Clim 850 hPa Divergence (in s^{-1})

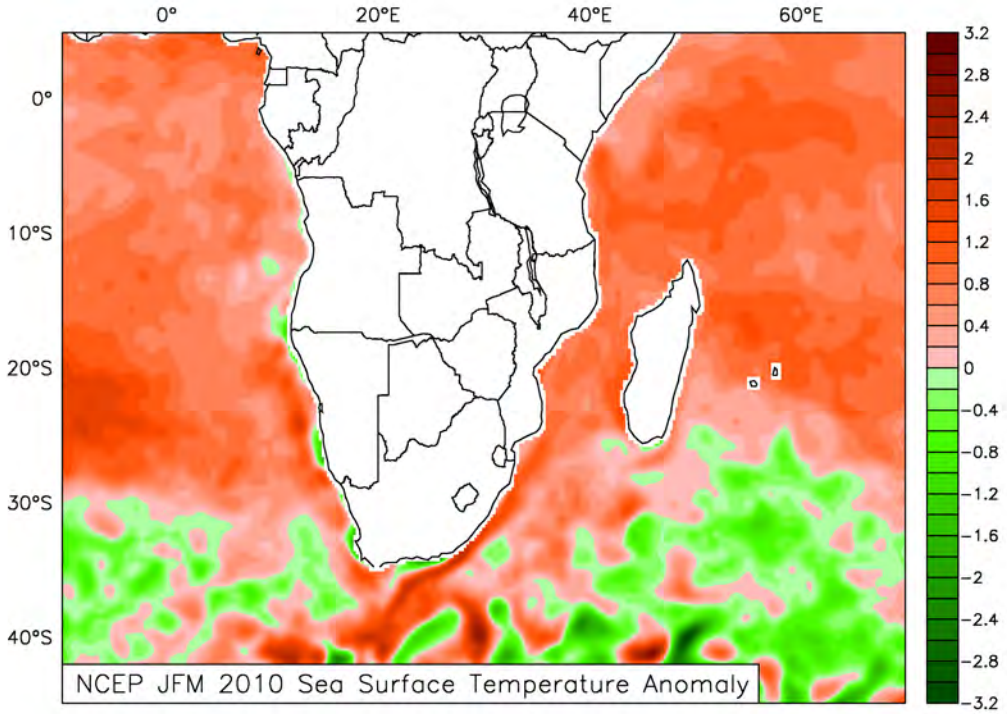

Figure 5.26: NOAA JFM 2010 Regional Sea Surface Temperature Anomaly (in ^{o}C)

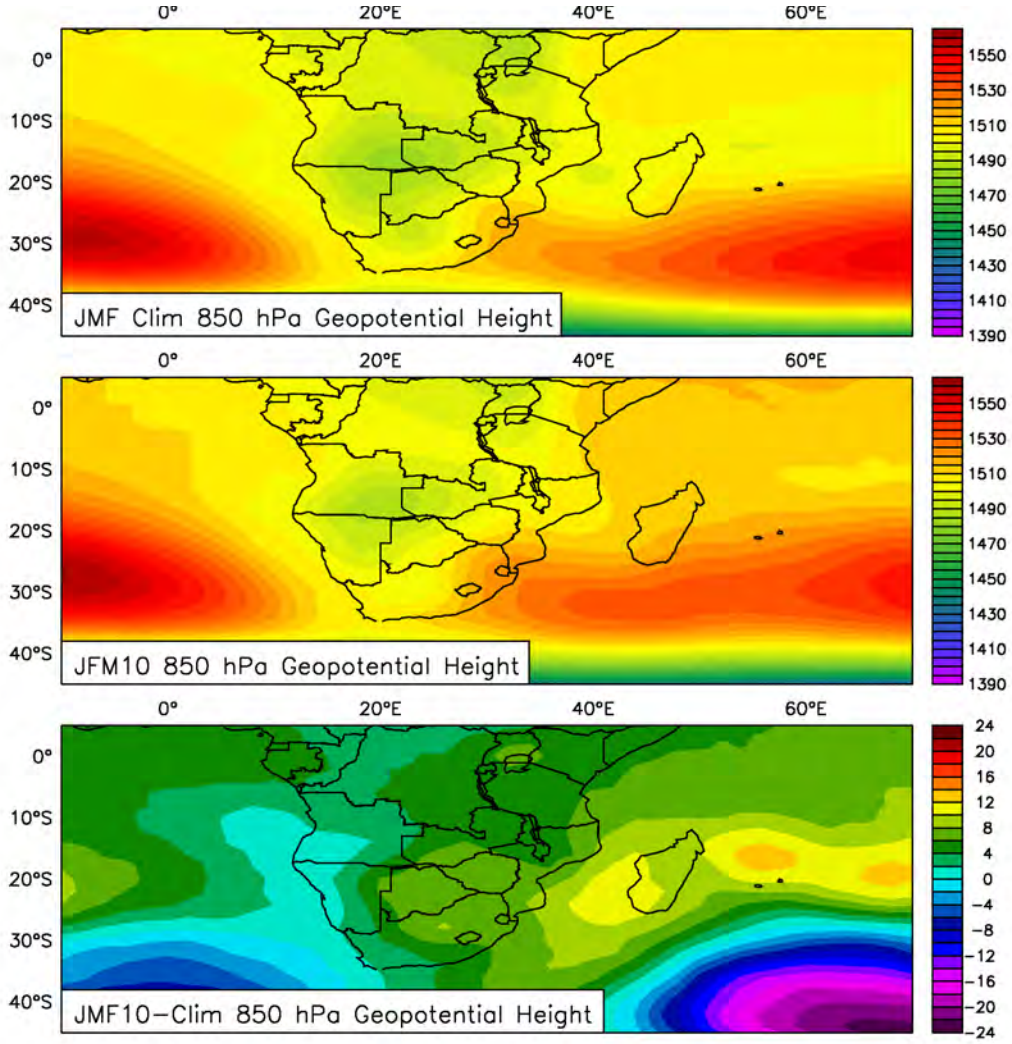

Figure 5.27: 20th Century JFM 2010 - Clim 850 hPa Geopotential Height (in hPa)

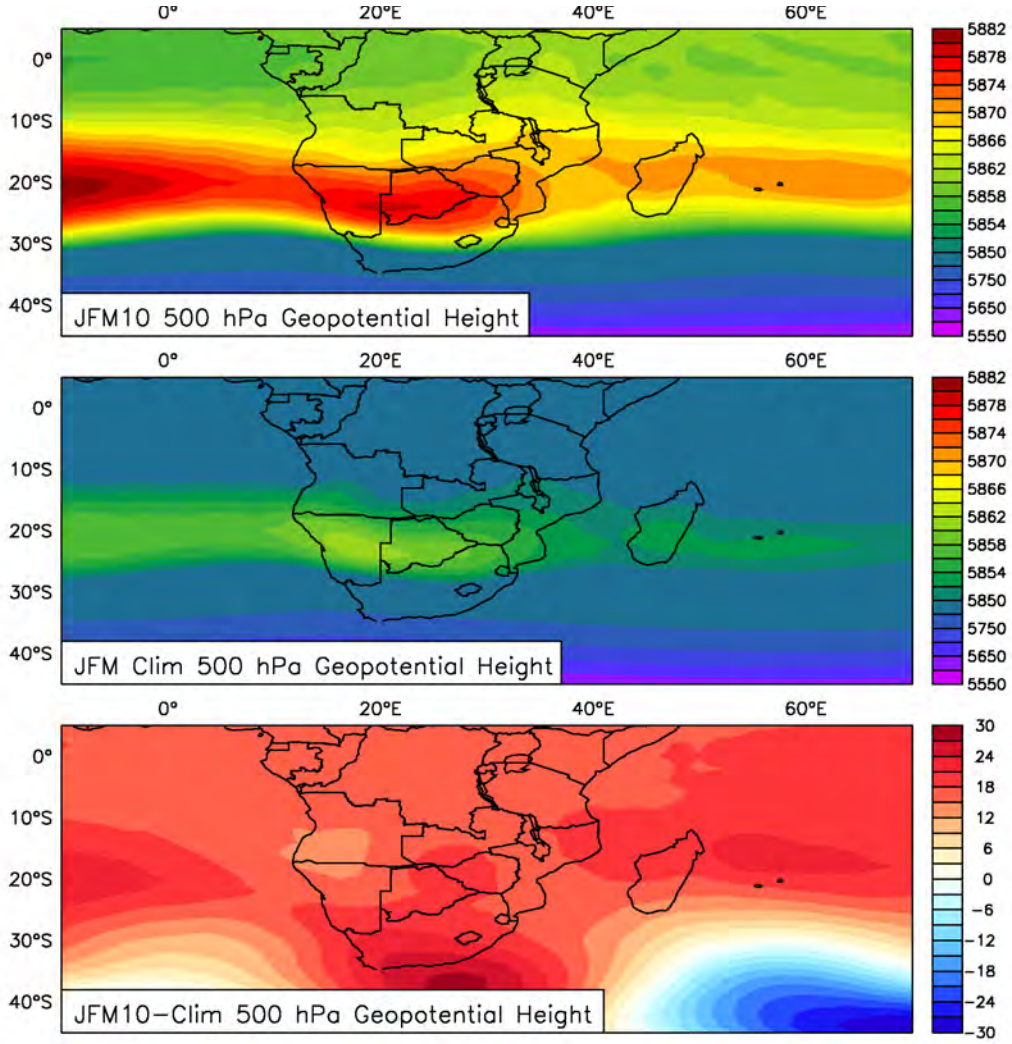

Figure 5.28: 20th Century JFM 2010 - Clim 500 hPa Geopotential Height (in hPa)

Angola and AMO			**Angola and NAO**		
Lag	Correlation	% Significance	Lag	Correlation	% Significance
-3	0.16	62	-3	-0.08	34
-2	**0.38**	**97**	-2	-0.01	2
-1	**0.56**	**100**	-1	0.20	74
0	**0.51**	**100**	**0**	**0.38**	**97**
1	**0.50**	**100**	**1**	**0.50**	**100**
2	**0.45**	**99**	2	0.32	92
3	**0.45**	**99**	3	0.21	75

Table 5.1: Summary of correlations between the area averaged dry day frequency over coastal northern Angola with the AMO as well as the NAO for the JFM seasons during 1979-2011

Angola and SAM		
Lag	Correlation	% Significance
-3	-0.05	23
-2	0.05	22
-1	0.30	91
0	**0.50**	**100**
1	**0.50**	**100**
2	0.18	68
3	0.00	0

Table 5.2: Summary of correlations between the area averaged dry day frequency over coastal northern Angola with the SAM for the JFM seasons during 1979-2011

Coastal Angola	JFM 1997-2012		JFM 1998		JFM 2010	
	Mean	STD	Value	Std Anom	Value	Std Anom
Total rainfall	397.9	61.0	450.9	0.9	323.2	-1.2
Number of dry days	12.9	7.1	8.0	-0.7	25.0	1.7
Number of wet days	5.8	3.1	6.0	0.1	2.0	-1.2
Max conc dry days	4.0	2.2	3.0	-0.5	6.0	0.9
Max conc wet days	1.6	0.8	2.0	0.5	1.0	-0.8
Max rainfall amount	16.8	4.0	19.6	0.7	15.6	-0.3

Table 5.3: Summary of GPCP data over coastal Angola

SA and TIOD			**SA and AMO**		
Lag	Correlation	% Significance	Lag	Correlation	% Significance
-3	-0.26	85	-3	-0.04	18
-2	**-0.35**	**95**	-2	0.16	62
-1	**-0.37**	**97**	**-1**	**0.36**	**96**
0	**-0.36**	**96**	**0**	**0.47**	**99**
1	**-0.37**	**96**	**1**	**0.43**	**99**
2	0.29	90	**2**	**0.42**	**98**
3	0.18	67	3	0.27	86

Table 5.4: Summary of correlations between the area averaged dry day frequency over central South Africa with the TIOD as well as the AMO for the JFM seasons during 1979-2011

Limpopo and Niño 3.4			**Limpopo and Botswana High**		
Lag	Correlation	% Significance	Lag	Correlation	% Significance
-3	**0.41**	**98**	-3	0.27	87
-2	**0.44**	**99**	-2	0.27	86
-1	**0.41**	**98**	-1	0.29	89
0	**0.37**	**96**	**0**	**0.37**	**96**
1	0.32	92	1	0.31	90
2	0.27	87	2	0.18	66
3	0.23	80	3	-0.13	53

Table 5.5: Summary of correlations between the area averaged dry day frequency over the Limpopo with the Niño 3.4 index as well as the Botswana high for the JFM seasons during 1979-2011

Zambia and Niño 3.4			**Zambia and Benguela Niño**		
Lag	Correlation	% Significance	Lag	Correlation	% Significance
-3	**0.50**	**100**	-3	-0.29	88
-2	**0.54**	**100**	-2	-0.34	93
-1	**0.50**	**99**	-1	-0.35	94
0	**0.48**	**99**	**0**	**-0.36**	**95**
1	**0.47**	**99**	1	-0.25	83
2	**0.47**	**99**	2	-0.12	43
3	**0.48**	**99**	3	0.00	3

Table 5.6: Summary of correlations between the area averaged dry day frequency over North East Zambia with the Niño 3.4 index as well as the Benguela Niño for the JFM seasons during 1979-2011

Coastal Angola	JFM 1997-2012		JFM 1998		JFM 2010	
	Mean	STD	Value	Std Anom	Value	Std Anom
Total rainfall	397.9	61.0	450.9	0.9	323.2	-1.2
Number of dry days	12.9	7.1	8.0	-0.7	25.0	1.7
Number of wet days	5.8	3.1	6.0	0.1	2.0	-1.2
Max conc dry days	4.0	2.2	3.0	-0.5	6.0	0.9
Max conc wet days	1.6	0.8	2.0	0.5	1.0	-0.8
Max rainfall amount	16.8	4.0	19.6	0.7	15.6	-0.3

Table 5.7: Summary of GPCP data over coastal Angola

Central SA	JFM 1997-2012		JFM 1998		JFM 2010	
	Mean	STD	Value	Std Anom	Value	Std Anom
Total rainfall	261.2	88.9	305.1	0.5	340.8	0.9
Number of dry days	47.1	8.8	55.0	0.9	37.0	-1.1
Number of wet days	6.6	3.8	11.0	1.2	10.0	0.9
Max conc dry days	10.7	2.8	10.0	-0.3	7.0	-1.3
Max conc wet days	2.0	1.0	2.0	0.0	3.0	1.0
Max rainfall amount	25.1	11.0	42.8	1.6	34.5	0.9

Table 5.8: Summary of GPCP data over Central South Africa

Limpopo	JFM 1997-2012		JFM 1998		JFM 2010	
	Mean	STD	Value	Std Anom	Value	Std Anom
Total rainfall	271.6	151.8	184.4	-0.6	210.7	-0.4
Number of dry days	51.3	7.4	51.0	0.0	54.0	0.4
Number of wet days	8.1	6.7	1.0	-1.1	5.0	-0.5
Max conc dry days	10.3	2.3	10.0	-0.1	14.0	1.6
Max conc wet days	2.8	2.0	1.0	-0.9	2.0	-0.4
Max rainfall amount	27.3	12.4	22.6	-0.4	28.7	0.1

Table 5.9: Summary of GPCP data over Limpopo

NE Zambia	JFM 1997-2012		JFM 1998		JFM 2010	
	Mean	STD	Value	Std Anom	Value	Std Anom
Total rainfall	662.4	54.9	662.3	0.0	678.5	0.3
Number of dry days	4.7	2.8	6.0	0.5	3.0	-0.6
Number of wet days	23.1	3.5	24.0	0.3	24.0	0.3
Max conc dry days	1.9	0.9	2.0	0.1	2.0	0.1
Max conc wet days	3.9	1.2	4.0	0.3	4.0	0.3
Max rainfall amount	24.8	4.5	20.0	-1.1	24.9	0.0

Table 5.10: Summary of GPCP data over North East Zambia

Chapter 6

Model Validation

Climate modelling is a powerful tool that can be used to investigate aspects of climate circulation that observational data and statistical analysis may not be as well suited to. In particular, sensitivity experiments can help uncover the relative importance of different forcing factors on a system, which in turn can lead to better understanding and hence better forecasting. The 1997-1998 and 2009-2010 El Niños and their impact on southern African rainfall are investigated through sensitivity experiments using the model CEU (introduced in Chapter 3). This chapter provides a detailed validation of the model.

Model validation is conducted in order to confirm the ability of the model to represent the observed climate and its variability (Oreskes et al., 1994). A comparison is performed in this chapter to investigate whether the model

is quantitatively and/or qualitatively consistent with observational data. It is also important to try to understand possible reasons why CEU may differ from observational data sets in order to better understand the strengths and weaknesses of the model when analysing results.

The CEU climatology simulation is compared to CRU observational data as well as 20th Century, ERA-Interim and GPCP reanalysis data sets for the late summer rainfall season from January to March (JFM). Since it is known that, for some variables like precipitation, there are sizeable differences between various observational data sets, the comparison with the model output is performed with several different observational data sets. For the circulation fields, both 20th Century and ERA reanalysis data are used. Since reanalysis data sets incorporate model output, care must be taken when interpreting comparisons with the model.

The validation is performed for variables including rainfall, temperature, winds, vertical velocity, zonal wind, sea level pressure, moisture flux, surface pressure and latent heat flux. The primary region of interest in this study is southern Africa. However, global-scale validation is necessary to confirm that the model adequately captures global climate features and processes that are important for southern African climate including the ITCZ, Hadley and Polar cells, the correct location of temperature minima and maxima, and the strong westerly jets in the midlatitudes.

6.1 CEU Climatology

The grid used in each of the simulations performed in this thesis is shown in the previous chapter (**Figure 3.1**). The grid is stretched to a resolution of 0.5^ox0.5^o over southern Africa, 1^ox1^o over much of the rest of the globe and 2^ox2.5^o over the Pacific Ocean and the poles. Due to the high resolution of the model experiments and the limitations of the facilities available, a model month took approximately 2 real time weeks to complete. As a result, rather than run one 21 year simulation to create a climatology for the JFM season, 21 simulations of 5 months each were run. Computational limitations and the calculated spin up time of 35 days (see Chapter 3) meant that each experiment was run from the 15th of November of the previous year until the 31st of March for each of the years from 1990 to 2010. The climatology run, referred to as Clim, was created by averaging the JFM values for each of these 21 years. Due to the space and time restrictions a climatology was not created for the winter months and hence validation is only performed for the austral summer.

6.2 Zonally Averaged Data

Zonally averaged precipitation for JFM (**Figure 6.1**) shows that CEU generally captures the correct distribution of global precipitation. The model exhibits an equatorial double maximum associated with the position of the ITCZ, which may indicate that CEU produces a double ITCZ which is com-

mon in many models. The southern hemisphere rainfall maximum just south of the equator is almost identical in both magnitude and position when compared with GPCP. It is underestimated by 1-3 mm·day^{-1} and shifted slightly northward when compared with 20th Century and CRU. The local minimum at 35^{o}S associated with the subtropical highs falls within the average of the rainfall levels of the different observational data, although both CEU and 20th Century reanalysis shift the minima poleward when compared to GPCP data. The local maximum at 50^{o}S associated with the westerly storm-track region is also well represented in CEU. North of the equator, the model captures the local minimum at 20^{o}N during JFM, the maximum at 40^{o}N, and the decline of rainfall levels north of that latitude.

CEU zonally averaged sea level pressure reflects the presence of the equatorial trough, as well as subtropical highs at approximately 30^o, together with the circumpolar trough near the south pole (**Figure 6.2**). Pressure between 50^{o}S and 90^{o}S is significantly lower in the model than it is in observations (up to 110 hPa) and the location of the local minimum is further south in the model by about 20^o. This may be due to the smoothing of the model topography over Antarctica, the higher resolution of the model over the poles, or a warm bias in the model at the poles. The lower pressure between 30^{o}N and 70^{o}N represents the location of the ascending branch of the Polar cells although the pressure is lower in CEU than it is in observations and the drop in pressure around 30^{o}N is rather sharp. The only regions over which CEU

slightly overestimates sea level pressure are at the local maxima at 30^oS and 85^oN.

Figure 6.3 shows that the equatorial maximum in zonally averaged specific humidity during JFM is reasonably well reflected in the model, although the magnitude is $2 - 4$ g kg^{-1} less than observations which indicates that CEU underestimates the mean meridional moisture.

The seasonal magnitude and location of zonally averaged moisture flux at the 850 hPa level during JFM is well captured in the model (**Figure 6.4**). The low-level southern (northern) maximum of westerly moisture flux in JFM around 50^oS (35^oN) is a few degrees further south (north) in CEU than in observations, as well as being approximately 10 (5) g kg^{-1} m$\cdot$s^{-1} stronger. The low-level southern (northern) easterly moisture flux around 20^oS (10^oN) is slightly further south in CEU than observations, as well as being approximately 10 g kg^{-1} m$\cdot$s^{-1} weaker (stronger).

The structure of zonally averaged zonal wind at 200 hPa is well represented in CEU with westerly maxima at 50^oS and 40^oN, although both are overestimated in CEU. The tropical easterly jet stream is positioned slightly further south in CEU when compared to ERA, but the magnitude is well reproduced and the position is in line with 20th Century data (**Figure 6.5**).

6.3 Global validation

The main characteristics of JFM precipitation are fairly well represented by CEU when compared with 20th Century, GPCP, and CRU (**Figure 6.6**). The model captures the subtropical dry regions over the oceans (west of the Americas, Africa and Australia) and over the continents (northern Africa, western southern Africa, the Middle East and Asia). There are a few regions over which CEU produces a seasonal total of up to 2 mm·day^{-1} of rainfall although observational data suggests that those regions do not receive any rainfall. In particular, CEU comes close to producing the correct dry conditions over inland Alaska, central and northern Canada, the central US, Venezuela, Patagonia, Greenland, eastern India, Kazakhstan, southern China, eastern Russia and southern Australia. The dry regions around 30^{o}S caused by the descending arms of the Hadley cell and the dry areas closer to the poles due to the descending arm of the Polar cells are also evident in the model output. The band of maximum precipitation in the tropics is associated with the strong convection of the ITCZ and this zone is clearly visible in the CEU simulations, spanning South America south of the equator, tropical southern Africa, Madagascar and South East Asia. The model also reproduces rainfall over the northern Pacific and Atlantic Oceans over the midlatitude storm tracks which results from cold, dry continental air being destabilised as it moves over the warm western boundary currents. Observed rainfall over the southern tip of South America associated with the impact

of the westerlies on the southern Andes is also well simulated by the model. Over the tropical Pacific, the double maximum associated with the ITCZ and the SPCZ is evident in the model as well as the 20th Century reanalysis and GPCP data sets.

CEU has an anomalous dry region near Zimbabwe over southern Africa and does not capture the very dry JFM conditions over southwest South Africa and Namibia. Rainfall totals over South America and southern Africa are lower in the model than the observations, which is atypical model behaviour as overestimated rainfall is more common (Landman and Beraki, 2012; Joubert and Hewitson, 1997; Goddard and Mason, 2002). There are some regions where CEU does overestimate rainfall, but these appear mostly over the oceans. The most notable differences (about 10 mm·day^{-1}) occur over the equatorial western Pacific, the eastern Indian Ocean, and the Mozambique channel.

Figure 6.7 confirms that the surface pressure of CEU has the same pattern of distribution as those seen in 20th Century and ERA although its magnitude is lower over the continents. The model captures the pattern of lowest surface pressures over higher topography as can be seen over the Himalayas in Asia, the Andes in South America, the Rockies in North America, Greenland, and Antarctica. CEU also captures the correct pattern of pressure over the oceans, although the magnitude is higher in CEU than

in reanalysis and most of the highs are slightly westward of their positions in reanalysis (**Figure 6.8**). The subtropical highs over the ocean and the Antarctic Circumpolar Trough are particularly overestimated, which is reflected in the anomalous low level circulation in CEU (**Figure 6.9**). The 850 hPa wind flow in CEU displays the general features of the global circulation correctly, although the magnitude of winds over some regions are up to 18 $m{\cdot}s^{-1}$ higher in the model than those in the reanalysis data sets (**Figure 6.10**). The model simulates both the circulation associated with the subtropical highs as well as their location between 10^oS and 40^oS and 20^oN and 50^oN which is characteristic of the season. The midlatitude westerlies between 40^oS and 60^oS and between 30^oN and 60^oN are also well represented in CEU in terms of location, while the magnitude of the flow is noticeably higher in the model. This is also visible in the zonally averaged zonal winds at the 850 hPa level (**Figure 6.11**). The northern hemisphere northeasterly trade winds are well positionally represented in CEU, as are the southern hemisphere southeasterly trade winds, although there is an easterly bias present. The model appears to increase its overestimation of the magnitude of the midlatitude westerlies over land (**Figure 6.10**). The northeasterly trades over West Africa are stronger and more easterly in direction in the model in comparison to 20th Century and ERA. The monsoonal winds along the east coast of Africa are stronger in the model and the easterly flow into southern Africa from the South Indian Ocean is also stronger.

The mid-level flow at 500 hPa is well captured in CEU when compared with observations although the winds are stronger in CEU (**Figure 6.12**). The locations of the westerly midlatitude jet streams at 30^oN to 50^oN and 40^oS to 60^oS are well reproduced. The winter (northern) hemisphere jet stream is stronger than the summer (southern) hemisphere jet stream and flow is also stronger in the eastern hemisphere than in the western hemisphere in JFM, and this feature is present in both the model and the reanalysis data sets. The difference in wind speeds in CEU and the reanalysis when considering the northern hemisphere jet is up to 42 $m{\cdot}s^{-1}$. CEU produces a very strong jet over land which is not present in the reanalysis data. The anticyclonic circulations over South America, southern Africa and the western Pacific are associated with summer deep convection and are well reproduced in CEU. The anticyclonic circulation over South America is known as the Bolivian high and its strength and position has been associated with rainfall over the Altiplano (Lenters and Cook, 1997, 1999), while the anticyclonic feature over southern Africa is consistent with the Botswana high discussed in Chapter 4.

Much like the 850 and 500 hPa global pattern of wind flow, the upper-atmosphere 200 hPa wind pattern is also well reproduced in CEU, although the wind speeds are higher (**Figure 6.14**). The jet streams at 30^oN to 50^oN and 40^oS to 60^oS are well positioned in the model although the winds are stronger in the model than observations (up to 22 $m{\cdot}s^{-1}$). The zonally aver-

aged zonal winds indicate that the jet streams are well positioned although their magnitude is higher, however, the northern hemisphere jet appears to be narrower in CEU than those in the reanalysis data sets. Winds over the North Atlantic poleward of 50^{o}N are not well represented in CEU when compared with 20th Century and ERA (**Figure 6.15**). The anticyclonic circulation over southern Africa is stronger in CEU and the easterlies making up the top of the circulation over 25^{o}S occur further to the north than in observations.

Figure 6.16 shows that CEU captures the general pattern of observed global temperature during JFM. Both observed and simulated temperature fields show that temperatures are maximum over the tropical regions where the incoming solar radiation is at its strongest. In agreement with observations, the simulated temperatures decrease as latitude increases and reach minimum values over the polar regions. In addition, the decrease in temperature arising from increased altitude can be seen over the mountainous regions of the Himalayas, the Andes, the Rocky Mountains and the Drakensberg range in South Africa.

However, CEU shows warm bias over some regions and cold bias over others. There is a band of warm water over the equatorial region in CEU that is not as pronounced or as large in 20th Century, ERA, or CRU. Maximum temperatures over northern Australia are lower in the model than in

observations, while temperatures over western North America are not as cool in the observations as those in CEU. Furthermore, a cold bias is evident over the Himalayas, while temperatures over the Andes mountains are not as low as those observed.

Further confirmation that the Polar and Hadley cells are well captured in CEU is evident in **Figure 6.17** where the zonally averaged vertical velocity compare well with observations, although not in the far south. Although the locations of these cells are well positioned, the speed at which air ascends and descends is higher in the model. The strong vertical motion over the southern polar region is evident in the model although it is weaker in magnitude than the reanalysis data. There is a band of vertical motion centred on the equator indicating that air over this region is rising where the Hadley cells meet and form the ITCZ. This motion is both stronger and closer to the surface in the model than in observations and causes CEU to produce higher levels of precipitation than those observed. This anomaly is also evident in the midlatitudes around 40^o - 50^o.

6.4 Regional validation

Rainfall is one of the most difficult variables to model with accuracy (Joubert and Hewitson, 1997; Landman and Beraki, 2012). CEU captures some of the main features of rainfall over southern Africa, such as the band of

precipitation associated with the ITCZ around and north of approximately 15^{o}S in eastern South Africa, as well as the region of minimal rainfall over the South Atlantic Ocean and along the west coast (**Figure 6.18**).

The anomalously high rainfall over the Mozambique Channel in CEU can be largely explained by examining the 850 hPa winds in **Figure 6.19**. The model winds are generally much stronger than those in the reanalysis, and, in particular, the northeast monsoonal flow from the North Indian Ocean towards Tanzania, the monsoonal northwesterlies towards Madagascar and the southeasterly flow from the South Indian Ocean are too strong in CEU. This may indicate that the model struggles to adequately capture circulation over areas with sharp topography gradients. The two air flows lead to a strong cyclonic feature over the Mozambique Channel which is much weaker in the other two data sets. This, coupled with the anomalously high latent heat flux there (**Figure 6.20**), promotes rainfall over the Channel. It is worth noting, however, that the latent heat flux in CEU south of about 25^{o}S appears to capture the Agulhas current and retroflection reasonably well which is often not the case in forecasting models (Rouault et al., 2003b).

The anomalous winds may also explain the rainfall anomalies over southern Africa south of 20^{o}S. Due to the strength of the southeasterlies from the South Indian Ocean, this flow continues much further across the continent in CEU than it does in the 20th Century reanalysis. Although the South

Atlantic Anticyclone does appear to be stronger in CEU than observations, the strength of the continental winds pushes the anticyclonic flow further west over the Atlantic Ocean. As a result, western southern Africa is dominated by northerly winds rather than southerly winds, which leads to the anomalously high rainfall over Namibia and western South Africa in CEU. This also forms an anticyclonic flow which produces the dry region over eastern Botswana, Limpopo, and western Zimbabwe. This anticyclonic flow is reminiscent of the Botswana high discussed in Chapter 4.

Sea level pressure in CEU is highest in the South Atlantic and Indian Oceans over the subtropical high pressure systems and these features are also displayed in observations (**Figure 6.21**). The maximum pressure levels over the South Indian Ocean are concentrated further east in CEU than in observations. However, the magnitude is up to 7 hPa higher in CEU and this higher sea level pressure may contribute to stronger winds over those regions. The sea level pressure over the South Atlantic Ocean is also slightly eastward in CEU when compared with reanalysis and is also up to 7 hPa higher. This may be related to the stronger Hadley cell produced by CEU.

The full cyclonic circulation of the Angola low is not captured in CEU unlike in 20th Century reanalysis, although there are westerlies over northern Angola which reflect some aspects of the Angola low in the model. Compared with 20th Century, it is located north east of the reanalysis. The Angola low

is often poorly captured in models (Reason and Jagadheesha, 2005; Lyon and Mason, 2007) and in particular it is not visible in the ERA reanalysis. The anticyclone centred over eastern South Africa in the model is substantially stronger than the flow seen in either reanalysis.

In **Figure 6.22**, it can be seen that the zonally averaged surface easterlies between 20^oS and 30^oS are stronger in CEU than in the reanalysis. The model shows weak westerlies between approximately 10^oS and 0^o which are not evident in the ERA reanalysis data and only very weakly present in the 20th Century reanalysis. The upper level zonal winds south of 25^oS are a bit stronger in CEU than observations, particularly near the top of the column, but otherwise display the correct pattern.

The convergence and divergence of moisture at 850 hPa as well as the moisture flux is displayed in **Figure 6.23**. The model more or less simulates the correct general pattern of divergence and convergence of moisture over southern Africa with two notable exceptions. Firstly, for the region along the western coast of Namibia and South Africa as well as the southern part of South Africa, the reanalysis data indicates divergence whereas the model displays convergence. Secondly, the region over northern Zambia / southern DRC displays convergence in the model while reanalysis mainly show divergence.

The moisture flux vectors show similar problems to those discussed above when looking at the 850 hPa winds. In particular, the northeast monsoonal flow from the North Indian Ocean, the northwesterly monsoonal flow towards Madagascar and the southeasterly flow from the South Indian Ocean are much stronger in CEU than reanalysis. It is hard to make a statement about the moisture influx from the Atlantic Ocean because the two reanalysis data sets differ so strongly.

Figure 6.24 illustrates that CEU surface temperatures are comparable with those observed. The cool temperatures observed over the high altitude regions of Tanzania, Zambia, Malawi, Zimbabwe, Angola, and Lesotho as well as warmer conditions over Botswana are well represented in CEU. However, the warm conditions over the DRC, Namibia and western South Africa are not well captured by the model. The cold temperature bias over the Drakensberg mountains may be due to model distortion of topographical features, which is further supported by the bias seen over the mountainous regions of Tanzania and Kenya (**Figure 6.25**). The cold bias over the Karoo desert is likely to be a result of the enhanced precipitation produced in the model (**Figure 6.18**).

Some of the precipitation anomalies between CEU and observations may be explained by considering the vertical overturning over the southern African region (**Figure 6.26**). The negative vertical velocity between 5^{o}S and 25^{o}S

in CEU is also apparent in ERA reanalysis, but only occurs in 20th Century data above approximately 700 hPa. South of 25^{o}S, the air descends faster in the model than it does in the observations.

The moisture flux into and out of southern Africa produced in CEU is compared to that of 20th Century and ERA by considering the vertical and horizontal transects of moisture flux with height. A boundary around southern Africa is formed by the box shown in **Figure 6.27**. **Figure 6.28** keeps longitude fixed at 10^{o}E forming a boundary parallel to the west coast of Africa; **Figure 6.29** keeps latitude fixed at 32^{o}S which forms the lower boundary of the summer rainfall region of southern Africa therefore excluding the Western Cape; **Figure 6.30** keeps longitude fixed at 42^{o}E so that the right boundary cuts across the Mozambique Channel; and **Figure 6.31** keeps latitude fixed at 10^{o}S which cuts through northern Angola, southern DRC and south Tanzania.

The zonal moisture flux at 10^{o}E indicates that near-surface flow is easterly between approximately 35^{o}S and 15^{o}S and westerly north of 15^{o}S and south of 35^{o}S, which is well captured in the model although the magnitudes in CEU are higher (**Figure 6.28**). In the upper-atmosphere, CEU compares well with ERA, but less so with 20th Century reanalysis. In the Mozambique channel along 42^{o}E (**Figure 6.30**) the model and reanalysis zonal moisture flux agree positionally, but CEU overestimates the magnitude consistently

with too strong and too deep low level westerlies north of 15^oS and easterlies south of 15^oS (**Figure 6.19**).

The transect of the meridional moisture flux along 32^oS is displayed in **Figure 6.29**. The model simulates southerly flow of moisture between 5^oW and 25^oE although it slightly overestimates the magnitude. The direction of weak flow between 30^oE and 60^oE is reversed in CEU when compared with reanalysis. However, the magnitude of the near-surface flow is relatively small. Along 10^oS (**Figure 6.31**), the general pattern of alternating positive and negative values of meridional moisture flux is well captured in CEU although the magnitude is stronger in the model between 35^oE and 50^oE and weaker between 10^oW and 15^oE.

6.5 CAM3 vs CEU

CEU is made up of CAM3 physics and EULAG dynamics, so it is useful to compare validation of CEU with those of CAM3. Validation of CAM3 has been carried out in a number of studies (Collins et al., 2006; Hurrell et al., 2006; Hack et al., 2006a,b). A comparison of the results of these studies of CAM3 and those found in this study might help diagnose potential areas for improvement in CEU. For instance, if an error persists regardless of which dynamics core is used or at what resolution, that might indicate that the problem rests in the physics parametrisation.

CAM3, which forms the physics core in CEU, incorporated several improvements from the previous version CAM2, however, several systematic biases are still present in the model (Collins et al., 2006). These biases include underestimation of implied ocean heat transport in the southern hemisphere, biases in the midlatitude continental precipitation and surface temperatures, errors in the radiative fluxes and surface stress in western coastal regions, and excessive surface stress in the storm tracks. CAM3 also underestimates the variability associated with the Madden-Julian oscillation, and does not produce realistic MJO activity (Collins et al., 2006).

Many GCMs are unable to reproduce the seasonal migration of the ITCZ across the equator (Gates et al., 1999). In particular, the peak of DJF ITCZ precipitation simulated in CAM3 lies more than 10^o north of the CMAP maximum, and illustrates the persistence of ITCZ precipitation north of the equator throughout the year (Hack et al., 2006b). Hack et al. (2006a) investigated the sensitivity of CAM3 to changes in horizontal resolution by comparing the output of simulations run at T42 (approximately 2.8^ox2.8^o) and T85 (approximately 1.4^ox1.4^o) configurations. They found that the radiative response to ENSO was greatly enhanced in the higher resolution experiments as well as local improvements to the representation of clouds and precipitation regimes, such as the improved structure of the Atlantic ITCZ (Hack et al., 2006a). However, the Pacific double ITCZ is largely indepen-

dent of horizontal resolution . Hurrell et al. (2006) also found that there is a tendency for the tropical precipitation maxima to remain in the northern hemisphere throughout the year, while precipitation tends to be higher than observations over tropical Africa. CEU also displays a tendency to produce a double ITCZ, which may just be the SPCZ and a shifted ITCZ (**Figure 6.1**). Hack et al. (2006b) also found that CAM3 overestimates rainfall poleward of the extratropical storm tracks, which is not evident in CEU. Hack et al. (2006b) found that CAM3 overestimated rainfall over much of Africa, particularly over the Congo region and western southern Africa, a characteristic that is also evident in CEU.

Wu et al. (2003) identified convective momentum transport (CTM) as a potential solution to the problem AGCMs have in correctly simulating ITCZ rainfall. The CTM-induced secondary circulation suppresses precipitation along the equator and enhances it away from the equator. It is possible that CTM or new convection parametrisation schemes could improve CEU rainfall performance.

Hurrell et al. (2006) also found that CAM3 reproduces the basic observed patterns of the pressure field but simulated surface pressures are higher than observed over the subtropics which is consistent with an easterly bias in the simulated trade winds and low-latitude surface wind stress. The zonal wind structure in CAM3 is close to observational data, although the middle-

latitude westerlies are too strong in both hemispheres throughout the year, consistent with errors in the simulated pressure field. These errors persisted in CEU and these anomalous wind conditions may have contributed to the anomalies seen in CEU rainfall and other circulation fields (Hurrell et al., 2006).

Representing surface topography at high resolution in models can result in gravity waves that generate noise and are sometimes referred to as "Gibbs ripples" (Lindberg and Broccoli, 1996). The spurious, small-scale errors in model output tend to increase with increased resolution. Various methods of smoothing are applied to topography to avoid this problem. In this study the topography used can be seen in **Figure 6.25**. Unfortunately, the modified topography does appear to affect circulation around regions that experience moderate-to-high topography gradients, which in turn may affect rainfall.

6.6 Two Particular Years of Interest

Rainfall over southern Africa during the late summer seasons of JFM 1998 and JFM 2010 are studied using CEU in Chapter 8. These seasons were chosen because they correspond to strong El Niño summers when the expected rainfall anomalies over southern Africa did not occur. A validation of these two seasons is performed in order to evaluate how well the model performed in capturing climate features over this region. It should be noted that most

numerical forecasting models performed relatively poorly when predicting rainfall over southern Africa during these seasons (Lyon and Mason, 2009; Landman and Beraki, 2010).

6.6.1 JFM 1998

Each of the different observational and reanalysis data sets CMAP, CRU, 20th Century and GPCP display stark inconsistencies in JFM 1998 seasonal rainfall when compared with one another (**Figure 6.32**). However, a general pattern of rainfall anomalies is discernible when considering all these data sets together. Overall, the observational data shows that northern Zimbabwe, Botswana, South Africa (excluding the northeastern part), Angola (except the southwestern part), southern Mozambique, Zambia and Tanzania experienced near or above average rainfall while Namibia, northeastern South Africa, northern Mozambique and most of the DRC experienced below average rainfall. While CEU reflects the same rainfall anomalies as observations over Tanzania, southern Mozambique, Zambia, Zimbabwe and western Angola, it has the opposite rainfall anomalies over Namibia, eastern Angola, South Africa, Botswana and the DRC. The positive rainfall anomalies in CEU over the western Indian Ocean are also evident in CMAP, GPCP and 20th Century, as is the positive rainfall anomaly over the Mozambique channel.

The reanalysis data sets both display a strengthening of the South At-

lantic anticyclone during JFM 1998, and, although this is also captured in CEU, the anomaly is not as large and the anomalous southerlies form further off the coast (as opposed to alongside the coast) as in the case of the reanalysis (**Figure 6.33**). The subtropical high also appears to have shifted southwestward in both the reanalysis and model data (**Figure 6.34**).

The midlatitude westerlies in the southern hemisphere were stronger in JFM 1998 in the reanalysis and in CEU, although in CEU the anomalies persist further north (**Figure 6.33**). The anomalous westerlies over southern South Africa may contribute to the anomalously low rainfall seen in CEU since they bring cooler and drier South Atlantic Ocean air over the region.

The reanalysis data sets both display stronger moisture flux anomalies from the South Atlantic Ocean than are seen in CEU (**Figure 6.35**), which may help to explain the reduced rainfall in CEU over Botswana and South Africa (**Figure 6.32**). The moisture flux input from the South Indian Ocean, on the other hand, is stronger in CEU than it is in reanalysis which may explain the enhanced rainfall over Mozambique in the model.

There was fairly strong relative subsidence between approximately 5^oS and 15^oS in CEU which is not evident in either of the reanalysis data sets (**Figure 6.36**). This position roughly corresponds to the strip of negative rainfall anomalies in CEU across central Angola and the southernmost part

of the DRC. There was also reduced latent heat flux over this region in CEU (**Figure 6.37**) which, coupled with the strong subsidence, could have resulted in conditions that were unfavourable for rainfall over the region. Although ERA also displays negative latent heat flux anomalies over this region, it does not display subsidence and so may not have resulted in below average rainfall.

6.6.2 JFM 2010

Figure 6.38 shows the percentage difference between JFM 2010 rainfall and climatology for CEU as well as the observational and reanalysis data sets CRU, CMAP, 20th Century and GPCP. The observational data sets each display some inconsistency when compared to one another individually, but, when viewed together, a pattern becomes clearer. In particular, there was above average rainfall over South Africa (except the southwest and northeast parts), Botswana, southern Namibia, Zambia, Angola, and the northeastern DRC, while below average rainfall was experienced over much of Zimbabwe, northeast South Africa, southern Mozambique, Tanzania, and northern Namibia in most of the data sets. These precipitation anomalies are generally well reproduced in the model CEU, except over Angola, Zimbabwe and southern Mozambique which all display the opposite rainfall anomaly in the model than that in the observational data.

It is evident in the moisture flux anomalies that there was an anoma-

lously strong Angola low during JFM 2010 which is well captured by CEU (**Figure 6.39**), although it is shifted eastward. This shift in location may partially account for the anomalously high rainfall over Zimbabwe and southern Mozambique seen in the model. The South Atlantic Ocean moisture flux anomalies in the ERA and 20th Century reanalysis are substantially different, with the model anomalies comparing favourably with ERA (**Figure 6.39**). However, in the South Indian Ocean, the reanalysis agree that a weaker South Indian anticyclone occurred during JFM 2010, while CEU indicates that it was stronger. This discrepancy is also reflected in the sea level pressure anomalies (**Figure 6.40**).

6.7 Ensemble Runs

Climate models that make predictions and projections of climate and weather from time scales of days to centuries typically involve parametrisation and approximation and therefore contain some uncertainty (Tebaldi and Knutti, 2007). These uncertainties can be grouped into parameter uncertainty and initial condition uncertainty. Parameter uncertainty is addressed by testing different parametrisations used in models and identifying which give the best approximation to observed fields. Initial condition uncertainty can be tested by initialising the model with slightly perturbed initial conditions and observing how the output fields behave over time.

Most studies that utilise climate models perform an ensemble of simulations and use the average of the output to perform their analysis. The reason for using an ensemble mean rather than a single run is to reduce model error. Ensembles can consist of anything from 2 to 11 simulations and almost always consider the initial condition uncertainty (Washington and Preston, 2006; Rocha and Simmonds (1997); Richard et al (2000); Reason and Jagadeesha (2005); Reason (2002); Ratnam et al. (2012); Landman and Mason (1999); Goddard and Graham (1999)). An ensemble of 6 runs was performed for Ctr98, Ctr10 using slightly perturbed temperature and vertical velocity fields in each ensemble run. It would have been ideal to run an ensemble for each of the idealised experiments as well as climatology experiments, but unfortunately the high computational cost of each simulation, coupled with computational restrictions, did not allow for this. The ensemble members for Ctr98 and Ctr10 are used to illustrate the relatively robust nature of the model.

Figures 6.41, 6.42, 6.43, 6.44, 6.45 and **6.46** display the average ensemble (top left), single ensemble (top middle), and climatology (top right) for JFM 1998 in each of the identified variables. The remaining six plots show each of the ensemble members. **Figures 6.47, 6.48, 6.49, 6.50, 6.51** and **6.52** display the same variables, except they are for JFM 2010. In each case, there are some differences between each of the ensemble members, but the differences between the average ensemble and the single ensemble are

not very large. The experiments run in the following chapter focus on large scale seasonal dynamics, and the single ensemble run is sufficient for these purposes.

6.8 Summary

Global validation indicates that CEU does reasonably well in capturing the general circulation, although the magnitude of most variables is overestimated by the model. CEU captures the ITCZ although more strongly than in observations and the South Indian Convergence Zone in particular is also found to be anomalously strong in the model. The Hadley and Polar cells are well positioned in CEU, although the speed at which air ascends and descends is faster in the model than in reanalysis. The trades, midlatitude westerlies and westerly subtropical jets are all faster and form over land in CEU which is anomalous. Global surface temperatures are reasonably well captured but there is a warm bias over the tropical oceans and a cold bias over Australia, North America and the Himalayas.

Regional validation of CEU over southern Africa indicates that CEU captures many of the regional features, but produces higher magnitudes for some variables than those in the observational and reanalysis data sets. Climatological rainfall north of approximately 20^oS is fairly well captured in CEU when compared with observations, however south of 20^oS the model

does not do as well. In particular, CEU displays anomalously high rainfall over southwest Angola, Namibia and western South Africa and has a region of anomalously low rainfall over eastern Botswana, western Zimbabwe and northern South Africa. The model also produces very high levels of rainfall over the Mozambique Channel. These rainfall anomalies are mostly explained by looking at the 850 hPa winds. The northeast monsoonal flow from the North Indian Ocean, the northeasterly monsoonal flow towards northern Madagascar, as well as the southeasterly flow from the South Indian Ocean are all much stronger in CEU than reanalysis. These winds lead to a strong cyclonic feature over the Mozambique Channel which, coupled with anomalously high latent heat flux there, results in high rainfall. Western southern Africa is dominated by northerly rather than southerly winds, probably due in part to the strong flow from the South Indian Ocean, which leads to anomalously high rainfall over Namibia and western South Africa. These wind anomalies lead to a substantially stronger anticyclone centred over western South Africa which in turn leads to the anomalous dry conditions over eastern Botswana, western Zimbabwe and northern South Africa. Many of the anomalous circulation features could be attributed to the model not performing well over regions that are impacted strongly by topographic effects. The cyclonic circulation of the Angola low is not properly captured in CEU, although the westerlies over northern Angola partially reflect this feature. Compared with 20th Century, this feature in CEU is located north east of the reanalysis. The Angola low is often poorly captured in models

(Reason and Jagadheesha, 2005; Lyon and Mason, 2007) and in particular it is not visible in the ERA reanalysis. The anticyclone centred over eastern South Africa in CEU is substantially stronger than the flow seen in either reanalysis. The Atlantic ITCZ is shifted south by about 6^o in CEU, but this southward shift in the ITCZ may be mitigated over the continent by the anomalously strong easterlies from the South Indian Ocean. Surface temperatures are well captured by CEU except for a cold bias over topographical features.

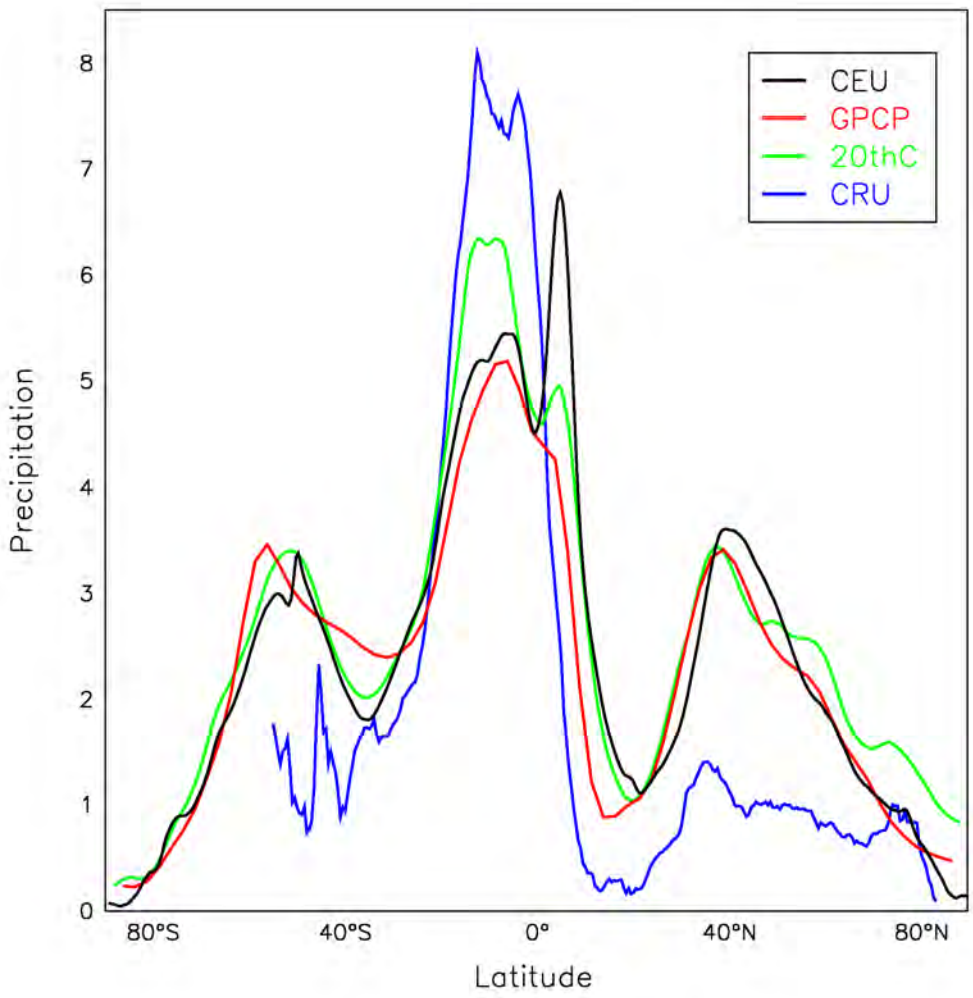

Figure 6.1: Zonally averaged JFM climatological precipitation for CEU, GPCP, 20th Century and CRU (in mm·day^{-1})

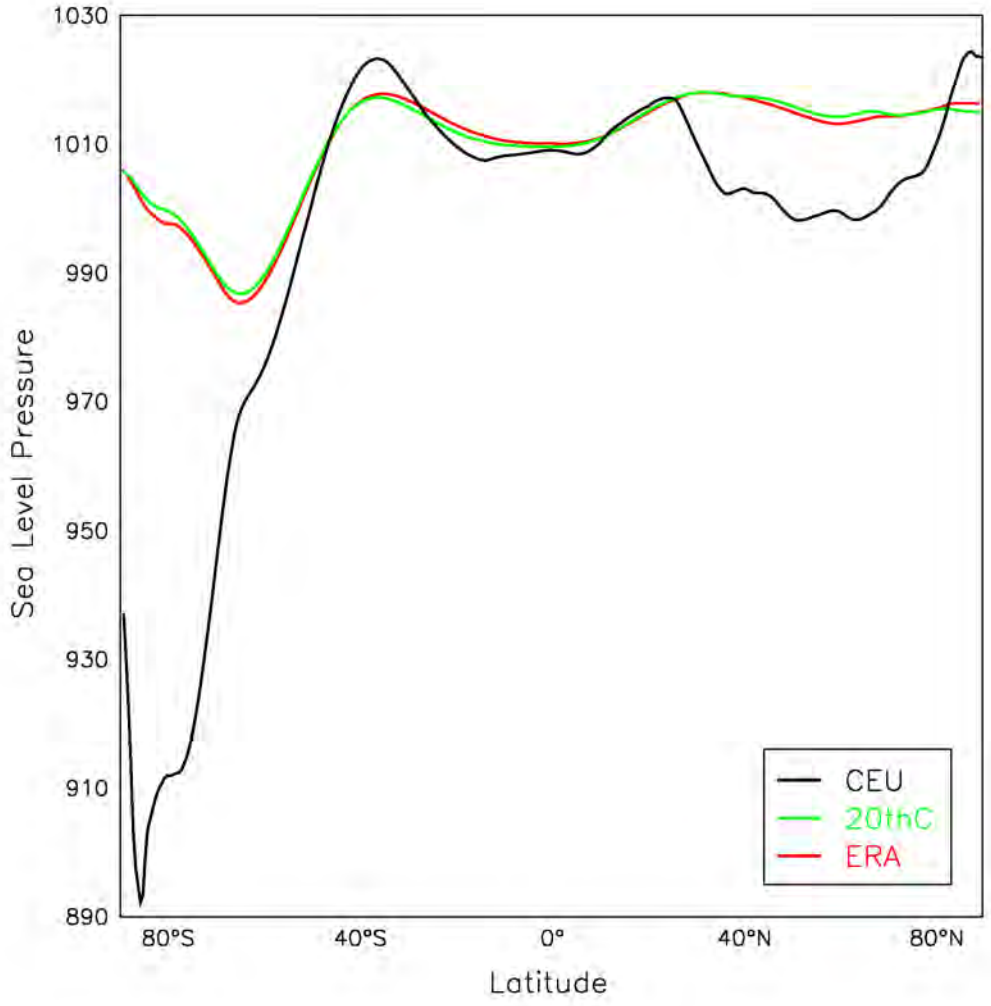

Figure 6.2: Zonally averaged JFM climatological sea level pressure for CEU, 20th Century and ERA (in hPa)

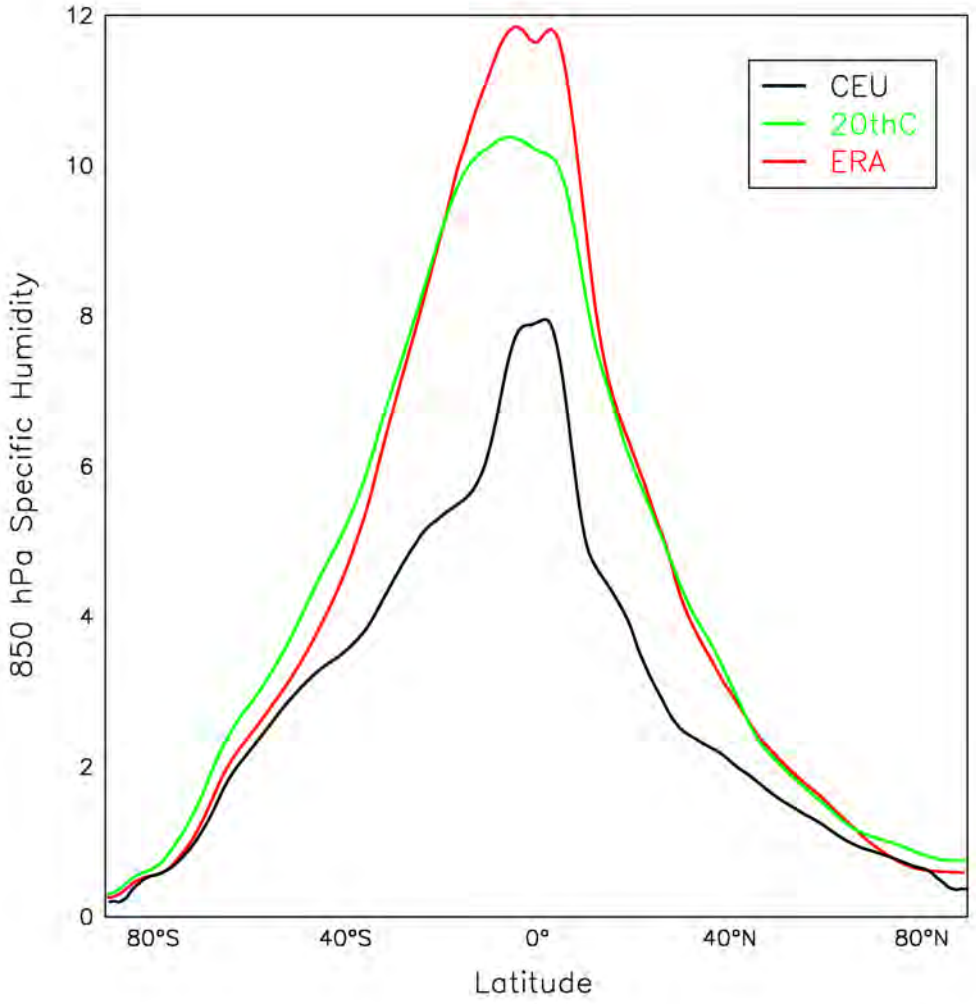

Figure 6.3: Zonally averaged JFM climatological specific humidity for CEU, 20th Century and ERA (in 10^{-3} kg·kg^{-1})

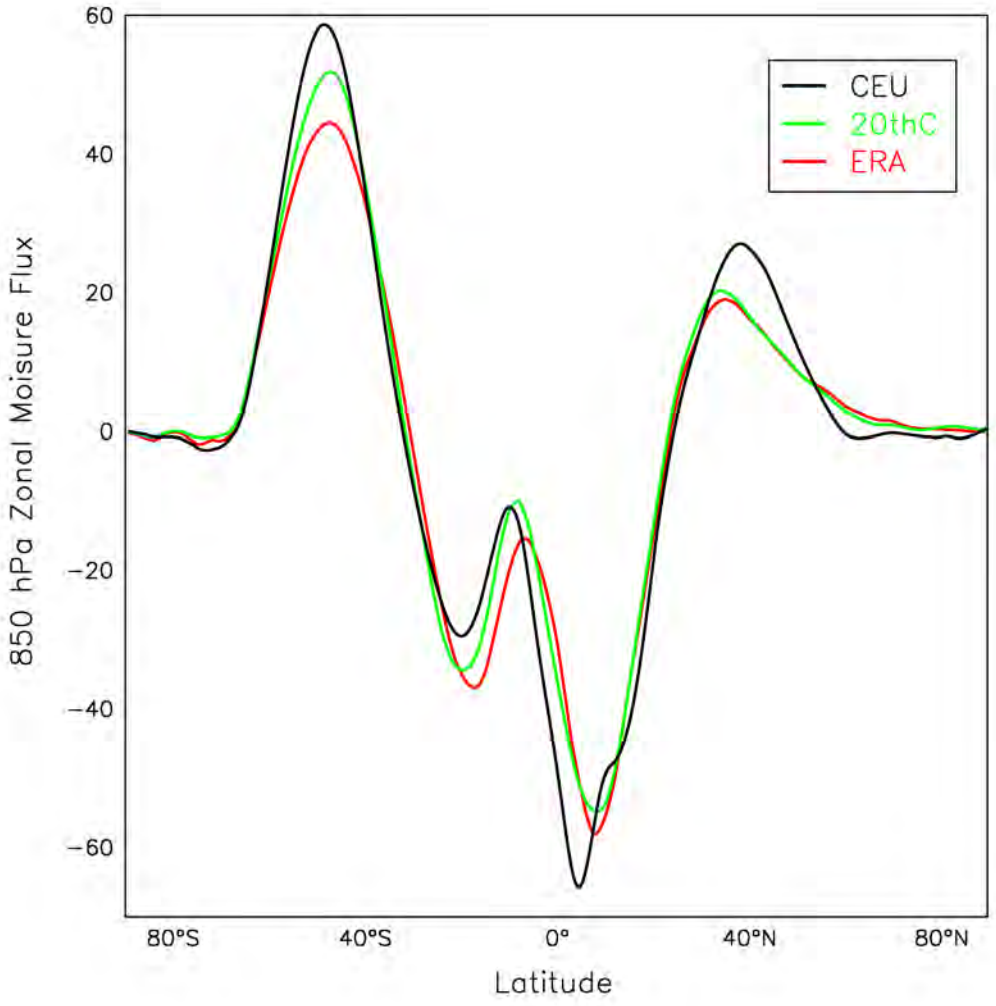

Figure 6.4: Zonally averaged JFM climatological moisture flux for CEU, 20th Century and ERA (in 10^{-3} kg·kg^{-1}·m·s^{-1})

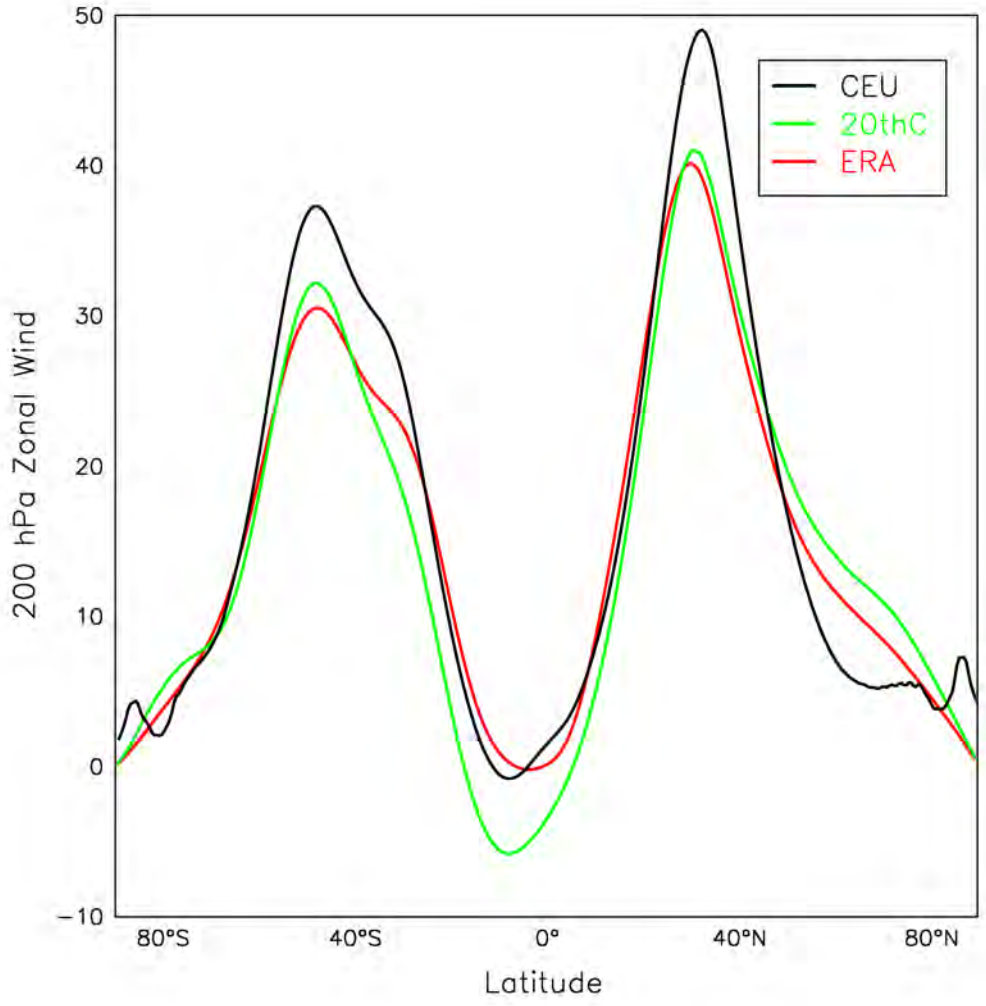

Figure 6.5: Zonally averaged JFM climatological zonal wind for CEU, 20th Century and ERA (in 10^{-3} kg·kg^{-1})

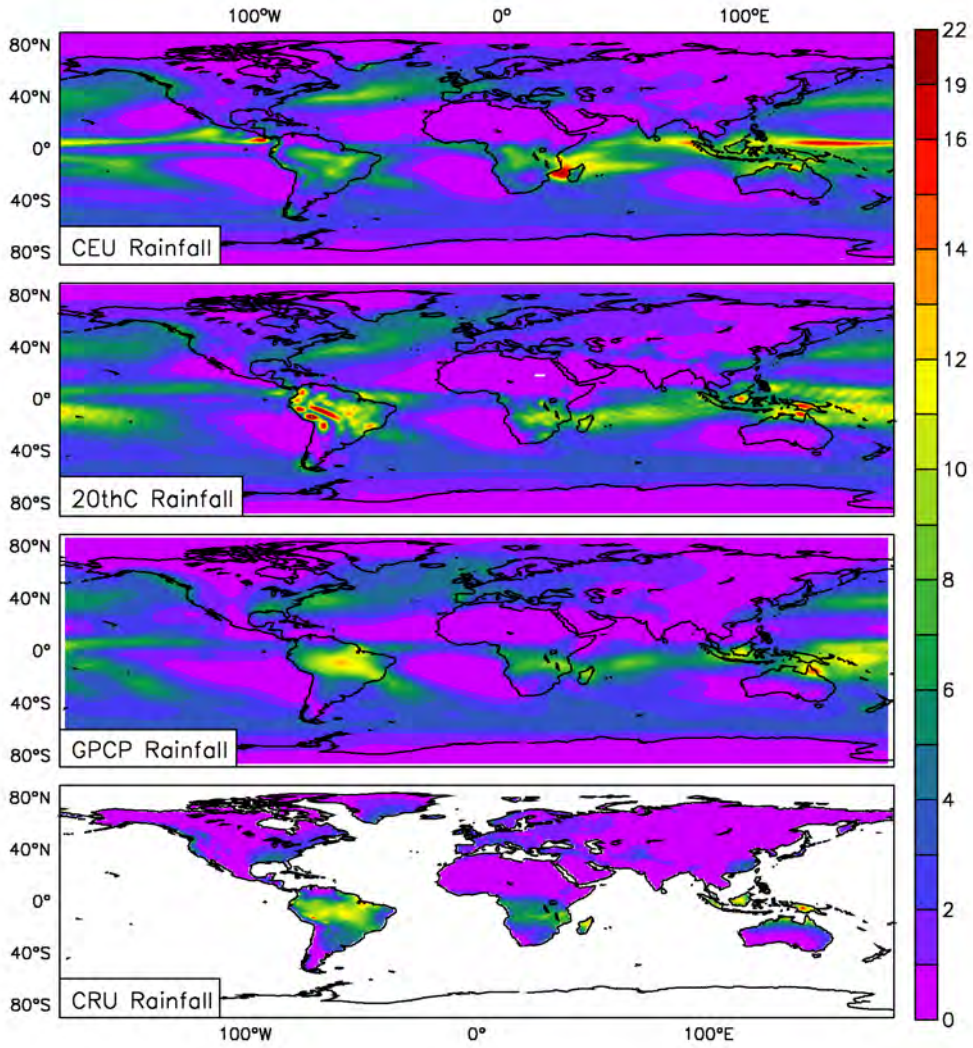

Figure 6.6: JFM climatological precipitation for CEU, 20th Century, GPCP and CRU (in mm·day^{-1})

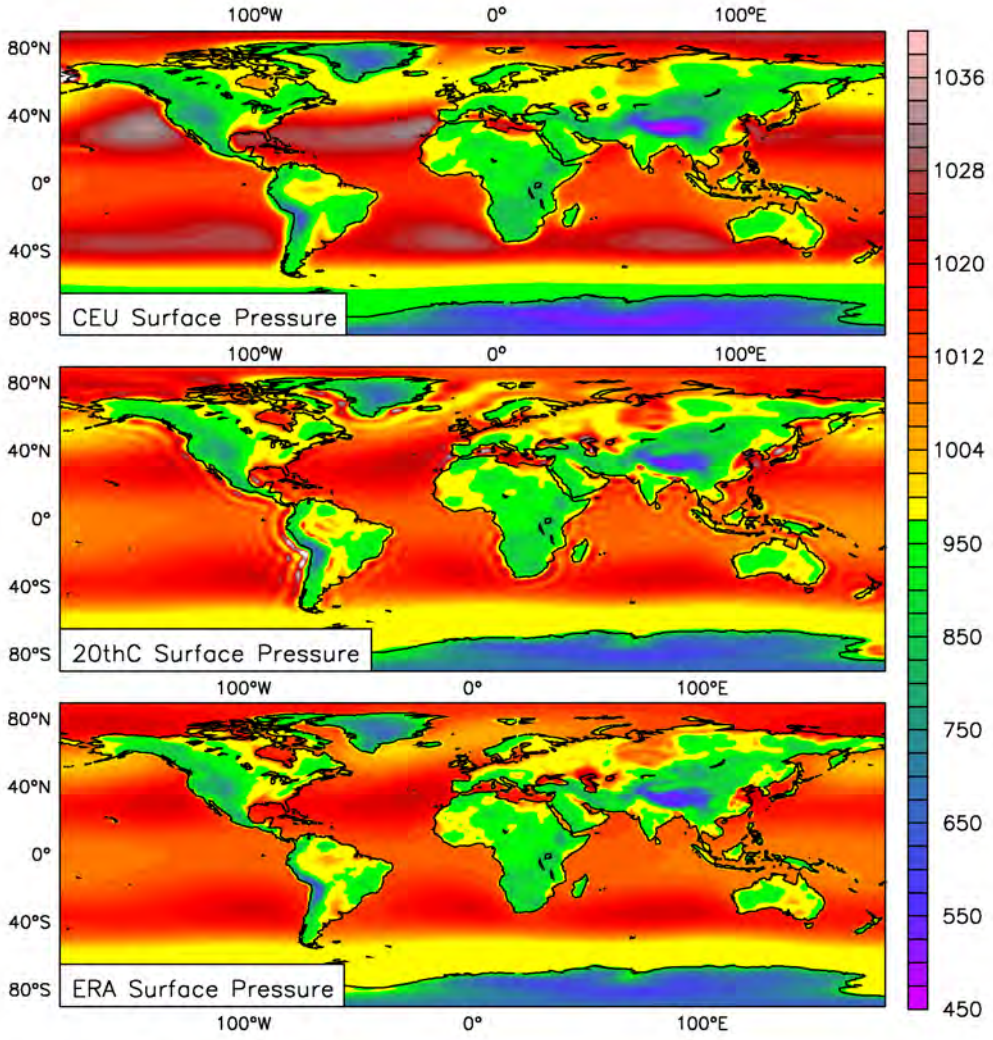

Figure 6.7: JFM climatological surface pressure for CEU, 20th Century and ERA (in hPa)

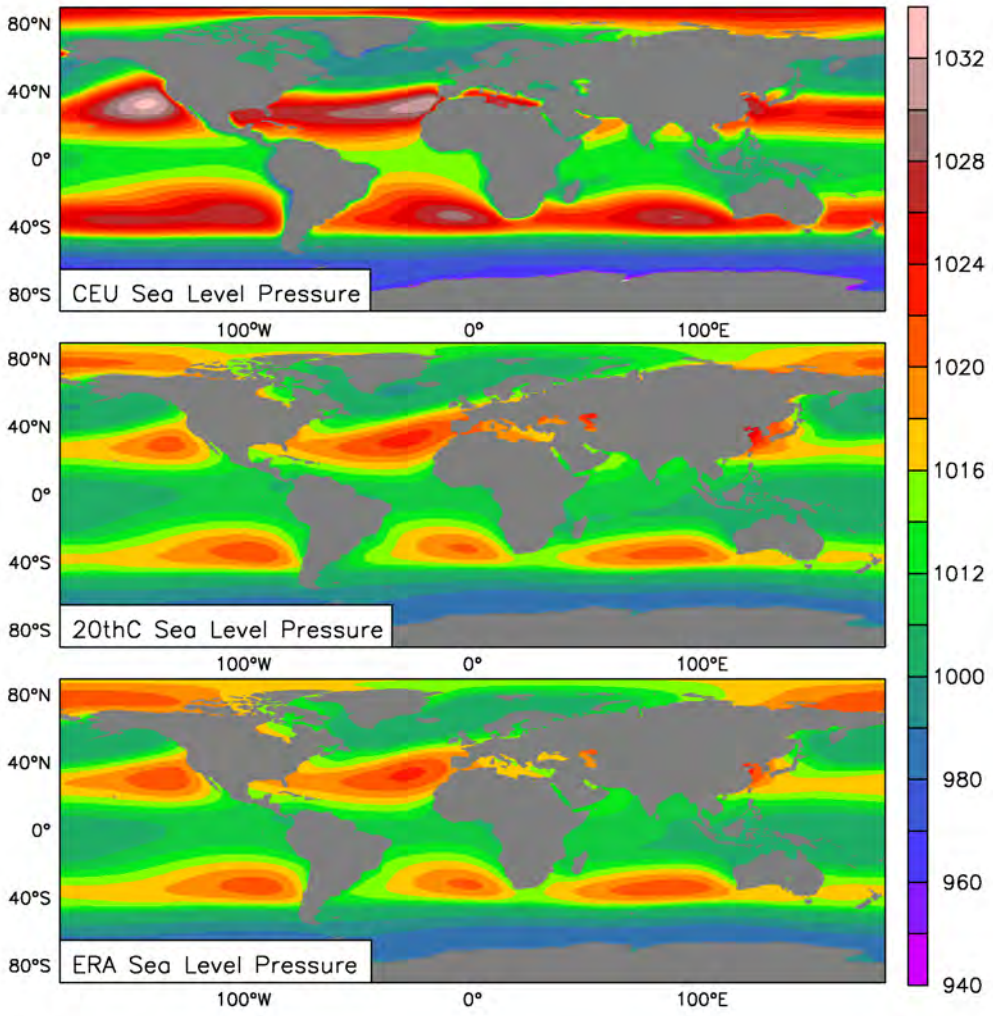

Figure 6.8: JFM climatological sea level pressure for CEU, 20th Century and ERA (in hPa)

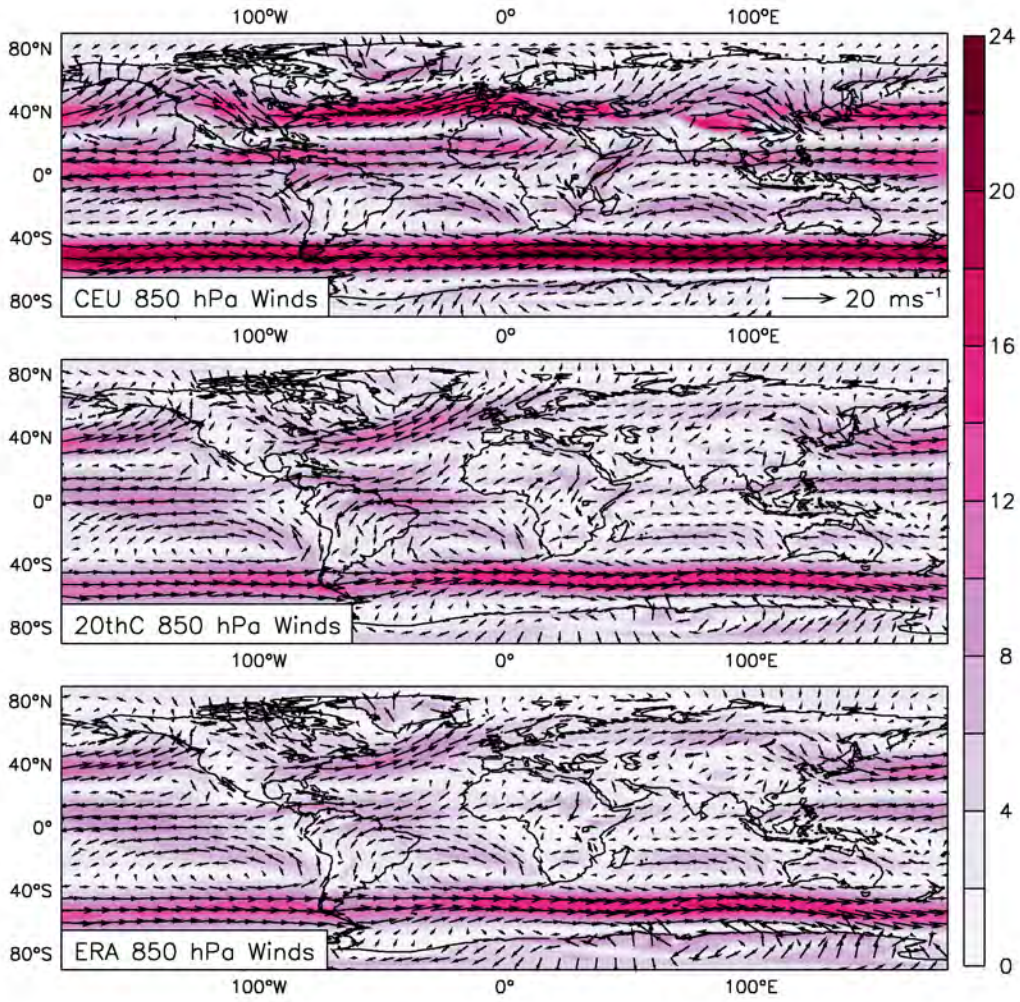

Figure 6.9: JFM climatological wind flow at 850 hPa for CEU, 20th Century and ERA (in $m \cdot s^{-1}$)

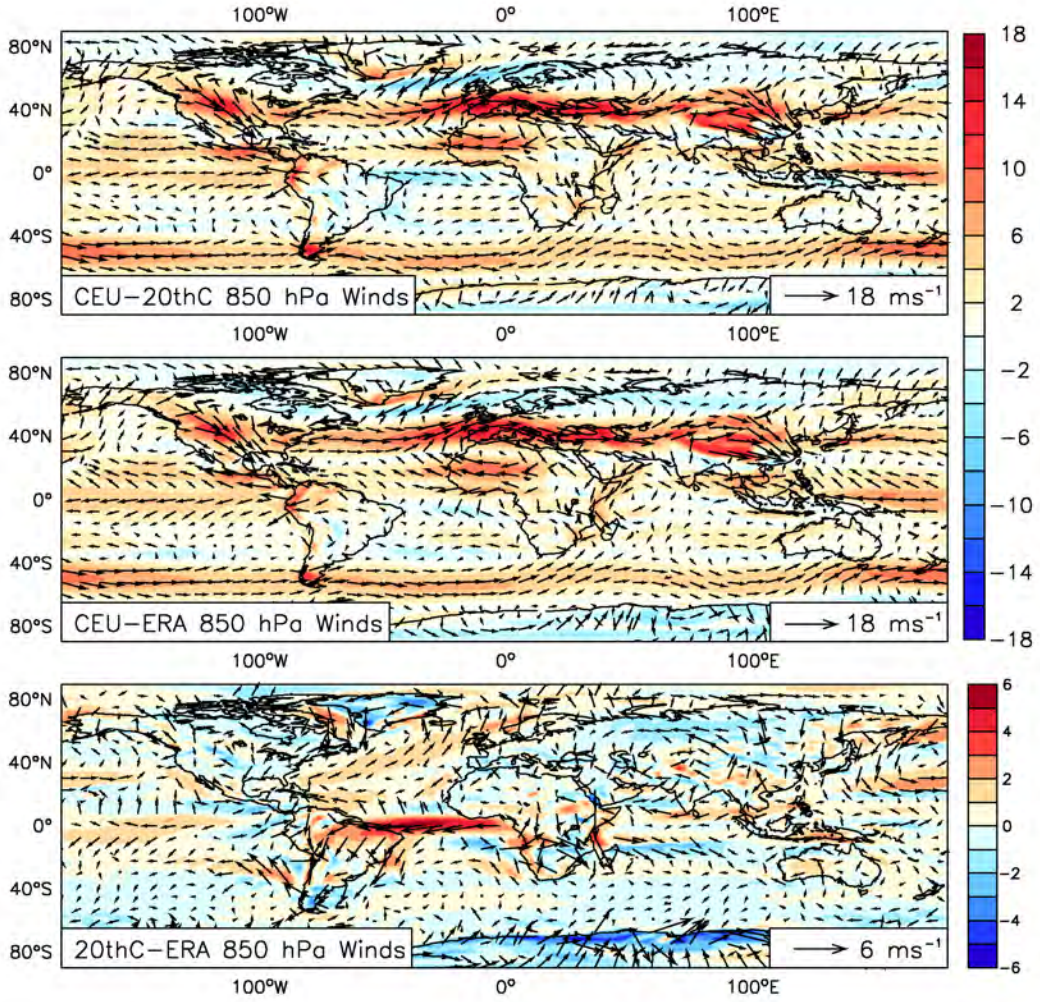

Figure 6.10: JFM climatological wind flow difference at 850 hPa for CEU compared with 20th Century; CEU compared with ERA; and 20th Century compared with ERA (in $m \cdot s^{-1}$)

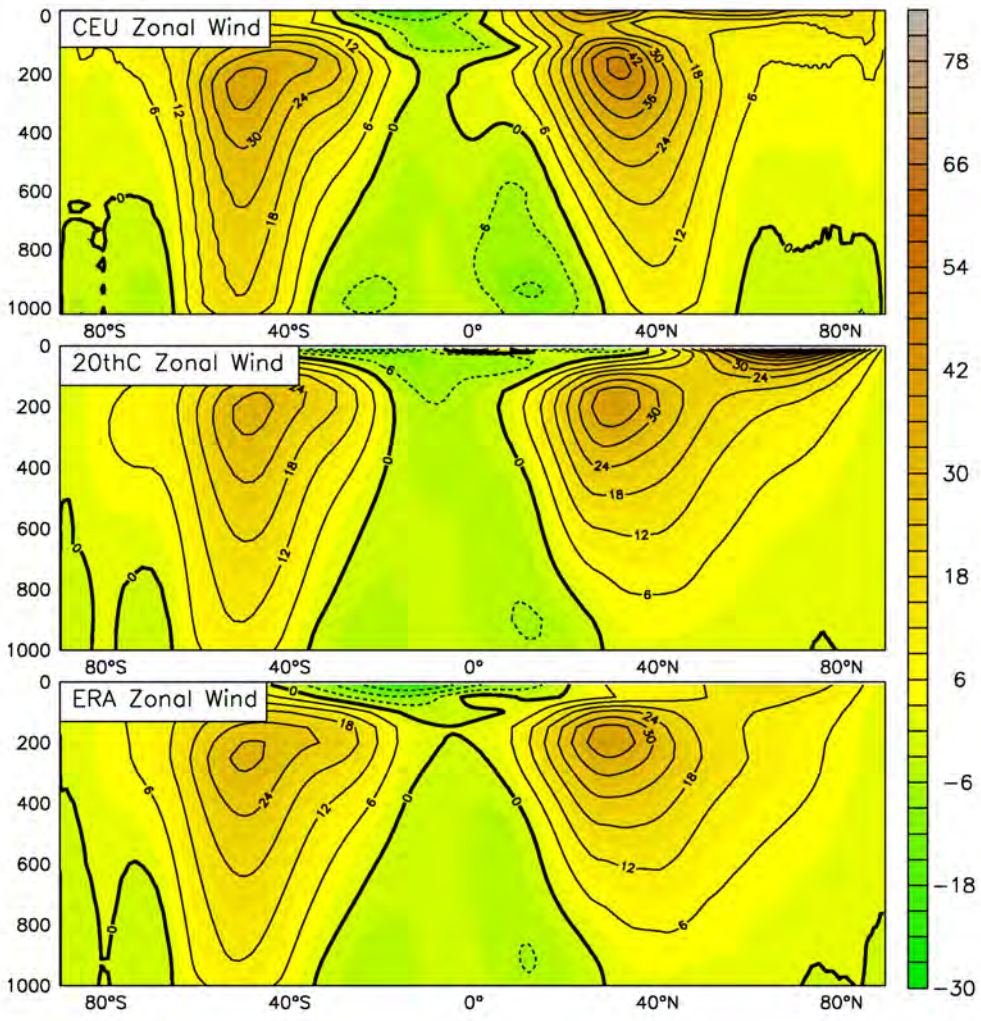

Figure 6.11: JFM climatological global zonal-mean cross sections of the zonal wind component for CEU, 20th Century and ERA (in $m \cdot s^{-1}$)

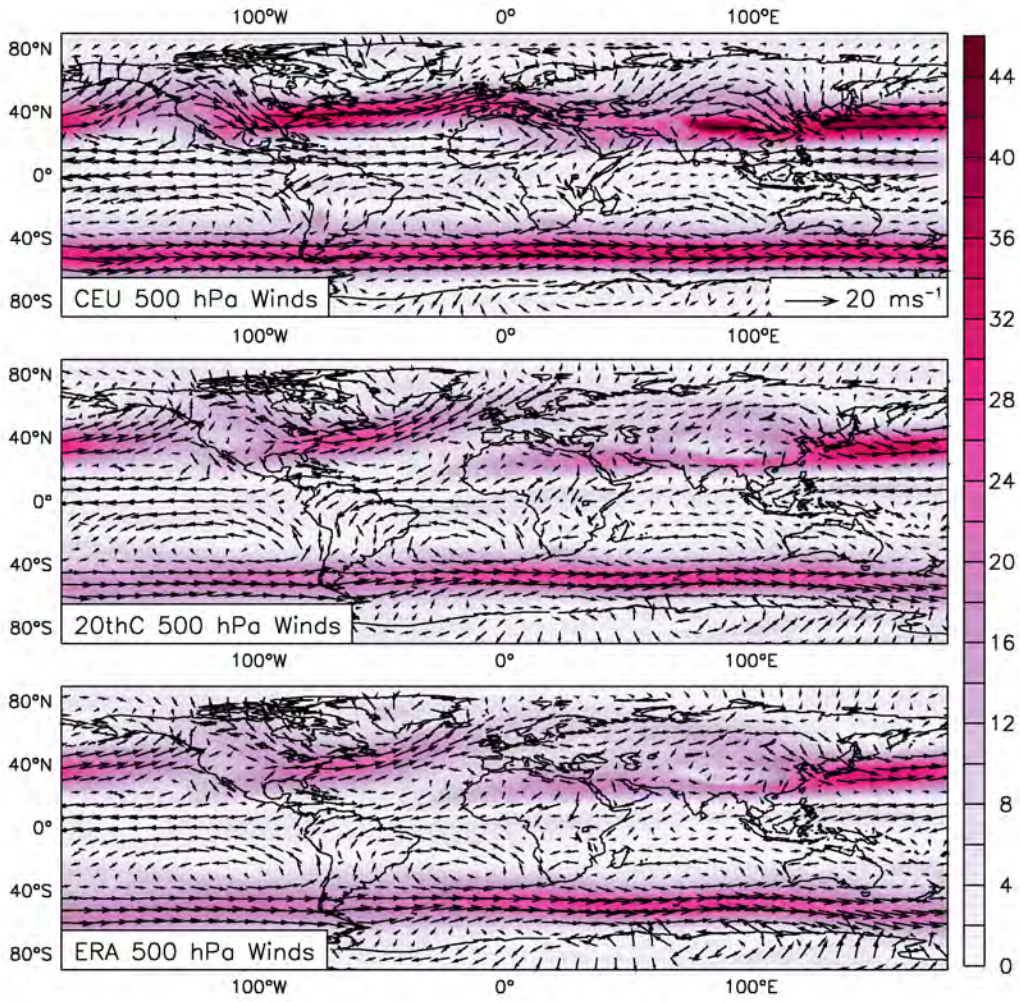

Figure 6.12: JFM climatological wind flow at 500 hPa for CEU, 20th Century and ERA (in $m \cdot s^{-1}$)

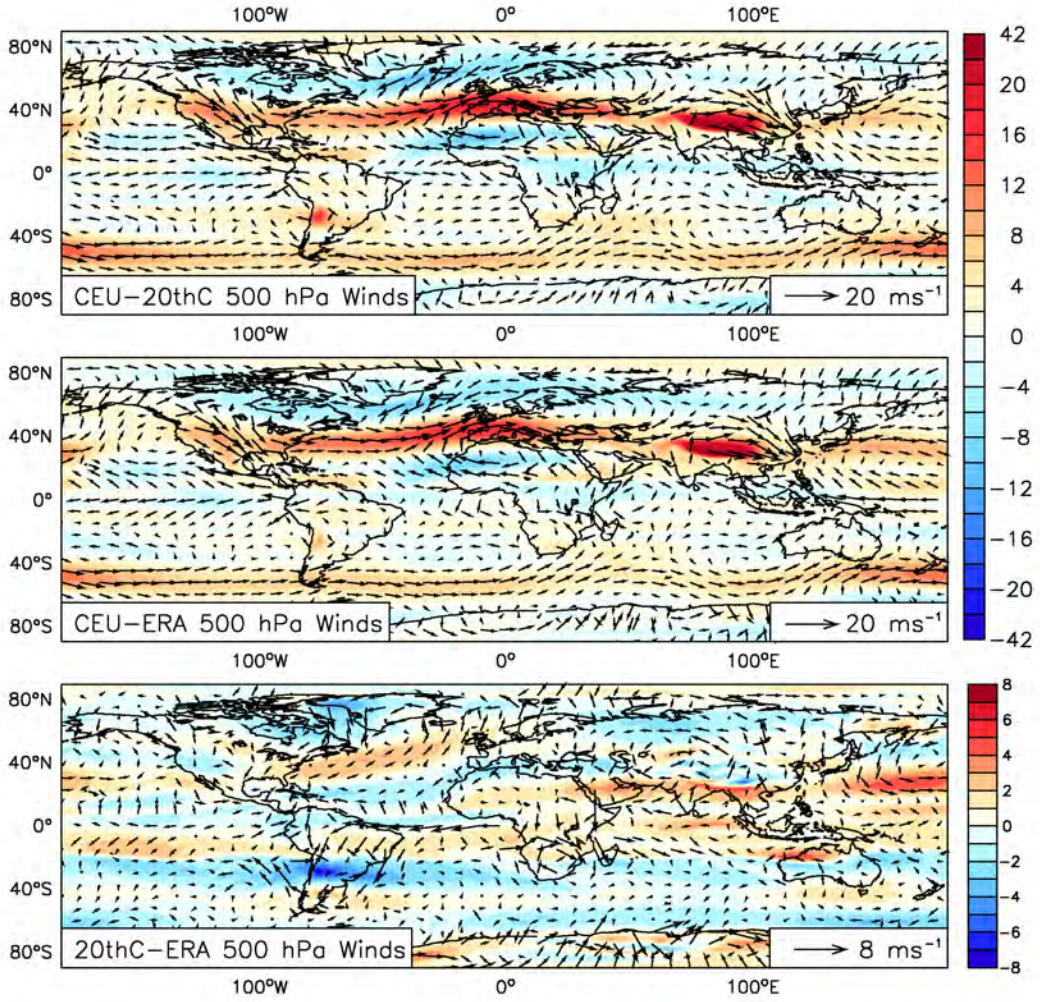

Figure 6.13: JFM climatological wind flow difference at 500 hPa CEU compared with 20th Century; CEU compared with ERA; and 20th Century compared with ERA (in $m \cdot s^{-1}$)

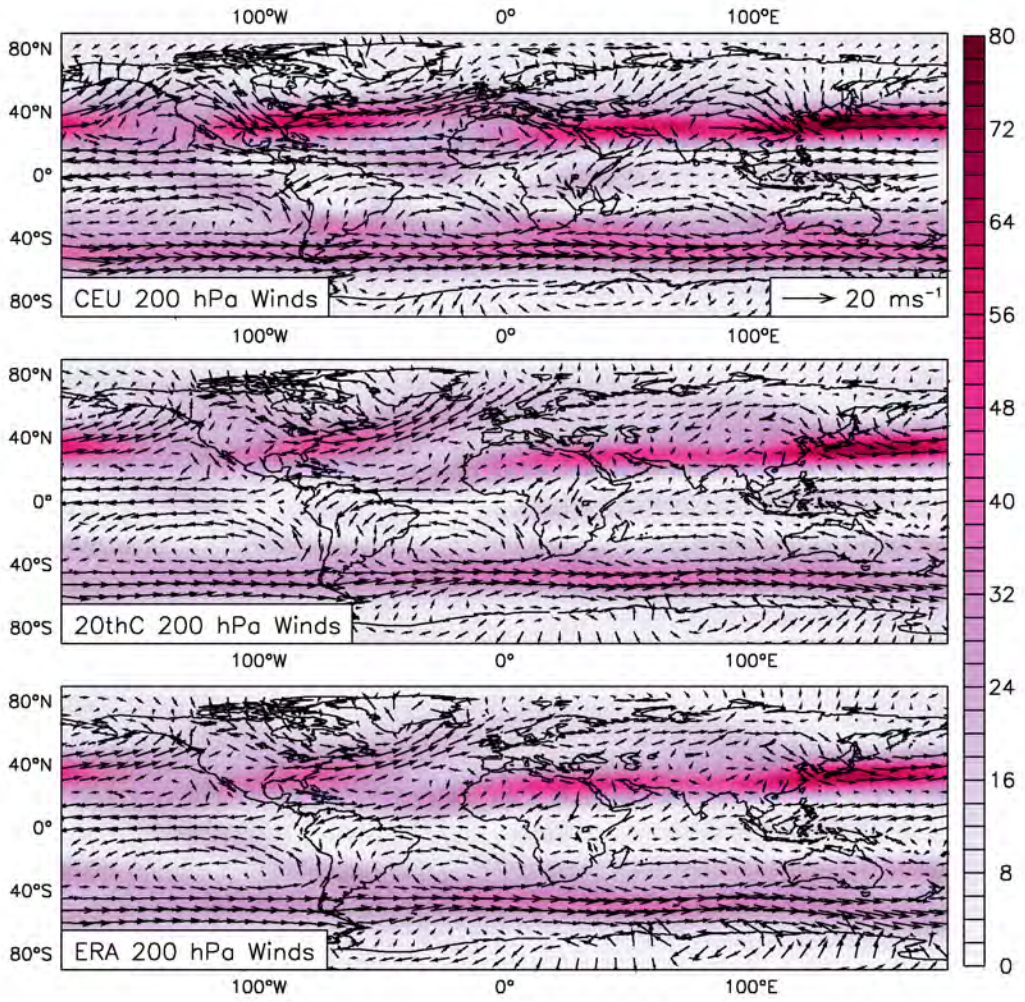

Figure 6.14: JFM climatological wind flow at 200 hPa for CEU, 20th Century and ERA (in $m \cdot s^{-1}$)

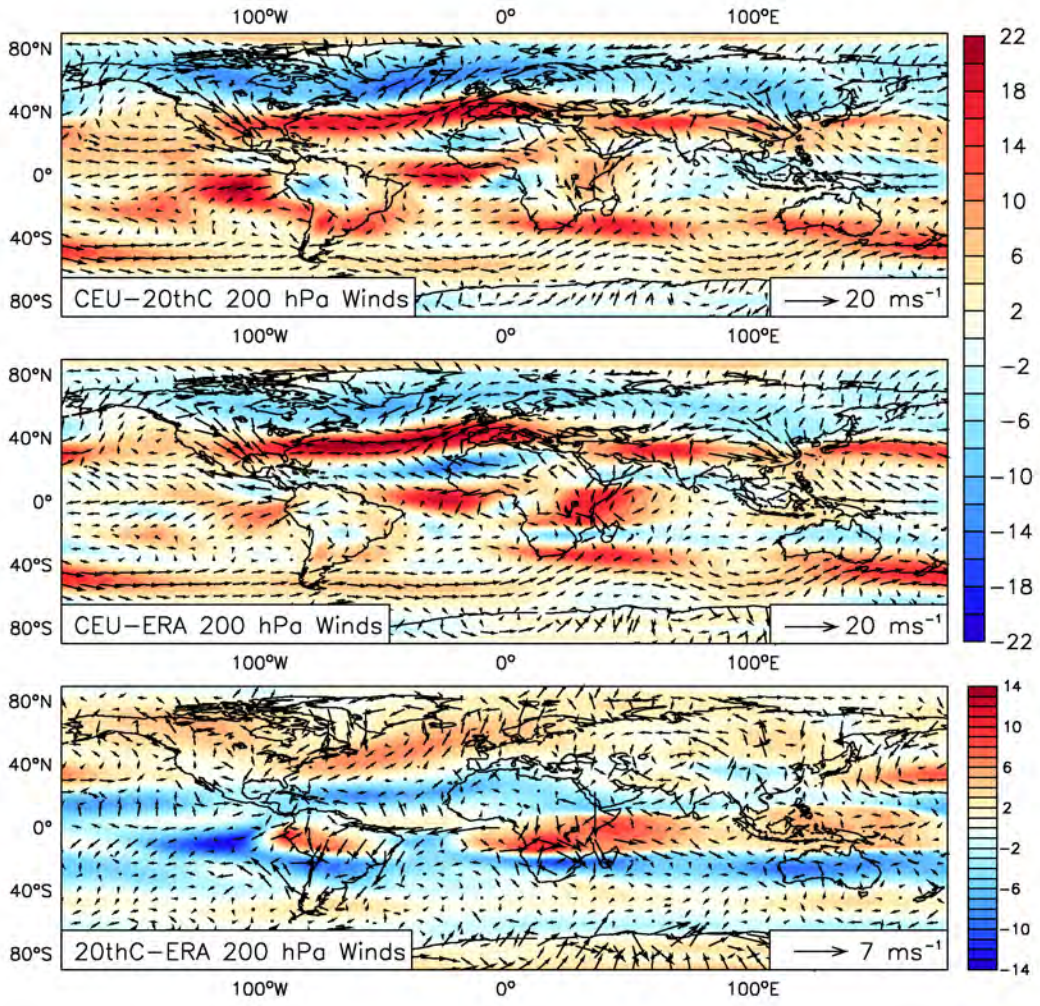

Figure 6.15: JFM climatological wind flow difference at 200 hPa for CEU compared with 20th Century; CEU compared with ERA; and 20th Century compared with ERA (in $m \cdot s^{-1}$)

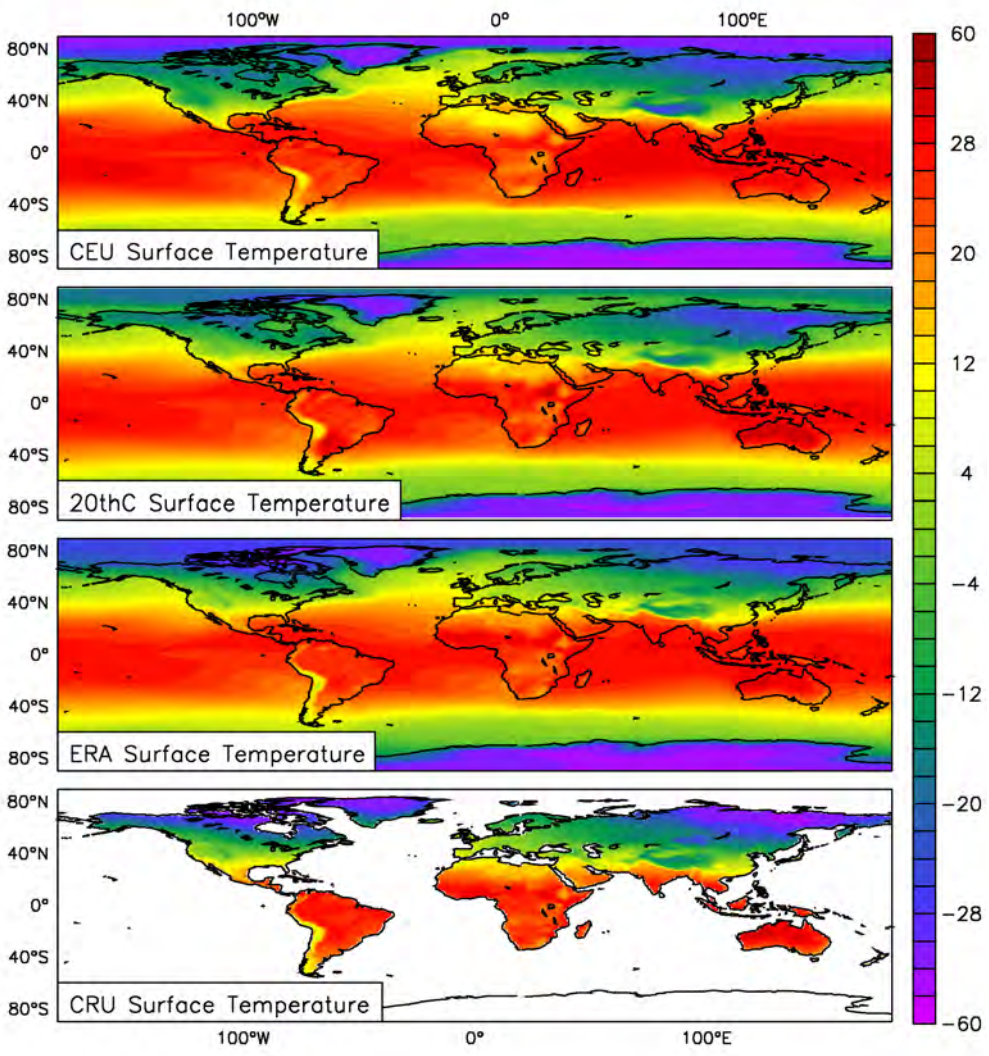

Figure 6.16: JFM climatological surface temperature for CEU, 20th Century and ERA (in ^{o}C)

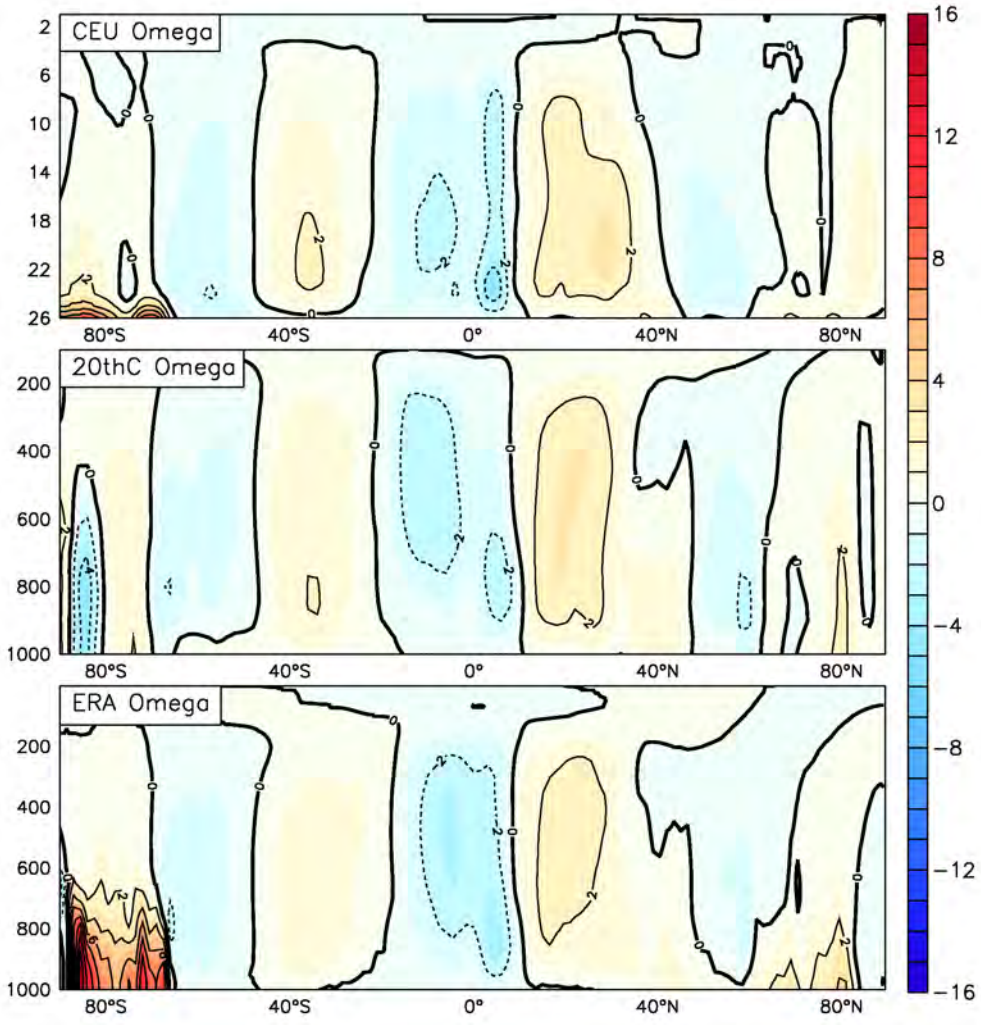

Figure 6.17: JFM climatological global zonal-mean cross sections of the vertical velocity for CEU, 20th Century and ERA (in 10^2 kg·m^{-1}·s^{-3})

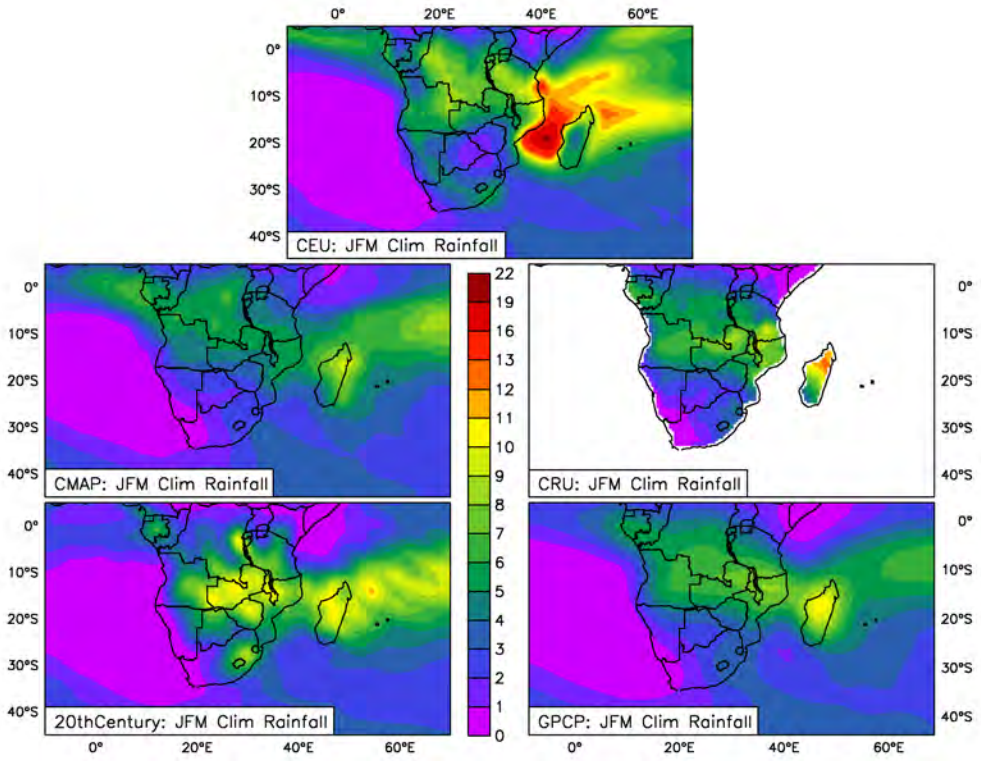

Figure 6.18: JFM climatological precipitation over southern Africa for CEU, CMAP, 20th Century, CRU and GPCP (in mm·day^{-1})

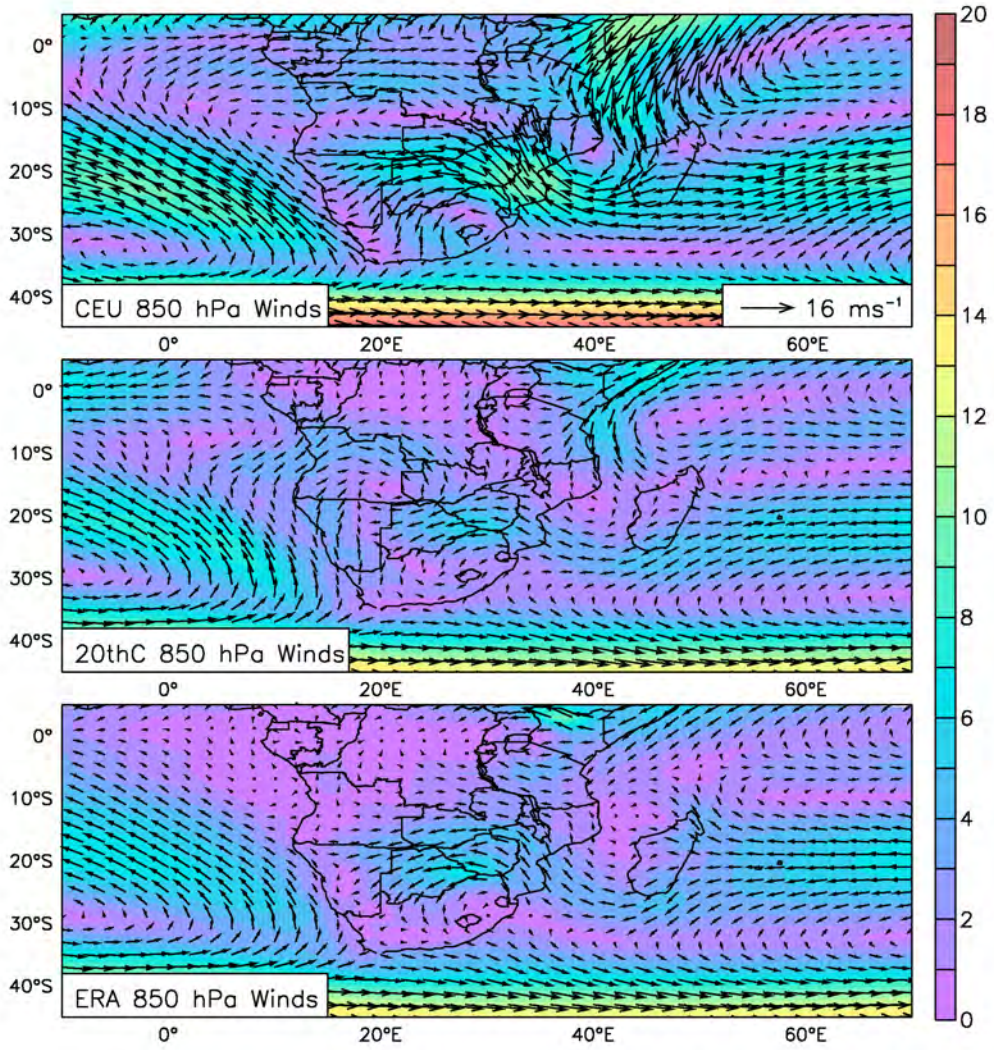

Figure 6.19: JFM climatological winds at 850 hPa over southern Africa for CEU, 20th Century and ERA (in $m \cdot s^{-1}$)

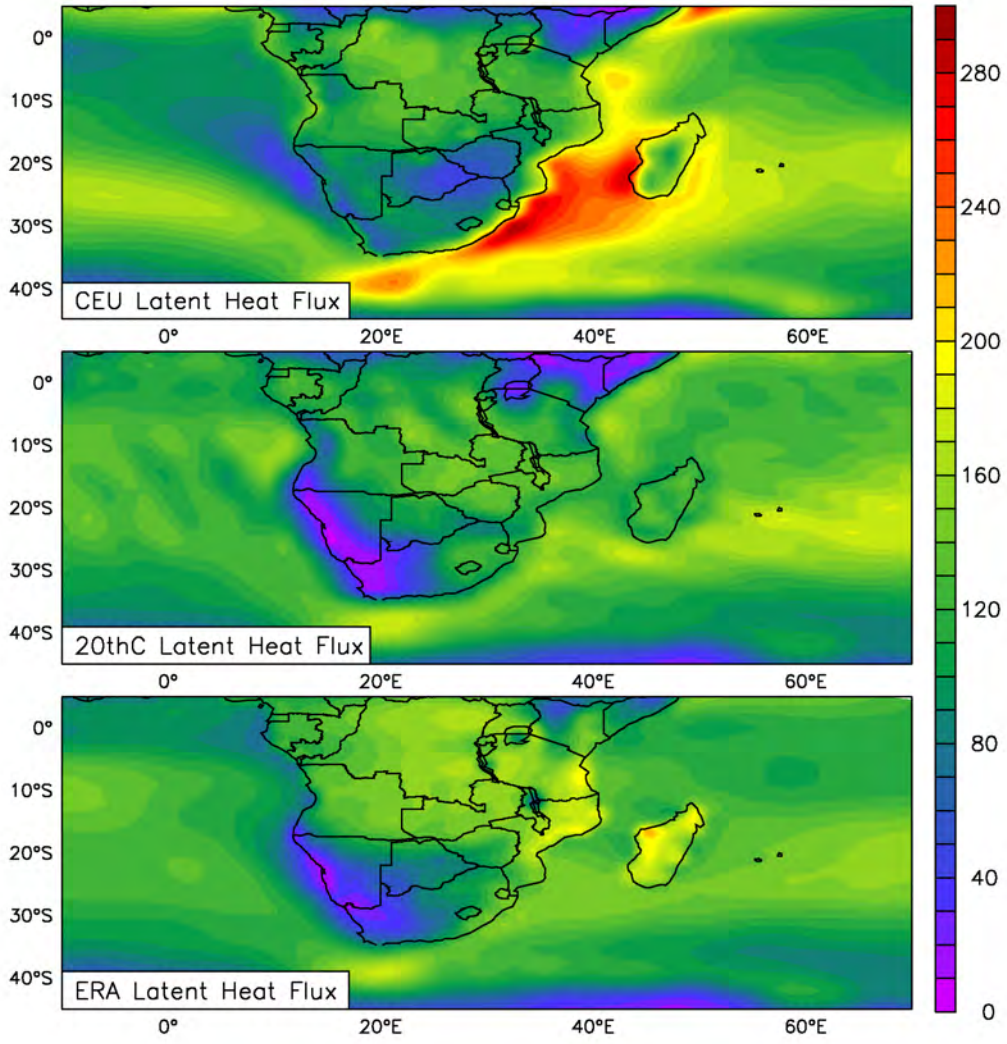

Figure 6.20: JFM climatological latent heat flux over southern Africa for CEU, 20th Century and ERA (in $kg{\cdot}s^{-3}$)

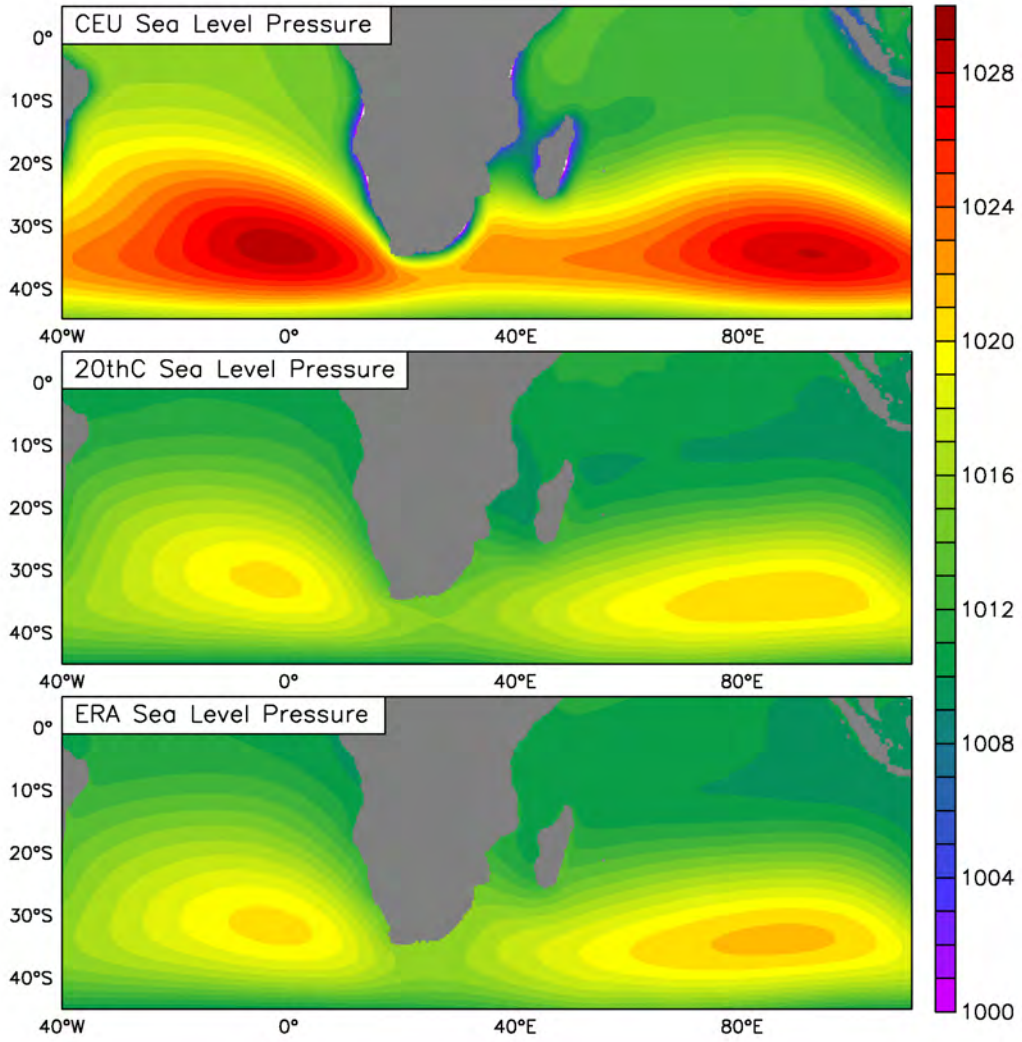

Figure 6.21: JFM climatological sea level pressure over southern Africa for CEU, 20th Century and ERA (in hPa)

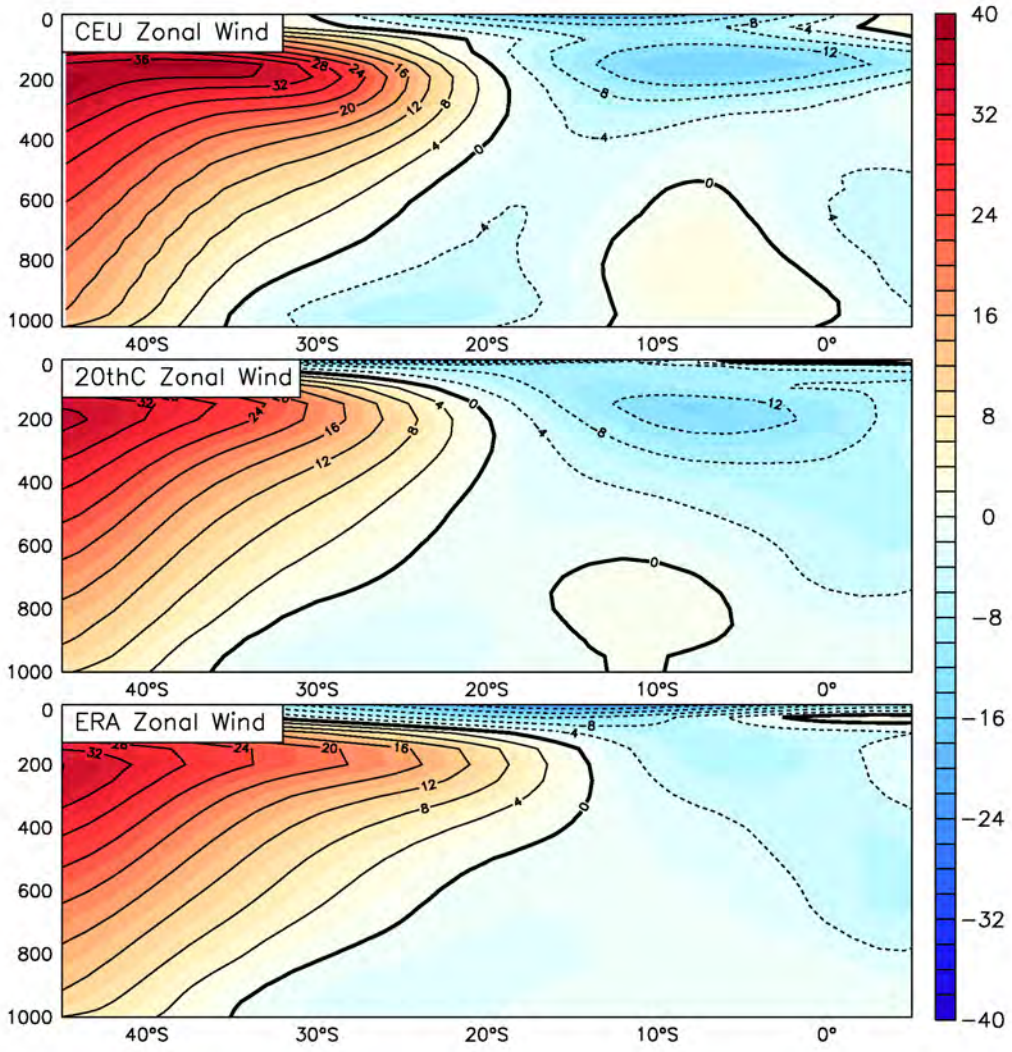

Figure 6.22: JFM climatological zonal winds over southern Africa zonally averaged from 0^o to 50^oE and for for CEU, 20th Century and ERA (in $\mathrm{m{\cdot}s^{-1}}$)

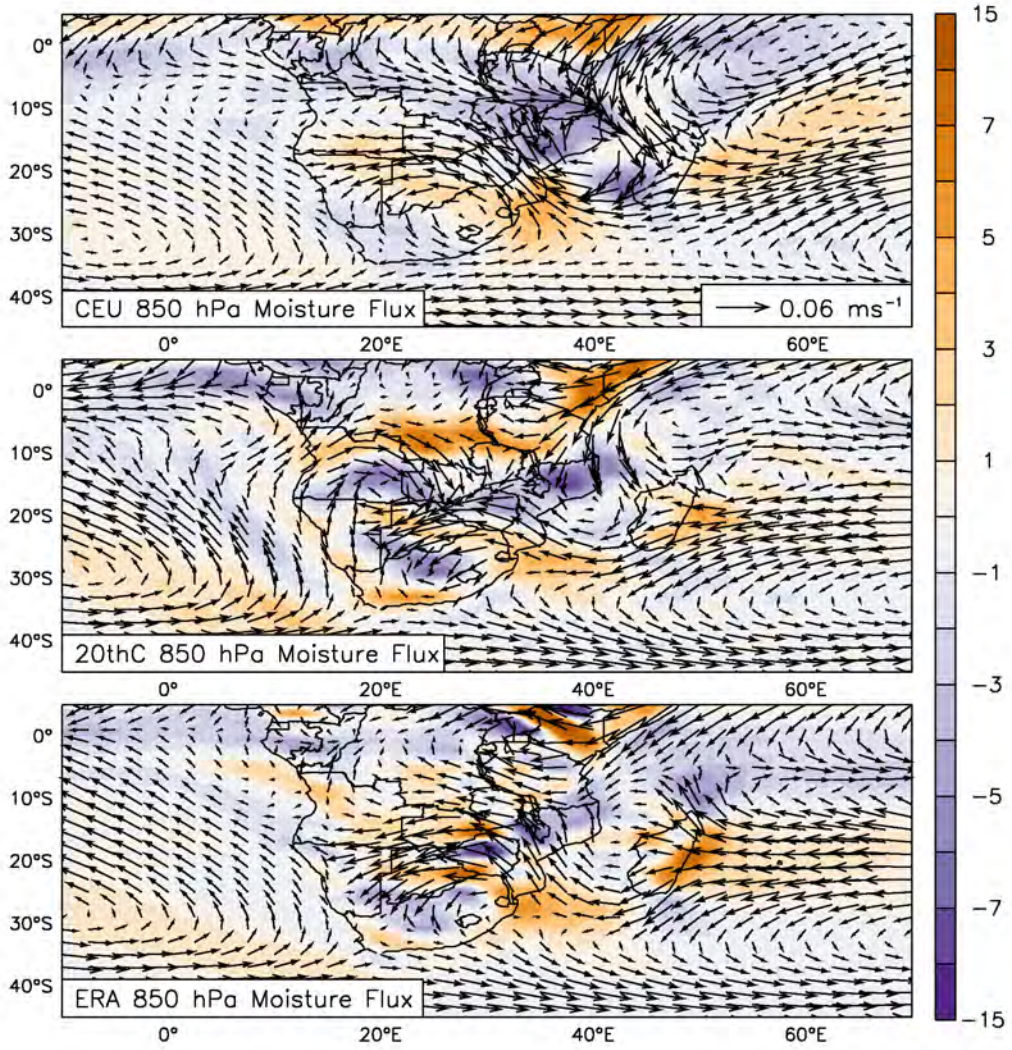

Figure 6.23: JFM climatological convergence and divergence at 850 hPa over southern Africa (in 10^8 s^{-1}) as well as the moisture flux at the same level for CEU, 20th Century and ERA (in $m \cdot s^{-1}$)

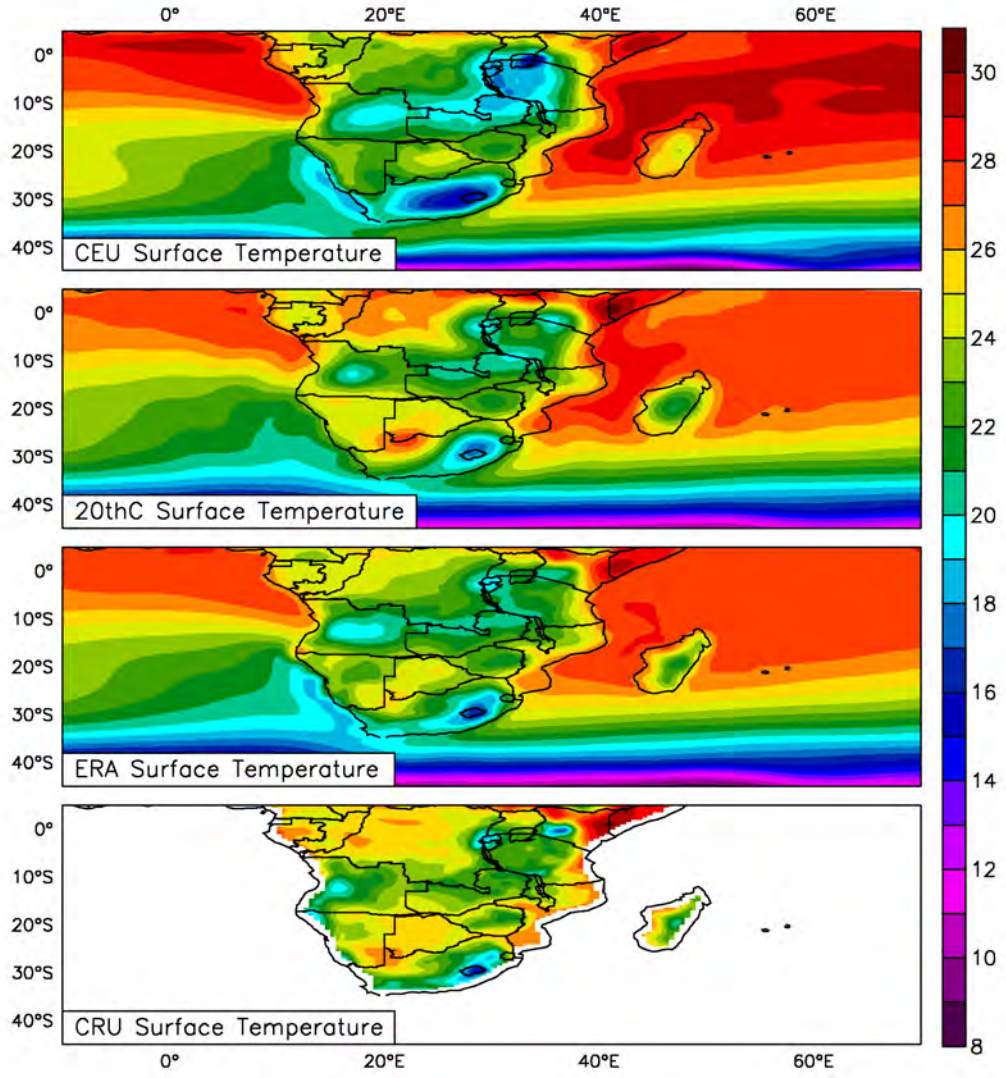

Figure 6.24: JFM climatological temperature over southern Africa for CEU, 20th Century, ERA and CRU (in ^{o}C)

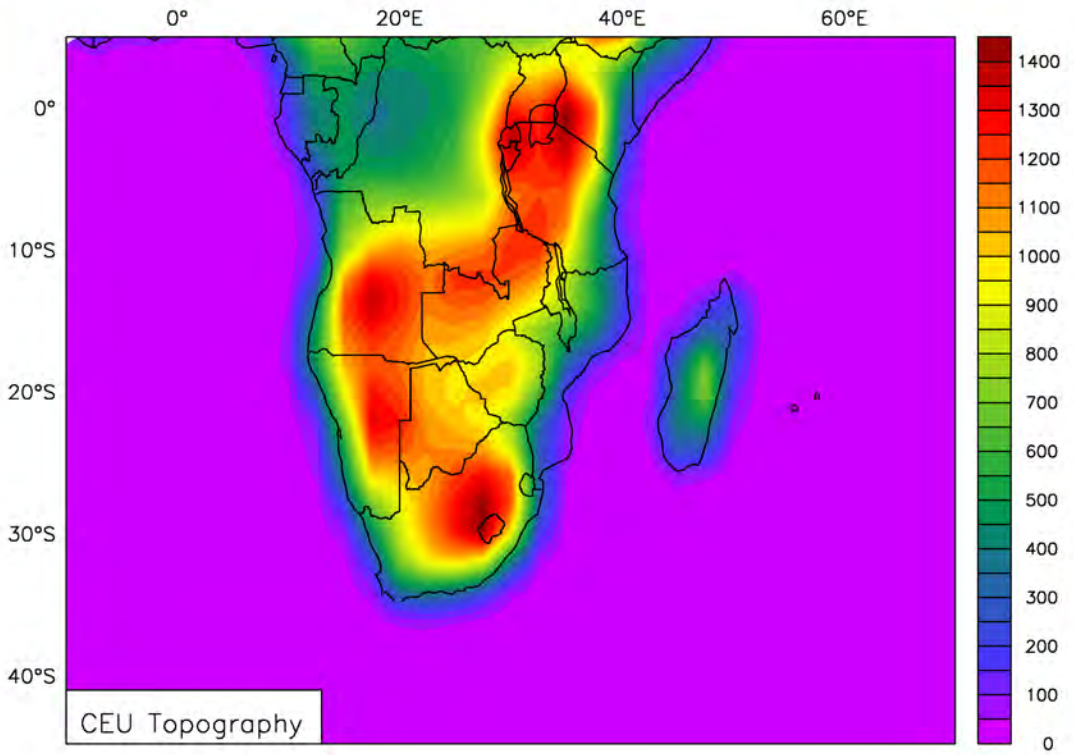

Figure 6.25: Topography over southern Africa in meters above sea level

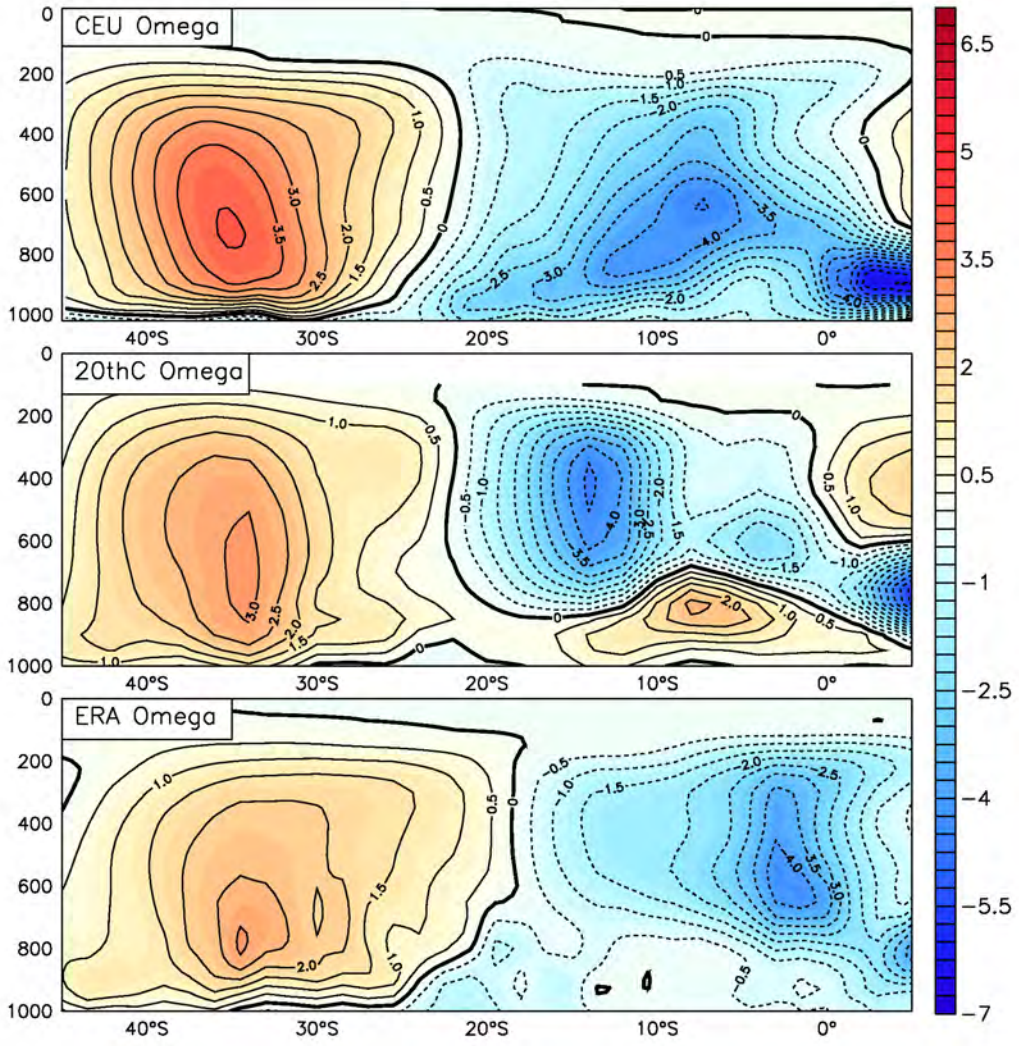

Figure 6.26: JFM climatological vertical velocity over southern Africa zonally averaged from 0^o to 50^oE and for CEU, 20th Century and ERA (in 10^2 kg·m^{-1}·s^{-3})

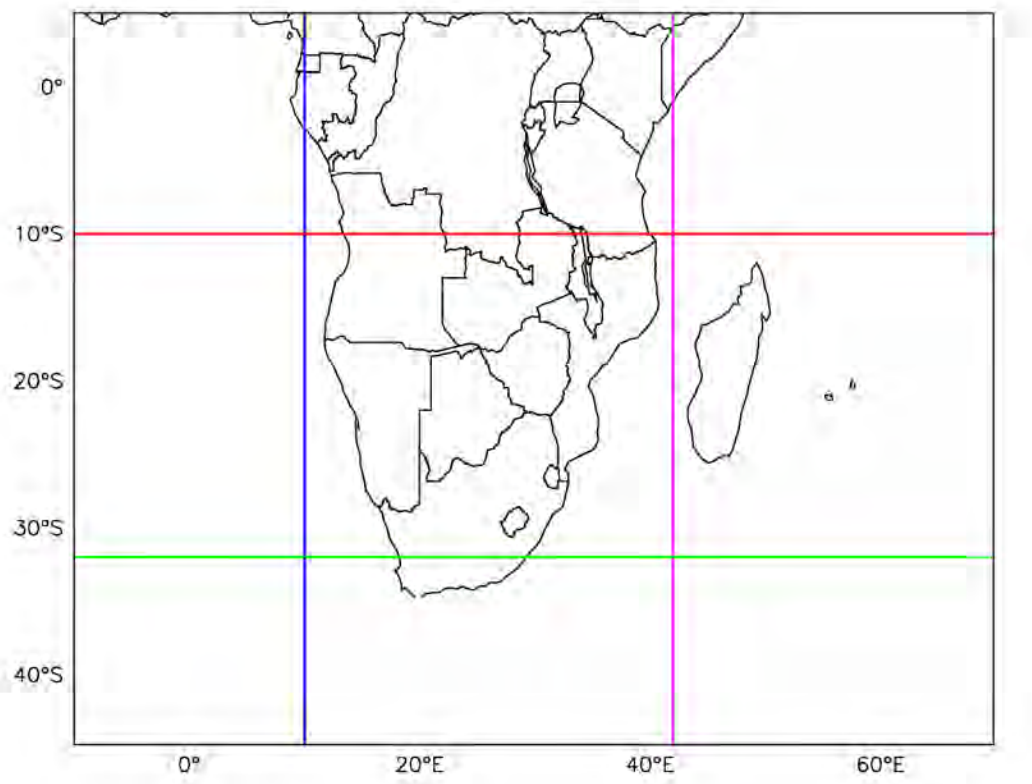

Figure 6.27: Position of vertical and horizontal transects around southern Africa

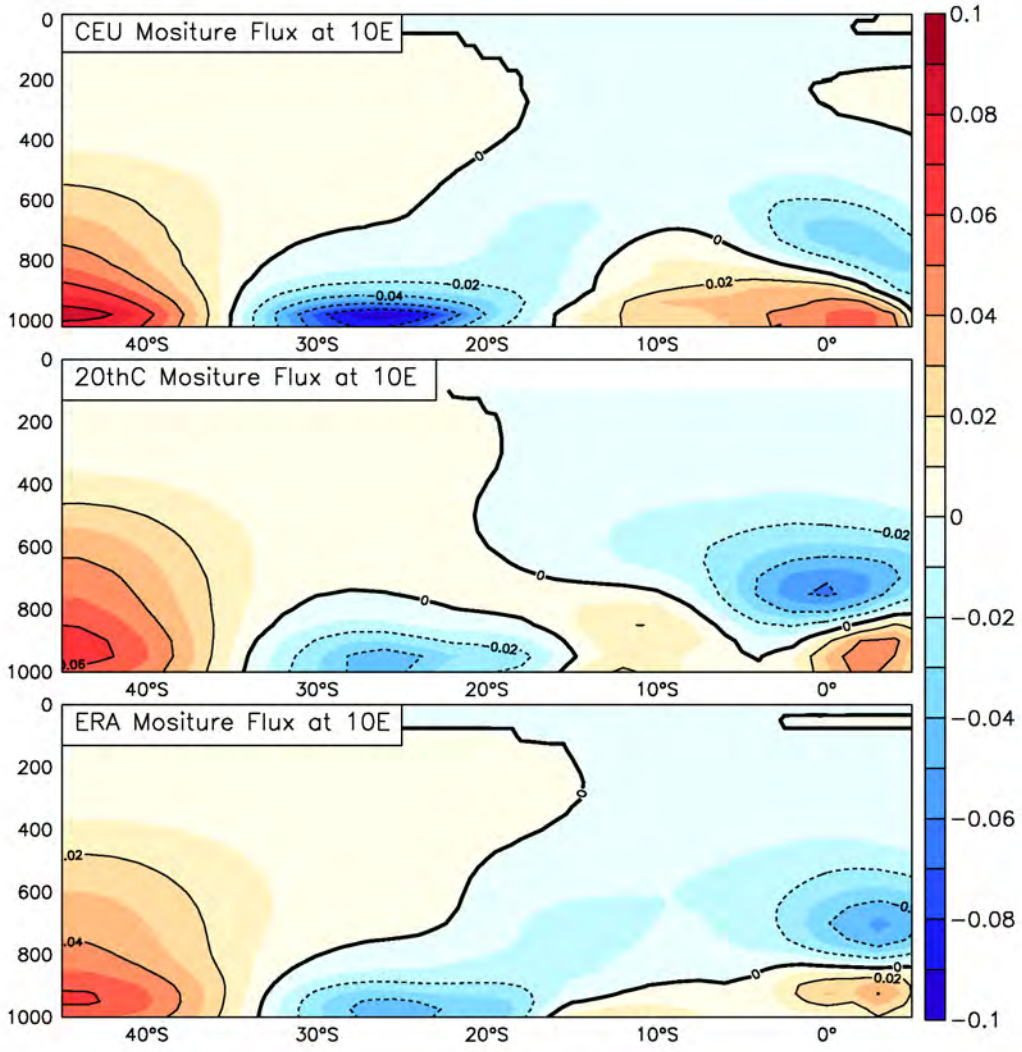

Figure 6.28: JFM climatological moisture flux at 10^oE for CEU, 20th Century and ERA (in 10^{-3} kg·kg^{-1}·m·s^{-1})

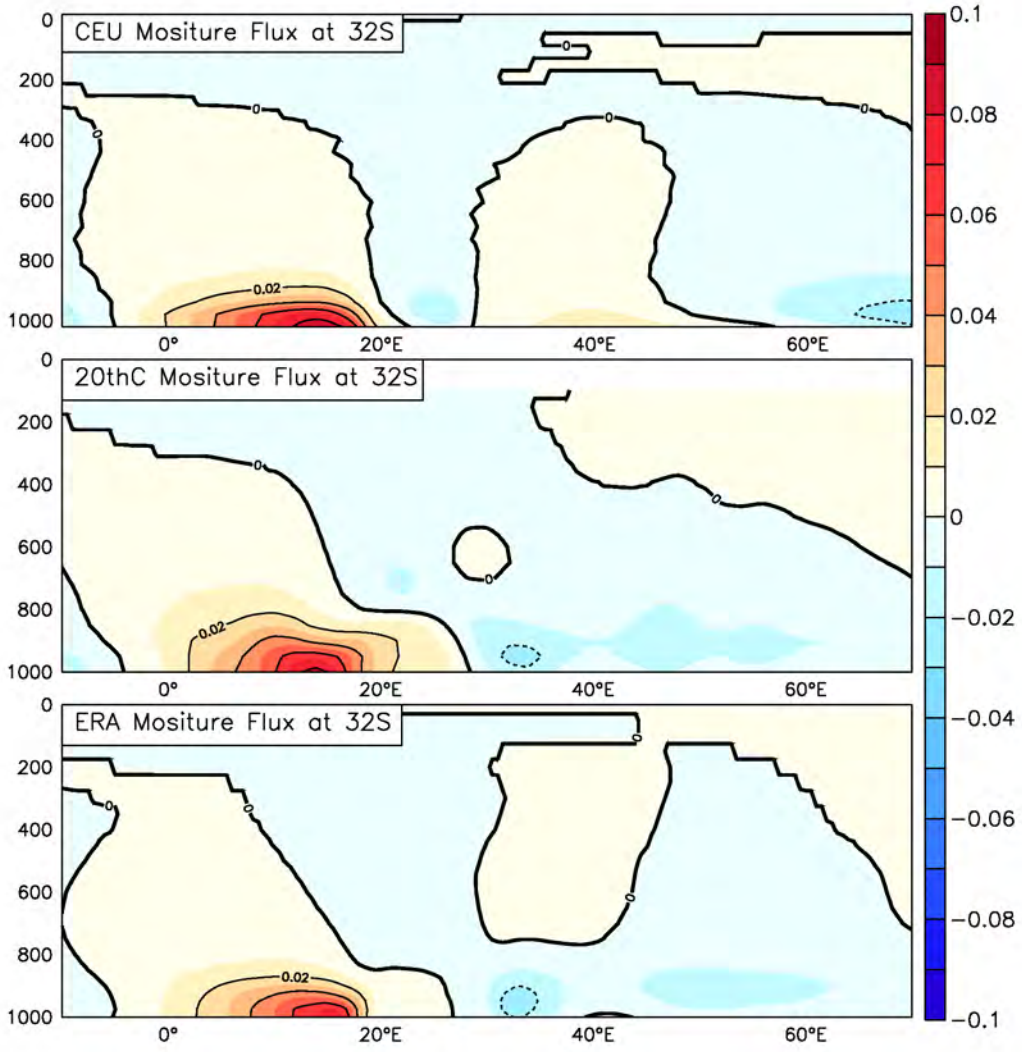

Figure 6.29: JFM climatological moisture flux at 32^{o}S for CEU, 20th Century and ERA (in 10^{-3} kg·kg^{-1}·m·s^{-1})

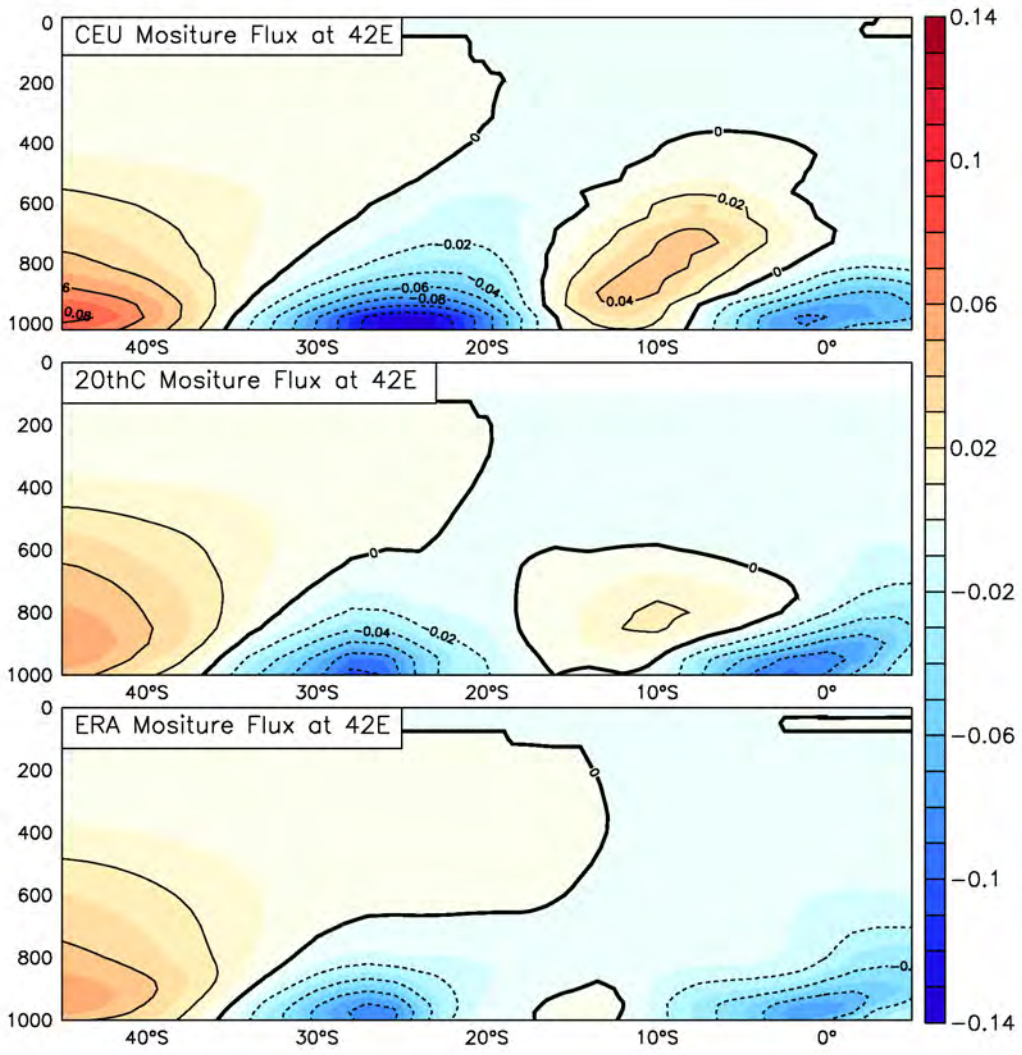

Figure 6.30: JFM climatological moisture flux at 42^{o}E for CEU, 20th Century and ERA (in 10^{-3} kg·kg^{-1}·m·s^{-1})

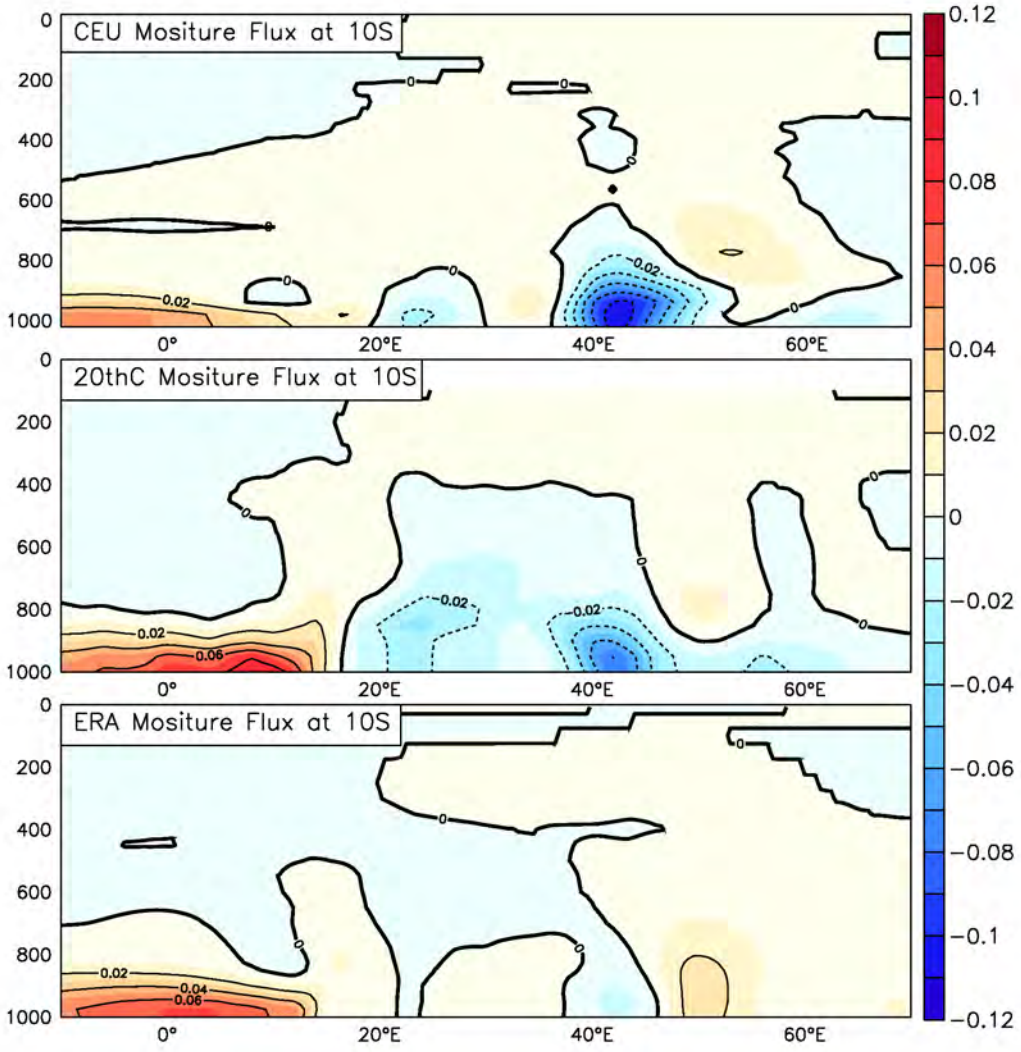

Figure 6.31: JFM climatological moisture flux at 10^oS for CEU, 20th Century and ERA (in 10^{-3} kg·kg^{-1}·m·s^{-1})

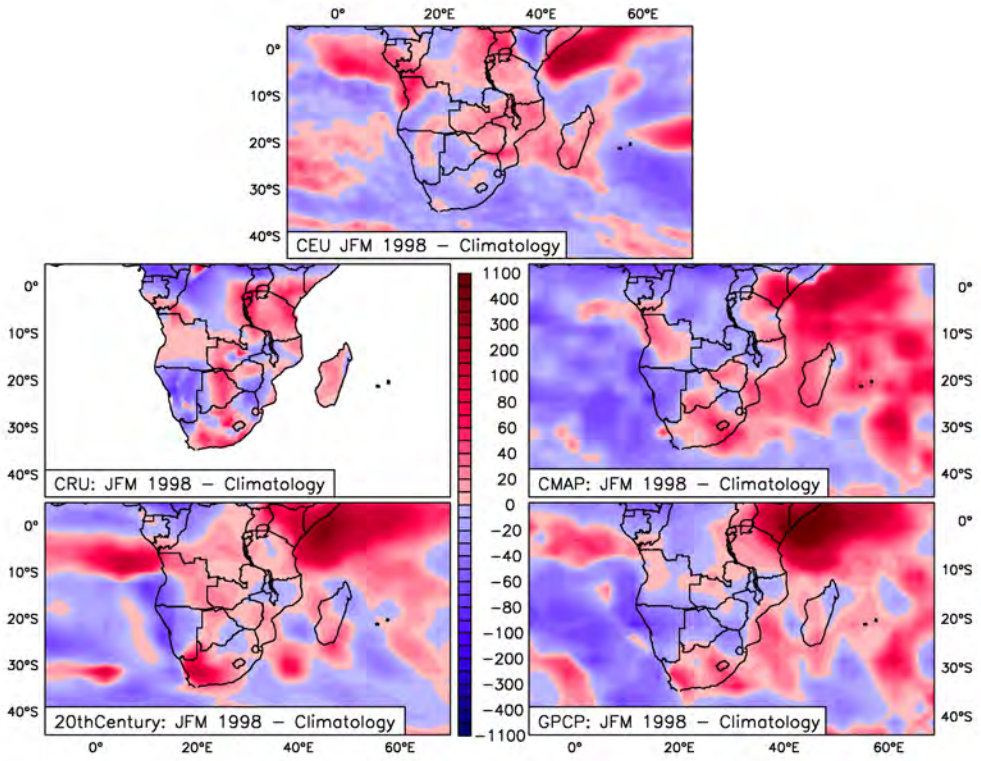

Figure 6.32: JFM 1998 percentage difference with Clim of rainfall over southern Africa for CEU, CMAP, CRU, 20th Century and GPCP (in mm·day^{-1})

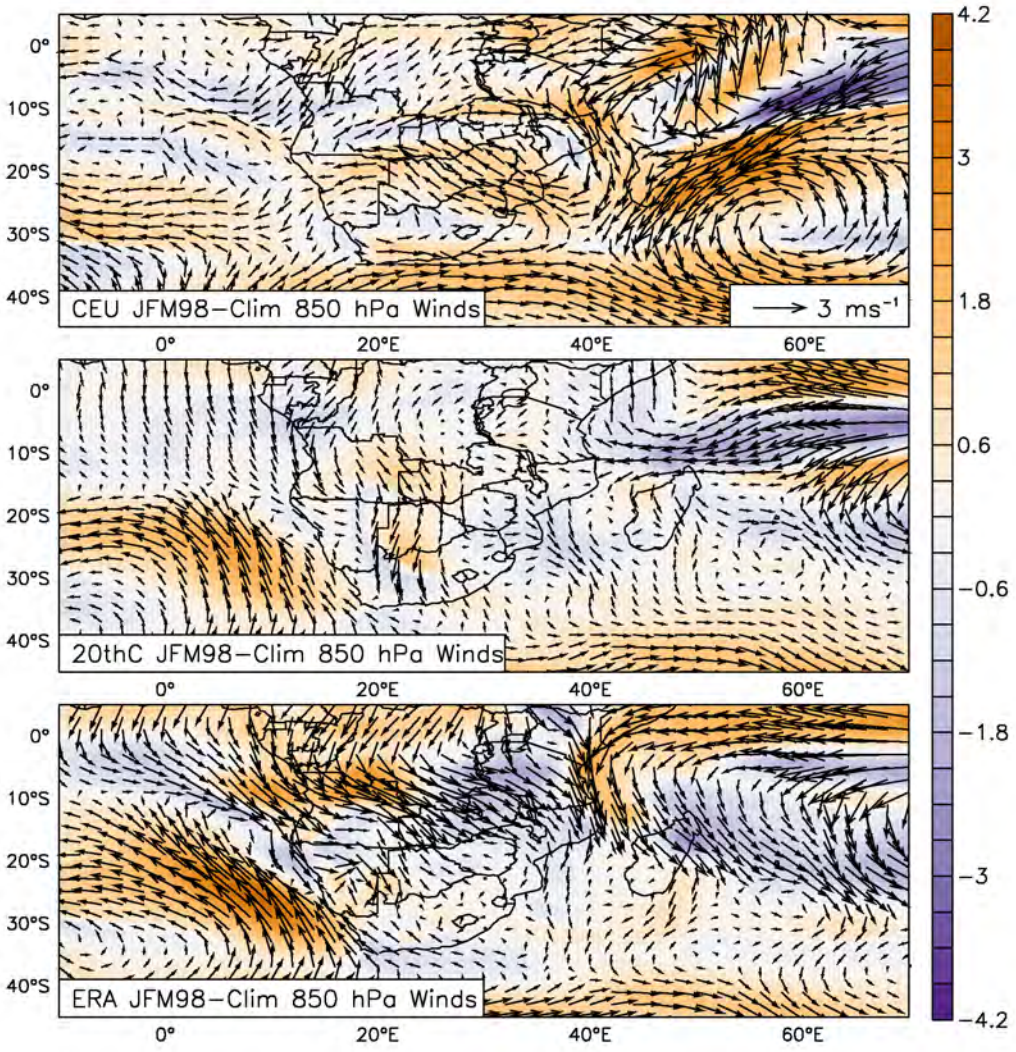

Figure 6.33: JFM 1998 850 hPa wind anomalies over southern Africa for CEU, 20th Century, ERA and CRU (in $m \cdot s^{-1}$)

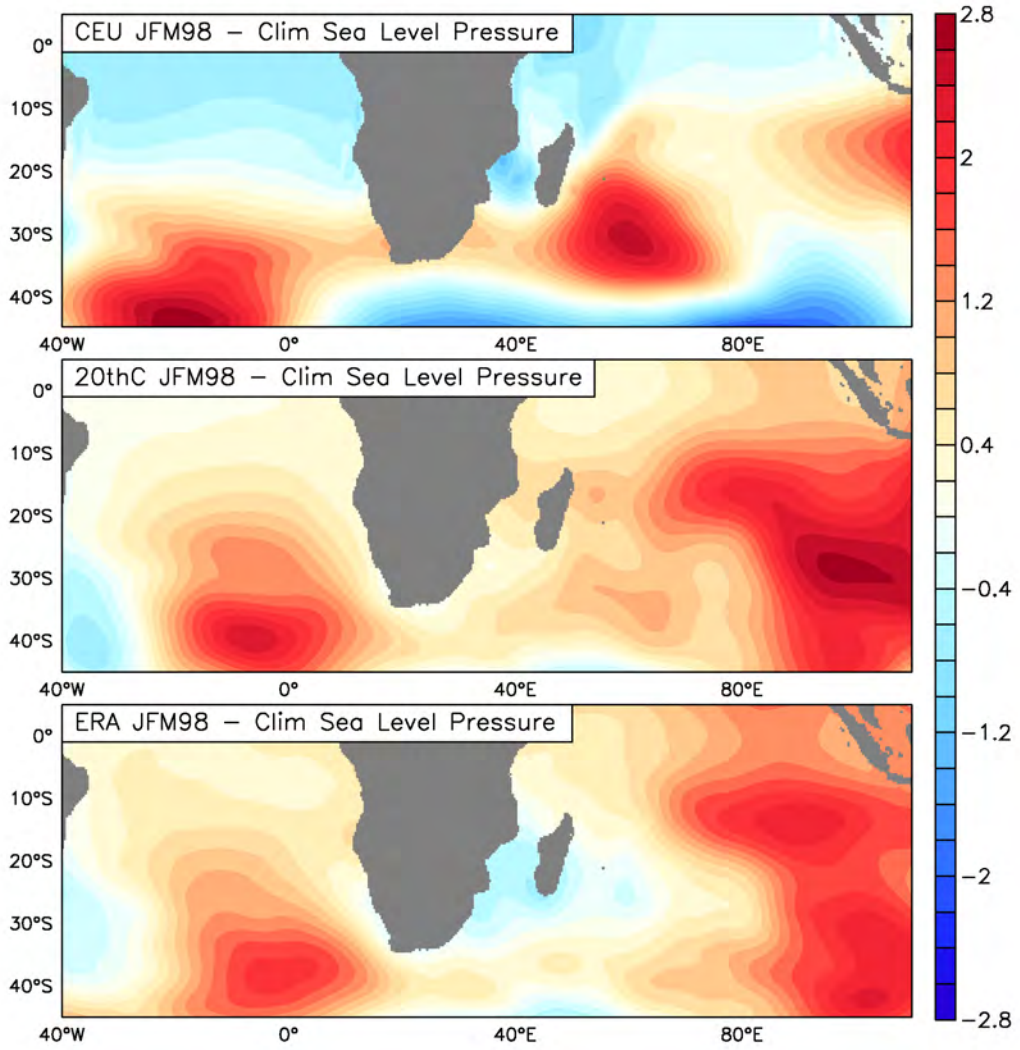

Figure 6.34: JFM 1998 sea level pressure anomalies over southern Africa for CEU, 20th Century, ERA and CRU (in hPa)

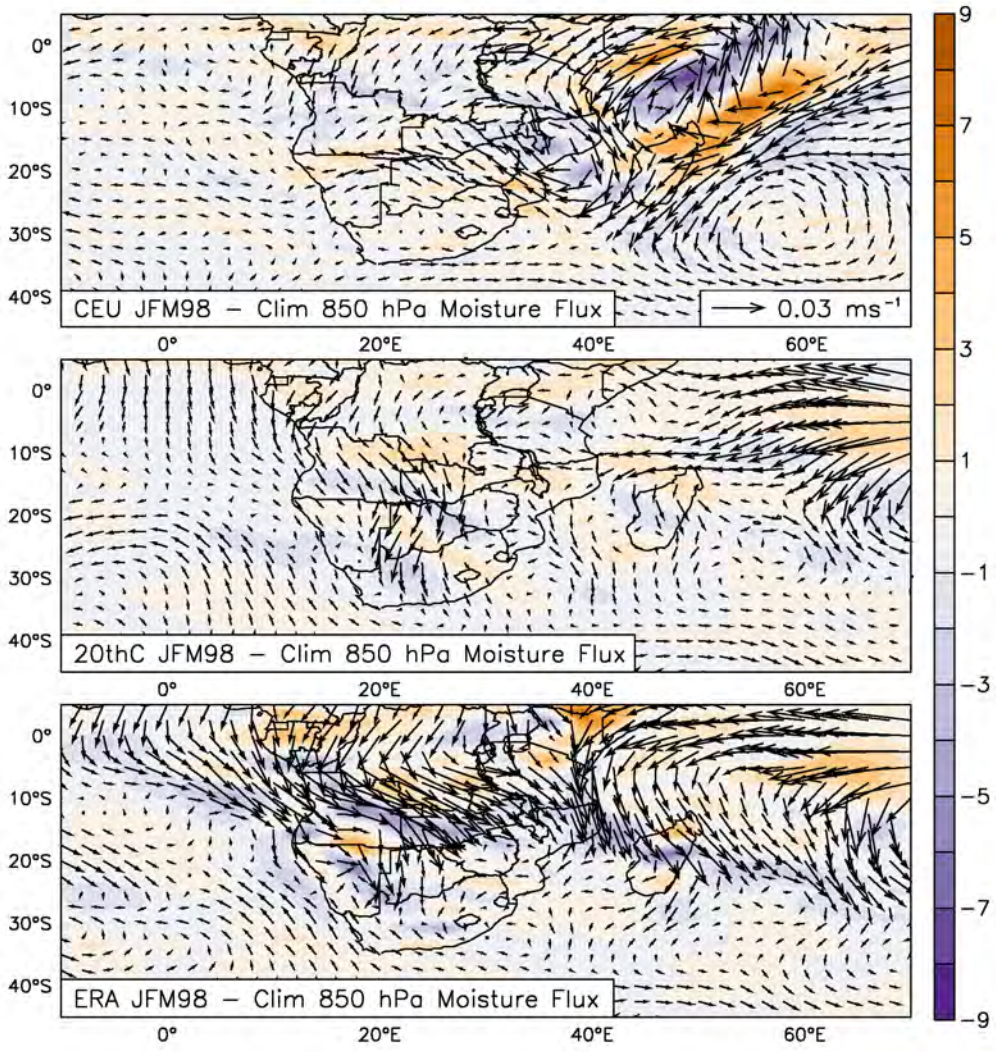

Figure 6.35: JFM 1998 moisture flux divergence (in 10^8 s^{-1}) and moisture flux (vectors) over southern Africa for CEU, 20th Century and ERA (in 10^{-3} $kg{\cdot}kg^{-1}{\cdot}m{\cdot}s^{-1}$)

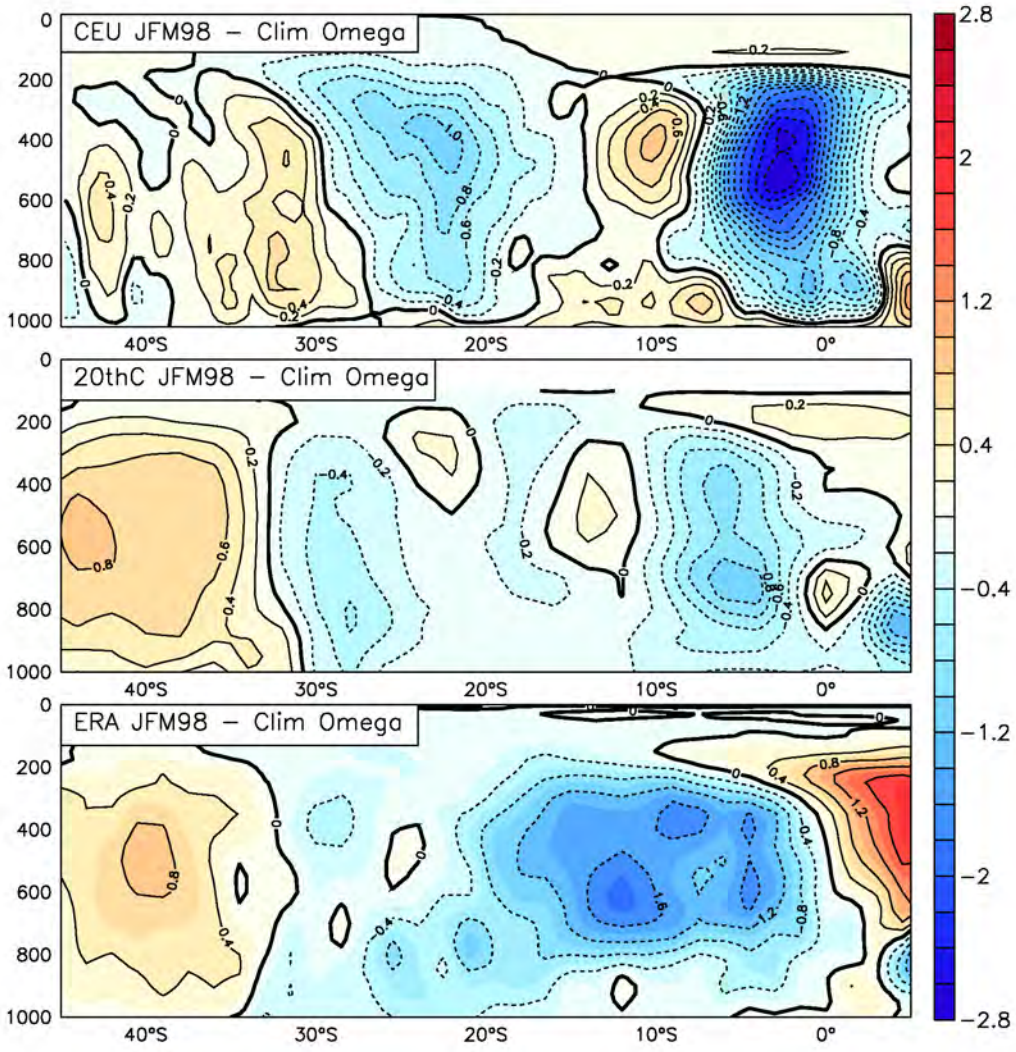

Figure 6.36: JFM 1998 omega anomalies over southern Africa for CEU, 20th Century, ERA and CRU (in in 10^2 kg·m^{-1}·s^{-3})

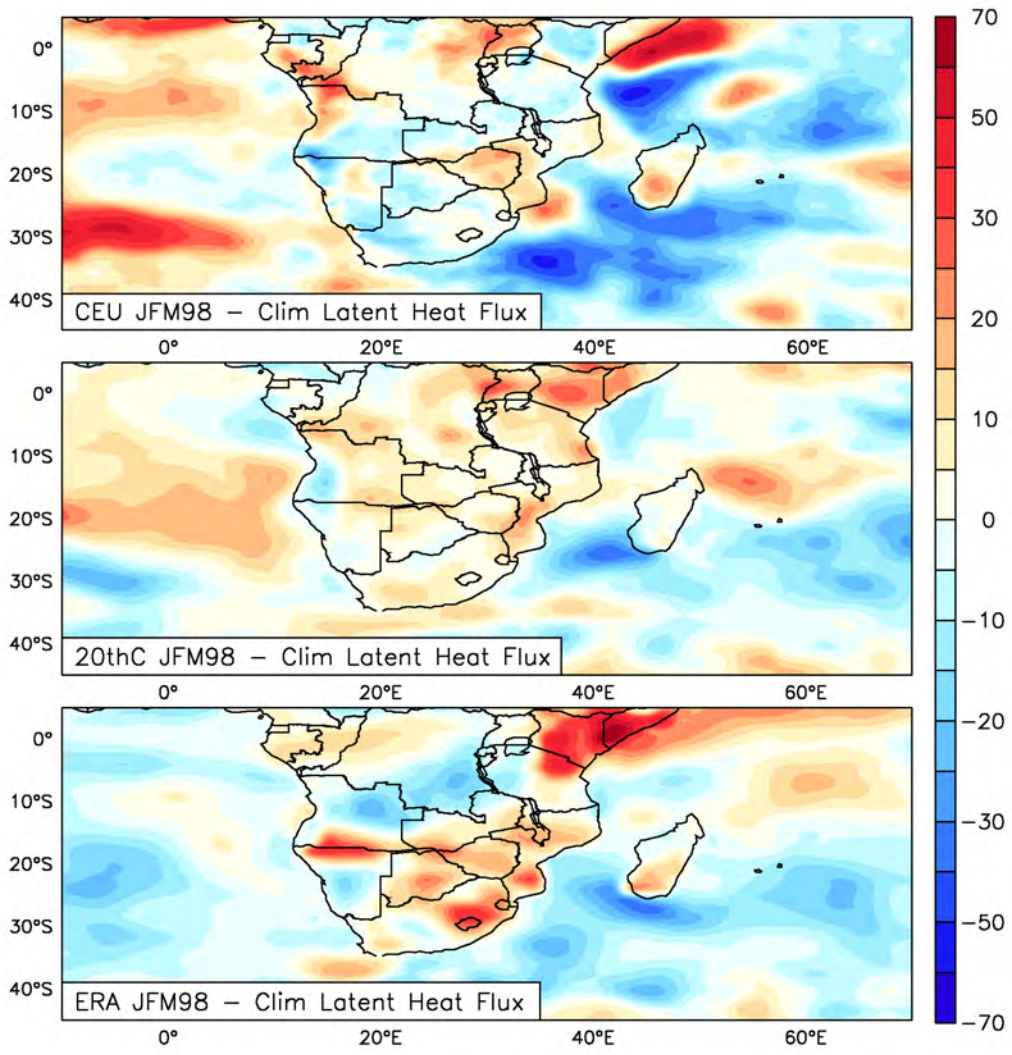

Figure 6.37: JFM 1998 latent heat flux anomalies over southern Africa for CEU, 20th Century, ERA and CRU (in $kg{\cdot}s^{-3}$)

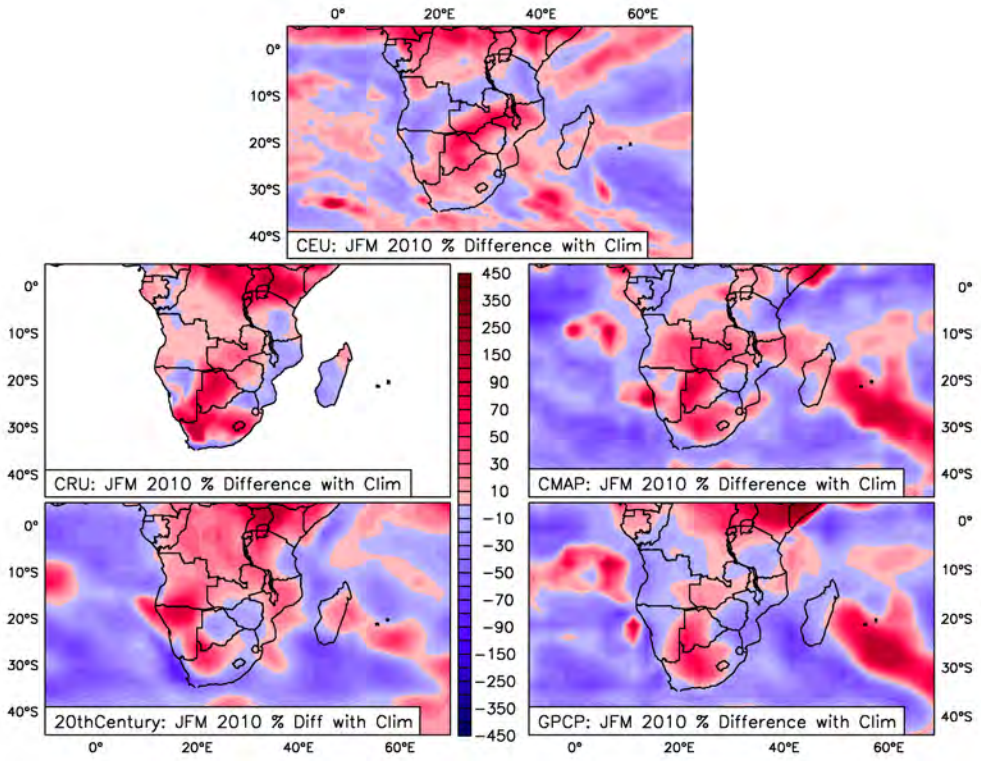

Figure 6.38: JFM 2010 percentage difference with Clim of rainfall over southern Africa for CEU, CMAP, CRU, 20th Century and GPCP (in mm·day^{-1})

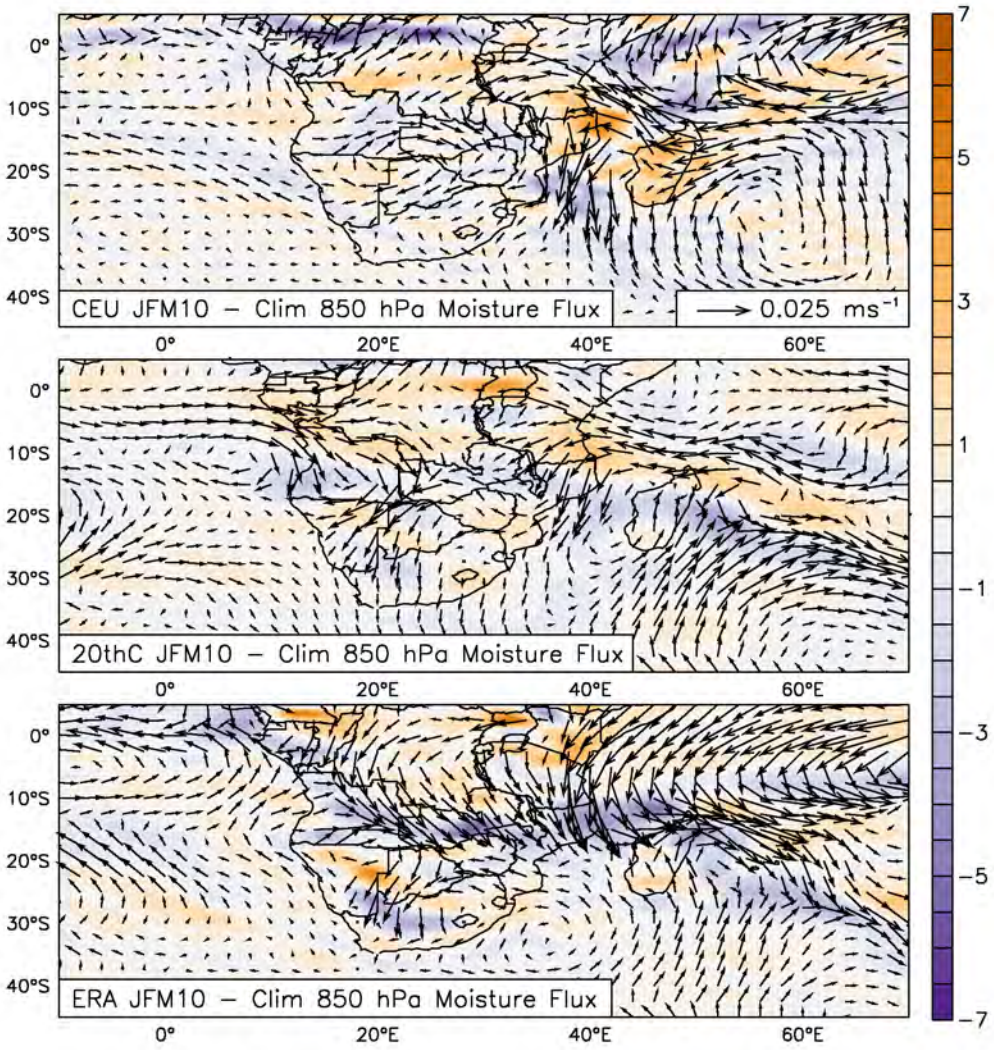

Figure 6.39: JFM 2010 moisture flux divergence (in 10^8 s^{-1}) and moisture flux over southern Africa for CEU, 20th Century and ERA (in 10^{-3} $kg{\cdot}kg^{-1}{\cdot}m{\cdot}s^{-1}$)

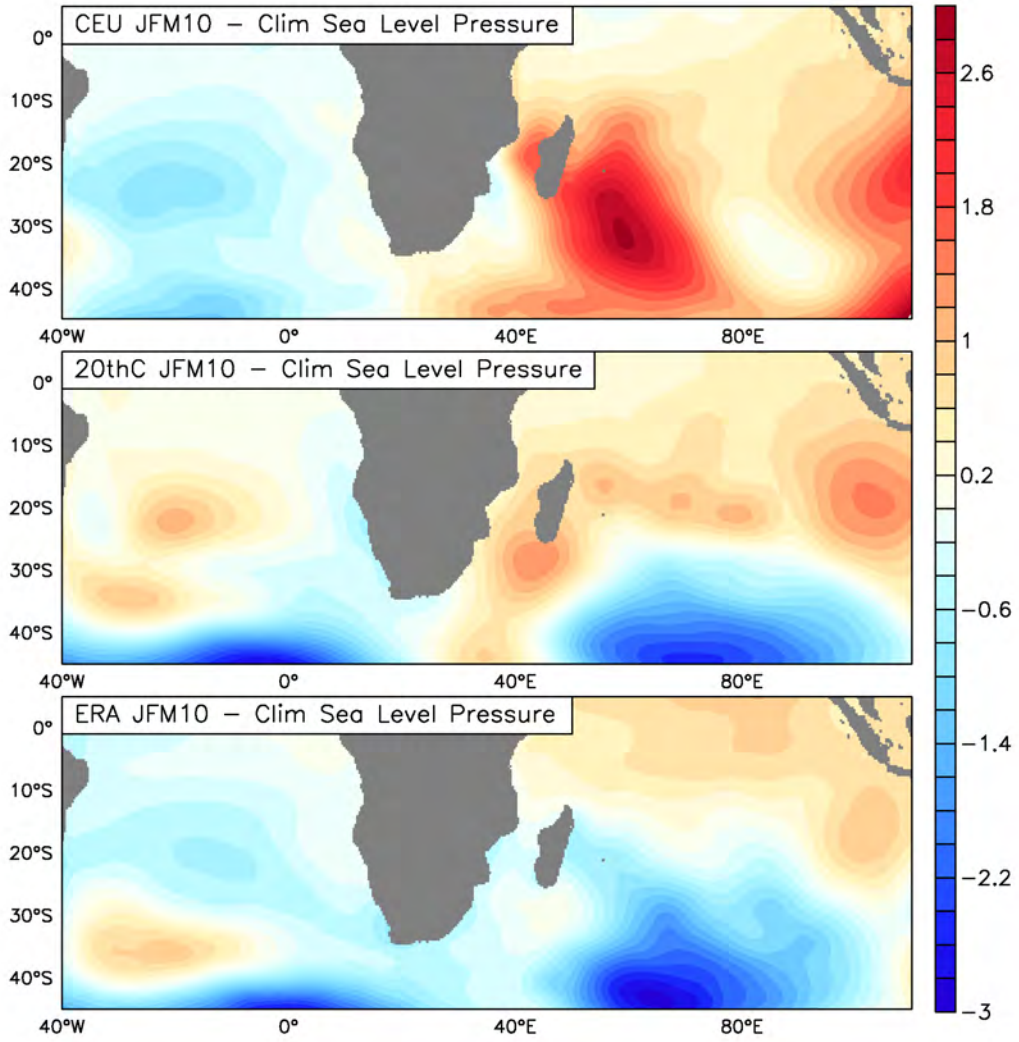

Figure 6.40: JFM 2010 sea level pressure anomalies over southern Africa for CEU, 20th Century, ERA and CRU (in hPa)

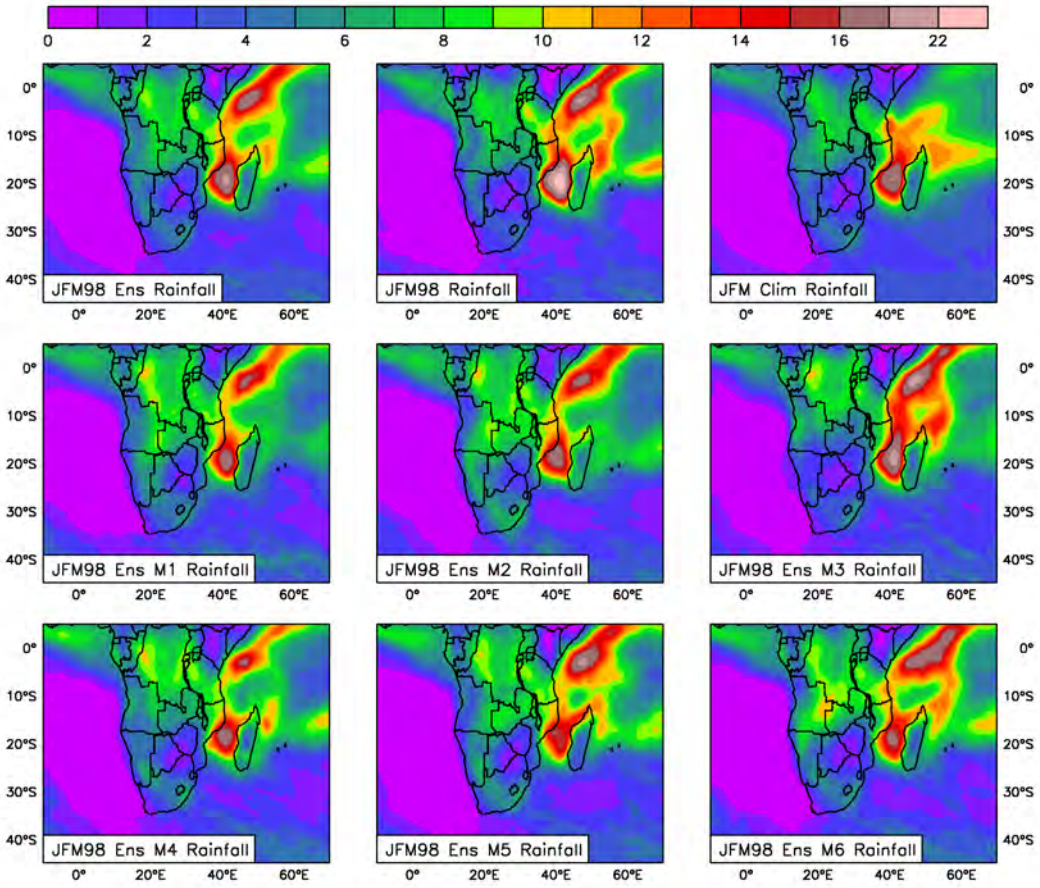

Figure 6.41: JFM 1998 rainfall over southern Africa for the ensemble average, JFM 1998, climatology, and each ensemble member (in mm·day^{-1})

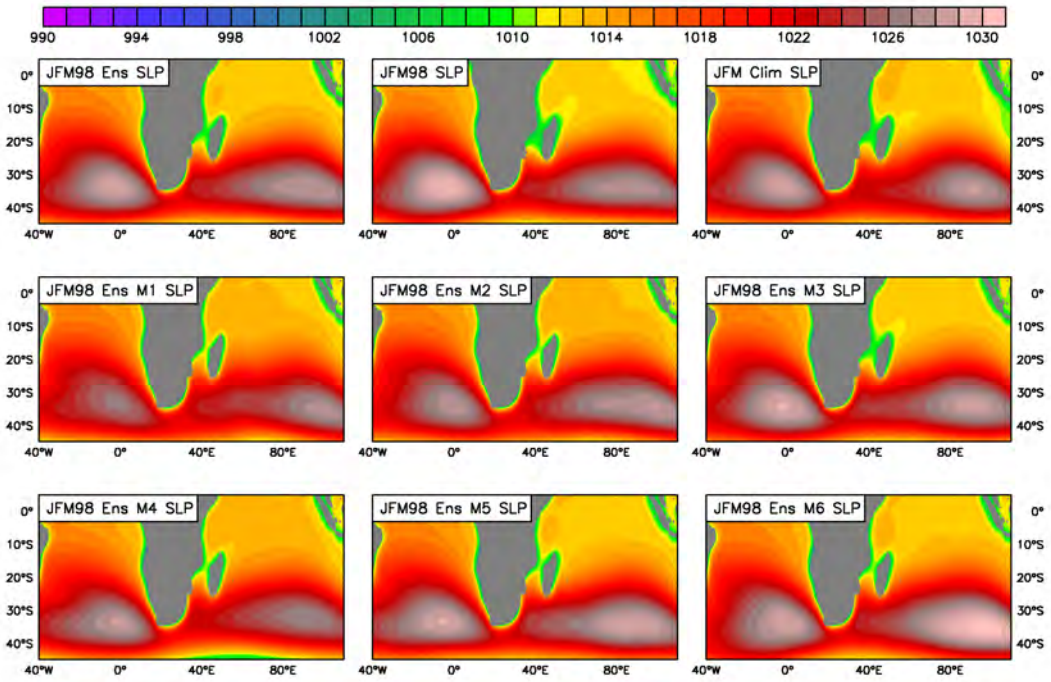

Figure 6.42: JFM 1998 sea level pressure over southern Africa for the ensemble average, JFM 1998, climatology, and each ensemble member (in hPa)

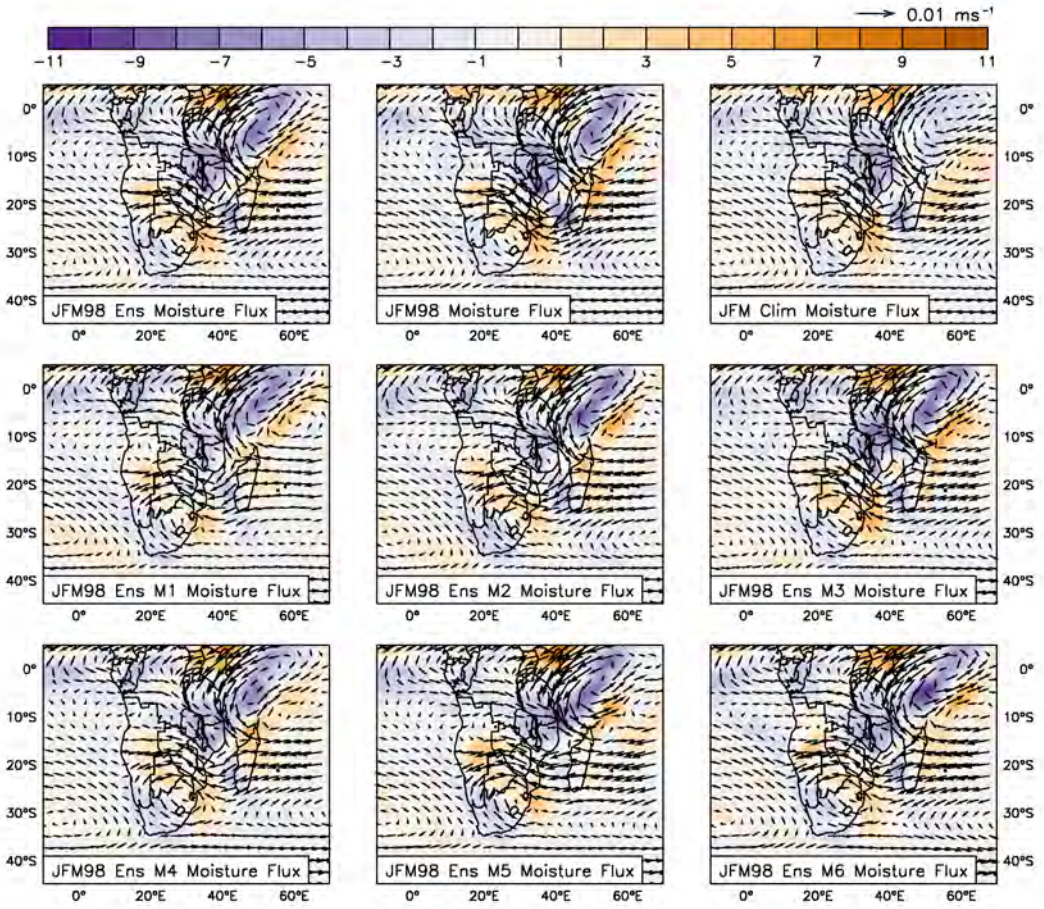

Figure 6.43: JFM 1998 850 hPa moisture flux convergence (in 10^8 s^{-1}) and moisture flux over southern Africa for the ensemble average, JFM 1998, climatology, and each ensemble member (in 10^{-3} $kg{\cdot}kg^{-1}{\cdot}m{\cdot}s^{-1}$)

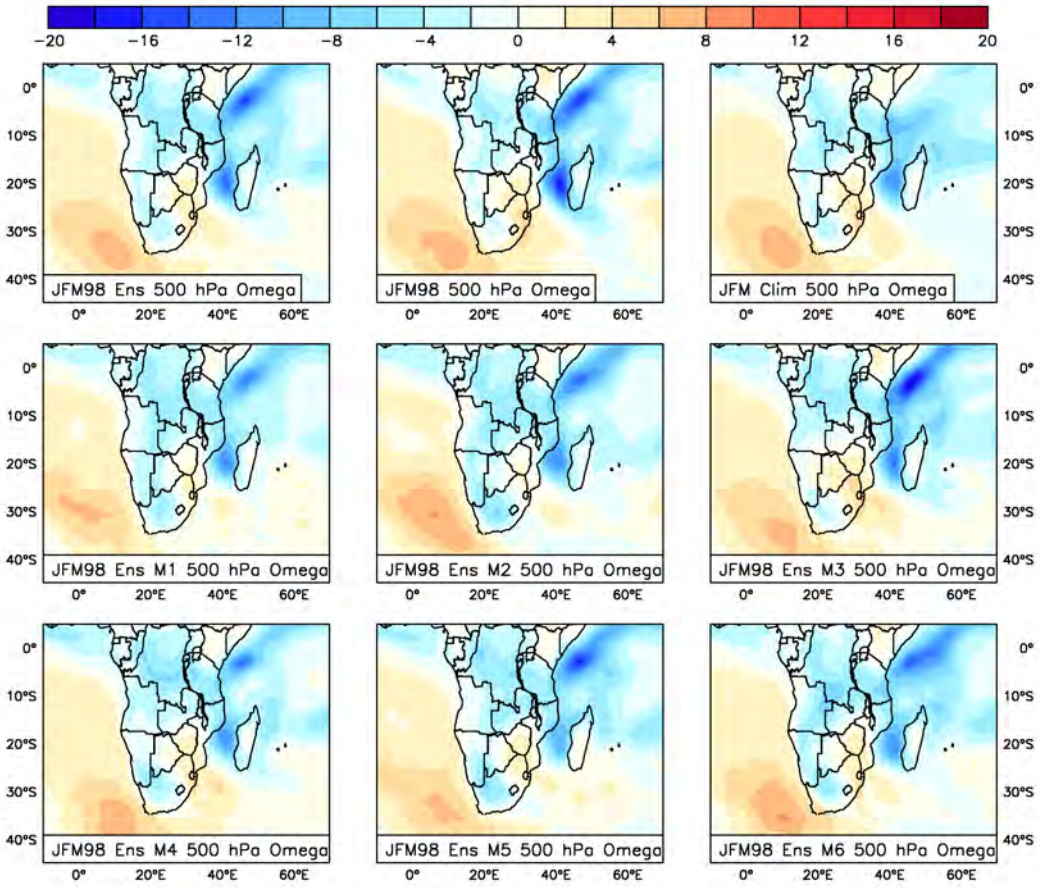

Figure 6.44: JFM 1998 omega over southern Africa for the ensemble average, JFM 1998, climatology, and each ensemble member (in 10^2 kg·m^{-1}·s^{-3})

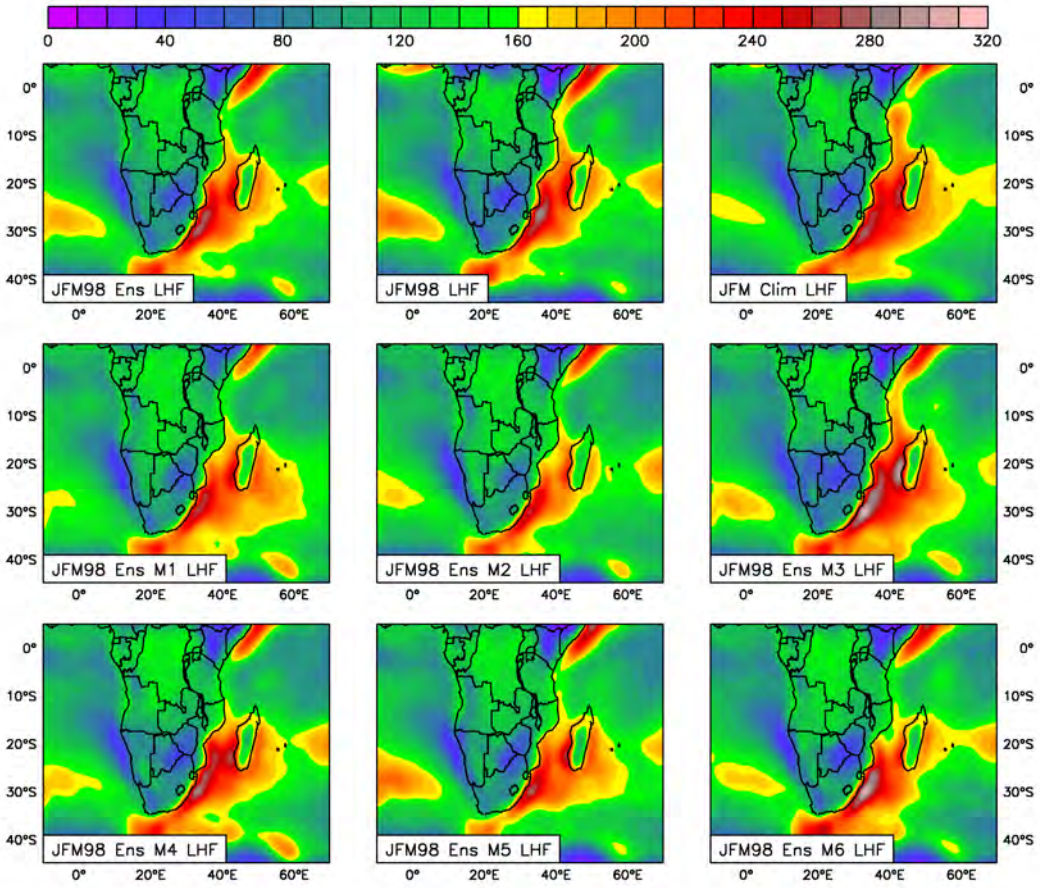

Figure 6.45: JFM 1998 latent heat flux over southern Africa for the ensemble average, JFM 1998, climatology, and each ensemble member (in $\mathrm{kg{\cdot}s^{-3}}$)

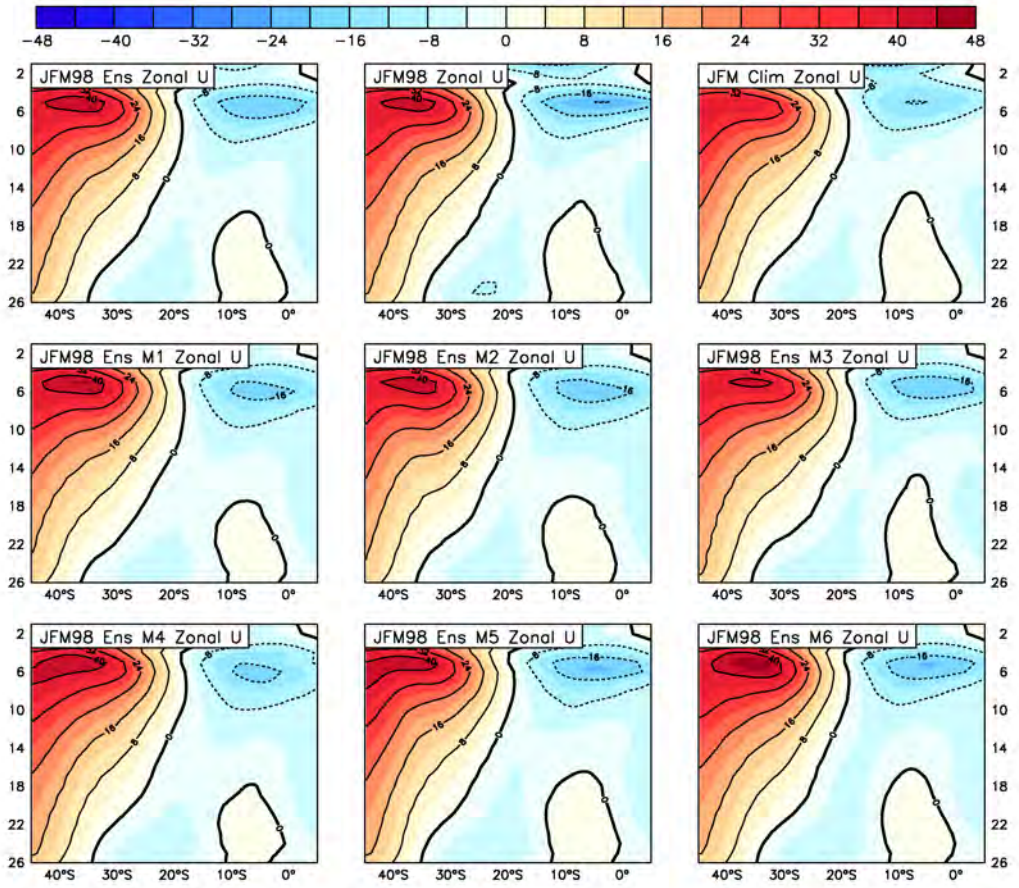

Figure 6.46: JFM 1998 zonally averaged zonal winds over southern Africa for the ensemble average, JFM 1998, climatology, and each ensemble member (in $\mathrm{m{\cdot}s^{-1}}$)

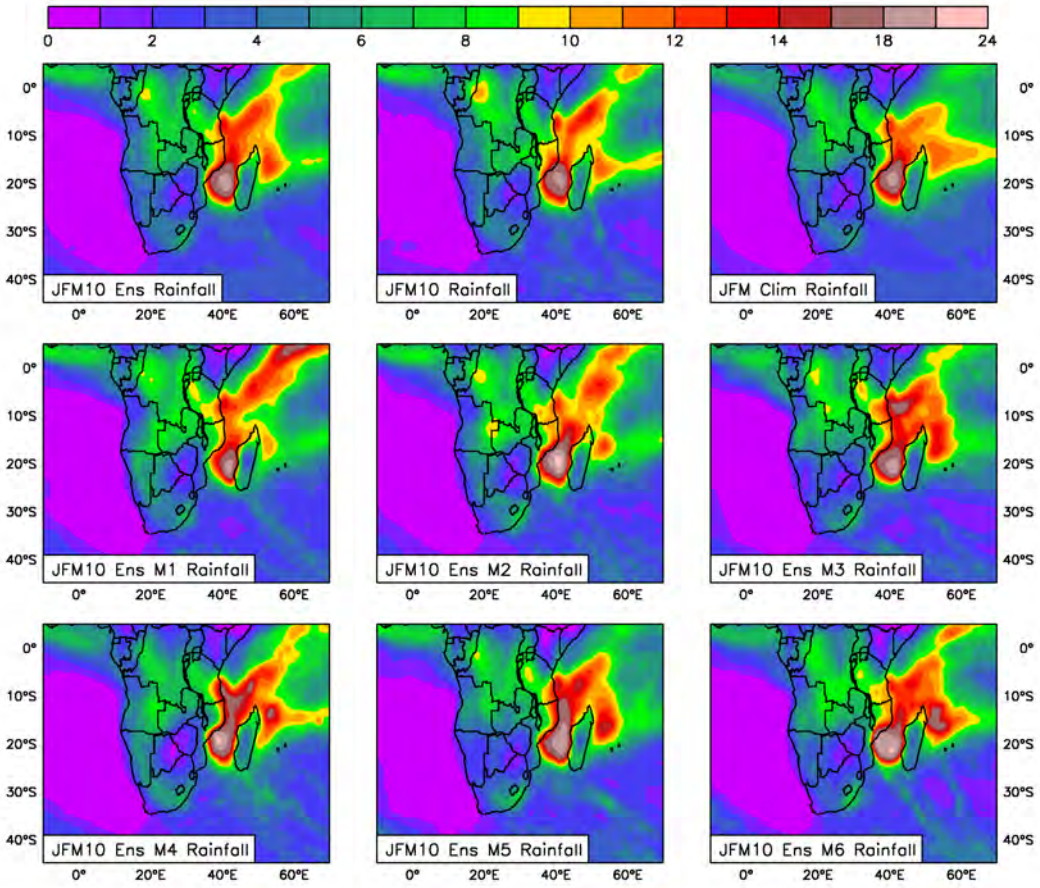

Figure 6.47: JFM 2010 rainfall over southern Africa for the ensemble average, JFM 2010, climatology, and each ensemble member (in mm·day^{-1})

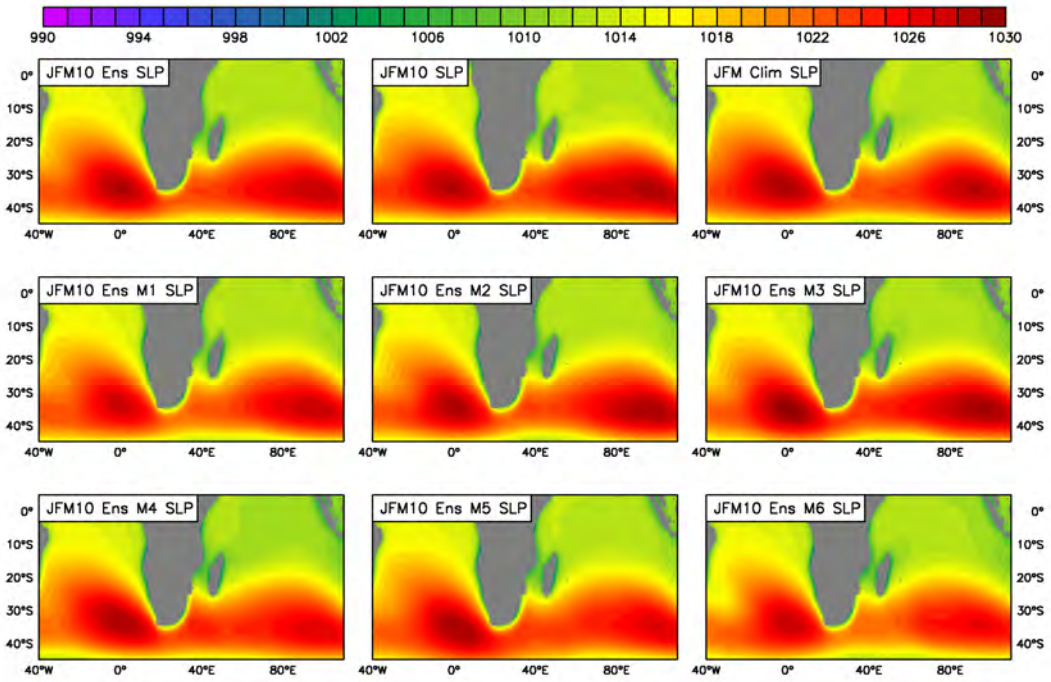

Figure 6.48: JFM 2010 sea level pressure over southern Africa for the ensemble average, JFM 2010, climatology, and each ensemble member (in hPa)

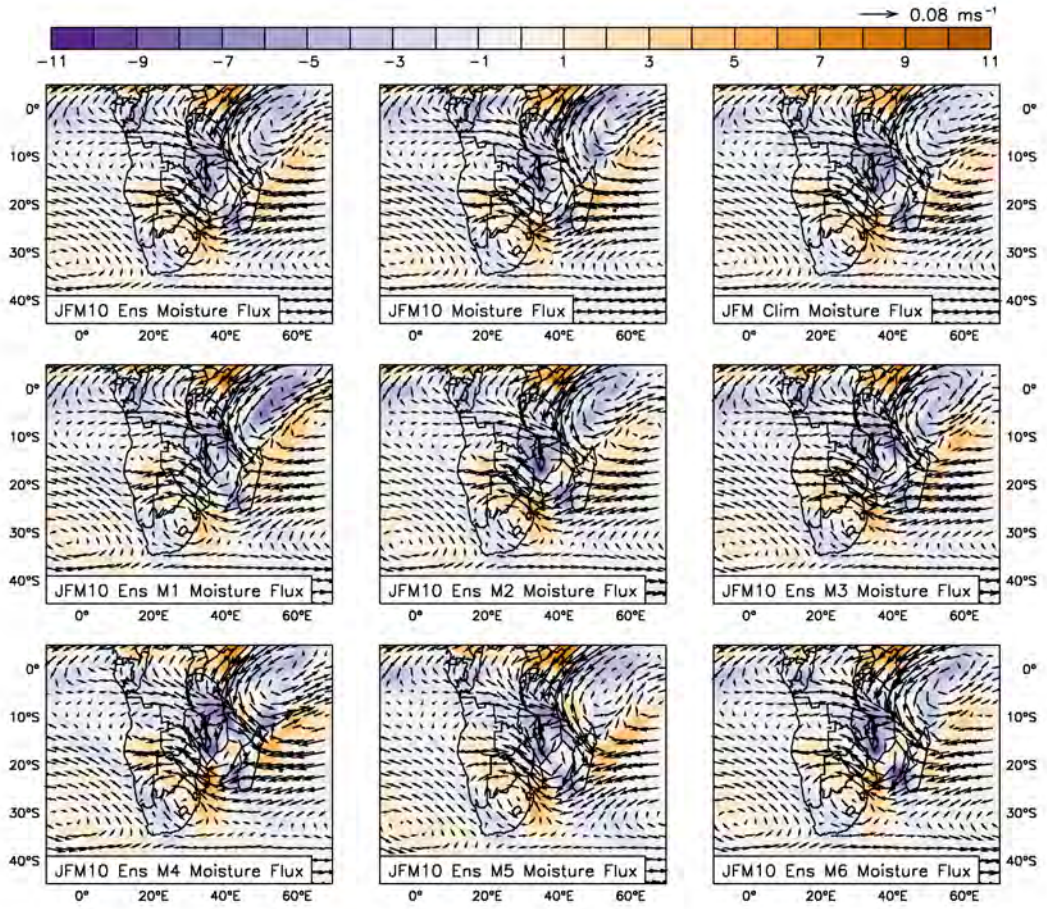

Figure 6.49: JFM 2010 moisture flux convergence at 850 hPa (in 10^8 s^{-1}) and moisture flux over southern Africa for the ensemble average, JFM 2010, climatology, and each ensemble member (in 10^{-3} $kg{\cdot}kg^{-1}{\cdot}m{\cdot}s^{-1}$)

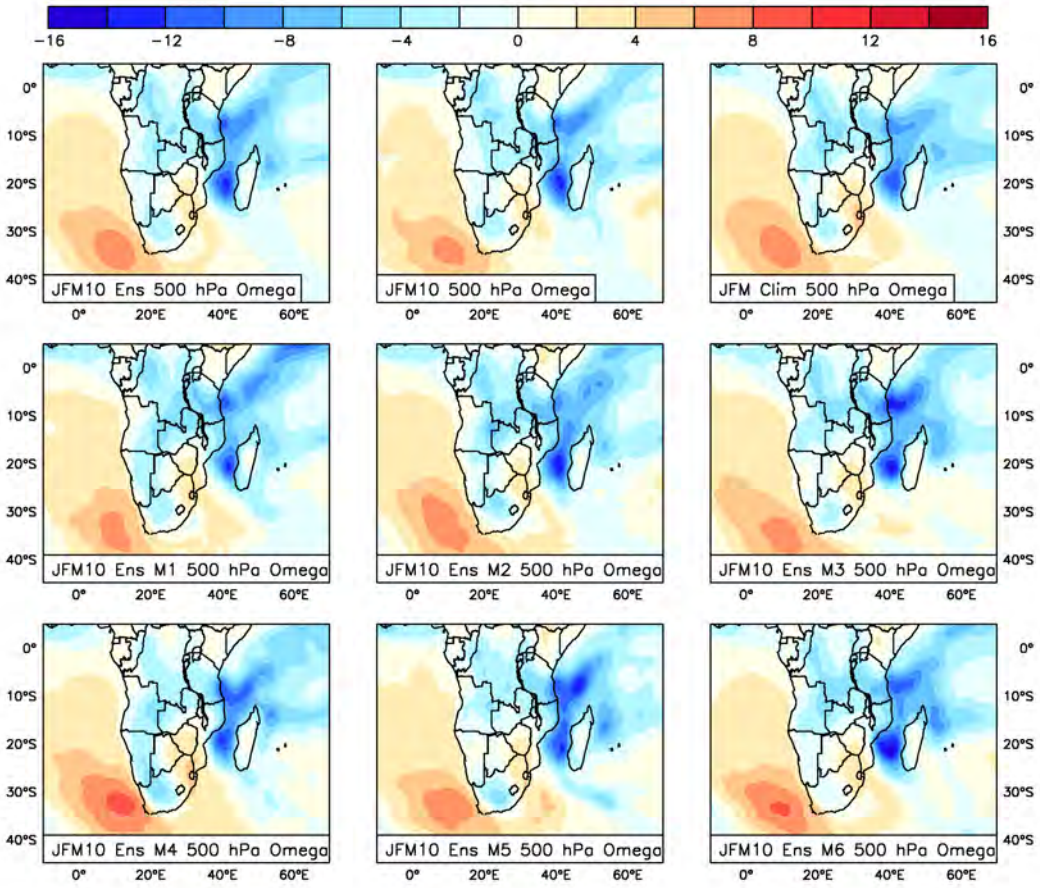

Figure 6.50: JFM 2010 omega over southern Africa for the ensemble average, JFM 2010, climatology, and each ensemble member (in 10^2 kg·m^{-1}·s^{-3})

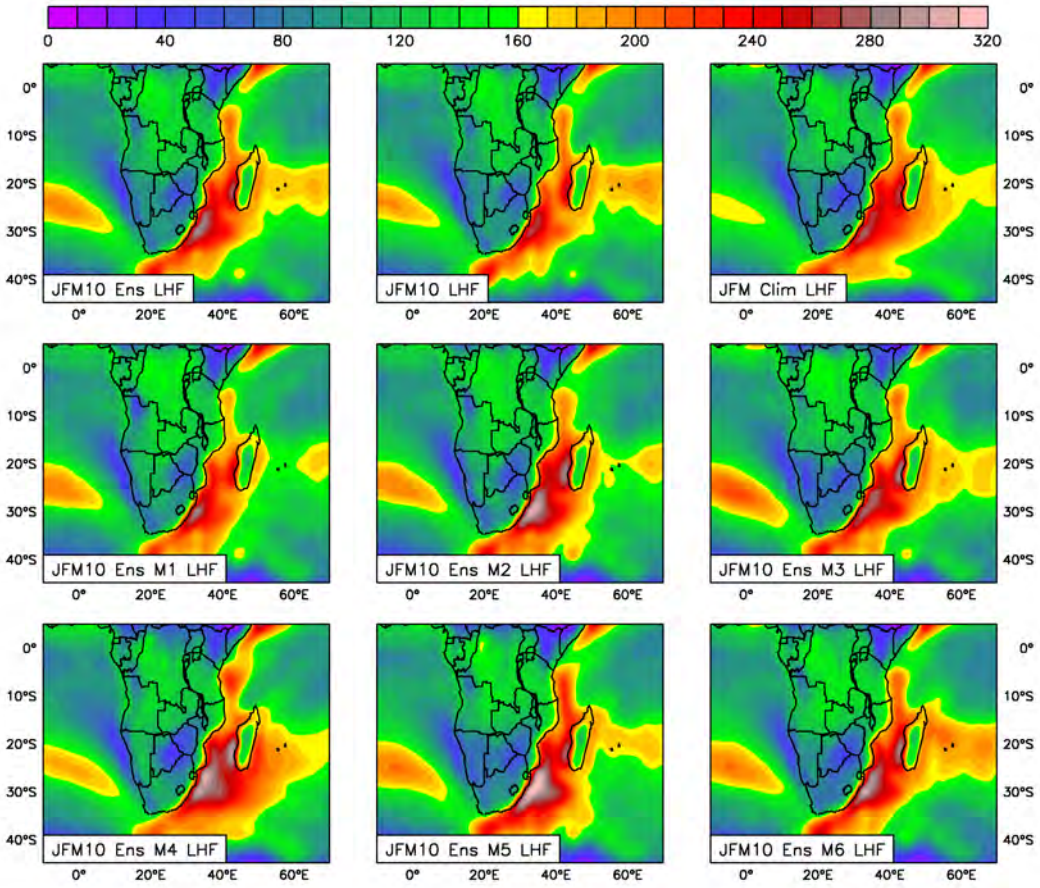

Figure 6.51: JFM 2010 latent heat flux over southern Africa for the ensemble average, JFM 2010, climatology, and each ensemble member (in $\mathrm{kg{\cdot}s^{-3}}$)

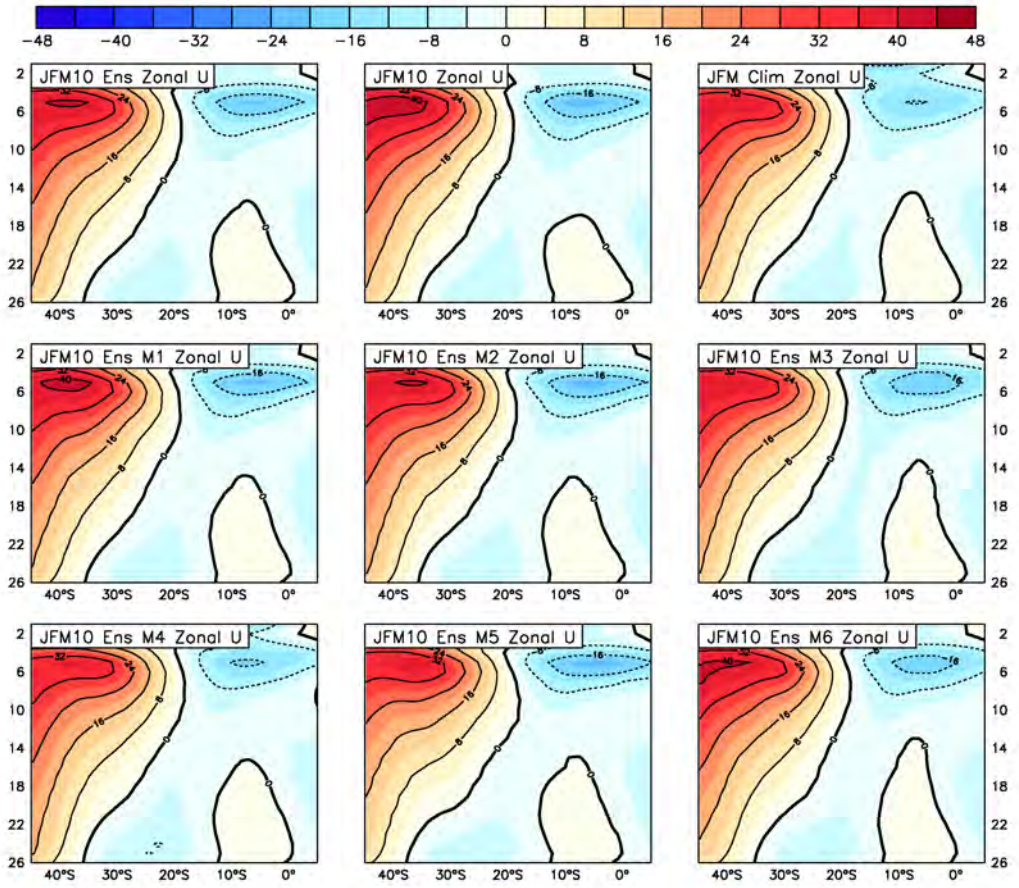

Figure 6.52: JFM 2010 zonally averaged zonal winds over southern Africa for the ensemble average, JFM 2010, climatology, and each ensemble member (in $\mathrm{m{\cdot}s^{-1}}$)

Chapter 7

Model Experiments

Many seasonal climate forecasts indicated an enhanced probability of below-average rainfall over southern Africa during the austral summer rainfall season 1997-1998 (Mason et al., 1999b; Buizer et al., 2000; Lyon and Mason, 2007). This prediction of dry conditions was probably linked to the strong El Niño that occurred during 1997-1998 and the typical association of El Niño with drought conditions over southern Africa in both models and observations (Hastenrath et al., 1993; Goddard and Graham, 1999; Reason et al., 2000; Reason and Rouault, 2002; Reason and Jagadheesha, 2005; Richard et al., 2000, 2001; Lyon and Mason, 2007, 2009). However, the widespread drought conditions that were expected generally failed to materialise and in fact, seasonal rainfall in some regions was observed to be near or above average (Kane, 1999; Richard et al., 2001). Landman and Beraki (2010) assessed the probabilistic rainfall forecast skill over southern Africa during

DJF for the period 1980-2002 using a number of multi-model ensembles and one of the main results of their study was that the forecasts perform better during El Niño and La Niña seasons than during neutral years. The rainfall forecast for the 2009-2010 DJF El Niño season that were made by the three coupled models discussed in Landman and Beraki (2010) also showed mostly enhanced probabilities for dry conditions over southern Africa. A similar forecast was also made by international centres such as the IRI and the South African Weather Service. However, DJF 2009-2010 rainfall over South Africa was anomalously high, something that was largely missed by most forecasting systems. The association of enhanced forecast skill with El Niño years may partially explain the level of confidence in the forecast of dry conditions for the austral summer seasons during 1997-1998 and 2009-2010.

The 1997-1998 and 2009-2010 summer rainfall seasons over southern Africa are often cited as examples of an unexpected rainfall response over the region to ENSO, and studies have been conducted to investigate what may have occurred during 1997-1998 in particular. Reason and Jagadheesha (2005) postulated that the enhanced moisture levels resulting from the positive TIOD and Benguela Niño events during the austral summer of 1997-1998, together with the relatively strong Angola low, mitigated the drought conditions that often coincide with an El Niño event. Lyon and Mason (2007) suggested that two primary factors associated with the unexpected rainfall conditions over subtropical southern Africa during JFM 1998, were the anomalous stationary

wave pattern observed over the Southern Hemisphere and its connection with the enhanced Angola low, as well as enhanced moisture flux into southern Africa from the western Indian Ocean due to the strong tropical Indian Ocean dipole event. To further investigate these factors, a set of model experiments with different idealised SST forcing were performed. These experiments are analysed in this chapter.

7.1 Idealised Experiments

Seven experiments were performed using CEU forced with prescribed SSTs during the months of, and leading up to, JFM 1998. The control run, referred to as Ctr98, was forced with observed global SSTs. The remaining six experiments were designed to isolate the impact of SSTAs in each major ocean basin on southern African rainfall during JFM 1998. Three experiments, namely NoAtl98, NoInd98 and NoPac98, replace SSTs in one major ocean basin by the climatology of that ocean. The remaining three experiments, namely OnlyAtl98, OnlyInd98, and OnlyPac98, replace SSTs in two ocean basins by their climatology. The Only"Ocean"98 experiments emphasise the impact of SSTAs in each ocean basin individually while the No"Ocean"98 experiments highlight the contribution of a combination of SSTAs from the other two ocean basins.

The same method was applied to produce simulations for JFM 2010.

The climatology described in **Chapter 7** is used here to calculate anomaly features and called Clim.

7.1.1 SST Forcings JFM 1998

Figure 7.1 shows the difference between global observed SSTs during JFM 1998 and climatological SSTs during the JFM season. Global SSTs were generally warmer than average during JFM 1998 over most of the Indian Ocean and the tropical - subtropical Atlantic Ocean with a particularly strong El Niño event occurring that year. A strong positive TIOD event occurred during the second half of 1997 and, although it is not typical for these events to last into the beginning of the following year, the DMI remained greater than 0.5 during February 1998, only decaying in March 1998 (Webster et al., 1999). In addition to the TIOD, the South Indian Ocean showed SSTAs reminiscent of a negative phase SIOD event which is confirmed in Feng et al. (2014). Behera and Yagamata (2001) also noted that the positive SIOD of 1997 changed phase to become a negative SIOD in early 1998. Apart from the pool of cool water just off the coast of Namibia, the Atlantic Ocean was generally warmer than average and there were warm SSTAs off the coast of Angola. It has been suggested that 1998 was a Benguela Niño year (Rouault et al., 2009). El Niño events typically lead to drought conditions over southern Africa (Lindesay, 1988; Reason et al., 2000), and negative SIOD events have been associated with dry conditions over parts of southern Africa, while a Benguela Niño, and positive TIOD events usually result in

above average rainfall over parts of southern Africa (Rouault et al., 2003a; Behera and Yagamata, 2001).

7.1.2 SST Forcings JFM 2010

The global SSTAs during JFM 2010 are shown in **Figure 7.2**. An El Niño is evident in the Pacific Ocean where SSTAs are approximately 2.5^o warmer over the central equatorial Pacific Ocean. A new type of El Niño, characterised by anomalously warm SSTAs in the central equatorial Pacific Ocean, has been occurring with more frequency in the last few decades. These events can be described using the Niño 4 index and are known as central Pacific (CP) El Niños, while canonical El Niño events are called Eastern Pacific (EP) El Niños (Kao and Yu, 2009; Yeh et al., 2009). The differences between CP and EP El Niños were discussed in more detail in **Chapter 2**. The El Niño event of 2009-2010 is considered to have been a CP El Niño event, however it was unusual since SSTAs over the eastern equatorial Pacific Ocean were also high. The SSTAs over the south eastern Pacific Ocean were below average which is typical of an CP El Niño and despite the anomalous warm equatorial eastern Pacific waters, the 2009-2010 event falls into the categorization of CP El Niño when the indices are consulted (Lee and McPhaden, 2010; Kim et al., 2011; Ratnam et al., 2012). There is also a region of positive SSTAs in the southern Pacific and negative SSTAs over the southeast Pacific along the coast of South America. There was a strong negative phase NAO during JFM 2010 and a tripole SSTA pattern is evident

in the North Atlantic Ocean. The warming of the subtropical North Atlantic SSTs can probably be attributed to the combined forcings from the El Niño and negative NAO that often warms the subtropical and high latitude SSTs and cools the midlatitude SSTs in the North Atlantic by modifying evaporative heat loss (Deser and Blackmon, 1993). There was also a weak positive TIOD during JFMA 2010 although the strength, and therefore its classification as a dipole event, varies depending on which SST data set is used (Blunden et al., 2011). CP El Niño events have been associated with below average rainfall over southern Africa although they do not produce dry conditions to the same extent as EP El Niño events (Ratnam et al., 2012, 2014), while positive TIOD events usually result in below average rainfall over parts of southern Africa. McHugh and Rogers (2001) found that heavier, convective, DJF rainfall occurs over Tanzania, northern Mozambique, Zambia and part of the western DRC during the negative NAO phase, when the North Atlantic westerlies are unusually weak. Todd and Washington (2004) also found a negative correlation between the NAO and central African rainfall, although their study focused on the FMA season.

7.2 Results

An assessment of the impact of SSTAs over each ocean basin on rainfall over southern Africa can be made by comparing the difference map computed for each experiment using the model climatology referred to earlier. In this

study, Only"OceanX" and No"OceanX" are compared as though the impact of OceanX can be completely isolated in the first case and completely removed in the second case. This approach assumes that the impacts of each ocean basin SSTAs on rainfall are independent of one another. However, this linear simplification of a highly complex interactive system can yield interesting and useful results and is commonly used to analyse sensitivity experiments.

7.2.1 JFM 1998

Figure 7.3 shows the rainfall percentage difference with Clim for Ctr98 and the six idealised experiments for the JFM 1998 season. Analysis of these experiments suggests five regions over which the rainfall response is relatively robust, namely the equatorial West Indian Ocean; the equatorial East Atlantic Ocean; South Africa and Botswana; Zimbabwe and Zambia; and the Democratic Republic of Congo (DRC). In some cases, multiple countries are discussed in the same section because of their proximity and the observation that they experience similar rainfall anomalies in each of the experiments.

The Equatorial West Indian Ocean

For clarification, the region referred to as the equatorial West Indian Ocean refers to the section of the Indian Ocean bordering the coast of East Africa up to approximately 60^oE and between approximately 5^oN and 7^oS. It stands out as a region of very high rainfall in the top panel of **Figure 7.3**. In

fact, the equatorial West Indian Ocean experienced up to three times more rainfall in Ctr98 than it did in the Clim experiment. This strong positive signal is evident in all idealised experiments in which the JFM 1998 Indian Ocean SSTs are present, namely Ctr98, NoAtl98, OnlyInd98 and NoPac98 (**Figure 7.3**). This region of high rainfall occurred over the warm pole of the TIOD in the western Indian Ocean where SSTs were as much as 2^oC warmer than average (**Figure 7.4**). The presence of an anomalously warm pool of water led to enhanced evaporation over this region, which is evident in the latent heat flux in all the experiments with Indian Ocean SST forcing (**Figure 7.5**). Relative uplift over the region (**Figure 7.6**), combined with increased moisture flux from the North Indian Ocean (**Figure 7.7**) and moisture flux convergence, is favourable for enhanced rainfall. High levels of rainfall over the equatorial west Indian Ocean are a coherent feature of strong TIOD events such as the one that occurred during 1997-1998 (Saji et al., 1999).

The Equatorial East Atlantic Ocean

The region of anomalously high rainfall over the Atlantic Ocean east of 5^oW and lying between approximately 7^oS and 3^oN is referred to as the equatorial east Atlantic Ocean (**Figure 7.3**). SSTs over this region were up to 1^oC higher than average during JFM 1998. The anomalously high rainfall over the equatorial east Atlantic Ocean in Ctr98 was also evident in those experiments that included the Atlantic Ocean SSTs, namely OnlyAtl98, NoInd98 and NoPac98 (**Figure 7.3**). The positive SSTAs are associated with posi-

tive latent heat flux anomalies over the region in these experiments which indicate enhanced evaporation (**Figure 7.5**) which, coupled with the anomalously strong uplift (**Figure 7.6**), created favourable rainfall conditions. The region of high rainfall over the equatorial east Atlantic Ocean appears to be a response to the local SST warming that occurred during JFM 1998. These results are consistent with enhanced rainfall in this region in the HadAM3 model when forced with warm SSTAs in the tropical South East Atlantic Ocean (Hansingo and Reason, 2009).

South Africa and Botswana

This region received below average rainfall during the JFM 1998 season (**Figure 7.3**, top panel). A similar pattern of rainfall anomalies is evident in each of the experiments that included the Indian Ocean SSTs, namely NoAtl98, OnlyInd98 and NoPac98, while the remaining three experiments all display strong positive anomalies over these two countries. The relative impact of the Pacific and Atlantic Ocean SSTs appear to be approximately equal given that the positive rainfall response to each individually, which can be seen in OnlyAtl98 and OnlyPac98, is roughly the same. The Pacific and Atlantic Ocean SSTs also show similar negative rainfall anomalies over South Africa and Botswana when paired with the Indian Ocean SSTs in NoPac98 and NoAtl98. These results suggest that while the Indian Ocean SSTs resulted in reduced rainfall over South Africa and Botswana, the Atlantic and Pacific Ocean SSTs acted in opposition to increase rainfall. Since

the combined impact of all three Ocean basin SSTs on rainfall over this region resulted in negative rainfall anomalies, it appears that the Indian Ocean SSTs had the greatest influence on rainfall over this region during JFM 1998 while the Pacific and Atlantic Ocean SSTs worked to oppose this impact.

The SIOD that occurred during 1997-1998 changed phase from positive to negative (Behera and Yagamata, 2001) and SSTAs south of Madagascar and southeast of South Africa are predominantly negative during the JFM 1998 season (**Figure 7.4**). Negative SSTAs in this region are usually associated with below average rainfall over South Africa and surrounding regions (Reason and Mulenga, 1999; Reason, 2001). The mechanism presented in Reason and Mulenga (1999) by which rainfall responds to this SSTA involves changes in the convergence over southeastern Africa of moist air streams originating from either the tropical South Indian Ocean or the tropical South Atlantic Ocean. Reason (1998) found that cold SSTs south of South Africa, such as those present in JFM 1998 (**Figure 7.4**), are associated with decreased rainfall over Botswana during austral summer. The decrease in rainfall was also found to be related to the moisture flux from the South Indian and Atlantic Oceans (Reason, 1998).

South Africa and Botswana experienced below average latent heat flux over both the land and over the ocean southeast of South Africa during JFM 1998 in Ctr98, NoAtl98, OnlyInd98 and NoPac98 (**Figure 7.5**) which, com-

bined with relative subsidence (**Figure 7.6**), and relative divergence over these countries (**Figure 7.7**), created conditions that were unfavourable for rainfall. These four experiments also have southeasterly moisture flux anomalies from the South Indian Ocean that pass over a region of relative moisture flux divergence over southern Mozambique (**Figure 7.7**). The moisture usually transported over South Africa and Botswana from the South Indian Ocean is transferred further northward than usual which can also be seen in the 850 hPa wind anomalies (**Figure 7.8**).

This analysis suggests that South Africa and Botswana were influenced most strongly by Indian Ocean SSTs during JFM 1998. The response of this region to the SIOD is in keeping with Reason and Mulenga (1999) and Reason (1998) who used a different AGCM to the one used in this study.

Zimbabwe and Zambia

Zimbabwe and Zambia both experienced above average rainfall in Ctr98, with the exception of a small section of northwest Zambia (**Figure 7.3**). This rainfall anomaly is also present when only the Atlantic Ocean SSTs are present in OnlyAtl98, but not in NoAtl98 pointing to the potential significance of this basin for Zimbabwean and Zambian rainfall during JFM 1998. There are also predominantly positive rainfall anomalies over these countries in OnlyPac98 except over the eastern half of Zimbabwe, while OnlyInd98 has strong negative rainfall anomalies over the region. This information

alone could lead to the conclusion that both the Atlantic and Pacific Ocean SSTs encourage positive rainfall anomalies over this region, while the Indian Ocean SSTs work to produce negative rainfall anomalies. Since the combined influence of the Pacific and Indian Ocean SSTs result in below average rainfall in NoAtl98, this implies that the Atlantic Ocean SSTs are necessary to produce above average rainfall over the region. Both experiments in which the Atlantic Ocean is coupled with one of the other ocean basins result in approximately the same pattern of rainfall anomalies over Zimbabwe and Zambia as in the Ctr98 anomalies (top panel). From these experiments, it appears that the positive rainfall anomalies over Zimbabwe and Zambia during JFM 1998 were primarily influenced by Atlantic Ocean SSTs, while the Indian Ocean SSTs worked to moderate rainfall over this region and the Pacific Ocean SSTs did not play as substantial a role in rainfall over these countries as for some of the other southern African countries.

Nicholson and Entekhabi (1987) established a link between the occurrence of a Benguela Niño event and an increase in coastal rainfall over the African continent lying approximately between the equator and 25^{o}S . Further studies, including those by Florenchie et al. (2003), Rouault et al. (2003a) and Hansingo and Reason (2009) have confirmed that there is a significant increase in rainfall over adjacent western Southern Africa, as well as further inland as far as Zambia, during Benguela Niño events.

The circulation anomalies in OnlyAtl98 caused by the presence of the JFM 1998 Atlantic Ocean SST forcing only are similar but generally stronger than those seen in OnlyPac98, much like the rainfall anomalies (**Figures 7.3, 7.5-7.8**). There are positive latent heat flux anomalies (**Figure 7.5**) as well as increased uplift (**Figure 7.6**) over these two countries in both experiments, although their magnitude is higher in OnlyAtl98 than it is in OnlyPac98. There is also increased relative convergence over Zambia in both experiments (**Figure 7.7**). Both experiments receive weakly increased moisture flux from the South Atlantic Ocean into the region, as well as from the tropical Indian Ocean (**Figure 7.7**). There is evidence of a stronger Angola low in the experiment OnlyAtl98 which displays a cyclonic moisture flux anomaly centred over the area where the countries Angola, Namibia, Botswana and Zambia have a common boundary (**Figure 7.7**). The Angola low is also strengthened in OnlyPac98 where a similar anomaly indicates increased flow eastward from the South Atlantic Ocean and southward over Zimbabwe although the return flow to the Atlantic is not strengthened in this experiment (**Figure 7.7**). In the case of OnlyInd98, there is an anticyclone over the approximate location of the Angola low, indicating that the Indian Ocean SST forcing alone produced conditions which were unfavourable for rainfall over this region.

The increased moisture from the Atlantic Ocean together with a stronger Angola low associated with the Atlantic Ocean SSTs during JFM 1998 seem

to have had the greatest impact on rainfall over Zimbabwe and Zambia.

The Democratic Republic of Congo

The DRC generally experiences above average rainfall in Ctr98, although there are negative rainfall anomalies in the southeast and northwest of the country (**Figure 7.3**). An overestimated, but otherwise similar, pattern of rainfall can be seen in OnlyPac98 which indicates that the Pacific Ocean SSTs may have contributed to the positive rainfall anomalies over the DRC during JFM 1998. OnlyAtl98 also displays some positive anomalies over a section of the DRC and may have added to an increase in rainfall, while the Indian Ocean SSTs in OnlyInd98 resulted in negative rainfall anomalies over the country. Indeed, the combination of the Pacific and Atlantic SSTs results in above average rainfall over the DRC as can be seen in NoInd98, while the combined impact of the Indian and Atlantic Ocean SSTs in NoPac98 results in mainly below average rainfall over the region. This implies that the positive rainfall signal from the Atlantic Ocean SSTs is small, but present. The combination of the Pacific and Indian Ocean SSTs in NoAtl98 results in anomalies that are very similar to those seen in Ctr98. Thus, the Pacific Ocean SSTs appear to have the greatest impact on rainfall over the DRC during JFM 1998, while the Indian Ocean SSTs acted to moderate this influence and the Atlantic Ocean SSTs had comparatively less impact, although they did seem to act in favour of enhanced rainfall over the region.

The DRC is the second largest country in Africa and while a large portion of the country lies in the vast central basin which is a low-lying plateau, there are also mountains in the east and dense tropical rain forest in the central river basin and the eastern highlands. Central equatorial Africa is a region of deep atmospheric convection and the tropospheric heating associated with this convection is a primary driver of the tropical circulation over Africa and the neighbouring oceans (Todd and Washington, 2004). This region has not been extensively studied due in part to the paucity of high quality long-term data sets, but some attempt has been made to link rainfall over the region with global SSTs. Studies by Hirst and Hastenrath (1983) and Nicholson and Entekhabi (1987) suggested a relationship between rainfall over central Africa and tropical southern Atlantic SSTs. Washington (2000) ran model simulations using historical SSTs and found that central equatorial African rainfall is not sensitive to global SST changes. Camberlin et al. (2001) confirmed these results when they found that, although ENSO-related and Atlantic SSTs play a key role in rainfall over much of Africa, they do not exhibit significant teleconnections with the Congo Basin. However, Todd and Washington (2004) did find a negative correlation between the FMA NAO and central African rainfall.

The Pacific and Atlantic experiments OnlyPac98 and OnlyAtl98 have similar circulation with regard to the DRC, but the anomalies are generally higher in OnlyPac98 than they are in OnlyAtl98. The same is true of

NoInd98 in which both ocean basin SSTs are present, and in this case the anomalies are larger still. The increased rainfall over the DRC in these experiments, as well as in Ctr98, appears to be a consequence of increased latent heat flux (**Figure 7.5**), enhanced relative uplift (**Figure 7.6**), and relative convergence along the eastern part of the country (**Figure 7.7**), which together create conditions which are favourable for increased rainfall. There is also a strong influx of moisture from the tropical Indian Ocean (**Figure 7.7**) in each case.

7.2.2 JFM 2010

Figure 7.9 shows the rainfall percentage difference with Clim for Ctr10 and the six idealised experiments for the JFM 2010 season. Analysis of these experiments suggests three regions over which the rainfall response is relatively robust, namely Zimbabwe and Mozambique; Zambia, Namibia, South Africa and Botswana; and the DRC.

Zimbabwe and Mozambique

Zimbabwe and Mozambique both experienced above average rainfall during Ctr10 (**Figure 7.9**). The OnlyInd10 experiment similarly shows positive rainfall anomalies over these countries, as does OnlyPac10 although not over the entire area. Of the single ocean only experiments, OnlyAtl10 has entirely negative rainfall anomalies over these two countries which indicates that it

may act to reduce rainfall here. The combined impact of the Indian and Atlantic Ocean SSTs during JFM 2010 produces predominantly positive rainfall anomalies over this region as can be seen in NoPac10, which indicates that the Indian Ocean SSTs exert more influence over this region than the Atlantic Ocean SSTs. The combined impact of the Atlantic and Pacific Ocean SSTs in NoInd10 result in below average rainfall over Zimbabwe and Mozambique, which implies that the Atlantic Ocean SSTs may have a greater influence on reducing rainfall over this region than the Pacific Ocean SSTs. There are positive rainfall anomalies over most of Mozambique and negative rainfall anomalies over northern Mozambique and Zimbabwe in NoAtl10 which is surprising given that the single ocean contribution of the Indian and Pacific SSTs led to increased rainfall over the region. It appears that the Indian Ocean SSTs had the greatest influence in increasing rainfall over Zimbabwe and Mozambique during JFM 2010, while the Atlantic Ocean SSTs worked to reduce rainfall here and the region was less sensitive to Pacific Ocean SST forcing.

When only Indian Ocean SSTs are present in experiment OnlyInd10, there is a substantial increase in latent heat flux in the western Indian Ocean and Mozambique Channel as well as over Zimbabwe and Mozambique (**Figure 7.10**). There is also strong relative uplift (**Figure 7.11**) and low level convergence (**Figure 7.12**) over this region and in the Mozambique Channel which create conditions that are favourable for rainfall.

OnlyAtl10 displays negative latent heat flux anomalies over these countries (**Figure 7.10**), relative subsidence over Zimbabwe and Mozambique (**Figure 7.11**) and relative divergence over these countries (**Figure 7.12**) which result in conditions that are unfavourable for rainfall. The moisture flux anomalies shows easterly anomalies over the Indian Ocean north of Madagascar and east of Tanzania implying a weaker monsoonal flow. There are westerly anomalies over the central and southern Mozambique Channel also in the opposite direction to the mean flow. Hence, there is reduced moisture influx from the South Indian Ocean towards Mozambique and Zimbabwe in this experiment, which is consistent with the reduced rainfall.

The experiment OnlyPac10 has positive latent heat flux anomalies over these two countries (**Figure 7.10**), as well as relative uplift (**Figure 7.11**) and convergence over most of Zimbabwe and Mozambique (**Figure 7.12**). In OnlyPac10, there is a large anticyclonic anomaly over Madagascar and the Mozambique Channel whereas in OnlyInd10, there is a cyclonic anomaly here. OnlyPac10 also shows an increase in moisture flux for the tropical South Atlantic into the Angola low (**Figure 7.12**).

Zambia, Namibia, South Africa and Botswana

Zambia, Botswana, and South Africa, as well as western and southern Namibia, are discussed together since they all display mainly positive rain-

fall anomalies in Ctr10 and OnlyPac10, and negative rainfall anomalies in OnlyInd10 while showing a relatively small and mixed sign responses in OnlyAtl10 (**Figure 7.9**). When the JFM 2010 Pacific Ocean SSTs are not present in NoPac10, the region displays mainly negative rainfall anomalies, which implies that the Pacific Ocean SSTs during JFM 2010 contributed to wet conditions. The rainfall anomalies over this region in NoPac10 and OnlyInd10 are similar, which suggests that Atlantic Ocean SSTs did not contribute significantly to the increased rainfall in these countries. Indeed, the OnlyAtl10 experiment shows weak rainfall anomalies over these countries which are mainly negative. The Pacific Ocean SSTs appear to have had more impact over the region than the opposing Indian Ocean SSTs. This can be seen when those two are present without the input of the Atlantic Ocean SSTs in NoAtl10 and the rainfall anomalies are mainly positive over these countries except for Zambia.

Both the experiments Ctr10 and OnlyPac10 display increased latent heat flux over these countries (**Figure 7.10**), increased relative uplift (**Figure 7.11**), and mainly relative moisture flux convergence over these countries (**Figure 7.12**). They also have increased moisture flux from the South Atlantic Ocean which, coupled with an anomalously strong Angola low, resulted in increased rainfall over Zambia, Botswana, South Africa and western Namibia (**Figure 7.12**). Increased moisture flux from the tropical western Indian Ocean flowed over Tanzania, Zambia and eastern Angola and hence

fed into the Angola low. This is consistent with the moisture sources important for South African rainfall outlined in Reason et al. (2006b).

On the other hand, the OnlyInd10 experiment displayed negative latent heat flux anomalies over these countries (**Figure 7.10**), strong relative subsidence (**Figure 7.11**), and mainly relative divergence in these countries (**Figure 7.12**). The moisture flux increase from the South Indian Ocean, coupled with a cyclonic anomaly over the Mozambique Channel and Madagascar as well as relative convergence over northern Mozambique and Madagascar, led to increased rainfall there. This resulted in less moisture input from the South Indian Ocean into southern Africa and there was also a decrease in moisture flux input from the South Atlantic Ocean (**Figure 7.12**).

The Democratic Republic of Congo

Rainfall anomalies over the DRC are positive in Ctr10 except for the southeastern region of the country where there are negative rainfall anomalies (**Figure 7.9**). The experiments in which the JFM 2010 Atlantic Ocean SSTs are present, namely OnlyAtl10, NoInd10, and NoPac10, also display predominantly positive rainfall anomalies over the DRC, while those without, namely OnlyInd10, OnlyPac10 and NoAtl10, display predominantly negative rainfall anomalies over the country. These results suggest that the Atlantic Ocean SSTs had the greatest impact on rainfall over this region during the JFM 2010 season.

Some insight into these results may come from the work of Vigaud et al. (2007, 2009). Vigaud et al. (2007) discussed two strong modes of variability affecting the onshore flow of moisture along the west coast of southern Africa. The first of these modes is linked to the South Atlantic anticyclone and the other is linked with the zonal mode of the westerly flux of moisture from the Atlantic. In a subsequent study, Vigaud et al. (2009) further explored the connection between southern African climate and the South Atlantic Ocean during the austral summer. They found that increased rainfall over the Congo basin is associated with increased moisture flux input from the tropical Atlantic Ocean and increased convection. This excess water vapour is then channelled from the Congo basin to the east and southeast at the surface, while the African Easterly Jet may transport moist air southward at mid-tropospheric levels.

The experiments Ctr10, OnlyAtl10, NoInd10 and NoPac10 display many of the same circulation features as in Vigaud et al. (2007, 2009). Each experiment has above average latent heat flux over the DRC, except OnlyAtl10 which provides re-cycled moisture to the region (**Figure 7.10**). They also all display relatively strong uplift over the DRC (**Figure 7.11**) and are predominantly convergent (**Figure 7.12**) which produces conditions that are favourable for rainfall. Ctr10 and NoPac10 both display an increase in moisture flux from the tropical South Atlantic Ocean northeast into the DRC

(**Figure 7.12**) as well as increased moisture flux from Africa north of the DRC. The experiments OnlyAtl10 and NoInd10, on the other hand, both show a decrease in moisture flux from the South Atlantic Ocean and strong easterly anomalies from the tropical Indian Ocean.

7.3 Summary

The 1997-1998 and 2009-2010 summer rainfall seasons over southern Africa are often cited as examples of an unexpected rainfall response to ENSO since, in both cases, drought conditions were predicted but near or above average rainfall was observed over many regions (Kane, 1999; Richard et al., 2001; Landman and Beraki, 2010). Studies indicate that some models may be over-confident in simulating the link between ENSO and southern African rainfall and that problem may have contributed to the discrepancy between the forecasts for these two years and observations (Landman and Beraki, 2010; Yuan et al., 2014). The anomalously strong Angola low during JFM 1998 together with a positive TIOD and Benguela Niño have been suggested as possible reasons for the increased rainfall over southern Africa during the summer season of 1997-1998 (Lyon and Mason, 2007; Reason and Jagadheesha, 2005).

The strongest El Niño on record occurred during 1997-1998 as well as a strong positive TIOD that persisted until March 1998. A positive SIOD switched phase to become a negative SIOD in early 1998 and there was a

Benguela Niño during JFM 1998. El Niño events typically lead to drought conditions over southern Africa (Lindesay, 1988; Reason et al., 2000) and negative SIOD events have been associated with dry conditions over parts of southern Africa (Behera and Yagamata, 2001; Reason, 2001, 2002) while a Benguela Niño events usually result in above average rainfall over parts of southern Africa (Rouault et al., 2003a).

The 2009-2010 CP El Niño was the strongest CP El Niño on record to date and the JFM 2010 season also had a strong negative phase NAO and a weak positive TIOD. CP El Niño events have been associated with below average rainfall over southern Africa although they do not produce dry conditions to the same extent as EP El Niño events (Ratnam et al., 2012, 2014) while positive TIOD events usually result in above average rainfall over parts of southern Africa. McHugh and Rogers (2001) found that heavier, convective, DJF rainfall occurs over Tanzania, northern Mozambique, Zambia and part of the western DRC during the negative NAO phase when the North Atlantic westerlies are unusually weak. Todd and Washington (2004) also found a negative correlation between the NAO and central African rainfall, although their study focused on the FMA season.

In an effort to determine the relative impact of the SST forcing in each ocean basin on rainfall over southern Africa during these two anomalous years, idealised sensitivity experiments were constructed using CEU. The

control runs, Ctr98 and Ctr10, were forced with observed global SSTs. In each of the three No"Ocean" experiments, input SSTs in that major ocean basin were replaced by the climatology of that ocean, while in each of the Only"Ocean" experiments, input SSTs of the other two ocean basins were replaced by their climatology. For example, NoPac98 was forced with SSTs made up of observed Atlantic Ocean SSTs (from November 1997 to March 1998), observed Indian Ocean SSTs (from November 1997 to March 1998), and climatological Pacific Ocean SSTs, and OnlyPac98 was forced with SSTs made up of climatological Atlantic Ocean SSTs, climatological Indian Ocean SSTs, and observed Pacific Ocean SSTs (from November 1997 to March 1998). The Only"Ocean"98 experiments emphasise the impact of SSTAs in each ocean basin individually while the No"Ocean"98 experiments highlight the contribution of a combination of SSTAs from the remaining two ocean basins.

The analysis of JFM 1998 rainfall anomalies suggested five different regions of interest, two of which are located over the oceans, namely the equatorial West Indian Ocean and the equatorial East Atlantic Ocean. The main focus of this study is on land based rainfall anomalies, but these two regions are included because they show that the local rainfall response to SSTs is robust in CEU. The equatorial West Indian Ocean rainfall is attributed to the Indian Ocean SSTs, and the equatorial East Atlantic Ocean rainfall is likewise attributed to the Atlantic Ocean SSTs. The other regions

discussed during this season appear to all have different dominant ocean forcings. South Africa and Botswana were influenced most strongly by the Indian Ocean SSTs during JFM 1998 which led to mainly negative rainfall anomalies, while the Pacific and Atlantic Ocean SSTs favoured increased rainfall over the region. Zimbabwe and Zambia were primarily influenced by Atlantic Ocean SSTs where increased moisture from the South East Atlantic Ocean, coupled with a stronger Angola low, led to increased rainfall, while the Indian Ocean SSTs worked to moderate rainfall over these countries and the Pacific Ocean SSTs did not seem to play as substantial a role. Rainfall over the DRC appeared to be largely forced by Pacific Ocean SSTs during JFM 1998, while the Indian Ocean SSTs acted to moderate this influence and the Atlantic Ocean SSTs seemed to have comparatively less impact.

The Angola low was stronger than average in the experiments which used only Atlantic or Pacific Ocean SST forcing and the modelled rainfall response in these experiments shows enhanced rainfall over much of southern Africa south of Angola. The strengthened Angola low was implicated directly in the above average rainfall over Zimbabwe and Zambia during JFM 1998. These results are in line with previous studies that have identified that the unexpectedly strong Angola low during JFM 1998 may have contributed to the above average rainfall experienced over southern Africa during this season (Reason and Jagadheesha, 2005; Lyon and Mason, 2007).

Analysis of the JFM 2010 rainfall anomalies suggested three separate regions of interest, namely Zimbabwe and Mozambique; Zambia, Namibia, South Africa and Botswana; and the DRC. Again, each of these regions seem to have been most influenced by a different ocean. The positive rainfall anomalies over Zimbabwe and Mozambique appear to be a result of the Indian Ocean SSTs during JFM 2010 while the Atlantic Ocean SSTs worked to reduce rainfall here and the region was less sensitive to Pacific Ocean SST forcing. Zambia, Namibia, South Africa and Botswana seem to have been influenced most by the Pacific Ocean SSTs while the Indian Ocean SSTs moderated rainfall over the region and rainfall was not particularly sensitive to the Atlantic Ocean SSTs. Rainfall over the DRC seems to have been influenced most by Atlantic Ocean SSTs during the JFM 2010 season.

The JFM 2010 Angola low was anomalously strong much like the JFM 1998 Angola low. The experiment OnlyPac10, which used only Pacific Ocean SST forcing, displayed an anomalously strong Angola low. The enhanced rainfall over Zambia, Namibia, South Africa and Botswana appears to have been a result of increased moisture flux from the South Atlantic Ocean coupled with an anomalously strong Angola low. These results indicate that the strength of the Angola low may be of great importance when considering rainfall forecasting over southern Africa.

Although there is an assumption of linearity which needs to be viewed

with caution, the results of these experiments suggests, as do many other analyses, that the southern Africa rainfall response to SST forcing is very complex and that the results of seasonal forecasting efforts need to be very carefully examined before making statements concerning the next season's rainfall.

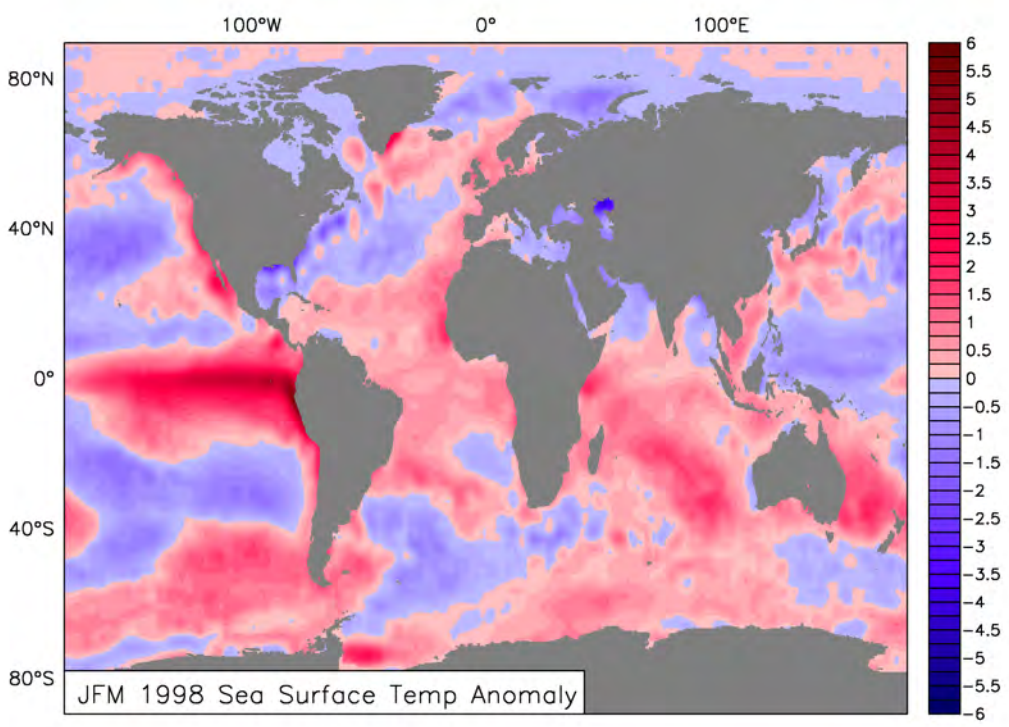

Figure 7.1: Sea surface temperature anomalies for JFM 1998 (in ^{o}C)

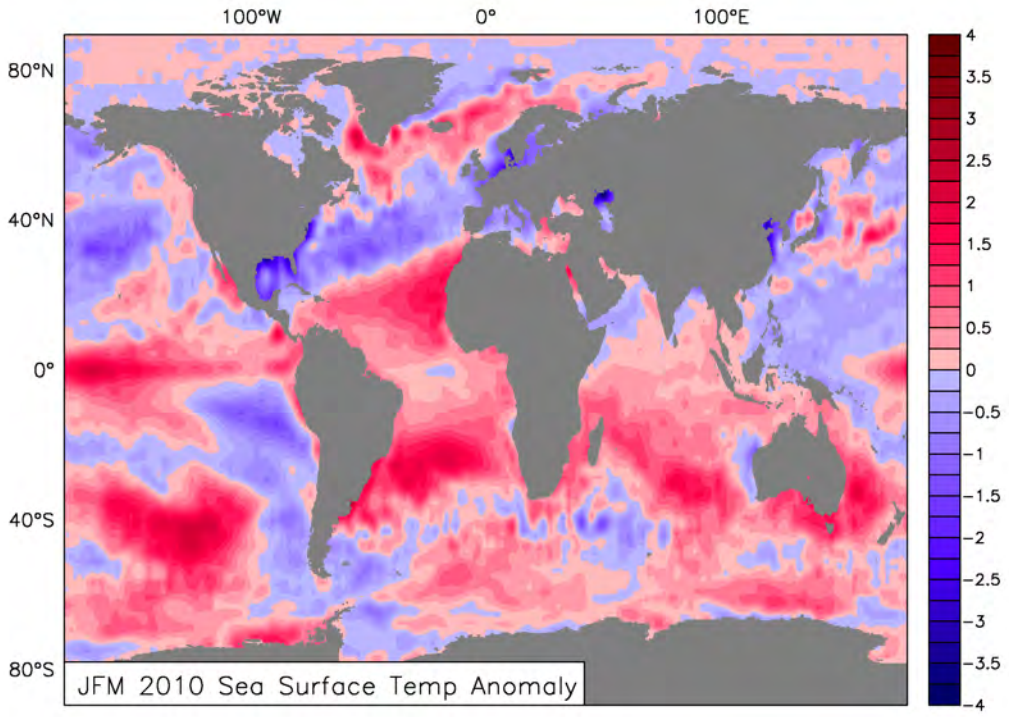

Figure 7.2: Sea surface temperature anomalies for JFM 2010 (in ^{o}C)

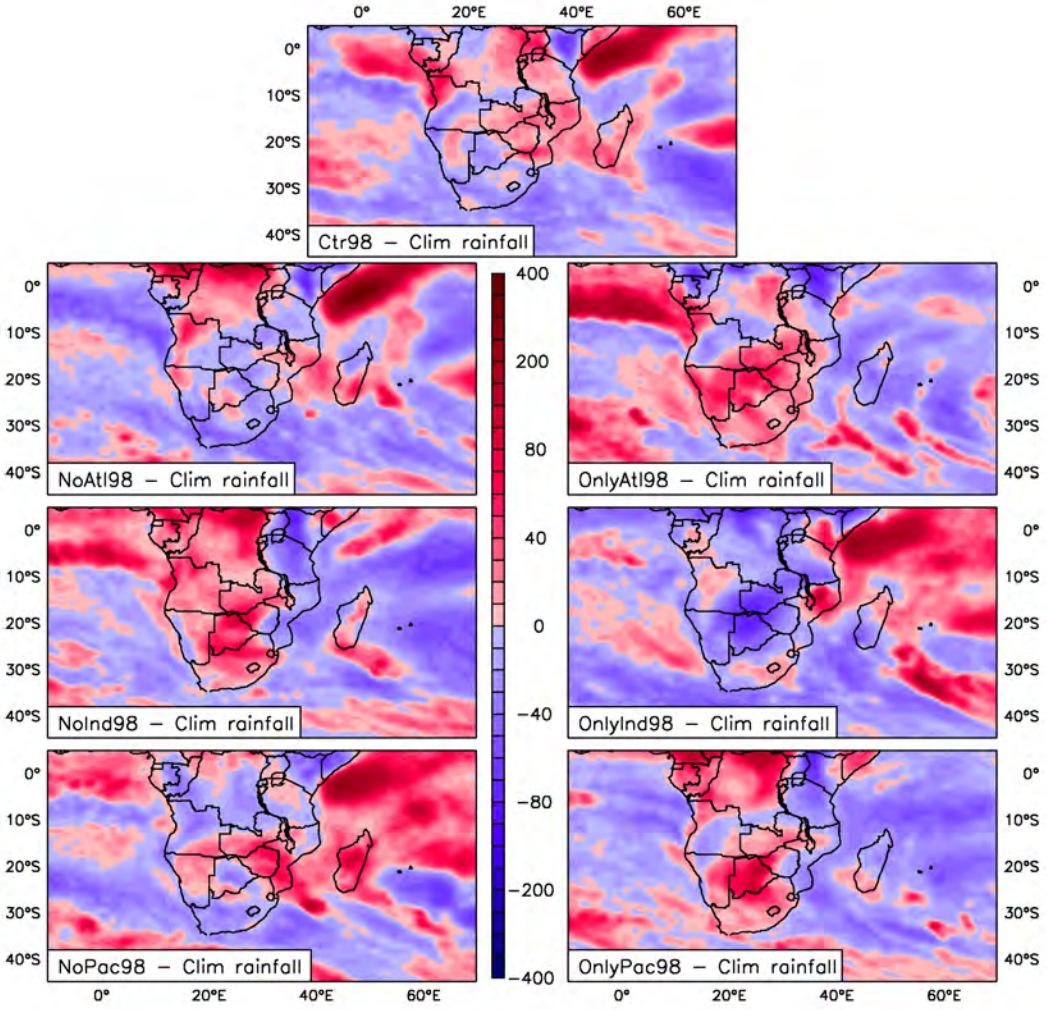

Figure 7.3: JFM 1998 percentage difference with Clim of rainfall for Ctr98, NoAtl98, NoInd98, NoPac98, OnlyAtl98, OnlyInd98 and OnlyPac98 (in mm·day^{-1})

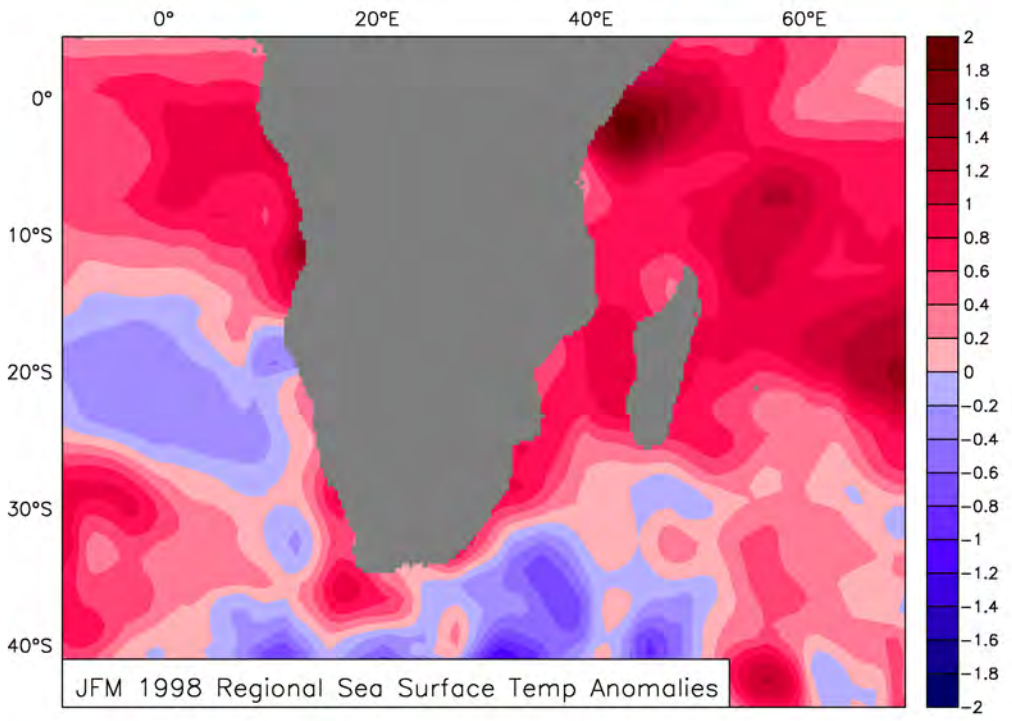

Figure 7.4: Regional sea surface temperature anomalies for JFM 1998 (in ^{o}C)

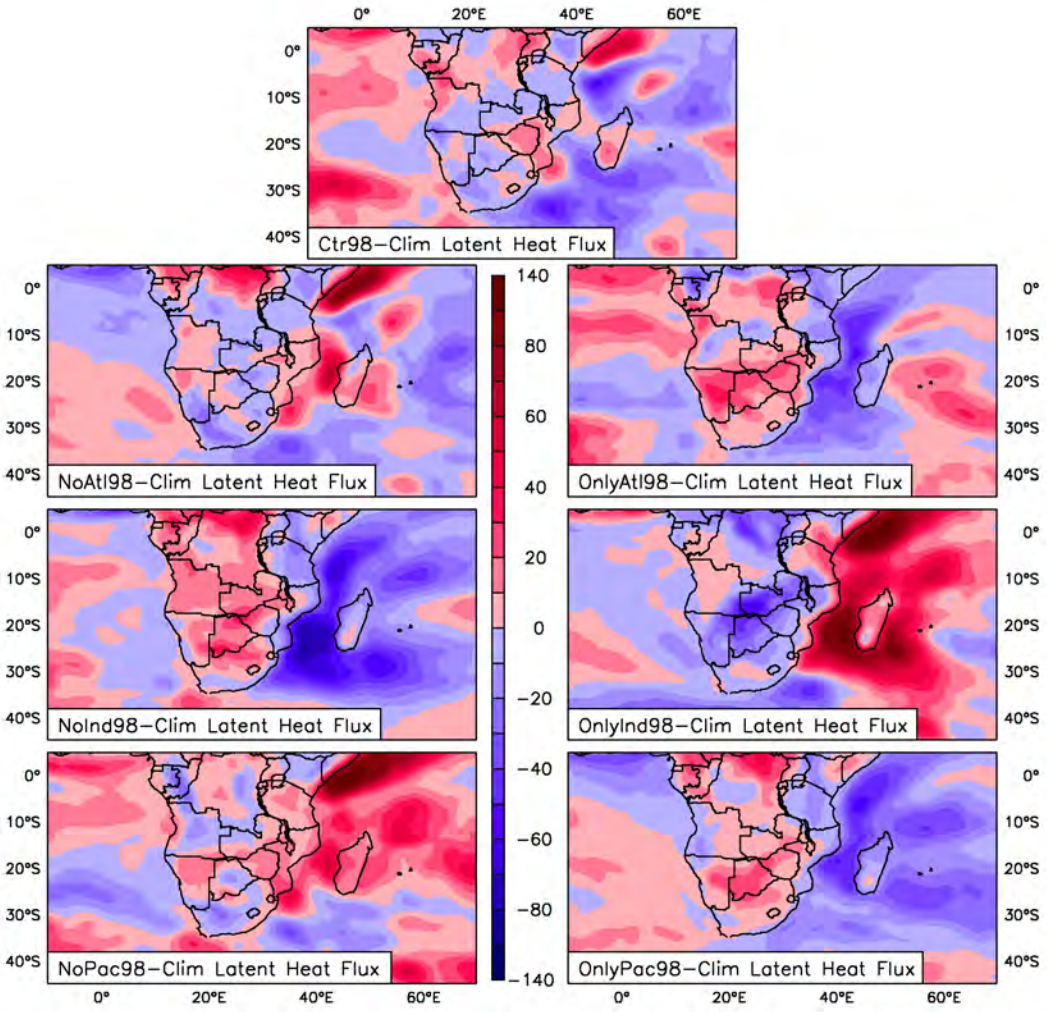

Figure 7.5: JFM 1998 latent heat flux for Ctr98, NoAtl98, NoInd98, NoPac98, OnlyAtl98, OnlyInd98 and OnlyPac98 (in kg·s^{-3})

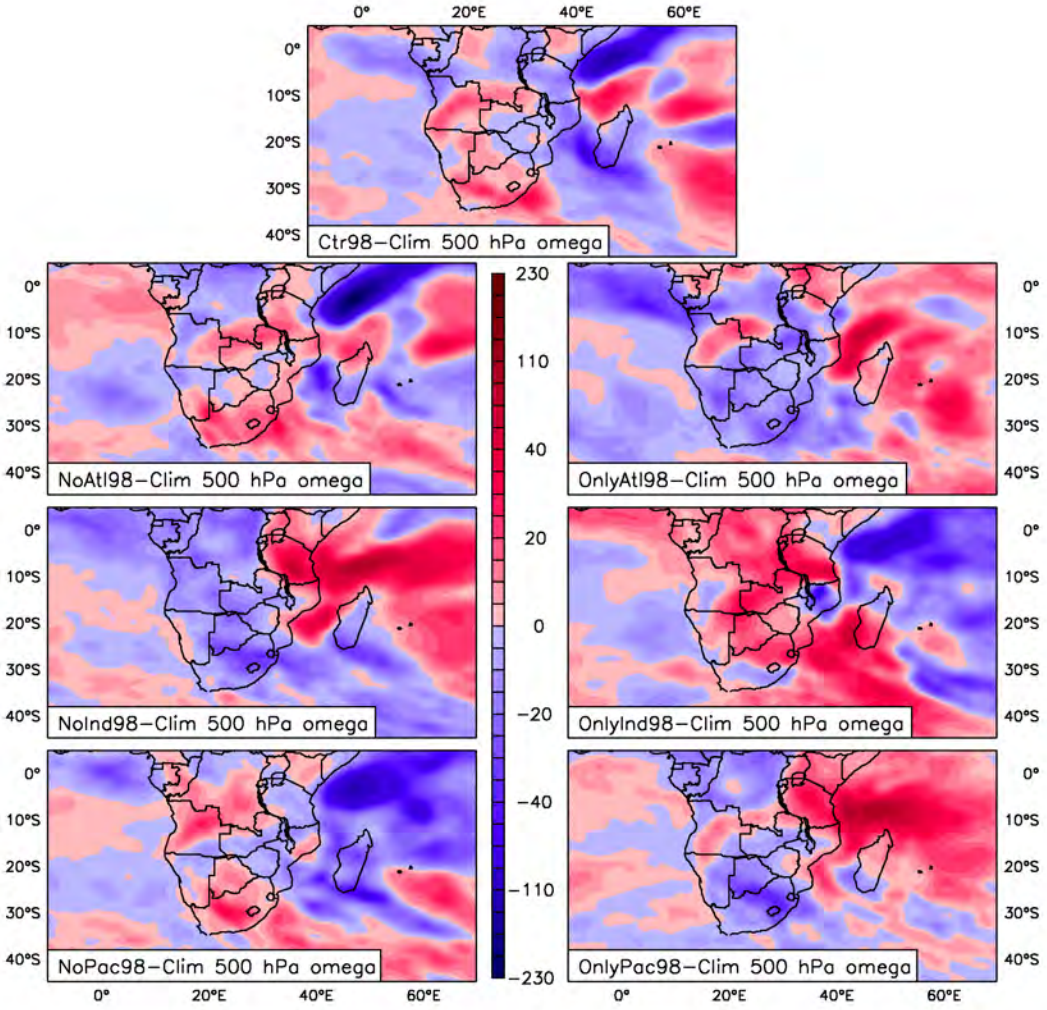

Figure 7.6: JFM 1998 500 hPa omega for Ctr98, NoAtl98, NoInd98, NoPac98, OnlyAtl98, OnlyInd98 and OnlyPac98 (in 10^2 kg·m^{-1}·s^{-3})

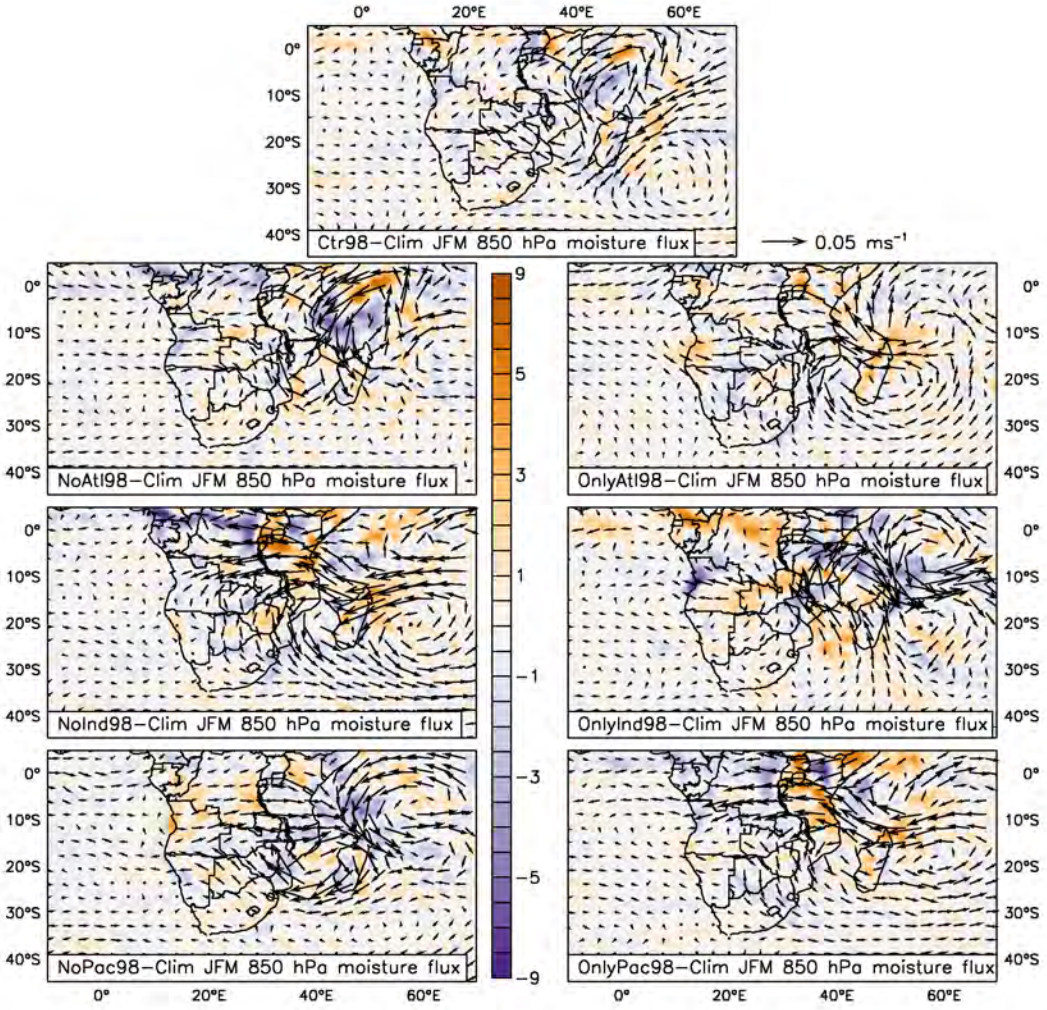

Figure 7.7: JFM 1998 moisture flux divergence anomaly (shaded 10^6 s^{-1}) and moisture flux ($m \cdot s^{-1}$) for Ctr98, NoAtl98, NoInd98, NoPac98, OnlyAtl98, OnlyInd98 and OnlyPac98

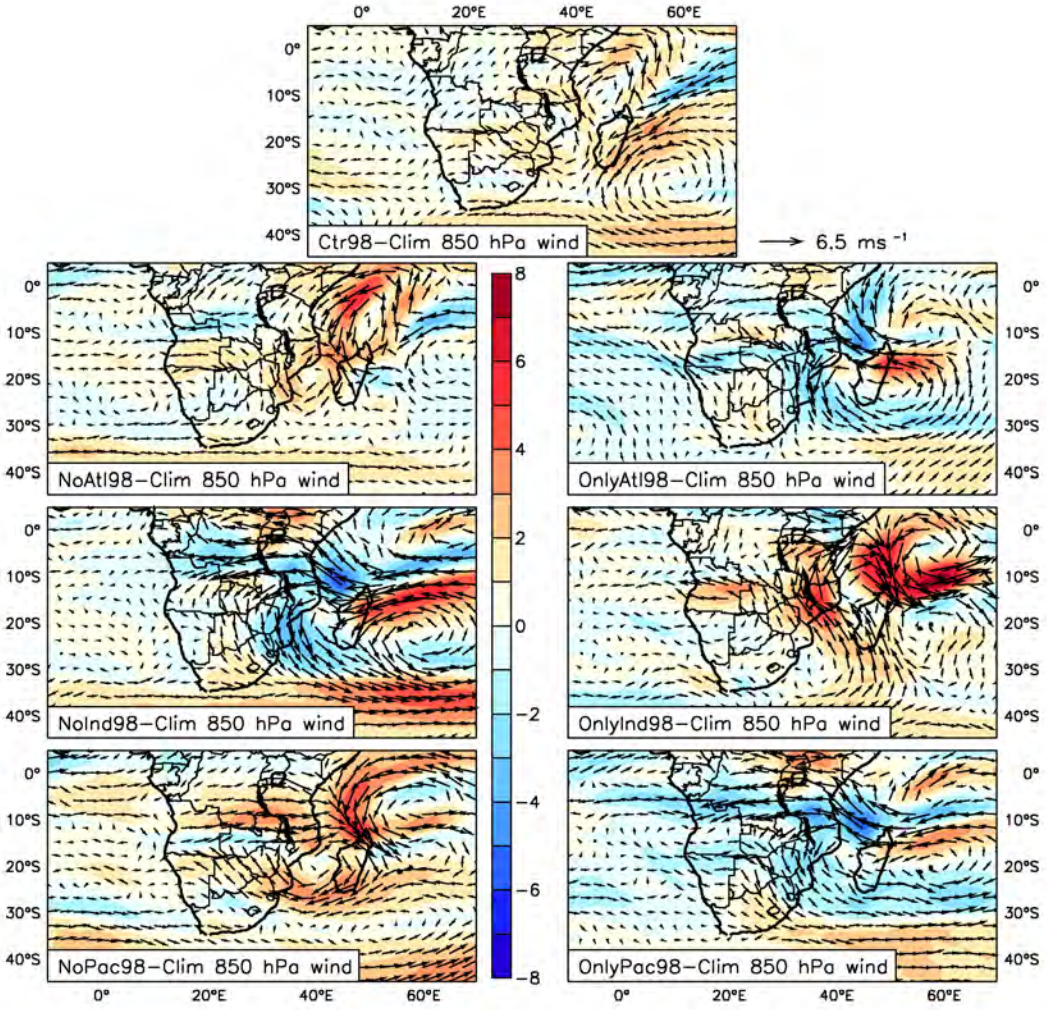

Figure 7.8: JFM 1998 850 wind anomaly (magnitude shaded) for Ctr98, NoAtl98, NoInd98, NoPac98, OnlyAtl98, OnlyInd98 and OnlyPac98 (in $\mathrm{m{\cdot}s^{-1}}$)

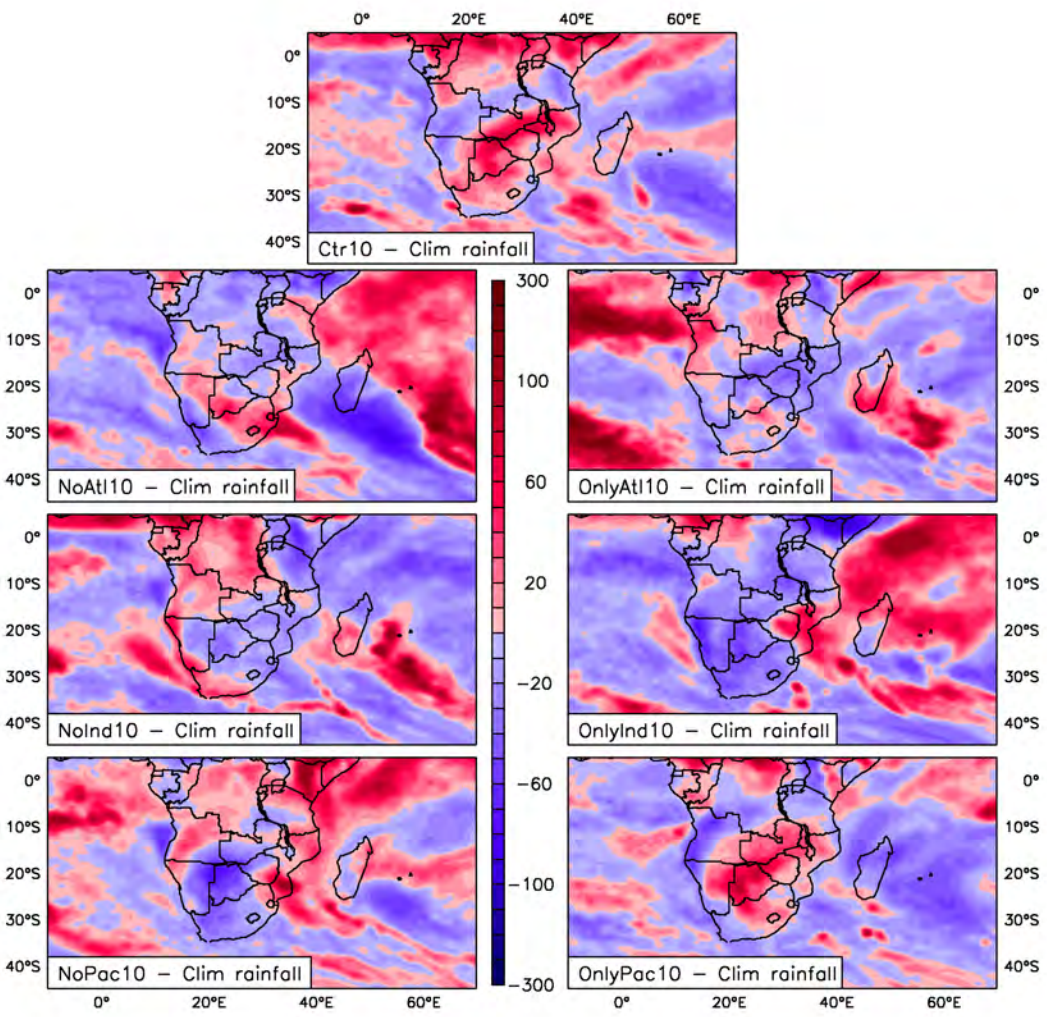

Figure 7.9: JFM 2010 percentage difference with Clim of rainfall for Ctr10, NoAtl10, NoInd10, NoPac10, OnlyAtl10, OnlyInd10 and OnlyPac10 (in mm·day^{-1})

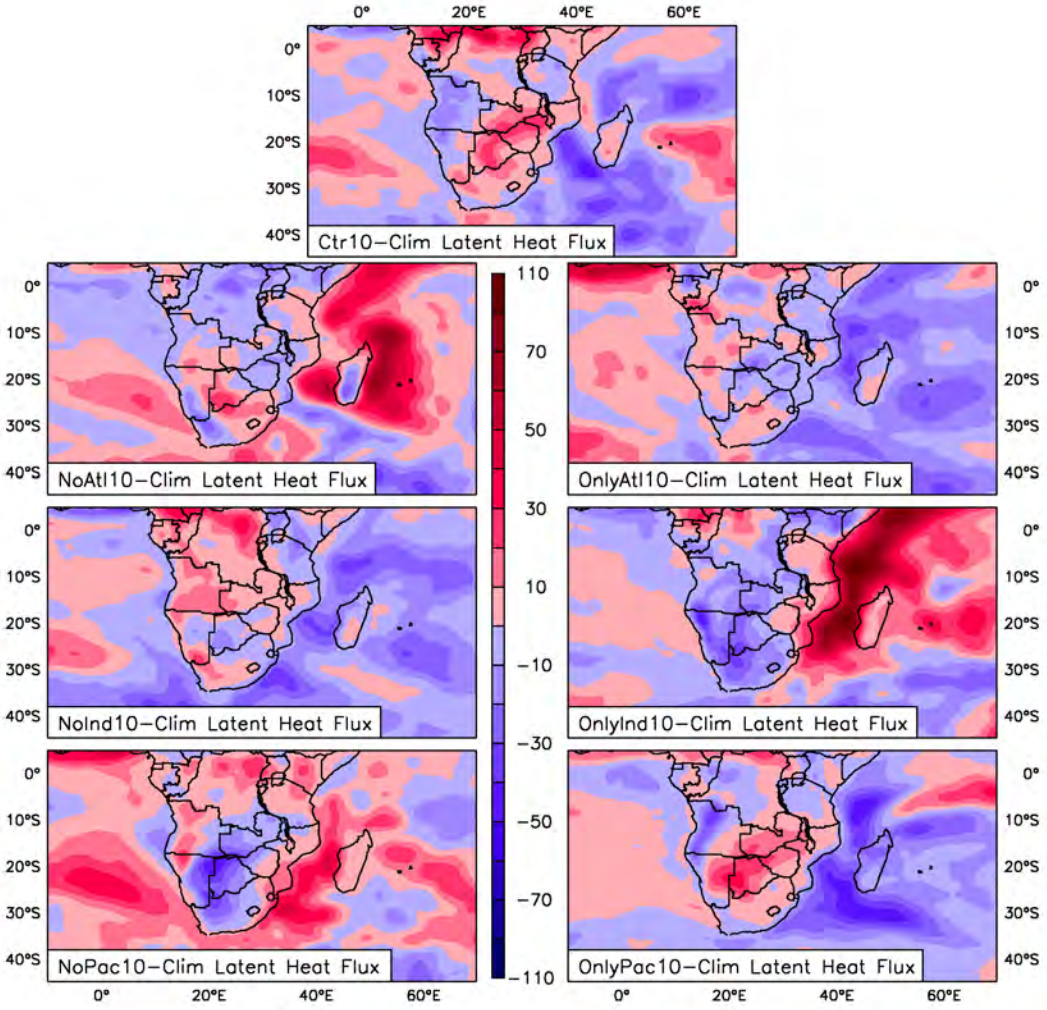

Figure 7.10: JFM 2010 latent heat flux for Ctr10, NoAtl10, NoInd10, NoPac10, OnlyAtl10, OnlyInd10 and OnlyPac10 (in $kg{\cdot}s^{-3}$)

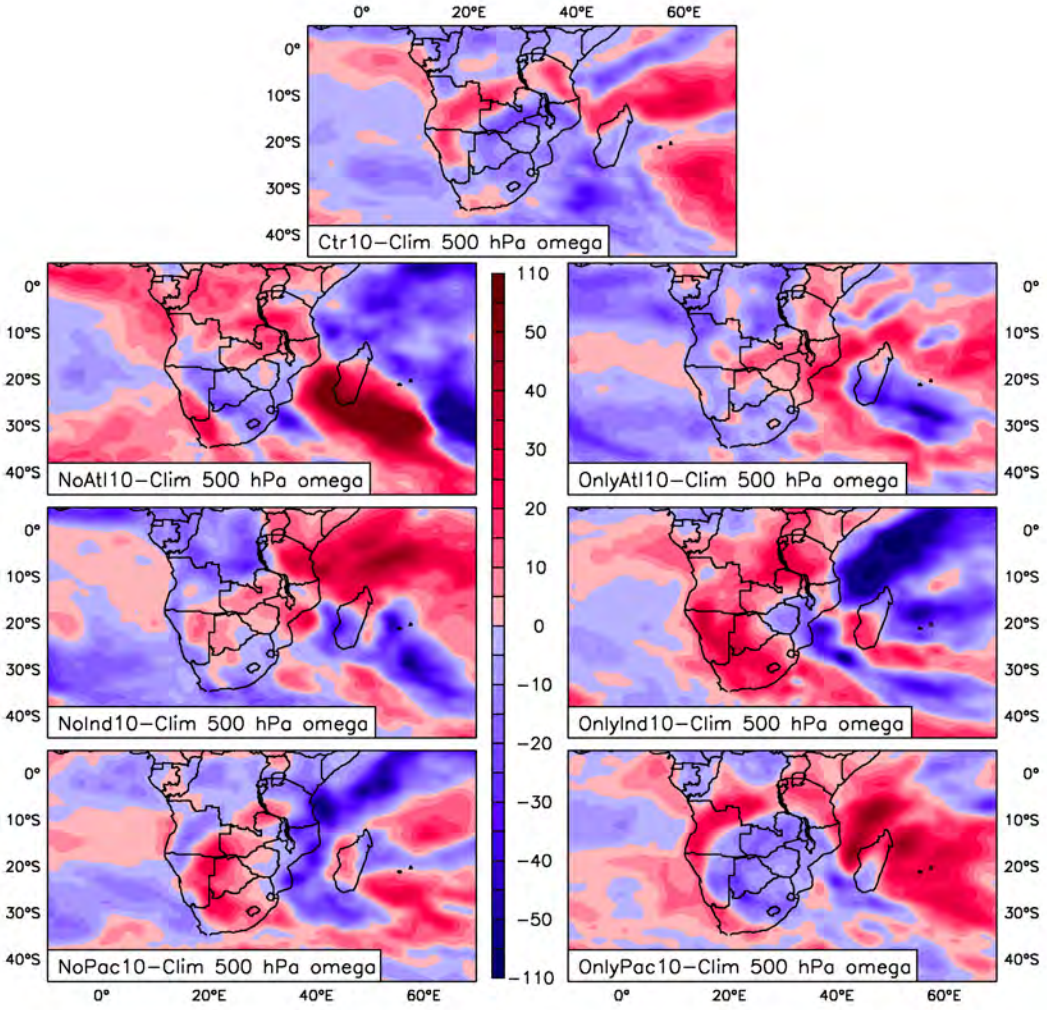

Figure 7.11: JFM 2010 500 hPa omega for Ctr10, NoAtl10, NoInd10, NoPac10, OnlyAtl10, OnlyInd10 and OnlyPac10 (in 10^2 kg·m^{-1}·s^{-3})

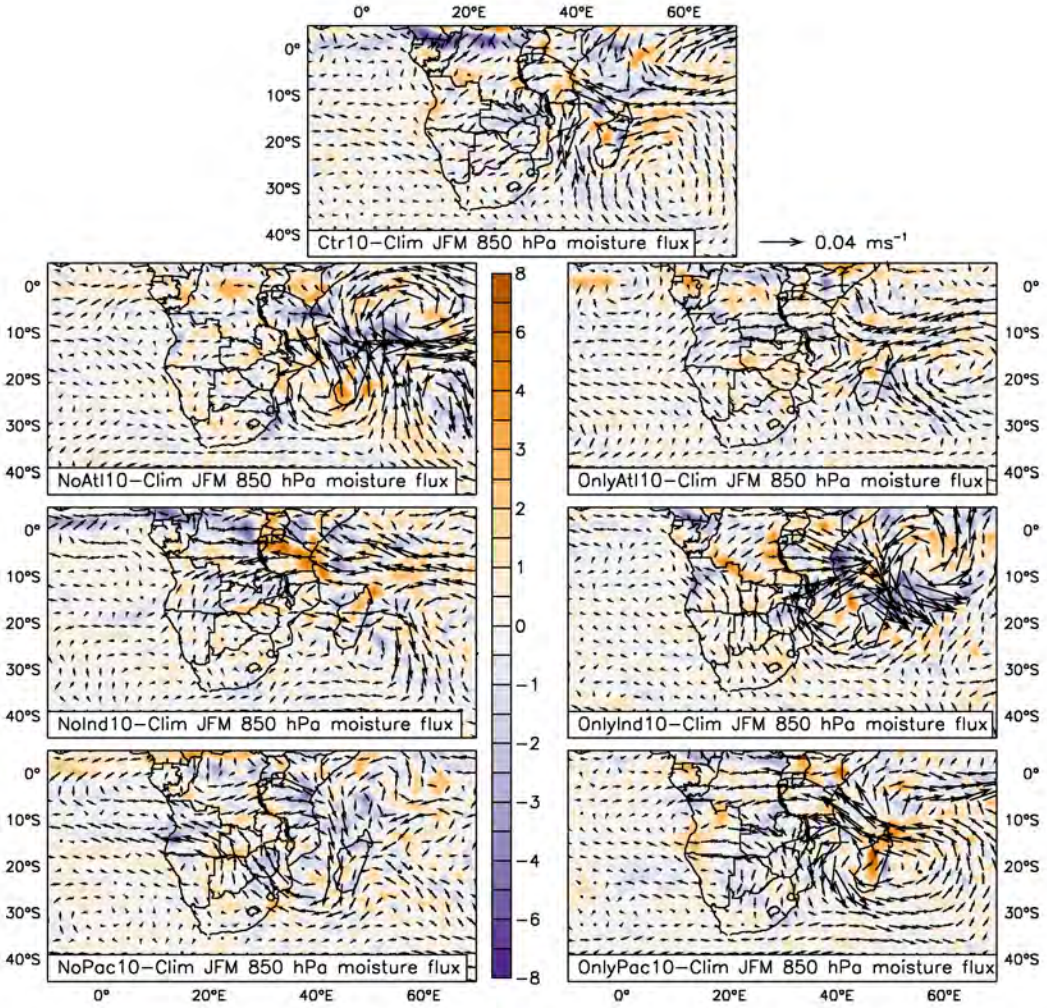

Figure 7.12: JFM 2010 moisture flux divergence anomaly (shaded 10^6 s^{-1}) and moisture flux ($m \cdot s^{-1}$) for Ctr10, NoAtl10, NoInd10, NoPac10, OnlyAtl10, OnlyInd10 and OnlyPac10

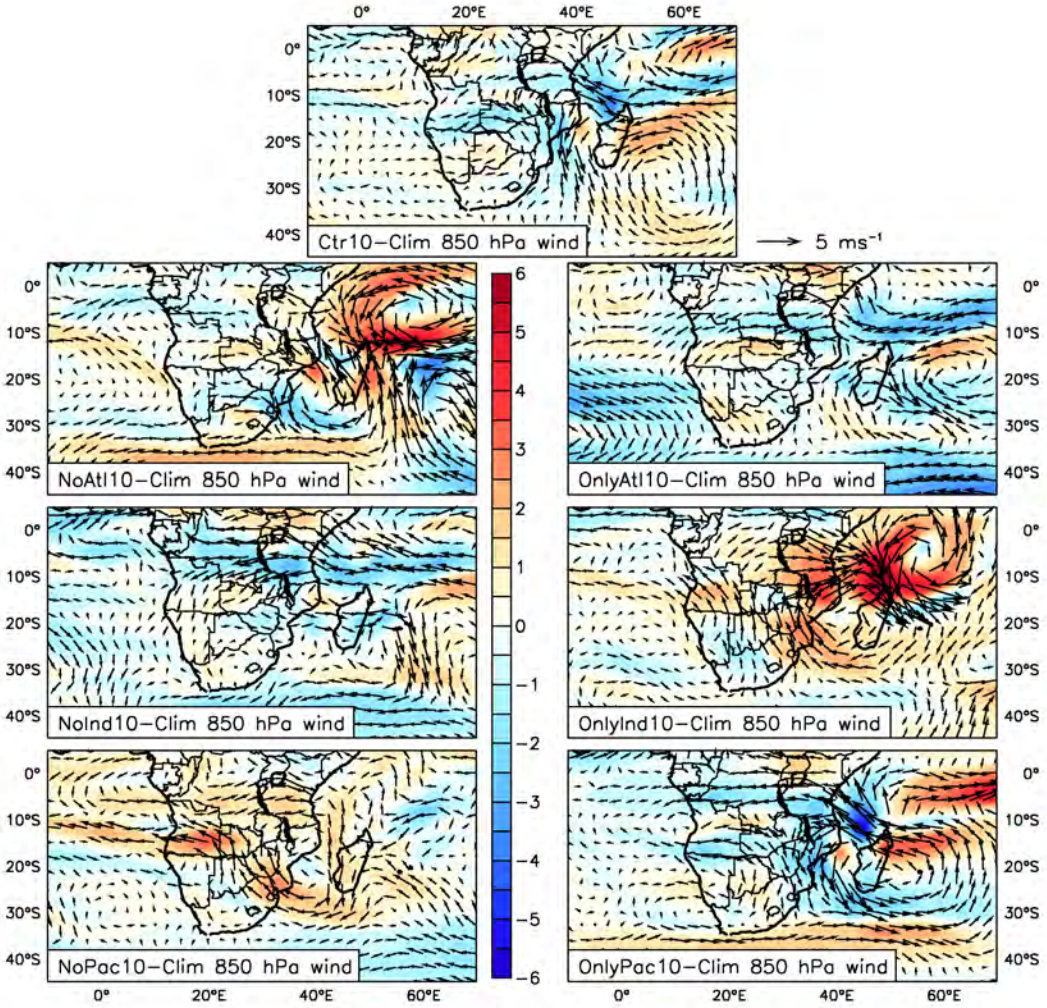

Figure 7.13: JFM 2010 850 wind anomaly (magnitude shaded) for Ctr10, NoAtl10, NoInd10, NoPac10, OnlyAtl10, OnlyInd10 and OnlyPac10 (in $m \cdot s^{-1}$)

Chapter 8

Summary and Conclusions

Southern Africa is a mainly semi-arid region that receives the majority of its annual rainfall during the austral summer months. The region is particularly vulnerable to severe weather events such as drought or floods due to the predominance of rain-fed agriculture as a source of food and income. The ability of many of the countries in southern Africa to adapt to climate stresses is hampered by extensive poverty, political instability. Unfortunately, climate change models for southern Africa indicate that the region will only face increased challenges in the future with predictions of reduced rainfall, agricultural drought, and increased rainfall variability for most parts of southern Africa (Collins et al., 2013). A better understanding of the climate processes that influence rainfall variability over southern Africa may prove useful in adaptating to the future climate and may also improve the reliability of forecasting anomalous events, both of which could have positive

implications for the quality of life and economic well being of the population of southern Africa.

8.1 Summary of Southern African Rainfall During JFM 1998 and JFM 2010

The 1997-1998 El Niño is the strongest El Niño event recorded, with an Oceanic Niño Index (ONI) peaking at 2.4 during the OND 1997 season (McPhaden, 1999; Latif et al., 1999; Murtugudde et al., 2000; Reason and Jagadheesha, 2005; Lyon and Mason, 2007). ENSO was not intensively studied until the El Niño of 1982-1983 (Wang et al., 2012), the second strongest El Niño event on record. The 1982-1983 El Niño sparked international interest in the ENSO phenomenon with the result that many observational systems and predictive models were in place when the 1997-1998 event occurred (McPhaden et al., 2009). The association between El Niño and dry conditions over southern Africa was well studied and established (Ropelewski and Halpert, 1987; Hastenrath et al., 1993; Goddard and Graham, 1999; Reason et al., 2000; Reason and Rouault, 2002; Reason and Jagadheesha, 2005; Richard et al., 2000, 2001; Lyon and Mason, 2007, 2009; Meque and Abiodun, 2014). However, although southern Zimbabwe and Namibia experienced drought during the summer of 1997-1998, the rest of southern Africa received average seasonal rainfall totals despite a dry start to the summer rainy season (Cook, 2000). In particular, there was drought in South Africa before

December 1997, but heavy rains occurred thereafter and rainfall was low in Namibia, almost normal in south southern Africa, and excessive in south-eastern southern Africa (Kane, 1999).

Many seasonal climate forecasts indicated an enhanced probability of dry conditions over the subcontinent during the austral summer season 1997-1998 (Mason et al., 1999b; Buizer et al., 2000; Lyon and Mason, 2007; Kane, 1999; Curtis et al., 2001).Yuan et al. (2014) found that the model SINTEX-F simulated too strong a link between ENSO and southern African rainfall and suggested this might explain why the forecasts for the 1997-1998 summer rainfall season were not in line with observations. The rainfall forecast for the 2009-2010 DJF El Niño season that were made by the three coupled models discussed in Landman and Beraki (2010) also showed mostly enhanced probabilities for dry conditions over southern Africa. A similar forecast was also made by centres such as the IRI and the South African Weather Service.

As well as a strong El Niño, 1997-1998 also experienced a strong positive TIOD (Webster et al., 1999; Latif et al., 1999; Murtugudde et al., 2000) that persisted until March 1998, a positive SIOD that switched phase to become a negative SIOD in early 1998 (Behera and Yagamata, 2001), and a Benguela Niño during JFM 1998 (Rouault et al., 2009). El Niño events typically lead to drought conditions over southern Africa (Lindesay, 1988; Reason et al., 2000), and negative SIOD events have been associated with dry conditions

over parts of southern Africa (Behera and Yagamata, 2001; Reason, 2001, 2002), while a Benguela Niño usually results in above average rainfall over parts of southern Africa (Rouault et al., 2003a).

During strong ENSO events, the Angola low is typically weakened and therefore supplies less moisture to the cloudbands over southern Africa with resulting dryer-than-average conditions (Mulenga et al., 2003; Reason and Jagadheesha, 2005). However, this connection between a strong ENSO and an anonymously weak Angola low was not observed during 1997-1998 and may have been partially responsible for the wetter-than-expected conditions over southern Africa (Reason and Jagadheesha, 2005).

Compared with the 1997-1998 El Niño, the 2009-2010 event has received relatively less attention, although both events are often cited as examples of anomalous rainfall responses to El Niño. A new type of El Niño, characterised by anomalously warm SSTAs in the central equatorial Pacific Ocean as opposed to the typical warming over the eastern Pacific Ocean, has been occurring with more frequency in the last few decades. These events can be described using the Niño 4 index (Kao and Yu, 2009; Yeh et al., 2009). It is known by many names including the central Pacific (CP) El Niño, dateline El Niño, warm pool (WP) El Niño or El Niño Modoki (Ashok et al., 2007a; Kao and Yu, 2009; Yu and Kim, 2010; Kug et al., 2009; Larkin and Harrison, 2005). The El Niño event of 2009-2010 is considered to have been

a CP El Niño event, however it was unusual since SSTAs over the eastern equatorial Pacific Ocean were also high. The SSTAs over the midlatitude south eastern Pacific Ocean were below average which is typical of an CP El Niño and despite the anomalous warm equatorial eastern Pacific waters, the 2009-2010 event falls into the categorization of CP El Niño when the indices are consulted (Lee and McPhaden, 2010; Kim et al., 2011; Ratnam et al., 2012).

DJF 2009-2010 rainfall over South Africa was anomalously high during JFM 2010 and the Vaal Dam in South Africa was more than 100% full for the first time in 13 years. As was the case during 1997-1998, the association of enhanced forecasting skill with El Niño years may partially explain the level of confidence in the forecast of dry conditions for the austral summer seasons during 2009-2010.

The 2009-2010 season experienced a strong CP El Niño, as well as a strong negative phase NAO, and a weak positive TIOD. CP El Niño events have been associated with below average rainfall over southern Africa, although they do not produce the same extent of dry conditions as EP El Niño events (Ratnam et al., 2012, 2014), while positive TIOD events usually result in above average rainfall over parts of southern Africa. McHugh and Rogers (2001) found that heavier, convective, DJF rainfall occurs over Tanzania, northern Mozambique, Zambia and part of the western DRC during the neg-

ative NAO phase, when the North Atlantic westerlies are unusually weak. Todd and Washington (2004) also found a negative correlation between the NAO and central African rainfall, although their study focused on the FMA season.

The late summer rainfall seasons JFM 1998 and JFM 2010 were both considered in each of the results chapters in this thesis and findings regarding these two seasons have been included in the relevant section below.

8.2 The Botswana High

The Botswana high has been implicated in rainfall anomalies over small regions of southern Africa in a few studies (Matarira, 1990; Magadza, 1994; Unganai and Mason, 2002; Ratna et al., 2013), but a thorough investigation of the importance of this feature could not be found in the existing literature. An analysis of the monthly evolution of the Botswana high reveals that it appears to track a similar migration pattern as that of the ITCZ.

Analysis was performed for both the early (OND) and late (JFM) summer seasons, but the results were more robust for the late summer season. An EOF analysis of 500 hPa geopotential height over southern Africa reveals that the Botswana high accounts for approximately 25% of the variance of geopotential height during the early summer OND season and the majority

of years in which a strong (weak) Botswana high occurred were El Niño (La Niña) years indicating a possible relationship between the Botswana high and ENSO. Correlation analysis confirmed this association as a correlation coefficient of 0.51 (at approximately 100% statistical significance) was found between the OND Botswana high and ENSO. However, no obvious pattern was found when investigating a possible association between the early summer Botswana high and rainfall variability over southern Africa.

For the later summer JFM season, EOF analysis revealed that the Botswana high accounts for approximately 75% of the variance of geopotential height at 500 hPa and the JFM season showed an even stronger relationship with ENSO than the early summer season since every strong (weak) Botswana high occurred during an El Niño (La Niña) year. Correlation analysis was used to further investigate the relationship between the JFM Botswana high and ENSO. The correlation coefficient of 0.87 (at approximately 100% statistical significance) confirmed the EOF analysis. Since the relationship between ENSO and rainfall over southern Africa has been well established, the question arises as to whether or not the Botswana high is simply another manifestation of ENSO. To address this, the association between rainfall over southern Africa and the relative strength and position of the Botswana high was investigated.

The general pattern of Botswana highs during El Niño years tends to

display the highest values over land and is usually centred in the typical region over the western part of southern Africa. If there are high values over the adjacent oceans, they are usually higher over the subtropical South Atlantic Ocean. However, the general pattern of Botswana highs during La Niña years tend to have their highest values split across each of the adjacent oceans. Alternatively, if the strongest values occur over land, they are not restricted to the usual location of the Botswana high and may occur much further east than is typical. During non-ENSO years that display the El Niño-like Botswana high, rainfall over southern Africa is usually below average, while rainfall during years that display La Niña-like Botswana highs is mostly above average. Thus, the correlation between the shape and position of the Botswana high exists during both ENSO and during neutral years. This result could be particularly useful because seasonal rainfall predictions over the region only seem to be reasonably accurate during strong ENSO seasons (Landman and Goddard, 2002). The results presented suggest that seasonal forecasters and climate scientists should pay attention not only to ENSO indicators but also to the Botswana high in investigating rainfall variability over southern Africa.

Future work on the relationship between the Botswana high and southern African rainfall should include calculation of an index to better identify Botswana highs during neutral years that can be classified as being either El Niño or La Niña -like. The relative impact of the Botswana high and

the Angola low on rainfall over the region is another potential area of future study. It would also be useful to identify factors that influence the position and strength of the Botswana high so that forecasting is possible.

8.3 Dry Day Frequency over Southern Africa

While the Botswana high was investigated on a monthly and seasonal basis, it is also of considerable interest to show how the rainy season behaves for shorter time periods. One of the parameters that user groups find useful is dry day frequency. Hence, the frequency of dry days over southern Africa during JFM was investigated using GPCP observational data. The climatology of DDF over southern Africa during JFM was calculated using daily GPCP data from 1997 to 2012. There are two large dry regions over the oceans corresponding to the South Atlantic and South Indian Anticyclones. A region of low DDF associated with the seasonal position of the ITCZ is also evident. It can be seen as a band of relatively low DDF that extends from the equatorial Atlantic Ocean south-eastward centred over northeast Angola, southern DRC, northeast Zambia, extending to a lesser extent into northern Mozambique, which then moves south-eastward to northern Madagascar before heading in a slightly northeastern direction over the Indian Ocean. Just to the south of this region, running from southern Namibia, across South Botswana, over southern Zimbabwe, most of the Limpopo region, southern Mozambique and into the southern Mozambique Channel is another band,

only this time it is one of high DDF. Usman and Reason (2004) identified this band of high DDF between 20^o and 25^oS as the drought corridor that runs across subtropical southern Africa. There is also a low DDF region over eastern South Africa below the drought corridor which is related to the Drakensberg and Maluti Mountains and the onshore flow of moist marine air as migratory anticyclones ridge into the South West Indian Ocean.

Correlation analysis between DDF and global SSTs was performed using GPCP pentad data from 1979 to 2011. The correlation analysis was generally in agreement with previous studies (Usman and Reason, 2004; Todd and Washington, 2004; Reason et al., 2005; Hachigonta and Reason, 2006) and found that DDF over the Limpopo and North East Zambia regions is correlated with ENSO, while DDF over coastal northern Angola and central South Africa are correlated with SSTs in the Indian and Atlantic Oceans. In particular, DDF over coastal northern Angola has a correlation of 0.51 with the AMO (at 100% statistical significance), although the AMO has not previously been associated with rainfall variability over southern Africa. DDF over coastal northern Angola was also found to be correlated with the NAO and the SAM. DDF over central South Africa was also correlated with the AMO, as well as the TIOD. These results indicate that the AMO may have an impact on DDF over some regions of southern Africa and may warrant further study. DDF over the Limpopo and North East Zambia were both found to be correlated with ENSO and DDF over North East Zambia is also

correlated with Benguela Niño events off the coast of Angola.

DDF during JFM over three of the four regions chosen in this study is also correlated with the Botswana high. The seasonal DDF over North East Zambia is correlated with the DJF Botswana high, which could be due to the northward position of the Botswana high during December as well as its elongated shape extending eastward over much of the subcontinent (**Figure 4.2**). DDF during JFM over the Limpopo is correlated with the Botswana high at zero lag, and DDF during JFM over coastal northern Angola is correlated with the Botswana high at a lag of -1. A possible explanation for this correlation is the northward shift of the Botswana high in April when it centres over southern Angola (**Figure 4.2**).

The late summer rainfall seasons JFM 1998 and JFM 2010 are of particular interest due to the fact that most climate prediction models forecast dry conditions over southern Africa but the expected dry conditions were not as widespread as anticipated. During JFM 1998, the drought corridor expanded and moved northward and the DDF along the rough seasonal position of the ITCZ increased. This behaviour might be linked to a northward shift in the position in the ITCZ. During El Niño events, the ITCZ is typically weakened as high pressure anomalies occur over the South Indian Ocean and southern Africa. The anomalously strong and unusually elongated Botswana high may also have contributed to the increase in size of the drought cor-

ridor, as well as the increase in DDF. The decreased moisture flux input from the South Indian Ocean may have been another contributing factor in this region. The stronger South Atlantic Anticyclone may have contributed to the eastward expansion of DDF over western Namibia and South Africa. DDF over Tanzania was reduced which was likely due to a combination of ENSO and TIOD influences. The distribution of DDF over southern Africa during JFM 2010 was rather different from that of JFM 1998 and the climatology. The drought corridor developed a more pronounced weakening over Botswana and the band to the right of Botswana increased and expanded further northward into Zimbabwe and Mozambique. This behaviour may have been linked to a reduction in moisture flux input from the South Indian Ocean. The movement of the drought corridor may also indicate a northward shift in the ITCZ.

8.4 Model results

Given that many studies have looked at the influence of SSTAs from a particular basin (and very occasionally two basins) on southern African rainfall using AGCMs, it is of interest to better understand the relative influence of all these basins on the region. Almost all studies have used global AGCMs with horizontal resolutions of order 200-300 km or else regional models of limited domain at resolutions of order 50 km. It was therefore of interest to see whether a stretch grid model which is global in domain but also has horizon-

tal resolution of order 50 km over Africa could be used to assess the influence of the different SST forcings. Thus, the non-hydrostatic, stretch grid global atmospheric model CEU was used to investigate the relative impact of each of the three major ocean basins on rainfall over southern Africa during JFM 1998 and JFM 2010. A number of idealised experiments were performed in which the input SSTs were altered. The control runs, Ctr98 and Ctr10, were forced with observed global SSTs. In each of the three No"Ocean" experiments, input SSTs in that ocean basin were replaced by the climatology of that ocean. The circulation output of these experiments can be thought to represent either the combined influence of the remaining two ocean's SST forcing, or the the effect of removing that particular ocean's SST forcing. In each of the Only"Ocean" experiments, input SSTs of the remaining two ocean basins were replaced by their climatology which isolates the impact of that ocean's SST forcing on southern African rainfall. Note that these experiments are, at best, approximations of relative impact since it is assumed that Only"OceanX" and No"OceanX" can be compared to CtrX as if the impact of OceanX can be completely isolated in the first case and completely removed in the second.

The analysis of JFM 1998 and JFM 2010 rainfall anomalies showed that different regions of southern Africa were most strongly influenced by different ocean basin SSTs. There was no obvious association found between either the regions affected or the two seasons examined. However, a feature that

was present in both JFM 1998 and JFM 2010 that also appears to have been responsible for much of the increased rainfall over southern Africa during these two seasons, is an enhanced Angola low. During strong ENSO events, the Angola low is typically weakened and therefore supplies less moisture to the cloudbands over southern Africa with resulting dryer-than-average conditions (Mulenga et al., 2003; Reason and Jagadheesha, 2005). However, this connection between a strong ENSO and a weak Angola low was not observed during 1997-1998 and 2009-2010 and some studies have linked the anomalously strong Angola low of 1997-1998 with the above average rainfall experienced over southern Africa during this season (Reason and Jagadheesha, 2005; Lyon and Mason, 2007). The JFM 2010 Angola low was also anomalously strong and results of this chapter indicate that this feature played an important role in producing enhanced rainfall over southern Africa during this season.

Future development on CEU is planned to improve its performance over southern Africa. These plans focus mainly on the incorporation of different, and hopefully improved, physics parametrisation schemes. One of the first steps will include upgrading CEU from CAM3 to the newer CAM 5.2, which offers many improvements on the physics parametrisations. Another possible improvement could be to implement the parametrisation schemes of other regional models which have been shown to perform better over southern Africa than CEU does. Other future plans include creating a regional model from

CEU, and then coupling it to an ocean model.

The main results of this thesis indicate that closer attention should be paid to the Botswana high and the Angola low since these two features are linked to both southern African rainfall and ENSO. Future studies could investigate whether or not a relationship between the Botswana high and Angola low exists and, if so, how it affects rainfall over southern Africa. Another question of interest is whether or not the Angola low also has a relationship with southern African rainfall anomalies during ENSO-neutral years.

Better understanding of the Botswana high and the Angola low has the potential to shed new light on the complex and non-linear relationships between southern African rainfall and ENSO, as well as potentially leading to better forecasting of seasonal rainfall during non-ENSO years.

List of Figures

List of Tables

Bibliography

Abiodun B, Prusa J, and Gutowski W (2008) *Implementation of a non-hydrostatic, adaptive-grid dynamics core in CAM3. Part I: comparison of dynamics cores in aqua-planet simulations.* Climate dynamics 31(7):795–810. ISSN 0930-7575

Abiodun BJ, Gutowski WJ, Abatan AA, and Prusa JM (2011) *CAM-EULAG: A non-hydrostatic atmospheric climate model with grid stretching.* Acta Geophysica 59(6):1158–1167

Abram N, Gagan M, Cole J, Hantoro W, and Mudelsee M (2008) *Recent intensification of tropical climate variability in the Indian Ocean.* Nature Geoscience 1:849–853

Ashok K, Behera S, Rao S, Weng H, and Yamagata T (2007a) *El Niño Modoki and its possible teleconnection.* J. Geophys Res. 112 C11007. doi: 10.1029/2006JC003798

Ashok K, Behera SK, Rao SA, Weng H, and Yamagata T (2007b) *El Niño*

Modoki and its possible teleconnection. Journal of Geophysical Research: Oceans (1978–2012) 112(C11)

Ashok K and Yamagata T (2009) *The El Nino with a Difference.* Nature 461:481–484

Barnston AG, He Y, and Glantz MH (1999) *Predictive skill of statistical and dynamical climate models in SST forecasts during the 1997-98 El Niño episode and the 1998 La Niña onset.* Bulletin of the American Meteorological Society 80(2):217–243

Barnston AG and Livezey RE (1987) *Classification, seasonality and persistence of low-frequency atmospheric circulation patterns.* Monthly weather review 115(6):1083–1126

Barnston AG and Ropelewski CF (1992) *Prediction of ENSO episodes using canonical correlation analysis.* Journal of Climate 5(11):1316–1345

Behera S and Yagamata T (2001) *Subtropical SST dipole events in the southern Indian Ocean.* Geophys. Res. Lett. 28(2):327–330

Bjerknes J (1969) *Atmospheric teleconnections from the equatorial pacific 1.* Monthly Weather Review 97(3):163–172

Black E, Slingo J, and Sperber K (2003) *An Observational Study of the Relationship Between Excessively Strong Short Rains in Coastal East Africa and Indian Ocean SST.* Mon. Wea. Rev. 131:74–94

Blunden J, Arndt DS, and Baringer MO (2011) *State of the climate in 2010*. Special Supplement to the Bulletin of the American Meteorological Society 92(6)

Bolvin DT, Adler RF, Huffman GJ, Nelkin EJ, and Poutiainen JP (2009) *Comparison of GPCP monthly and daily precipitation estimates with high-latitude gauge observations*. Journal of Applied Meteorology and Climatology 48(9):1843–1857

Buizer JL, Foster J, and Lund D (2000) *Global impacts and regional actions: preparing for the 1997-98 El Niño*. Bulletin of the American Meteorological Society 81(9):2121–2139

Camberlin P, Janicot S, and Poccard I (2001) *Seasonality and atmospheric dynamics of the teleconnection between African rainfall and tropical sea-surface temperature: Atlantic vs. ENSO*. International Journal of Climatology 21(8):973–1005

Cane MA (2005) *The evolution of El Niño, past and future*. Earth and Planetary Science Letters 230(3):227–240

Chipanshi AC and Ringrose S (2001) *Reflections on the 1997/98 El Niño phenomenon in Botswana*. Weather 56(1):11–24

Collins M, Knutti R, Arblaster J, Dufresne JL, Fichefet T, Friedlingstein P, Gao X, Gutowski W, Johns T, Krinner G et al. (2013) *Climate Change 2013: The Physical Science Basis. Contribution of Working Group I to*

the Fifth Assessment Report of the Intergovernmental Panel on Climate Change. Cambridge University Press, Cambridge, United Kingdom and New York, NY, USA

Collins WD, Rasch PJ, Boville BA, Hack JJ, McCaa JR, Williamson DL, Briegleb BP, Bitz CM, Lin SJ, and Zhang M (2006) *The formulation and atmospheric simulation of the Community Atmosphere Model version 3 (CAM3)*. Journal of Climate 19(11):2144–2161

Collins WD, Rasch PJ, Boville BA, Hack JJ, McCaa JR, Williamson DL, Kiehl JT, Briegleb B, Bitz C, Lin S et al. (2004) *Description of the NCAR community atmosphere model (CAM 3.0)*. NCAR Tech. Note NCAR/TN-464+ STR

Compo GP, Whitaker JS, Sardeshmukh PD, Matsui N, Allan R, Yin X, Gleason B, Vose R, Rutledge G, Bessemoulin P et al. (2011) *The twentieth century reanalysis project*. Quarterly Journal of the Royal Meteorological Society 137(654):1–28

Cook C, Reason C, and Hewitson B (2004) *Wet and dry spells within particularly wet and dry summers in the South African summer rainfall region*. Climate Research 26(1):17–31. ISSN 0936-577X

Cook K (2000) *The South Indian convergence zone and interannual rainfall variability over southern Africa*. Journal of Climate 13(21):3789–3804

Cook K (2001) *A Southern Hemisphere wave response to ENSO with implications for southern Africa precipitation.* Journal of the Atmospheric Sciences 58(15):2146–2162. ISSN 1520-0469

Curtis S, Adler R, Huffman G, Nelkin E, and Bolvin D (2001) *Evolution of tropical and extratropical precipitation anomalies during the 1997–1999 ENSO cycle.* International Journal of Climatology 21(8):961–971. ISSN 1097-0088

De Groen M and Savenije H (1995) *Do land use induced changes of evaporation affect rainfall in Southeastern Africa?* Physics and Chemistry of the Earth 20(5):515–519

Dee D, Uppala S, Simmons A, Berrisford P, Poli P, Kobayashi S, Andrae U, Balmaseda M, Balsamo G, Bauer P et al. (2011) *The ERA-Interim reanalysis: Configuration and performance of the data assimilation system.* Quarterly Journal of the Royal Meteorological Society 137(656):553–597

Deser C and Blackmon ML (1993) *Surface climate variations over the North Atlantic Ocean during winter: 1900-1989.* Journal of Climate 6(9):1743–1753

Fauchereau N, Trzaska S, Richard Y, Roucou P, and Camberlin P (2003a) *Sea-surface temperature co-variability in the Southern Atlantic and Indian Oceans and its connections with the atmospheric circulation in the Southern Hemisphere.* International journal of climatology 23(6):663–677

Fauchereau N, Trzaska S, Rouault M, and Richard Y (2003b) *Rainfall variability and changes in southern Africa during the 20th century in the global warming context.* Natural Hazards 29(2):139–154

Feng J, Yu L, and Hu D (2014) *Influence of Indian Ocean subtropical dipole on spring rainfall over China.* International Journal of Climatology 34(4):954–963

Florenchie P, Lutjeharms J, Reason C, Masson S, and Rouault M (2003) *The source of Benguela Niños in the south Atlantic Ocean.* Geophys. Res. Lett 30(10):1505

Florenchie P, Reason C, Lutjeharms J, Rouault M, Roy C, and Masson S (2004) *Evolution of interannual warm and cold events in the southeast Atlantic Ocean.* Journal of Climate 17:2318–2334

Folland C, Palmer T, and Parker D (1986) *Sahel rainfall and worldwide sea temperatures, 1901–85.* Nature 320(6063):602–607

Folland CK, Colman AW, Rowell DP, and Davey MK (2001) *Predictability of northeast Brazil rainfall and real-time forecast skill, 1987-98.* Journal of Climate 14(9):1937–1958

Gates WL, Boyle JS, Covey C, Dease CG, Doutriaux CM, Drach RS, Fiorino M, Gleckler PJ, Hnilo JJ, Marlais SM et al. (1999) *An overview of the results of the Atmospheric Model Intercomparison Project (AMIP I).* Bulletin of the American Meteorological Society 80(1):29–55

Gillett N, Kell T, and Jones P (2006) *Regional climate impacts of the Southern Annular Mode.* Geophysical Research Letters 33(23)

Goddard L and Graham N (1999) *Importance of the Indian Ocean for simulating rainfall anomalies over eastern and southern Africa.* J. Geophys. Res. 104(D16):19099–19116

Goddard L and Mason S (2002) *Sensitivity of seasonal climate forecasts to persisted SST anomalies.* Climate Dynamics 19(7):619–632

Goldenberg SB, Landsea CW, Mestas-Nuñez AM, and Gray WM (2001) *The recent increase in Atlantic hurricane activity: Causes and implications.* Science 293(5529):474–479

Grabowski W and Smolarkiewicz P (2002) *A multiscale anelastic model for meteorological research.* Monthly weather review 130(4):939–956

Grimm AM and Reason CJ (2011) *Does the South American Monsoon Influence African Rainfall?* Journal of Climate 24(4)

Hachigonta S and Reason C (2006) *Interannual variability in dry and wet spell characteristics over Zambia.* Climate Research 32(1):49

Hachigonta S, Reason C, and Tadross M (2008) *An analysis of onset date and rainy season duration over Zambia.* Theoretical and Applied Climatology 91(1-4):229–243

Hack JJ, Caron JM, Danabasoglu G, Oleson KW, Bitz C, and Truesdale JE (2006a) *CCSM-CAM3 climate simulation sensitivity to changes in horizontal resolution.* Journal of climate 19(11):2267–2289

Hack JJ, Caron JM, Yeager SG, Oleson KW, Holland MM, Truesdale JE, and Rasch PJ (2006b) *Simulation of the global hydrological cycle in the CCSM Community Atmosphere Model version 3 (CAM3): Mean features.* Journal of climate 19(11):2199–2221

Hansingo K and Reason C (2009) *Modelling the atmospheric response over southern Africa to SST forcing in the southeast tropical Atlantic and southwest subtropical Indian Oceans.* International Journal of Climatology 29(7):1001–1012

Harris I, Jones P, Osborn T, and Lister D (2013) *Updated high-resolution grids of monthly climatic observations–the CRU TS3. 10 Dataset.* International Journal of Climatology

Harrison M (1984) *A generalized classification of South African summer rain-bearing synoptic systems.* Journal of Climatology 4(5):547–560

Harrison MSJ (1986) *A synoptic climatology of South African rainfall variations.* Ph.D. thesis, University of the Witwatersrand, 1986 Typescript (photocopy)

Hart N, Reason C, and Fauchereau N (2010) *Tropical-extratropical interac-*

tions over southern Africa: three cases of heavy summer season rainfall. Monthly Weather Review 138(7):2608–2623

Hart NC, Reason CJ, and Fauchereau N (2013) *Cloud bands over southern Africa: seasonality, contribution to rainfall variability and modulation by the MJO.* Climate dynamics 41(5-6):1199–1212

Hastenrath S, Nicklis A, and Greischar L (1993) *Atmospheric-hydropheric mechanisms of climate anomalies in the western equatorial Indian Ocean.* J. Geophys. Res. 98:20219–20235

Hélein F (2002) *Harmonic maps, conservation laws, and moving frames*, volume 150. Cambridge Univ Pr

Hermes J and Reason C (2005) *Ocean model diagnosis of interannual coevolving SST variability in the south Indian and South Atlantic Oceans.* Journal of climate 18(15):2864–2882

Hirst A and Hastenrath S (1983) *Atmosphere-Ocean Mechanisms of Climate Anomalies in the Angola-Tropical Atlantic Sector.* Journal of Physical Oceanography 13(7):1146–1157. ISSN 1520-0485

Huffman GJ, Adler RF, Morrissey MM, Bolvin DT, Curtis S, Joyce R, McGavock B, and Susskind J (2001) *Global precipitation at one-degree daily resolution from multisatellite observations.* Journal of Hydrometeorology 2(1):36–50

Hurrell JW, Hack JJ, Phillips AS, Caron J, and Yin J (2006) *The dynamical simulation of the Community Atmosphere Model version 3 (CAM3).* Journal of climate 19(11):2162–2183

Johns TC, Carnell RE, Crossley JF, Gregory JM, Mitchell JF, Senior CA, Tett SF, and Wood RA (1997) *The second Hadley Centre coupled ocean-atmosphere GCM: model description, spinup and validation.* Climate dynamics 13(2):103–134

Joubert A and Hewitson B (1997) *Simulating present and future climates of southern Africa using general circulation models.* Progress in physical geography 21(1):51. ISSN 0309-1333

Jury M and Pathack B (1991) *A study of climate and weather variability over the tropical southwest Indian Ocean.* Meteorology and Atmospheric Physics 47(1):37–48

Jury MR (2002) *Economic impacts of climate variability in South Africa and development of resource prediction models.* Journal of Applied Meteorology 41(1)

Kane R (1999) *Some characteristics and precipitation effects of the El Nino of 1997–1998.* Journal of Atmospheric and Solar-Terrestrial Physics 61(18):1325–1346

Kao HY and Yu JY (2009) *Contrasting eastern-Pacific and central-Pacific types of ENSO.* Journal of Climate 22(3):615–632

Kijazi A and Reason C (2005) *Relationships between intraseasonal rainfall variability of coastal Tanzania and ENSO.* Theoretical and applied climatology 82(3-4):153–176

Kim W, Yeh SW, Kim JH, Kug JS, and Kwon M (2011) *The unique 2009–2010 El Niño event: A fast phase transition of warm pool El Niño to La Niña.* Geophysical Research Letters 38(15)

Kug J and Kang I (2006) *Interactive feedback between ENSO and the Indian Ocean.* Journal of climate 19(9):1784–1801

Kug JS, Jin FF, and An SI (2009) *Two types of El Niño events: cold tongue El Niño and warm pool El Niño.* Journal of Climate 22(6):1499–1515

Kutzbach JE (1967) *Empirical eigenvectors of sea-level pressure, surface temperature and precipitation complexes over North America.* Journal of Applied Meteorology 6(5):791–802

Landman W and Beraki A (2010) *Multi-model forecast skill for mid-summer rainfall over southern Africa.* International Journal of Climatology

Landman W and Mason S (1999) *Change in the Association between Indian Ocean Sea-Surface Temperatures and Summer Rainfall over South Africa and Namibia.* Int. J. Climatol. 19:1477–1492

Landman WA and Beraki A (2012) *Multi-model forecast skill for mid-summer rainfall over southern Africa.* International Journal of Climatology 32(2):303–314

Landman WA and Goddard L (2002) *Statistical recalibration of GCM forecasts over southern Africa using model output statistics.* Journal of Climate 15(15):2038–2055

Larkin NK and Harrison D (2005) *On the definition of El Niño and associated seasonal average US weather anomalies.* Geophysical Research Letters 32(13)

Latif M, Dommenget D, Dime M, and Grotzner A (1999) *The Role of Indian Ocean Sea Surface Temperature in Forcing East African Rainfall Anomalies during December-January 1997/98.* Journal of Climate 12:3497–3502

Lee T and McPhaden MJ (2010) *Increasing intensity of El Niño in the central-equatorial Pacific.* Geophysical Research Letters 37(14)

Lenters J and Cook K (1997) *On the origin of the Bolivian high and related circulation features of the South American climate.* Journal of the Atmospheric Sciences 54(5):656–678

Lenters J and Cook K (1999) *Summertime precipitation variability over South America: Role of the large-scale circulation.* Monthly Weather Review 127(3):409–431

Limpasuvan V and Hartmann DL (1999) *Eddies and the annular modes of climate variability.* Geophysical Research Letters 26(20):3133–3136

Lindberg C and Broccoli AJ (1996) *Representation of topography in spectral*

climate models and its effect on simulated precipitation. Journal of climate 9(11):2641–2659

Lindesay J (1988) *South African rainfall, the Southern Oscillation and a Southern Hemisphere semi-annual cycle.* International Journal of Climatology 8(1):17–30. ISSN 1097-0088

Lipps FB and Hemler RS (1982) *A scale analysis of deep moist convection and some related numerical calculations.* Journal of the Atmospheric Sciences 39(10):2192–2210

Lipps FB and Hemler RS (1986) *Numerical simulation of deep tropical convection associated with large-scale convergence.* Journal of the atmospheric sciences 43(17):1796–1816

Lu R, Dong B, and Ding H (2006) *Impact of the Atlantic Multidecadal Oscillation on the Asian summer monsoon.* Geophysical research letters 33(24)

Lubbecke J, Boning C, Keenlyside N, and Xie SP (2010) *On the connection between Benguela and Equatorial Atlantic Niños and the role of the South Atlantic Anticyclone.* J. Geophys. Res. in press

Lyon B and Mason S (2007) *The 1997-98 summer rainfall season in southern Africa. Part I: observations.* Journal of climate 20(20):5134–5148. ISSN 0894-8755

Lyon B and Mason S (2009) *The 1997/98 Summer Rainfall Season in South-*

ern Africa. Part II: Model Simulations and Coupled Model Forecasts. Journal of Climate 22(13):3802–3818. ISSN 1520-0442

Magadza C (1994) *Climate change: some likely multiple impacts in Southern Africa*. Food Policy 19(2):165–191

Malherbe J, Landman WA, and Engelbrecht FA (2014) *The bi-decadal rainfall cycle, Southern Annular Mode and tropical cyclones over the Limpopo River Basin, southern Africa*. Climate Dynamics 42(11-12):3121–3138

Mason S and Jury M (1997) *Climatic variability and change over southern Africa: a reflection on underlying processes*. Progress in Physical Geography 21(1):23. ISSN 0309-1333

Mason S, Lindesay J, and Tyson P (1994) *Simulating drought in southern Africa using sea surface temperature variations*. WATER SA-PRETORIA-20:15–15. ISSN 0378-4738

Mason S, Waylen P, Mimmack G, Rajaratnam B, and Harrison J (1999a) *Changes in extreme rainfall events in South Africa*. Climatic Change 41(2):249–257

Mason SJ, Goddard L, Graham NE, Yulaeva E, Sun L, and Arkin PA (1999b) *The IRI seasonal climate prediction system and the 1997/98 El Niño event*. Bulletin of the American Meteorological Society 80(9):1853–1873

Matarira CH (1990) *Drought over Zimbabwe in a regional and global context*. International Journal of Climatology 10(6):609–625

McHugh MJ and Rogers JC (2001) *North Atlantic oscillation influence on precipitation variability around the southeast African convergence zone.* Journal of Climate 14(17):3631–3642

McPhaden M (1999) *Genesis and evolution of the 1997-98 El Niño.* Science 283(5404):950

McPhaden M, Ando K, Bourles B, Freitag H, Lumpkin R, Masumoto Y, Murty V, Nobre P, Ravichandran M, Vialard J et al. (2009) *The global tropical moored buoy array.* Community White Paper for OceanObs 9

McPhaden M, Lee T, and McClurg D (2011) *El Niño and its relationship to changing background conditions in the tropical Pacific Ocean.* Geophysical Research Letters 38(15)

Meque A and Abiodun BJ (2014) *Simulating the link between ENSO and summer drought in Southern Africa using regional climate models.* Climate Dynamics pages 1–20

Mo KC (2010) *Interdecadal modulation of the impact of ENSO on precipitation and temperature over the United States.* Journal of Climate 23(13):3639–3656

Mulenga H, Rouault M, and Reason C (2003) *Dry summers over northeastern South Africa and associated circulation anomalies.* Climate Research 25(1):29–41. ISSN 0936-577X

Murtugudde R, McCreary J, and Busalacchi A (2000) *Oceanic processes associated with anomalous events in the Indian Ocean with relevance to 1997-1998*. Journal of geophysical research 105(C2):3295–3306

New M, Hewitson B, Stephenson D, Tsiga A, Kruger A, Manhique A, Gomez B, Coelho C, Masisi D, Kululanga E et al. (2006) *Evidence of trends in daily climate extremes over southern and west Africa*. J. Geophys. Res 111:D14102

Newman M, Shin SI, and Alexander MA (2011) *Natural variation in ENSO flavors*. Geophysical Research Letters 38(14)

Nicholson S and Entekhabi D (1987) *Rainfall variability in equatorial and southern Africa: relationships with sea surface temperatures along the southwestern coast of Africa*. Journal of Climate and Applied Meteorology 26(5):561–578. ISSN 0733-3021

Nicholson S and Kim J (1997) *The Relationship of the El Nino-Southern Oscillation to African Rainfall*. Journal of Climate 17:117–135

Nicholson S and Selato J (2000) *The influence of La Nina on African rainfall*. International Journal of Climatology 20(14):1761–1776. ISSN 1097-0088

Nigam S, Guan B, and Ruiz-Barradas A (2011) *Key role of the Atlantic Multidecadal Oscillation in 20th century drought and wet periods over the Great Plains*. Geophysical Research Letters 38(16)

Nikulin G, Jones C, Giorgi F, Asrar G, Büchner M, Cerezo-Mota R, Christensen OB, Déqué M, Fernandez J, Hänsler A et al. (2012) *Precipitation climatology in an ensemble of CORDEX-Africa regional climate simulations.* Journal of Climate 25(18):6057–6078

Ogallo L (1988) *Relationships between seasonal rainfall in East Africa and the Southern Oscillation.* Journal of Climatology 8(1):31–43

Oreskes N, Shrader-Frechette K, and Belitz K (1994) *Verification, validation, and confirmation of numerical models in the earth sciences.* Science 263(5147):641–646

Pohl B, Fauchereau N, Reason C, and Rouault M (2010) *Relationships between the Antarctic Oscillation, the Madden-Julian Oscillation, and ENSO, and consequences for rainfall analysis.* Journal of Climate 23(2):238–254

Pohl B, Richard Y, and Fauchereau N (2007) *Influence of the Madden-Julian oscillation on Southern African summer rainfall.* Journal of Climate 20(16):4227–4242

Prusa J, Smolarkiewicz P, and Wyszogrodzki A (2008) *EULAG, a computational model for multiscale flows.* Computers & Fluids 37(9):1193–1207

Ratna SB, Behera S, Ratnam JV, Takahashi K, and Yamagata T (2013) *An index for tropical temperate troughs over southern Africa.* Climate dynamics 41(2):421–441

Ratnam J, Behera S, Masumoto Y, Takahashi K, and Yamagata T (2012) *Anomalous climatic conditions associated with the El Niño Modoki during boreal winter of 2009.* Climate dynamics 39(1-2):227–238

Ratnam J, Behera S, Masumoto Y, and Yamagata T (2014) *Remote Effects of El Niño and Modoki Events on the Austral Summer Precipitation of Southern Africa.* Journal of Climate 27(10):3802–3815

Reason C (1998) *Warm and cold events in the southeast Atlantic/southwest Indian Ocean region and potential impacts on circulation and rainfall over southern Africa.* Meteorology and Atmospheric Physics 69(1-2):49–65

Reason C (2001) *Subtropical Indian Ocean SST dipole events and southern African rainfall.* Geophys. Res. Lett. 28(11):2225–2227

Reason C (2002) *Sensitivity of the southern African circulation to dipole sea-surface temperature patterns in the South Indian Ocean.* Int. J. Climatol. 22:377–393

Reason C, Allan R, Lindesay J, and Ansell T (2000) *ENSO and climatic signals across the Indian Ocean basin in the global context: Part I, Interannual composite patterns.* International Journal of Climatology 20(11):1285–1327

Reason C, Florenchie P, Rouault M, and Veitch J (2006a) *10 Influences of large scale climate modes and agulhas system variability on the BCLME region.* Large Marine Ecosystems 14:223–238

Reason C, Hachigonta S, and Phaladi R (2005) *Interannual variability in rainy season characteristics over the Limpopo region of southern Africa.* International Journal of Climatology 25(14):1835–1853

Reason C and Jagadheesha D (2005) *A model investigation of recent ENSO impacts over southern Africa.* Meteorology and Atmospheric Physics 89(1):181–205. ISSN 0177-7971

Reason C, Landman W, and Tennant W (2006b) *Seasonal to Decadal Prediction of Southern African Climate and Its Links with Variability of the Atlantic Ocean.* Bulletin of the American Meteorological Society 87:941–955

Reason C and Mulenga H (1999) *Relationships between South African rainfall and SST anomalies in the southwest Indian Ocean.* International Journal of Climatology 19(15):1651–1673

Reason C and Rouault M (2002) *ENSO-like decadal variability and South African rainfall.* Geophysical Research Letters 29(13):1638. ISSN 0094-8276

Reason C and Rouault M (2005) *Links between the Antarctic Oscillation and winter rainfall over western South Africa.* Geophysical Research Letters 32(7)

Reynolds RW, Smith TM, Liu C, Chelton DB, Casey KS, and Schlax MG

(2007) *Daily high-resolution-blended analyses for sea surface temperature.* Journal of Climate 20(22):5473–5496

Richard Y, Fauchereau N, Poccard I, Rouault M, and Trzaska S (2001) *20th century droughts in southern Africa: spatial and temporal variability, teleconnections with oceanic and atmospheric conditions.* International Journal of Climatology 21(7):873–885

Richard Y, Trzaska S, Roucou P, and Rouault M (2000) *Modification of the southern African rainfall variability/ENSO relationship since the late 1960s.* Climate Dynamics 16(12):883–895. ISSN 0930-7575

Rocha A and Simmonds I (1997) *Interannual variability of south-eastern African summer rainfall. Part I: Relationships with air-sea interaction processes.* International Journal of Climatology 17(3):235–265

Ropelewski C and Halpert M (1987) *Global and regional scale precipitation patterns associated with the El Nifio/Southern Oscillation.* Hon. flea. Rev 115:1606–1635

Rouault M, Florenchie P, Fauchereau N, and Reason C (2003a) *South East tropical Atlantic warm events and southern African rainfall.* Geophys. Res. Lett 30(5):8009

Rouault M, Reason C, Lutjeharms J, and Beljaars A (2003b) *Underestimation of latent and sensible heat fluxes above the Agulhas Current in NCEP and ECMWF analyses.* Journal of climate 16(4):776–782

Rouault M and Richard Y (2005) *Intensity and spatial extent of droughts in southern Africa*. Geophysical research letters 32(15):L15702

Rouault M, Servain J, Reason C, Bourlès B, Rouault M, and Fauchereau N (2009) *Extension of PIRATA in the tropical South-East Atlantic: an initial one-year experiment*. African Journal of Marine Science 31(1):63–71

Saji N, Goswami B, Vinayachandran P, and Yamagata T (1999) *A Dipole Mode in the Tropical Indian Ocean*. Nature 401:360–363

Saji N, Xie SP, and Yamagata T (2006) *Tropical Indian Ocean Variability in the IPCC Twentieth-Century Climate Simulations*. Journal of Climate 19:4397–4417

Saji N and Yamagata T (2003) *Possible Impacts of Indian Ocean Dipole Mode Events on Global Climate*. Clim. Res. 25:151–169

Shannon L, Boyd A, Brundrit G, and Taunton-Clark J (1986) *On the existence of an El Niño-type phenomenon in the Benguela system*. Journal of Marine Research 44(3):495–520. ISSN 0022-2402

Shinoda T, Alexander M, and Hendon H (2004) *Remote response of the Indian Ocean to interannual SST variations in the tropical Pacific*. Journal of climate 17(2):362–372

Smolarkiewicz P and Prusa J (2004) *Forward-in-time differencing for fluids: simulation of geophysical turbulence*. Turbulent flow computation pages 279–312

Su H, Neelin JD, and Chou C (2001) *Tropical teleconnection and local response to SST anomalies during the 1997–1998 El Niño.* Journal of Geophysical Research: Atmospheres (1984–2012) 106(D17):20025–20043

Sutton RT and Hodson DL (2005) *Atlantic Ocean forcing of North American and European summer climate.* Science 309(5731):115–118

Suzuki R, Behera S, Iizuka S, and Yamagata T (2004) *Indian Ocean subtropical dipole simulated using a coupled general circulation model.* J. Geophys. Res 109:C09001

Tebaldi C and Knutti R (2007) *The use of the multi-model ensemble in probabilistic climate projections.* Philosophical Transactions of the Royal Society A: Mathematical, Physical and Engineering Sciences 365(1857):2053–2075

Thompson DW and Wallace JM (2000) *Annular modes in the extratropical circulation. Part I: month-to-month variability*.* Journal of Climate 13(5):1000–1016

Todd M and Washington R (1999) *Circulation anomalies associated with tropical-temperate troughs in southern Africa and the south west Indian Ocean.* Climate Dynamics 15(12):937–951

Todd MC and Washington R (2004) *Climate variability in central equatorial Africa: influence from the Atlantic sector.* Geophysical Research Letters 31(23)

Trenberth KE (1998) *Development and forecasts of the 1997/98 El Niño: CLIVAR scientific issues.* CLIVAR Exchanges 3:4–14

Trenberth KE and Shea DJ (2006) *Atlantic hurricanes and natural variability in 2005.* Geophysical Research Letters 33(12)

Tyson P (1986) *Climatic change and variability in southern Africa.* Oxford University Press

Unganai L and Mason S (2002) *Long-range predictability of Zimbabwe summer rainfall.* International Journal of Climatology 22(9):1091–1103

Usman MT and Reason C (2004) *Dry spell frequencies and their variability over southern Africa.* CLIMATE RESEARCH. 26(3):199–211

Vigaud N, Richard Y, Rouault M, and Fauchereau N (2007) *Water vapour transport from the tropical Atlantic and summer rainfall in tropical southern Africa.* Climate Dynamics 28(2):113–123

Vigaud N, Richard Y, Rouault M, and Fauchereau N (2009) *Moisture transport between the South Atlantic Ocean and southern Africa: relationships with summer rainfall and associated dynamics.* Climate Dynamics 32(1):113–123

Walker N (1990) *Links between South African summer rainfall and temperature variability of the Agulhas and Benguela Current systems.* Journal of Geophysical Research: Oceans (1978–2012) 95(C3):3297–3319

Wang C, Deser C, Yu JY, DiNezio P, and Clement A (2012) *El Niño-Southern Oscillation (ENSO): a review.* Coral Reefs of the Eastern Pacific, Spring Science Publisher

Washington R (2000) *Quantifying chaos in the atmosphere.* Progress in physical geography 24(4):499–514

Washington R and Preston A (2006) *Extreme wet years over southern Africa: Role of Indian Ocean sea surface temperatures.* J. Geophys. Res. 111, D15104. doi:10.1029/2005JD006724

Webster P, Moore A, Loschnigg J, and Leben R (1999) *Coupled Ocean-Atmosphere Dynamics in the Indian Ocean During 1997-98.* Nature 401:356–360

Weng H, Behera SK, and Yamagata T (2009) *Anomalous winter climate conditions in the Pacific rim during recent El Niño Modoki and El Niño events.* Climate dynamics 32(5):663–674

Wu X, Liang XZ, and Zhang GJ (2003) *Seasonal migration of ITCZ precipitation across the equator: Why can't GCMs simulate it?* Geophysical research letters 30(15)

Xie P and Arkin PA (1997) *Global precipitation: A 17-year monthly analysis based on gauge observations, satellite estimates, and numerical model outputs.* Bulletin of the American Meteorological Society 78(11):2539–2558

Yamagata T, Behera S, Luo J, Masson S, Jury M, and Rao S (2004) *Coupled ocean–atmosphere variability in the tropical Indian Ocean.* Earth Climate: The Ocean–Atmosphere Interaction, Geophys. Monogr 147:189–211

Yeh SW, Kug JS, and An SI (2014) *Recent progress on two types of El Niño: Observations, dynamics, and future changes.* Asia-Pacific Journal of Atmospheric Sciences 50(1):69–81

Yeh SW, Kug JS, Dewitte B, Kwon MH, Kirtman BP, and Jin FF (2009) *El Niño in a changing climate.* Nature 461(7263):511–514

Yeo SR and Kim KY (2013) *Global warming, low-frequency variability, and biennial oscillation: an attempt to understand the physical mechanisms driving major ENSO events.* Climate Dynamics pages 1–16

Yu JY and Kao HY (2007) *Decadal changes of ENSO persistence barrier in SST and ocean heat content indices: 1958–2001.* Journal of Geophysical Research: Atmospheres (1984–2012) 112(D13)

Yu JY and Kim ST (2010) *Three evolution patterns of central-Pacific El Niño.* Geophysical Research Letters 37(8)

Yuan C, Tozuka T, Luo JJ, and Yamagata T (2014) *Predictability of the subtropical dipole modes in a coupled ocean–atmosphere model.* Climate Dynamics 42(5-6):1291–1308